TEAM tAO

Science

Table of Contents

21 October 2005
Volume 310
Number 5747

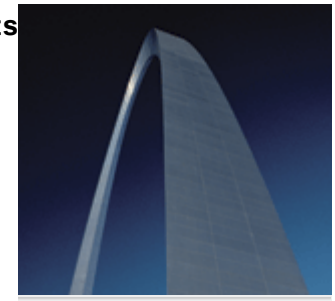

NEW THIS WEEK:

SPECIAL FEATURE

RESEARCH

NEWS

Ice Sheets and Sea Level

Increases in population near coastlines have added to the potential impact of the flooding dangers posed by sea-level rises that accompany global warming. Accurate projections of changes in the Greenland and Antarctic ice sheets are critical in this regard. **Alley *et al.*** (p. 456) review recent observational and modeling advances in the understanding of the response of those ice sheets. Confident projections in ice sheets and sea level in the coming decades and centuries still require additional observations to characterize rapid dynamic changes in ice sheets, as well as improved models.

Particle-Based Photovoltaics

The ability of organic materials to serve as low-cost replacements for silicon in solar cells is hampered by their limited absorption range for light and the low mobility of the charge carriers that are generated. The addition of colloidal semiconductor nanoparticles can enhance electron transport in these polymers. **Gur *et al.*** (p. 462) now show that a solar cell can be realized with only inorganic nanoparticles. They spin-cast bilayers of rod-shaped CdSe or CdTe nanoparticles, which act as donor-acceptor pairs, on indium oxide glass, and then coat them with a metallic top electrode. The highest efficiency for simulated solar illumination was ~3% for a device in which the top contact was made from calcium and the carrier trapping was minimized by sintering the nanoparticles.

Calcium Channel Regulation by Klotho

Klotho, a membrane protein with β-glucuronidase activity, also occurs in a soluble form that has recently been implicated as a hormone that regulates longevity in mice. **Chang *et al.*** (p. 490) now show that its enzymatic activity is required to activate the Ca^{2+} channel, TRPV5. Upon cleavage of sugar residues on TRPV5 by klotho, the channel becomes activated and accumulates at the surface of cells, increasing the influx of Ca^{2+}. This interaction may control Ca^{2+} homeostasis in tissues such as the kidney, where both proteins are abundantly expressed in the mouse.

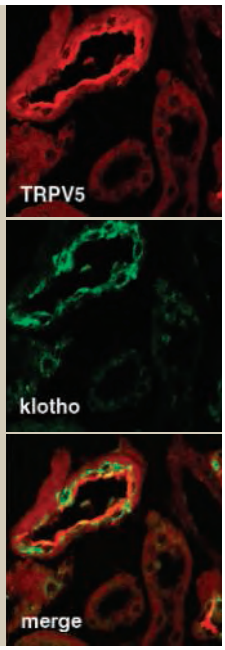

Metals Distort into Insulators

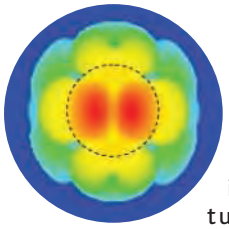

At room temperature, metals and insulators usually represent very different classes of materials, but a number of materials systems can undergo metal-to-insulator transitions at low temperatures. **Wachowiak *et al.*** (p. 468; see the Perspective by **O'Shea**) studied potassium-C_{60} monolayers at 7 K with scanning tunneling microscopy and spectroscopy and found that increasing the potassium to C_{60} ratio from 3 to 4 changed the films from metals into insulators. This charge-induced structural rearrangement was driven by distortions resulting from the Jahn-Teller effect, which helped enhance electron localization.

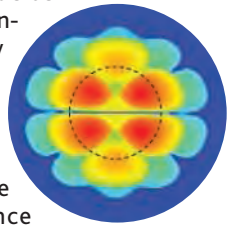

Holey Snowball

Snowball Earth episodes were periods during the Neoproterozoic when global glaciation persisted for time spans of millions of years. How much of the planet was actually covered by ice, and how thick it was, are topics that have been debated vigorously. **Olcott *et al.*** (p. 471, published online 29 September) report the discovery of a large body of black shales that was deposited in southeastern Brazil during one of the Neoproterozoic low-latitude glaciations, between 740 and 700 million years ago. These organic-rich deposits suggest that they were formed as a result of vigorous marine primary production, either in open waters or beneath relatively thin sea ice. Thus, in one area during one Snowball Earth glaciation, there existed spots with environmental conditions conducive to continued, intense biological activity.

Creating Clouds on Titan

Titan's atmosphere contains abundant methane that condenses to form clouds. The short lifetime of methane in the atmosphere, however, may require local sources on this moon. New observations from Cassini and ground-based telescopes are revealing the dynamics of these clouds and possible methane sources (see the news story by **Kerr**). **Roe *et al.*** (p. 477) describe observations from the Keck and Gemini telescopes which show that for several months, methane clouds were most abundant in one region in the southern hemisphere of Titan. **Griffith *et al.*** (p. 474), using Cassini observations over several days, show that typical mid-latitude clouds only persist for a few hours, and their dynamics reflect convective processes in Titan's atmosphere. Both results may be consistent with a local source of methane on this part of Titan.

Deforestation by Stealth?

For more than two decades, satellite imagery has been used to assess deforestation rates in the Brazilian Amazon, but this kind of remote sensing only detects large ''clear-cuts'' in tropical rainforests. **Asner *et al.*** (p. 480) developed an automated remote-sensing system for detection of forest disturbances down to the level of a few treefalls. They applied this system in the Brazilian Amazon to monitor selective logging, which is currently unaccounted for in most policy-making arenas. Selective logging doubles previous estimates of the amount of tropical rainforest that is degraded by humans each year; it occurs mostly in frontier areas, and via illegal operations on conservation and indigenous lands. The results lead to revised estimates of the amount of carbon removed from the region and the flux of carbon to the atmosphere.

CONTINUED ON PAGE 403

CREDITS (TOP TO BOTTOM): CHANG *ET AL.*, WACHOWIACK *ET AL.*

Published by AAAS

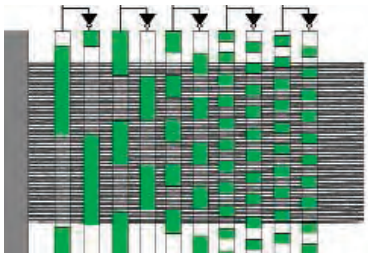

Addressing Nanowire Circuits

A number of methods have been developed for patterning nanowires into small circuits, but connecting these wires to electrical leads is still a challenge, as lithographic methods create patterns on much larger length scales. One possible method for integrating nanowires with larger-scale features is through a demultiplexer architecture. **Beckman *et al.*** (p. 465, published online 29 September) show that this architecture works for a series of circuits on various length scales. Unlike other designs, their configuration does not require precise doping of the nanowires, and it is reasonably fault tolerant with respect to the initial deposition of the nanowires.

Faster Testing for Prion Infection

In vitro tests are needed that replicate the in vivo infection characteristics of so-called prion diseases, such as scrapie in sheep and Creutzfeldt-Jakob disease (CJD) in humans. **Nishida *et al.*** (p. 493) now present an assay system using cultured neural cells that can replicate the mutual interference characteristics observed previously in mice between different strains responsible for CJD and scrapie. The coculture system reduces the time required to test agent interference characteristics from months to days.

A Model of Regulation

It is becoming possible to recognize basic principles of regulatory circuits that control biological processes. **Brandman *et al.*** (p. 496; see the Perspective by **Bornholdt**) compared three distinct biological regulatory systems and note that all contain multiple positive feedback loops with fast and slow time courses. They used mathematical models of the systems to show that these characteristics allow the systems to be relatively insensitive to fluctuations in signal input and allow for the kinetics of activation and inactivation to be adjusted independently to best fit the physiological requirements of the system.

Optimal Enzyme Landscape

Epistatic mutations, which have a nonadditive effect on phenotype, may be important in evolution because they could generate rugged adaptive landscapes. Alternatively, epistasis may be relatively unimportant in natural selection. **Lunzer *et al.*** (p. 499; see the Perspective by **Ellington and Bull**) construct a biochemical adaptive landscape for cofactor use by the *Escherchia coli* enzyme isopropylmalate dehydrogenase (IMDH). The enzyme normally uses nicotinamide adenine dinucleotide (NAD) as a coenzyme, but can be engineered through five amino acid changes to use nicotinamide adenine dinucleotide phosphate (NADP). More than 150 single and double intermediate mutants were assayed for performance and coenzyme preference, and mutant bacteria were assayed for fitness. Each amino acid change contributes additively to enzyme function, whereas they show epistatic contributions to fitness. All natural IMDHs use NAD, which suggests that an ancient adaptive landscape has been conserved.

Each to Their Own

In recent decades, the migration patterns of the European blackcap have diversified to include the British Isles in their overwintering habitat. This newly evolved habit has a genetic basis. However, birds using different locations to overwinter often share the same summer breeding territory, and this situation could allow for interbreeding. **Bearhop *et al.*** (p. 502; see the news story by **Pennisi**) show that birds in their breeding grounds mate with birds that have overwintered in the same location. Thus, divergence and ultimately speciation could occur despite overlapping territories. These studies may also reveal one way in which migratory species have responded to climate change.

CREDIT: BECKMAN *ET AL.*

Published by AAAS

Science and the Digital Divide

At the launch of the World Summit on the Information Society (WSIS) in Geneva in December 2003, the world community strongly affirmed the central role of science in developing an information society and affirmed the principle of "universal access with equal opportunities for all scientific knowledge and the creation and dissemination of scientific and technical information." The WSIS Declaration of Principles recognized the essential role of the public domain and public institutions such as libraries, archives, and museums in supporting the growth of the Information Society and providing free and equitable access to information.* The WSIS Plan of Action suggested numerous approaches to implement these principles, including "e-science" as a key application of information and communication technologies in support of sustainable development.†

The international scientific community succeeded in raising these issues at WSIS and securing widespread support from participating governments. Now, with the second phase of WSIS taking place in Tunis in November 2005, the scientific community needs to take the lead in demonstrating how science—and universal access to scientific data, information, and knowledge—can make a critical difference in sustainable development and overcoming the "digital divide."

The deadly South Asian tsunami in December 2004 and what many have called the "silent tsunamis" of millions of unnecessary deaths and untold suffering from malnutrition, disease, and poverty remind us that science has far to go. Scientists must work not only to predict future hazards and develop new medicines and vaccines, but also to make scientific data and information much more accessible and useful for real-world decision-making. These disasters underscore the need to better understand how societies can best organize themselves to address pressing problems posed by limited resources, conflict, poor infrastructure, and inadequate skills and knowledge. Scientists, the original developers of information and communication technologies, often take for granted their ready access to data and information, software and hardware, and networks of colleagues. But for billions of people, even the most rudimentary access to life-saving scientific expertise and knowledge, such as an early warning or a new cropping method, is a major challenge.

How can the international scientific community help reduce the digital divide? Already, many scientists and scientific institutions are working to improve the reach and effectiveness of science through information and communication technologies. The International Council for Science (ICSU) and its Committee on Data for Science and Technology (CODATA) are collaborating with WSIS to collect and document such efforts (www.wsis-online.net/science/home_EN/). But more needs to be done.

Scientists can support distance education and training; improve the accessibility of information and communication technologies to disadvantaged, marginalized, and vulnerable groups; communicate technical knowledge to the general public; and establish digital libraries, data archives, and other mechanisms to increase access to scientific information. We urge the scientific community to come up with more creative ideas and outcomes. Noteworthy examples on this front include the efforts by the Massachusetts Institute of Technology to provide electronic access to its course materials (http://ocw.mit.edu/index.html) and by the Global Biodiversity Information Facility to make primary scientific biodiversity data openly available (www.gbif.org). The scientific community should also consider new approaches to open electronic access, such as the Science Commons (http://sciencecommons.org), that, among other things, address the complex issue of licensing structures.

Immediately after the South Asian tsunami, critical data on elevation, population location, administrative boundaries, and damage could not be shared because of intellectual property and national security constraints. Even now, the 30-meter-resolution data from the Shuttle Radar Topographic Mission (SRTM) flown by NASA in the year 2000 is not publicly available, although it could potentially provide the best available elevation information regarding most of the world's coasts. The pending decision by the U.S. National Geospatial-Intelligence Agency to prohibit public access to various aeronautical products would be another step in the wrong direction. The scientific community needs to press governments not only to release specific data sets that are vital to disaster management and planning, but also to establish a "good Samaritan" principle for the use of data and information in humanitarian emergencies.

Science helped to create the Information Society—it can now help extend that society to all.

Shuichi Iwata and Robert S. Chen

Shuichi Iwata (University of Tokyo) is president of ICSU's CODATA. Robert S. Chen (Columbia University) is secretary-general of CODATA. CODATA is based in Paris, France.

10.1126/science.1119500

*WSIS, Declaration of Principles (document WSIS-03/GENEVA/DOC/4-E, 12 December 2003). †WSIS, Plan of Action (document WSIS-03/GENEVA/DOC/5-E, 12 December 2003).

Published by AAAS

EDITORS' CHOICE

edited by Stella Hurtley

VIROLOGY

Surveying Influenza

Wild influenza viruses circulate in waterfowl, and mallard ducks (*Anas platyrhynchos*) are particularly good reservoirs, capable of transmitting most of the 16 known hemagglutinin (HA) subtypes of influenza A. Viruses of HA subtype H5 and H7, commonly found in mallards, can transform into highly pathogenic forms when introduced into domesticated poultry via the addition of basic amino acid residues in the HA cleavage site, including that of H5N1, responsible for more than 100 human deaths in Southeast Asia and the current source of fears of a human pandemic. Over 4 years, Munster *et al.* have been surveying and sequencing influenza A subtypes circulating in migrant mallards in northern Europe. Unsurprisingly, but nonetheless alarming, they have discovered that highly related H5 and H7 were circulating in wild ducks before epidemics of highly pathogenic influenza in poultry in Italy (1997 and 2000) and the Netherlands (2003). This sort of surveillance could be a valuable early warning system, allowing time to make vaccines up-to-date. The World Health Organization has also been surveying H5N1 avian influenza viruses with a view to monitoring adamantane drug resistance and antigenic drift, and hence to developing a predictive strategy for vaccine preparation. — CA

Waterfowl trapped in the wild.

Emerg. Infect. Dis. **11**, 1545; 1515 (2005).

NEUROSCIENCE

Sleep Consolidates Visual Experience

Sleep is important for learning and for memory formation. However, there is much controversy about the impact of sleep on brain plasticity and the mechanisms underlying these observations. Jha *et al.* tested whether local brain activity during sleep was necessary for the establishment of brain plasticity. They used the well-established phenomenon of ocular dominance plasticity, in which monocular deprivation shifts synaptic activity in the primary visual cortex (area V1) of the cat in favor of the non-deprived eye only during a critical developmental period. By pharmacological blockade of action potentials they managed to reversibly silence area V1 only during sleep. Although control animals showed the normal critical period ocular dominance shift, this phenomenon could be prevented by selectively silencing area V1 during sleep. Additional undisturbed sleep after a period of cortical inactivation did not rescue this cortical plasticity. Thus, specific neuronal activity in the affected brain area during sleep immediately after waking experience is required for the consolidation of ocular dominance plasticity. — PRS

J. Neurosci. **25**, 9266 (2005).

MATERIALS SCIENCE

Spongy Clay?

Exfoliated clays have been used to reinforce and compatibilize polymeric materials. Clays have also been added to temperature-responsive hydrogels to improve their properties by strengthening the hydrogels without severely degrading their thermoresponsive behavior. Recently, a technique was found to make clay aerogels, which are highly porous structures with very low densities. Bandi *et al.* infiltrated a hydrophilic clay aerogel with *N*-isopropylacrylamide monomer, which was polymerized in situ in order to produce a polymer-clay composite that preserves the aerogel structure of the clay. The resulting composite retains a low density and good stability, with phase transition and swelling behavior similar to that of the unmodified polymer. The clay aerogel improved the structural integrity of the polymer. At the same time, the polymer prevented loss of the aerogel structure when the composite was immersed in water, even though the unmodified hydrogel has little structural integrity of its own. The composites could be cycled through several dehydration–hydration cycles without any breakdown in the structure or performance of the aerogel hydrogel. — MSL

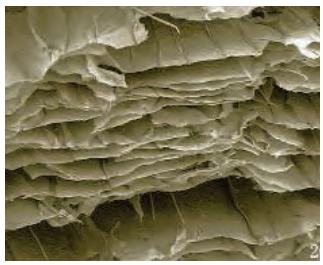

Clay aerogel structure.

Macromolecules 10.1021/ma051698+ (2005).

CELL BIOLOGY

Stem Cells by a Whisker

During normal mammalian hair growth, hair follicles undergo phases of growth, regression, and rest throughout the life of the animal. At the onset of the growth phase, cells recruited from the hair bulge form a hair germ, from which a new hair bulb develops. The adult hair bulge harbors keratinocyte cells, some of which are capable of clonal growth in cell culture, which may represent progenitor cells that underlie the formation of different hair follicle cell lineages or may be multipotent stem cells that can sustain long-term hair follicle renewal.

Claudinot *et al.* now show that these follicular cells are bona fide mammalian stem cells. Single keratinocytes were isolated from the whisker follicles of adult rats, labeled and expanded in cell culture, and then injected into the skin of newborn mice when pelage hair was just being formed. Grafts were subsequently transplanted into nude mice. In some mouse hair follicles, all eight cell lineages present were constituted of entirely transplanted cells, including the root sheaths, hair shaft, sebaceous glands, and epidermis. Transplanted cells were still found after several hair cycles, which suggests that clonogenic keratinocytes are true multipotent stem cells. Furthermore, the transplanted rat cells retained the capacity to recognize and home to the mouse follicle hair bulge. In the future, stem cells from human hair follicles could be exploited to regenerate hair and reconstruct tissue in patients. — LDC

Proc. Natl. Acad. Sci. U.S.A. 10.1073/pnas.0507250102 (2005).

CONTINUED ON PAGE 409

GEOLOGY

Sea Ice Amplification

Numerous, millennial-scale warming episodes, called Dansgaard-Oeschger (D-O) events, punctuated the last glacial period. These events, first discovered in deep ice cores from Greenland, are visible in climate records extending from pole to pole, and in Pacific as well as Atlantic marine sediments. One popular hypothesis about the cause of these abrupt climate

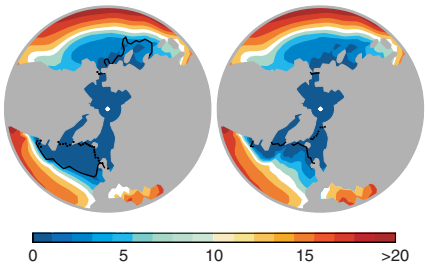

Extent of sea ice.

warmings invokes changes in the strength of the ocean's thermohaline circulation, which affect ocean heat transport. Such a model, however, cannot explain the size of the temperature swings in Greenland, which were as large as 5° to10°C. Li *et al.* use an atmospheric general circulation model to show that warming and cooling of the magnitude observed in Greenland can be caused by only small changes in the amount of sea ice around it. Furthermore, the sea ice changes that they suggest would also account for variations in snow accumulation and oxygen isotope composition similar to those measured in ice cores from Greenland. Finally, the amount of sea ice retreat proposed is consistent with forcing either by ocean thermohaline circulation variations, or by changes in surface wind stress in the North Atlantic. Thus, sea ice can provide a positive feedback strong enough to cause warming like that which occurred during D-O events. — HJS

Geophys. Res. Lett. **32**, L19702 (2005).

CHEMISTRY

One After Another

Multistep synthesis is more efficient when two or more reactions are run consecutively in the same flask, thereby eliminating isolation and purification steps. Huang *et al.* show that a single catalyst can sequentially facilitate nucleophilic and electrophilic additions to α,β-unsaturated aldehydes (compounds with adjacent C=C and C=O groups), with both steps proceeding in high enantioselectivity. Initial reaction of the chiral imidazolidinone catalyst at the C=O group yields an iminium intermediate that adds furan, indole, and thiophene-derived nucleophiles at the β-carbon of the C=C group. The product then remains activated toward addition of electrophilic chlorine at the α-carbon. Moreover, the catalyst–reagent interactions dominate the reaction kinetics, selecting for a syn addition geometry in which both nucleophile and electrophile bond to the same face of the olefin, despite the unfavorable sterics of this arrangement. Overall yields are in the 60 to 90% range, with 9 to 1 or greater syn selectivities, and 99% enantiomeric excess of the major product. Hydride nucleophiles can be added as well, and a fluorine electrophile substituted for the chloro compound. Selectivity switches with hydride to favor the anti product, although a syn geometry can still be induced by addition of an alternate catalyst after the nucleophilic step. — JSY

J. Am. Chem. Soc. 10.1021/ja055545d (2005).

CELL BIOLOGY

Quick-Release RNA

After it is transcribed from DNA, eukaryotic messenger RNA (mRNA) undergoes various types of processing, including the addition of a polyadenylate [poly(A)] tail. The mRNA then typically moves out of the nucleus and into the cytoplasm, where it is translated into protein. However, a large fraction of poly(A)$^+$ RNA stays within the nucleus.

Prasanth *et al.* now suggest that this nuclear-retained RNA may be part of a gene-regulatory mechanism that ensures rapid translation of mRNAs that are required for cellular defenses against stress. They found two populations of poly(A)$^+$ RNA derived from the mouse gene encoding cationic amino acid transporter 2, a protein critical for the activation of the nitric oxide signaling pathway (a common response to stress). In addition to the conventional protein-coding mCAT2 mRNA present in the cytoplasm, a second transcript (CTN-RNA) was retained in the nucleus by virtue of its distinct 3′ untranslated region (UTR). When cells were exposed to stress, the latter RNA was rapidly cleaved at its 3′UTR and released into the cytoplasm. This nuclear RNA release mechanism may thus control the expression of a variety of proteins whose activity is required rapidly in response to stress or other cellular signals. — PAK

Cell, in press.

CREDITS: LI *ET AL.*, *GEOPHYS. RES. LETT.* **32**, L19702 (2005)

Published by AAAS

This Week

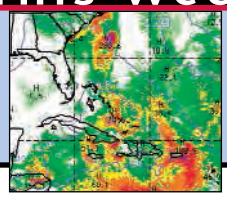

PAGE 420
Forecasts without forecasters

422
Phthalate risks reconsidered

STEM CELLS

Deriving 'Controversy-Free' ES Cells Is Controversial

Two methods that create embryonic stem (ES) cells without destroying viable embryos can work—at least in mice. But although some scientists and ethicists herald the research as a step toward finding an uncontroversial way to produce ES cells, it seems clear that neither method completely resolves the ethical debate.

One method, called altered nuclear transfer (ANT), uses nuclear transfer to create cells that are incapable of forming a normal embryo but can give rise to ES cells. In the second, researchers derive an ES cell line from a single cell taken from an early embryo—while allowing the remaining cells to develop into a live-born mouse. Ethicists and researchers have proffered both ideas in the past as alternative ways to create ES cells, which can become any kind of cell in the body, without destroying an embryo (*Science*, 24 December 2004, p. 2174). Until now, however, the discussions have been largely theoretical.

Developmental biologists Rudolf Jaenisch and Alexander Meissner of the Whitehead Institute at the Massachusetts Institute of Technology wanted to see if they could move ANT theory into practice. As they describe in a paper published online 16 October in *Nature*, they did so by interrupting the function of a gene called *Cdx2* in a donor skin cell and fusing that cell with an oocyte. This created cells that could form a type of early-stage embryo called a blastocyst and give rise to ES cells—but could not implant in a uterus and therefore had no chance of developing into a full organism.

William Hurlbut, a physician and ethicist at Stanford University and a strong proponent of the ANT idea on the President's Council on Bioethics, says that without Cdx2, the cell clusters lack the basic organizational capability that would merit the term "living organism." The lack of Cdx2, he explains, "is not a deficiency but an insufficiency. I think it's pretty reasonable to say [the resulting cells] are not a human."

Jaenisch says that although he and Meissner have no moral objections to research that uses human embryos, they pursued the ANT project to see if there might be a simple way to break the political and ethical impasse. In the United States, federal law prohibits funding for research that harms or destroys human embryos—including human nuclear transfer experiments. "Nuclear transfer is such an important technology, and if we want to do it in the States, we need federal funding. If this serves as a compromise, the modifications are so simple that one could accept them," Jaenisch says.

To others, however, the technique raises more questions than it answers, both ethical and scientific. Turning off *Cdx2* creates a severely disabled embryo but an embryo nonetheless, says Tadeusz Pacholczyk of the National Catholic Bioethics Center in Philadelphia. Stem cell researcher George Daley of Children's Hospital in Boston says the data Jaenisch and Meissner show suggest Pacholczyk has a point. "The embryo that is established in the first few days is substantially normal," he says.

Even so, Pacholczyk is encouraged by the work. "This study doesn't get around the ethical impasse yet. But … it does remind us how the power of science can be used to resolve some very grave moral concerns."

Although Jaenisch says their ANT method is not difficult to perform, it does introduce an additional complication. The technique involves inserting extra DNA into the donor cell genome, which can sometimes interrupt other genes and leave the cell's progeny prone to forming cancerous tumors. Jaenisch says that risk is small and preventable: Researchers can check their donor cells before nuclear transfer to see where the added DNA has integrated. The pair also demonstrated that the DNA that interferes with Cdx2 production can be removed from the resulting stem cells so that any later use of the cell line would not be affected by the blocked gene.

In a second paper also published in *Nature*, Robert Lanza and his colleagues at Advanced Cell Technology (ACT), a biotech company in Worcester, Massachusetts, showed that they can remove a single cell from a very early mouse embryo and grow it into a stem cell line. The technique the scientists used is similar to that used in preimplantation genetic diagnostics, performed at fertility clinics around the world. Scientists remove one or two cells from early embryos to test them for the presence of certain genes, so that an embryo is implanted only if it doesn't carry a genetic disease.

The ACT team showed that for mouse embryos at least, a single cell taken from an eight-cell embryo can grow into ES cell lines when it is cultured with other ES cells. The technique isn't as efficient as obtaining ES cells from later-stage embryos, although Lanza says his team is working on it: The team produced just five ES cell lines from 125 tries, while the usual success rate is about 30%. ▶

U.S. Public Supports Stem Cell Research

Although Senate leaders say their vote on proposals to loosen restrictions on federal stem cell policy may have to wait until next year, it looks as though Americans want change. Two-thirds of Americans approve of expanding use of human embryonic stem (hES) cells in research, saying they either support proposed legislative changes or favor more aggressively promoting this research. Johns Hopkins University's Genetics and Public Policy Center in Baltimore, Maryland, released the poll of 2212 people last week.

BAN 15.9% favor	Prohibit all research to create or study hES cell lines.
CURRENT 21.6% favor	Allow federal funding for research on a small number of hES cell lines created before August 2001.
PROPOSED 19.0% favor	Allow federally funded researchers to study new hES cell lines derived using private funds.
PROMOTE 39.7% favor	Use federal funds to create and study new hES cell lines.
DK/NA 3.8%	Don't know/no answer

CREDIT: CONSTANCE HOLDEN FROM GENETICS AND PUBLIC POLICY DATA

Published by AAAS

426
Are wild birds spreading H5N1?

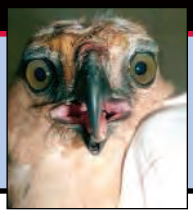

431
Return to the hidden planet

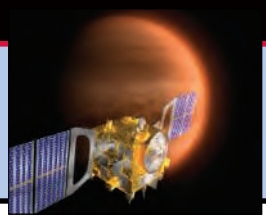

432
Climatic regime change

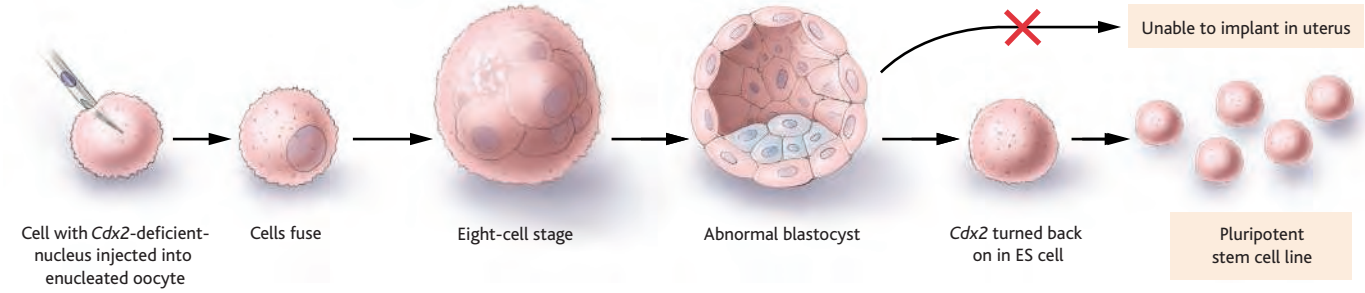

Ethical end run? Altered nuclear transfer produces blastocysts that lack a gene required for early development. The abnormal blastocysts can give rise to ES cells but cannot implant in a uterus.

Lanza and his colleagues showed that the seven-cell embryos had the same chance of survival after implantation into a surrogate mother as undisturbed control embryos had. He believes that fertility clinics could use similar techniques to derive new human ES cell lines under existing regulations and safety guidelines—and might even be eligible for federal funding.

But the ACT method raises issues of its own, says fertility and stem cell research expert John Gearhart of Johns Hopkins University in Baltimore, Maryland, among others. It is not clear whether in mice or in humans the cell taken from the early embryo might itself be able to form a complete organism—a genetic twin of the original embryo—in which case, some argue, the technique would still destroy a potential life. In addition, the biopsy procedure carries "a small but known risk," Gearhart says, not only to the embryo but also to the potential mother, because she might have to go through additional in vitro fertilization cycles if the embryo fails to develop.

Both proponents and critics agree that the ideal solution would be a way to reprogram a skin cell directly to an ES-like cell—without involving any embryolike entities. "That's the Holy Grail," says Lanza. Daley predicts that with increased understanding of the genes that control ES cells, such a method will eventually be possible. "Then you'd have a reasonable technical fix," he says—one that everyone could agree on.

–GRETCHEN VOGEL

AVIAN INFLUENZA

Europe Scrambles to Control Deadly H5N1 Strain

After confirming last week that the deadly H5N1 avian influenza virus circulating in Asia has now killed 1800 turkeys at a farm in Turkey and several ducks in Romania, European officials are bracing for further outbreaks among poultry. "It's a worrying development," says Michael Ryan, director of the Department of Epidemic and Pandemic Alert and Response for the World Health Organization (WHO) in Geneva, Switzerland. With migratory birds suspected of carrying the virus, "we may see further introductions [in other countries] in the coming weeks," he adds. As *Science* went to press, there were reports that an H5 bird flu strain had surfaced in Greece.

Alex Thiermann, a veterinarian at the World Organisation for Animal Health (OIE) in Paris, praises Turkey and Romania for their "early detection, rapid response, transparency, and cooperation with international agencies." Culling flocks quickly in an affected area, which the two countries are doing, is the best way to control local spread of the disease, he says. In Southeast Asia, the disease wasn't recognized until it had already spread widely among poultry.

H5N1, previously concentrated along Asia's Pacific coast, started moving across the continent toward Europe in July. Although the role of wild birds in this spread is still debated (see p. 426), the European Commission is urging farmers near wetlands to minimize the chance of contact between poultry and migratory birds.

So far, the virus has infected 117 people in Asia, mostly from direct contact with infected birds, and has killed 60 of them. H5N1 "is an avian virus and not a pandemic virus," emphasizes Ryan, who adds that its spread to Europe only slightly increases the chance that H5N1 will acquire the ability to pass easily among humans.

To prepare for a possible pandemic, many nations are stockpiling the antiflu drug oseltamivir (Tamiflu), considered the most effective antiviral available. But in the 20 October issue of *Nature*, a team led by Yoshihiro Kawaoka of the University of Tokyo, Japan, and the University of Wisconsin, Madison, reported that an H5N1 strain that infected a Vietnamese girl in February was resistant to oseltamivir. Kawaoka emphasizes that the vast majority of H5N1 strains in circulation are still sensitive to the drug, and

Quick action. Turkey's rapid response in collecting poultry for culling could minimize the inroads of H5N1 in the country.

"there is no point in changing the strategy for an outbreak" among humans. His team does suggest that as a backup, authorities consider stockpiling zanamivir, an antiviral that appears to maintain its effectiveness even against oseltamivir-resistant strains. **–DENNIS NORMILE**

CREDITS (TOP TO BOTTOM): ILLUSTRATION: CHRIS BICKEL/*SCIENCE*; ANATOLIAN/REUTERS

EVOLUTION

New Migration Route Could Lead To New Species of Bird

The cliché "birds of a feather flock together" doesn't hold for European blackcaps that breed in southern Germany and Austria. At one time, these birds migrated back and forth together, spending summers in northern Europe and winters in Portugal, Spain, and North Africa. But in the past 50 years, there's been a split in the avian ranks, with more and more heading northwest for the winter, not south.

On page 502, Stuart Bearhop, an animal ecologist at Queen's University Belfast, U.K., and his colleagues report that even though all the blackcaps gather each year at the same mating sites, they tend to reproduce with those from their particular wintering ground—a phenomenon called assortative mating. Moreover, the birds that stay north are reproducing more than those taking the southern route, which may improve the chances of the birds forming two species.

Gone astray. European blackcaps that moved to new wintering grounds outdo blackcaps taking the traditional route.

CREDIT: TIM LOSEB

Researchers considering how new species develop have speculated that differences in migration patterns could produce assortative mating, but "this is the first empirical demonstration that it actually occurs," says Michael Webster, a behavioral ecologist at Washington State University in Pullman. Moreover, he adds, the blackcap research helps explain how alternative migration patterns can evolve quickly.

Blackcaps were once typically seen in the United Kingdom only during the summer, but over the past 40 years, the number of them wintering in the U.K. has soared, prompting researchers to wonder how the birds' migration patterns were changing. Tracking migratory birds has posed quite a challenge. In 1997, however, researchers began using the ratio of hydrogen isotopes in bird tissue as a tool. Distinctive isotope patterns in rainfall, taken up by migrating birds, provide a signature to reveal where they have traveled.

In 2002 and 2003, Bearhop and Wolfgang Fiedler, an ornithologist at the Max Planck Institute for Ornithology in Radolfzell, Germany, used this technique to determine the winter origins of blackcaps landing in eight mating places in southern Germany and Austria. With these data, Bearhop, Fiedler, and Jason Newton of the Scottish Universities Environmental Research Centre in Glasgow found that blackcaps from the same winter home were 2.5 times more likely to mate with each other than with blackcaps from elsewhere. The findings "strongly indicate that this is assortative mating due to the different wintering areas," notes Darren Irwin, an evolutionary biologist at the University of British Columbia in Vancouver, Canada.

Assortative mating is a matter of timing, Bearhop says. The birds from Britain and Ireland have shorter migrations to their summer mating grounds in Germany and Austria and, prompted by the more dramatic changes in day length at their home locations as winter becomes spring, those more northern migrants leave about 2 weeks earlier than those wintering in Iberia. "Because [these birds] mate with whoever arrives first, they have tended to remain isolated from the later-arriving historical population," say Keith Hobson, an ecologist with the Canadian Wildlife Service in Saskatoon, Canada.

The recent shift in migratory pattern is a boon to the northern blackcaps. These frontrunners grab the prime real estate and seduce early-arriving females. They tend to lay about one more egg per season than the late arrivals from the south, says Bearhop. "[These data] may help explain why there has been such an increase in blackcaps wintering in Britain," Irwin notes.

Still, Hobson and others question whether the north-based birds are becoming a new species. They argue, for example, that there is not yet enough information about the fate of hybrids between the two bird populations. Nonetheless, says Peter Marra of the National Zoological Park in Washington, D.C., "this study provides us with a scenario of how [separate migratory] patterns may evolve and should stimulate some good discussion among students of migration ecology."

–ELIZABETH PENNISI

ScienceScope

South Korea Rolls Out Stem Cell Hub

South Korea, whose scientists last year became the first to produce stem cells from cloned human embryos (*Science*, 13 February 2004, p. 937), is hoping to score more firsts in efforts to turn human embryonic stem (ES) cell research into treatments for disease. This week, Seoul National University was scheduled to announce the creation of a World Stem Cell Hub centered at the school's hospital, spearheaded by cloning pioneer Woo Suk Hwang and funded by the Korean government. Hwang and University of Pittsburgh stem cell researcher Gerald Schatten have collaborated on the plan, which will include facilities in Europe and the United States, as well as a stem cell bank and a program allowing Korean technicians to teach cloning and the cultivation of human ES cell lines.

–CONSTANCE HOLDEN

Station Plans Buoyed

NASA is informally promising its foreign partners that there will be 18 more flights to the still-incomplete international space station, sources at NASA and industry say. The news should assuage many who feared that the agency would leave key components of the station earthbound. Agency officials had considered slashing the number of shuttle flights before it retires the fleet from a planned 24 to as few as 12. The higher number means the European Columbus and the Japanese experiment modules can be orbited, but the Japanese centrifuge and a Russian power module likely will be left behind, along with a host of U.S. research-related equipment. NASA plans to release more details on the station later this month.

–ANDREW LAWLER

Gene Hunters, Heal Ourselves

Currently deciphering genomes of species from macaques to zebra finches, the high-throughput sequencing centers funded by the National Human Genome Research Institute (NHGRI) are shifting toward solving medical problems. The program, whose annual budget is $130 million, will eventually devote half its output to disease gene searches, NHGRI says. Initial targets include seven rare, single-gene disorders and X-linked diseases. Moreover, until 4 November, NHGRI is soliciting more disease gene targets. "We have the possibility in one fell swoop of solving 50 or maybe 100 diseases," says Nelson Freimer, a geneticist at the University of California, Los Angeles.

–ELIZABETH PENNISI

Published by AAAS

PLANETARY SCIENCE

Titan Clouds Hint of Heavy Rains, Methane Gurglings

Astronomers monitoring Titan from Earth and planetary scientists watching it from the passing Cassini spacecraft are reporting some funny business on Saturn's giant moon. Titan's rare clouds pop up in midlatitudes like smoke from a chimney, they say, and then rain out their methane as they blow downwind. But these midlatitude clouds appear over just a few small spots. That suggests that there's something special about the surface beneath them, possibly the presence of erupting methane volcanoes or geysers.

As they report on page 474, planetary scientist Caitlin Griffith of the University of Arizona (UA), Tucson, and her teammates on Cassini's Visual and Infrared Mapping Spectrometer (VIMS) watched the four clouds visible last 15 January as Cassini approached Titan. Within a narrow range of wavelengths in the near-infrared, VIMS could make out small cores to the clouds where plumes rose as fast as 36 kilometers per hour, like a summer afternoon's thunderhead. "They're probably convective, and vigorously so," says Griffith. On reaching altitudes as high as 42 kilometers, some clouds then fell 10 kilometers in an hour as they blew downwind to the east.

To fall that fast, those clouds must have consisted of millimeter-size raindrops of liquid methane, the VIMS team says. Planetary scientist Ralph Lorenz of UA and colleagues showed early this year that Titan's lower atmosphere—loaded with methane but starved of heat energy by the distant sun and enshrouding haze—should produce such rare but intense convection. Methane rain probably reaches the surface from the kinds of clouds they saw, says Griffith. That would help explain the heavily eroded icy terrains seen through Cassini's Huygens probe (*Science*, 21 January, p. 330).

Astronomer Henry Roe of the California Institute of Technology in Pasadena and his colleagues had a far more distant observing perch at the Keck and Gemini observatories on Hawaii's Mauna Kea, but they were able to monitor Titan much longer. On page 477, they report spotting 24 clouds over 82 nights of observing. The abundance of examples enabled them to confirm that Titan clouds outside the south polar region—at least the larger ones they could detect—form almost exclusively near 40°S latitude.

Griffith and her colleagues see the same latitudinal preference. That's because the atmosphere's larger-scale circulation boosts rising plumes there, they say. Theory and modeling by others suggest that the moon's south-flowing near-surface winds rise near 40°S in the current southern-hemisphere summer. That would encourage convection at that latitude, they note.

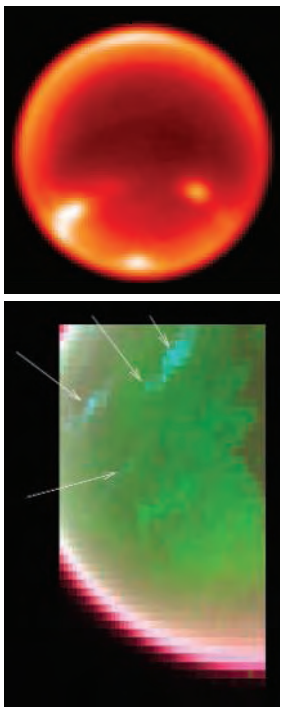

On track. Titan clouds tend to form in a line at mid southern latitudes, perhaps over methane eruptions. They are imaged here in the infrared from Earth (*top*) and by the Cassini spacecraft (*bottom*).

CREDITS (TOP TO BOTTOM): H. G. ROE *ET AL.*, *SCIENCE*; C. A. GRIFFITH *ET AL.*, *SCIENCE*

Roe and colleagues are more intrigued by another geographic preference of Titan's clouds. They found that three-quarters of their clouds appeared in one-quarter of the circumference of the 40°S latitudinal band. The clustering was centered at a longitude of 350°W. The other quarter of the observed clouds fell in a broader band just to the west, and the rest of 40°S had no detectable clouds. Everyone assumes that there's something different about the surface beneath the clouds—on Earth it might be a mountainous obstacle or a sun-warmed coast—that promotes towering plumes of rising air. On Titan, the clouds' longitudinal preference "is pretty much still a mystery," says Griffith.

Roe and his colleagues don't have an answer either, but they have ruled out some possibilities. Over time, the clouds appear in slightly different places within their preferred band, Roe notes, which argues against inevitably stationary mountains as triggers. And 40°S clouds come and go too quickly to be fueled by higher summertime solar heating. That leaves geysering or the volcanic eruption of methane from the icy interior, says Roe. The methane added to the atmosphere could destabilize it and trigger a rising plume, he says. Cassini has found signs of such "cryovolcanism" in icy lava flows and volcanolike edifices (*Science*, 8 April, p. 193) but no definite signs of ongoing activity—at least, not yet.

–RICHARD A. KERR

ScienceScope

Trials Target TB

PARIS—The amount of time required to treat tuberculosis (TB) could be halved if a series of phase II clinical trials of a new drug regimen, announced at a meeting here by Bayer HealthCare and the Global Alliance for TB Drug Development, bear fruit. TB takes more than a million lives annually, and curing it requires patients to take a four-drug cocktail for at least 6 months. Many patients don't complete the regimen, which can trigger antibiotic resistance.

Under the deal, researchers at the Centers for Disease Control and Prevention, Johns Hopkins University, and University College London will test in 2500 patients in eight countries whether replacing one drug in the current cocktail with a new Bayer antibiotic called moxifloxacin can, as mouse studies suggest, reduce treatment time by 2 to 3 months. Bayer will make the drug available cheaply in developing countries if the studies—and subsequent phase III trials—prove the new cocktail's value.

–MARTIN ENSERINK

South Dakota Digs In

One state made a preemptive move this week in the competition to host the proposed $300 million national Deep Underground Science and Engineering Laboratory (DUSEL) (*Science*, 29 July, p. 682). South Dakota announced it has struck a deal to open the upper levels of the abandoned Homestake gold mine in Lead as soon as 2007 as an interim underground laboratory. The National Science Foundation (NSF) is currently deliberating whether to build DUSEL at Homestake or at the Henderson Mine in Empire, Colorado.

South Dakota Governor Mike Rounds, a Republican, says scientists have an "open invitation" to use the space, which at 1500 meters deep would be the second deepest lab in the world. "We're available, and the resources are there," Rounds says. But Henderson bid spokesperson Chang Kee Jung, a physicist at Stony Brook University in New York, called the move "not kosher." He fears that a working lab would hand NSF what amounts to a fait accompli, as well as put the foundation in a tough position if a researcher were to propose work at Homestake before a DUSEL decision is finalized. NSF says it will maintain its standards during the DUSEL process.

–ADRIAN CHO

Published by AAAS

TOXICOLOGY

Panel Finds No Proof That Phthalates Harm Infant Reproductive Systems

An expert panel convened by the U.S. government has thrown cold water on a widely publicized study suggesting that hormonelike chemicals in consumer products are warping the reproductive systems of baby boys. Although animal studies raise concern about infants' exposure to these chemicals, known as phthalates, there is no solid human evidence that they are harming babies, the panel concluded last week after a 2.5-day meeting. "The data are insufficient," the panel's report states.

Vulnerable. Babies undergoing medical procedures may be at risk of effects from hormonelike chemicals called phthalates.

The phthalate review, organized by the National Toxicology Program (NTP), puts the burden of proof back on those who attribute harm to these so-called endocrine disrupters, humanmade chemicals that can act like hormones. Phthalates are found in everything from nail polish to plastic PVC plumbing. In studies with rats, high doses of phthalates act as antiandrogens, blocking the effects of testosterone, and can cause problems such as undescended testicles in male pups exposed in the womb. These findings led a 2000 NTP panel to express "concern" about possible exposures to the most common phthalate, DEHP, in healthy infants and "serious concern" about potential effects on very sick infants, who can be exposed to relatively high levels leaking from medical tubing and blood-storage bags. Such worries have already led Europe to ban certain phthalates from cosmetics and baby toys, and some companies are voluntarily removing DEHP from medical products.

In May, an explosive report seemed to confirm these fears, providing evidence that phthalates were subtly affecting sexual development in infants. In the online *Environmental Health Perspectives*, epidemiologist Shanna Swan of the University of Rochester, New York, and colleagues reported that in a study of 85 boy babies, those whose mothers were exposed during pregnancy to higher levels of four phthalate metabolites echoed a pattern seen in phthalate-exposed rat pups: The boys overall had a shorter anogenital distance (AGD)—the space between the anus and genitalia—and were more likely to have smaller genitals and partially descended testicles. Swan also found a less-than-significant association between shorter AGD and two DEHP metabolites. The Swan study made a huge splash in the press, most recently on the front page of the *Wall Street Journal*.

But the panel, 11 scientists charged to look at a wave of new research on reproductive risks of DEHP, found Swan's results inconclusive. Pointing to the lack of a significant association with DEHP metabolities, it notes that Swan's AGD measure is a "novel index" whose relevance in humans "has not been established." Two toxicologists on the panel questioned Swan's data on other phthalates as well. One of the strongest associations with AGD shortening was found with a compound that doesn't cause comparable effects in animals, says Kim Boekelheide of Brown University in Providence, Rhode Island. "It makes everybody scratch their head" and wonder, "Is this just noise?" adds Robert Chapin of Pfizer.

The NTP panel also found that the small number of subjects and possible confounding factors limited the usefulness of several other new human studies, including one linking higher phthalate exposure and lower testosterone levels in infant boys. The panel's conclusion: There is "insufficient evidence in humans" that DEHP exposure during pregnancy, childhood, or adulthood is causing harm. Swan says she's not surprised that the panel dismissed her report because its focus was DEHP, and her data finding an effect for that particular phthalate were only "suggestive." She defends her results for other phthalates, saying humans may respond differently than rats do to some of these chemicals.

The NTP panel did feel that Swan's study broke new ground: It recommends repeating the work with a larger sample size. Swan says she's in the middle of that. Boekelheide says others too will be looking at AGD, which he calls an "exciting" potential measure of endocrine effects in babies. "It's the kind of study we need to have more of," he says.

—JOCELYN KAISER

NATIONAL INSTITUTES OF HEALTH

NIH Aims to Create 'Homes' for Clinical Science

Elias Zerhouni's mantra since taking the helm of the National Institutes of Health (NIH) 3 years ago has been "translational research"—meaning he wants to find better ways to move basic discoveries into the clinic. Last week, Zerhouni unveiled perhaps his most radical proposal yet for achieving that goal. As he explained in a commentary in the 13 October *New England Journal of Medicine*, NIH plans to create academic "homes" for clinical and translational science over the next 7 years and establish "a new … academic discipline."

Research institutions are reacting with both excitement and anxiety. "It's really long overdue," says William Crowley, director of clinical research at Harvard's Massachusetts General Hospital in Boston. One worry, however, is that by mandating such medically oriented homes, NIH will force institutions to wall off clinical researchers instead of bringing them together with basic scientists. "The danger is separatism. Most people believe clinical and translational research should be part of the fabric of the whole institution," says Howard Dickler, director of the research division of the Association of American Medical Colleges.

NIH says inclusion is the goal of the new plan, part of Zerhouni's Roadmap, initiatives that pool money from all 27 NIH institutes and centers for common projects. The problem it addresses, notes Crowley, is that there are too few new clinical scientists in ▶

Architect. Elias Zerhouni wants academic institutions to build centers that combine basic science, clinical research, and training.

CREDITS (TOP TO BOTTOM): STEWART COHEN/GETTY IMAGES; NATIONAL INSTITUTES OF HEALTH

Published by AAAS

academia; many find research less appealing than other careers. The genomics explosion and rise in chronic disease, Zerhouni adds, require individualized treatments that move from bench to bedside "in a much more facile way."

NIH's solution is to restructure the 74 institutions that now have NIH-funded General Clinical Research Centers (GCRCs), units with beds for clinical research. Each institution will have to merge its GCRC, clinical research training, and resources such as biostatisticians, regulatory staff, and safety review boards into a new, more efficient "home." The homes will incorporate other translational research, such as animal testing and designing clinical trials. The final entity—a center, department, or institute—will award graduate and postgraduate degrees in clinical research and related disciplines. And the director must have some authority for hiring and promoting faculty, which NIH hopes will make clinical research a more attractive career path.

In 2006, NIH will spend $30 million on four to seven of these Clinical and Translational Science Awards (CTSAs),* which will supplant the recipient's GCRC. Another $11.5 million will go for planning grants up to 50 other institutions. All institutions with GCRCs will have to compete for a CTSA by 2012, when funding will total $500 million. About 60 CTSAs will be funded, fewer than the current 78 GCRCs.

At least one school, the University of Texas Southwestern Medical Center in Dallas, has already created a department of clinical research. Others are wary. It's "a huge deal" to set up a department, says Judith Swain of the University of California, San Diego (UCSD), and "it just silos clinical research." Instead, UCSD wants to keep clinical scientists in their present departments but give them joint appointments in the clinical home. Some institutions, such as the University of Kentucky (UK) in Lexington, are also putting clinical and basic scientists in groups focused on a disease process or problem, such as atherosclerosis. "It forces people to think differently," says UK research dean William Balke.

Although the program will be "flexible," says National Center for Research Resources acting director Barbara Alving, medical school leaders aren't yet clear on how to meet NIH's requirements. Many are also nervous about where the funds will come from at a time when NIH's budget is likely to be flat at best. NIH says it will not cut individual investigator-initiated grants to fund the CTSAs but will draw on Roadmap funds and existing clinical and translational programs. As always, says Dickler, "the devil is in the details." —JOCELYN KAISER

* www.ncrr.nih.gov/clinicaldiscipline.asp

U.S. ECONOMY

Panel Calls for More Science Funding to Preserve U.S. Prestige

Last week, a National Academies panel delivered a dire warning to Congress: Give science an extra $10 billion annually, or watch jobs and national status disappear to Asia. Many people may agree with the message, but details of the panel's ambitious prescriptions are already drawing criticism.

Tasked by Congress in May to assess U.S. technical competitiveness and offer recommendations to sustain or improve it, the 20-person panel included Nobel laureates and high-tech CEOs. Its report* found that U.S. scientific dominance is eroding. The worrisome indicators include a rapidly expanding Asian technical base, subpar U.S. precollege science and math education, and a U.S. shift away from fundamental research. "[A] frog that is heated slowly until it boils won't respond until it is too late," the committee explained in its report, *Rising Above the Gathering Storm*.

Lesson plan. An academies' report calls for funding more science teachers and extra money for physical sciences.

The group proposed new $20,000 college scholarships for students who commit to teaching science in public high schools and recommended expanding programs for graduate students in needed fields, including a quadrupling of current federal early-career awards. It further called for an eventual doubling of the $8 billion the United States currently spends on basic research in the physical sciences each year. And to encourage industrial research, the group proposed reforming the patent system, expanding visa programs for foreign scientists, and making permanent an expanded R&D tax credit. "We cannot afford not to [invest]," says panel chair and former Lockheed Martin CEO Norman Augustine.

The panel's sweeping recommendations may face a tough reception. The congressional Government Accountability Office reported last week that little is known about the effectiveness of current federal scholarship programs totaling $2.8 billion. And some science education experts worry that the higher education recommendations could create a glut of scientists. "There hasn't been a huge increase in the amount of biomedical scientists as the NIH [National Institutes of Health] budget has doubled," notes demographer Michael Teitelbaum of the Alfred P. Sloan Foundation in New York City.

Massive new federal investment in basic research would, counters retired Merck chair and panel member Roy Vagelos, "invent new industries." Those emerging fields, in turn, will create a "continuing wave of new jobs," says Association of American Universities president Nils Hasselmo. While acknowledging that the U.S. government spends more on R&D than the rest of the G7 industrialized nations combined, the report says that federal funding for the physical sciences has been flat in 2005 dollars since the 1970s. It calls for a new "small, agile" research agency within the Department of Energy akin to the Defense Advanced Research Projects Agency.

House Science Committee staff director David Goldston says that proposal ignores the fact that promising energy technologies are currently available but underutilized. "There might be much more of a deployment problem than an R&D problem," he says. Others question the broader call for a federal research boost. "We need a more precise policy than simply spending more money," says science policy specialist David Guston of Arizona State University in Tempe.

Panelists acknowledge that high-level groups have made sweeping calls like this before, with little effect. Given that science budgets are expected to stay flat or face small cuts in 2006, Guston and other policy watchers say they are skeptical that the report's call for billions in new funding will fly. Still, Senator Lamar Alexander (R–TN), who had called for the panel, says its proposals could garner support from many lawmakers who are concerned about U.S. jobs, especially if the White House endorses the report. "Now it needs the imprimatur of the president," he says. A White House spokesperson says the president welcomes the new report. —ELI KINTISCH

* books.nap.edu/catalog/11463.html

Published by AAAS

U.S. ASTRONOMY

You Make the Call, NASA Chief Tells Scientists

Faced with problems fixing the space shuttle, finishing the international space station, and winning support for an ambitious exploration effort, NASA Administrator Michael Griffin told researchers last week that he was "fed up" with conflicting advice from the science community. Instead of expecting more funds, Griffin explained to the federal Astronomy and Astrophysics Advisory Committee, researchers need to make tough choices about how to spend what money is available.

The NASA chief's blunt talk comes as he and the White House negotiate the agency's 2007 budget request, which will be released in February. Science accounts for nearly a third of NASA's $16 billion budget, which is unlikely to increase faster than inflation in coming years—and neither is science's share of it, Administration officials say. "The good news is that the NASA administrator is going to give us our fair share," says Lennard Fisk, a solar physicist at the University of Michigan, Ann Arbor, and chair of the National Academies' Space Studies Board. "The bad news is that … we can't execute the programs we have with the money available."

The community's intense—and successful—lobbying to repair the Hubble Space Telescope is a good example of how a sound scientific argument can conflict with a limited budget, Griffin told the advisory panel, which was formed 2 years ago to coordinate space and ground-based astronomy funded by NASA, the National Science Foundation, and the Department of Energy. "The astronomy community did this to itself," he said. Unless the James Webb Space Telescope—currently $1.5 billion over budget—is scaled back, he warned, "I just don't see how to pay for other missions."

Researchers say they are willing to make those choices, but they note that NASA has disbanded its own advisory council. The agency has not sought advice yet from the academy panel on how to manage its fiscal crisis and avoid a civil war among disciplines fighting for limited resources.

Tough talk. Michael Griffin wants scientists to figure out how best to spend NASA's shrinking science budget.

"How to give the advice is not clear," says Fisk. He notes that the NASA panel has been in limbo since Griffin arrived in March. The administrator is expected to make sweeping changes to the council's membership, including replacing chair Charles Kennel, an earth scientist and head of Scripps Institution of Oceanography in San Diego, California. Fisk adds that the academies' board is willing to lend a hand on setting scientific priorities if NASA asks.

Griffin reiterated his intention not to divert science funding to other areas within his agency, and his direct approach resonated with some federal advisory panel members. "Mike does listen to people," says chair Garth Illingworth, an astronomer at the University of California, Santa Cruz, adding that he was reassured by Griffin's invitation to astronomers to step up to the plate. "If the previous administrator had involved the community in the decision" to cut the planned Hubble mission, he notes, the astronomy community could have evaluated its choices more carefully before deciding to lobby legislators to save Hubble.

"We're all dealing with the collateral damage from inappropriate methods of thinking," said Griffin. On that point, adds Illingworth, "I couldn't agree more."

–CAROLYN GRAMLING AND ANDREW LAWLER

SCIENTIFIC PUBLISHING

Retracted Papers Spur Million-Dollar Lawsuit

One of the authors of two plant biology papers that were retracted last year is suing the senior author who withdrew the papers. She is alleging that her former lab chief threatened to ruin her career and then did so with the retractions.

In notices published almost a year ago, Daniel Klessig of the Boyce Thompson Institute (BTI) for Plant Research in Ithaca, New York, and several colleagues said they were retracting two papers, which described a new plant enzyme and had appeared in *Cell* and the *Proceedings of the National Academy of Sciences* (*PNAS*), because they had been unable to reproduce certain results. The retraction notices, however, were not approved or signed by the first author on both papers, Meena Chandok (*Science*, 5 November 2004, p. 960).

Chandok has now launched a legal counterattack. In late August, she filed a civil lawsuit in a U.S. district court in Syracuse, New York, seeking more than $1 million in punitive and compensatory damages from Klessig. (BTI, *Cell*, and *PNAS* were not named as co-defendants.) The lawsuit, which was first reported by *The Scientist*, states that Klessig had falsely leveled misconduct charges—including that Chandok fabricated data in the papers—and that a BTI investigation did not validate those allegations. In a 14 July memo to Klessig and Chandok, provided to *Science* by Chandok's lawyer, BTI president David Stern confirms that an investigation had not substantiated the charges but adds: "There are numerous disputes on factual issues and divergent viewpoints that I cannot or will not attempt to resolve or reconcile."

Among other claims in her lawsuit, Chandok alleges that after she resigned from the lab in March 2004, Klessig threatened to press misconduct charges and withhold support for her visa-extension application if she didn't help him with further research on the enzyme. "As a result of the false allegations, Dr. Chandok's reputation has been damaged in the scientific community," the suit states.

Klessig denies Chandok's charges. He told *Science*: "Because we were unable both to reproduce the critical data … and to verify certain biological reagents used in the original publication, I was ethically compelled to retract the papers." No trial date has yet been set.

–JOHN TRAVIS

CREDIT: CRAIG BAILEY/AP PHOTO

Published by AAAS

As H5N1 reaches Europe, scientists debate the role of wild birds but agree on the need for greater surveillance

Are Wild Birds to Blame?

Almost as soon as H5N1 avian influenza began its deadly sweep across Asia, people fingered migratory birds as likely culprits in its spread. Migrating birds offer an obvious way to connect the dots of H5N1 outbreaks along the east coast of Asia and, in just the past few months, its unexpected cross-continent jump to Siberia, Kazakhstan, and Turkey. Moreover, researchers have long known that these birds commonly harbor less virulent flu viruses, and many wild birds mingle with Asia's free-ranging domestic poultry, which have been decimated by H5N1.

But avian experts have been almost universally skeptical that wild birds are spreading the virus. One reason is that sampling of tens of thousands of birds has failed to turn up a single healthy wild bird carrying the pathogenic strain of H5N1, which has caused the death of more than 100 million domestic birds—and at least 60 humans—in Asia. Evidence so far suggests that H5N1 kills wild ducks and geese nearly as efficiently as it does chickens. "Dead ducks don't fly" has been the refrain, as avian experts point out that sick and dying birds simply can't spread viruses very far. Instead, epidemiologists investigating the virus's jump, even to geographically far-flung regions, keep turning up evidence suggesting that the poultry trade and other human activities are responsible.

Now, however, evidence implicating wild birds is starting to convince even some of the doubters. "Until about 2 months ago, I was pretty skeptical on whether wild birds were playing a role," says David Suarez, a virologist with the U.S. Department of Agriculture's (USDA's) Southeast Poultry Research Laboratory in Athens, Georgia. "But now I feel that there is much stronger evidence that wild birds are spreading the virus." What changed his mind, he says, was the death of 100 or so ducks, gulls, geese, and swans from H5N1 at a remote lake in Mongolia that he believes can't be explained by human activities. And, he and others add, in an unexpected twist, it's beginning to look as though the culprits might not be the long-suspected migratory waterfowl but another yet-unidentified wild species.

The implications are huge. If wild birds are carrying the disease, says Suarez, "it will be difficult or impossible to control the spread from country to country." Nailing down the answer became even more urgent last week with the confirmation that H5N1 has now entered Europe.

Even before that confirmation, the Netherlands ordered farms along migratory routes to keep poultry inside, and three German states asked farmers to voluntarily take similar precautions. Last month, the European Commission rejected proposals to extend such measures throughout the union, but E.U. officials were reassessing their stance with the news that H5N1 has reached Turkey (see p. 417). Everyone recognizes that if wild birds are involved, new strategies will be needed to halt the virus's spread to domestic flocks—and from them to people. A growing number of scientists and organizations are calling for dramatically increased global surveillance to profile all viruses circulating in wild birds. Says Kennedy Shortridge, a virologist and professor emeritus at the University of Hong Kong, "H5N1 is important, but we still need to be on the lookout for other flu viruses." The costs of surveillance are small, he says, considering the damage that could be done to the poultry industry—or, worse, the potential for a human pandemic.

Heads up. Researchers worry that bar-headed geese might carry the H5N1 virus from the sites of outbreaks in northern China and Mongolia to India and Bangladesh.

From low to high

One reason migratory waterfowl were high on the list of suspects for spreading H5N1 is because they are natural hosts for other bird flu viruses. But Ilaria Capua, a virologist at Italy's National Reference Laboratory for Avian Influenza in Padua, warns that Anatidae, the family that includes ducks and geese, are as genetically distant from gallinaceous birds (chickens, turkeys, and quail) as cats are from dogs. The different families interact with viruses very differently, she says.

Viruses are subtyped by the forms of two of their surface glycoproteins, hemagglutinin (H) and neuraminidase (N). There are 16 forms of hemagglutinin and nine of neuraminidase. Viruses are further classified as being of low or high pathogenicity. Low-pathogenicity viruses are typically carried in a bird's intestinal and respiratory tracts and usually cause mild or no symptoms. Highly pathogenic viruses can infect cells throughout a bird's body and cause systemic disease and, usually, death.

Waterfowl have been shown to carry low-pathogenicity viruses of virtually all possible combinations of H and N, including low-pathogenicity versions of H5N1. So far, however, there is no known natural reservoir for

CREDITS (TOP TO BOTTOM): WILLIAM B. KARESH/WILDLIFE CONSERVATION SOCIETY

Published by AAAS

highly pathogenic avian influenza viruses. They emerge only after low-pathogenicity viruses jump from water birds into chickens and turkeys. As the virus attempts to adapt to a new host, it somehow acquires the ability to infect cells throughout the bird's entire body. This mutation from low to high pathogenicity, with a resulting bird flu epidemic among poultry, has occurred at least 19 times since 1959. In some cases, researchers have traced the virus from its low-pathogenicity form in water birds to a low-pathogenicity virus that circulated in poultry before becoming highly pathogenic.

No one has yet uncovered the lineage of the highly pathogenic H5N1 strain now endemic in Asia. Presumably, it evolved from a low-pathogenicity H5N1 variant circulating in waterfowl in southern China before the first known outbreak of the disease in chickens in Hong Kong in 1997. By culling all 1.5 million domestic poultry in Hong Kong, authorities stamped out the outbreak. With a few exceptions, the virus was not seen again until December 2003, when a massive outbreak swept chicken farms in Korea. By January, the virus had turned up on farms in Japan and Vietnam; by February it was detected in Indonesia, and it was soon killing chickens in Thailand and China.

When public health experts pointed to migratory birds as a likely source, ornithologists and animal epidemiologists showed that the outbreaks did not neatly fit any known migratory patterns. If migratory birds were carriers, they argued, the virus should have turned up in the Philippines and Taiwan by now, but it hasn't. What's more, since the late 1990s, USDA has sampled more than 10,000 waterfowl crossing the Bering Sea from Asia to Alaska, while University of Hong Kong researchers have tested several thousand entering Hong Kong; neither group has found a single healthy bird carrying the H5N1 virus.

Instead, human movements of infected poultry have spread the virus over seemingly improbable distances. For instance, an outbreak of H5N1 among poultry in Lhasa, Tibet, in January 2004 was traced to a shipment of chickens from Lanzhou in China's Gansu Province, about 1500 kilometers away. An even more bizarre case surfaced in October 2004, when an air traveler was caught at Brussels Airport with two crested hawk eagles, infected with H5N1, in his carry-on bag. The smuggler had bought them at a Bangkok bird market on behalf of a Belgian falconer.

A new paradigm

As the epidemic continues, it's becoming increasingly clear that H5N1 represents a "change in the paradigm" of what is known about avian influenza viruses, says Les Sims, a veterinarian in Manunda, Australia. Before this strain of H5N1 appeared, for instance, waterfowl were thought to be resistant to infection by highly pathogenic viruses. Studies over the last several years have shown that domestic ducks can asymptomatically carry some strains of H5N1 that are lethal to chickens. (Yet other H5N1 strains are lethal to domestic ducks.)

Until last spring, however, there was no sign that H5N1 was infecting any wild birds in a significant way. That changed in April, when an H5N1 outbreak at Lake Qinghai in northwestern China killed an estimated 5000 to 6000 migratory water birds.

The die-off immediately raised alarms that surviving birds might carry the virus to India and beyond. But, apparently because of infighting between Chinese ministries and institutions, the government barred Chinese and outside scientists from sampling or tracking the travel of surviving birds. "It was a missed opportunity," says ornithologist David Melville from Nelson, New Zealand.

Stowaways. These crested hawk eagles, infected with H5N1, were smuggled from Bangkok to Brussels in an air traveler's carry-on bag.

Researchers are still wondering how the virus got to this remote corner of China. Just after the Lake Qinghai outbreak, the virus turned up on a poultry farm in the same province. This "makes it difficult to tell whether poultry or wild birds brought the virus to the area," says Suarez.

An August outbreak at Erkhel Lake in Mongolia, however, helped persuade Sims that wild birds are to blame, but his change of mind comes not from finding a positive link but from ruling out human movements of poultry, he warns. "All epidemiology is based on probabilities," he adds.

A group of veterinarians from the Wildlife Conservation Society was already in Mongolia in case H5N1 made the 600-kilometer leap when it heard of unusual bird deaths at Erkhel Lake. The group collected 774 samples from both dead and living birds. USDA confirmed highly pathogenic H5N1 in dead birds—but found no evidence of the virus in any samples from the live ducks, gulls, geese, or swans.

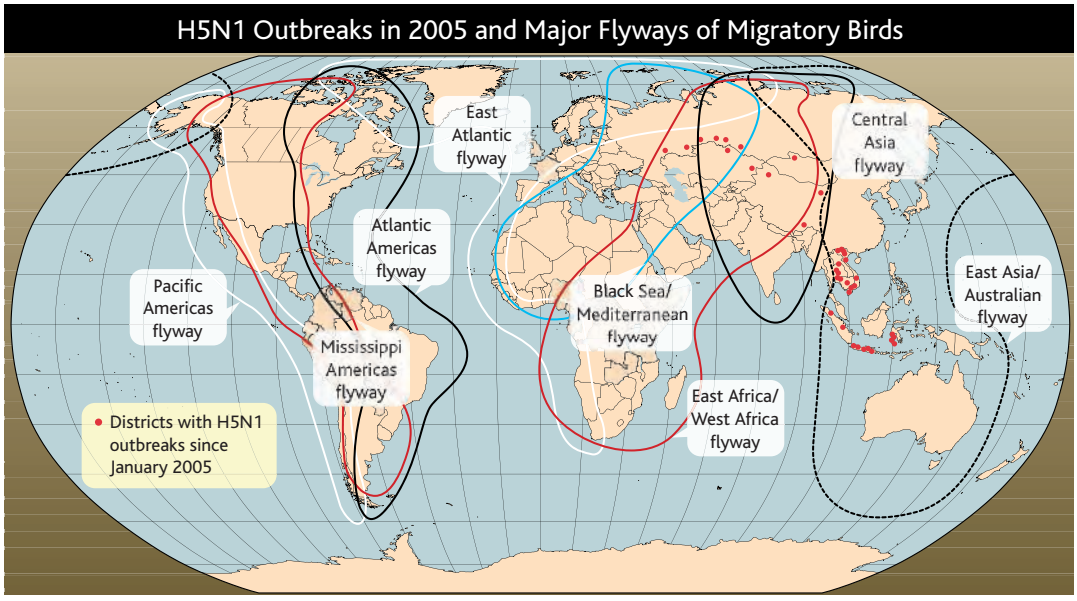

On the fly. Flyways might seem to connect the dots of H5N1 outbreaks, but the timings and locations aren't a perfect fit with known migratory patterns.

CREDITS (TOP TO BOTTOM): S. VAN BORM *ET AL.*, *EMERGING INFECTIOUS DISEASES* **11** (MAY 2005); AI OUTBREAKS: OIE, FAO, AND GOVERNMENT SOURCES; FLYWAYS: WETLANDS INTERNATIONAL

Keeping Track of Viral Air Traffic

BERKENWOUDE, THE NETHERLANDS—Catching wild ducks, an art that requires skill as well as patience, has a long tradition in this water-rich country. But these days, Dutch duck trappers are helping address a 21st century challenge by taking stock of the dizzying variety of bird flu strains flying overhead—and perhaps providing early warning should the fatal H5N1 strain arrive. At Erasmus Medical Center in Rotterdam, virologist Vincent Munster runs one of the largest surveillance programs for avian influenza in the world, and he relies on dozens of people who catch birds, either for a living or as a hobby, to send him more than 8000 samples a year.

Bert Pellegrom, a forester whose hobby is keeping a 200-year-old duck trap operational, is one of them. At his trap—really a small lake, surrounded by reed screens to hide the trapper from the birds and equipped with elaborate netting structures—Pellegrom catches ducks several times a week, which he kills and sells to the local poulterer. (They fetch about $4 a bird.) On a sunny afternoon last week, conditions weren't favorable—too warm and not enough wind—but Pellegrom caught two mallards. "This may look a bit unpleasant," he cautioned, before wringing their necks. Then he got some sterile cotton swabs from a shed, inserted one in each of the ducks' cloacas, and turned it around once before pulling it out and storing it in a small plastic bag.

Helping hands. Bert Pellegrom (*right*) is one of many people collecting samples for the avian influenza surveillance program run by Vincent Munster.

Between 1% and 20% of all ducks, depending on the species and season, are infected with an influenza strain, usually without symptoms, Munster says. Back at the lab, he and his colleagues culture viruses from the samples, determine the strain, sequence the signature hemagglutinin gene, and check whether they have low or high pathogenicity. Although duck trappers like Pellegrom supply some of the samples, the majority come from ornithologists—in the Netherlands, Sweden, and far-flung places such as Japan, Canada, and South America—who ring wild birds for migration studies and release them. Together, the samples cover hundreds of different bird species, mostly ducks, geese, gulls, and shorebirds. Bit by bit, the Rotterdam group, led by Ron Fouchier, is assembling a detailed picture of which viral strains are out there, which bird species each strain prefers to infect, and how patterns change with the seasons.

When the program started 5 years ago, it was a leisurely academic endeavor, and the researchers analyzed the samples only after the end of each migration season. But after H5N1 started its path of devastation from China to Turkey, the group realized that it offered a possible early warning system as well. Two months ago, they started collecting samples weekly and screening them as soon as they come in. If highly pathogenic H5N1 makes it to northern Europe, Munster hopes he will be the first to know. The group has applied for European Union funds to expand the network across Europe.

Munster rarely goes on field trips himself. But when he accompanied a reporter to Pellegrom's trap, his study produced an unexpected benefit: Rather than selling them, Pellegrom offered the two birds to Munster, who, for the first time in his life, got to carve up, roast, and eat his research subjects at home. **–MARTIN ENSERINK**

Because there are so few poultry in this isolated region, Suarez thinks their involvement is "unlikely." "The most likely scenario," he says, is that wild birds carried the virus to Erkhel Lake and infected the birds that eventually died. "We don't know which species were responsible for spreading the virus," says Sims, who is also involved in the project, although he suspects that those unidentified species could be spreading the virus elsewhere. (The researchers declined to provide further details because they are readying an article for publication.) Figuring out which species might be involved will be tough, others note, as next to nothing is known about avian influenza except in waterfowl.

Searching

Some answers may come from Fu-Min Lei, an ornithologist at the Institute of Zoology in Beijing, part of the Chinese Academy of Sciences (CAS). Since last March, he has collected more than 6000 viral and serological samples from a variety of wild animals throughout China, including 2000 samples from migratory and resident birds, and is searching for H5N1.

Another Chinese team led by George Gao, a virologist at CAS's Institute of Microbiology in Beijing, has collected several dozen serum samples from birds that survived the H5N1 outbreak at Qinghai Lake. If any test positive for antibodies to the H5N1 virus, says Gao, who is preparing to publish a paper, it would suggest that some mildly infected water birds might be carrying the virus long distances.

Even before the virus turned up in Turkey, the incidents at Qinghai and Erkhel and the spread of the H5N1 virus through Siberia and Kazakhstan had sparked new surveillance efforts. In Europe, Albert Osterhaus, a virologist at Erasmus University in Rotterdam, the Netherlands, has proposed a Europe-wide wild bird surveillance program. His group currently gathers cloacal samples from 6000 birds annually, primarily in the Netherlands (see sidebar). Extending such surveillance to critical migratory routes crossing Europe, which he estimates would cost about $2.5 million, would not only serve as an early warning system for a possible pandemic, he says, but also provide data on other viruses that pose a threat to domestic flocks. Osterhaus would like to see similar networks set up to cover flyways in Asia-Pacific and the Americas.

Other nations have not recognized the need, so surveillance is patchy, except in Asia, which has an aggressive program of sampling wild birds and birds brought to live poultry markets.

The United Nations Food and Agriculture Organization (FAO) is helping nascent surveillance efforts in South Asia, and the World Organisation for Animal Health recently sent an expert mission to support surveillance in Russia. "We're very concerned about India and Bangladesh," says FAO's Juan Lubroth, because the bar-headed geese that breed at China's Qinghai Lake winter in South Asia. But Lubroth notes that wild bird surveillance is just one on a long list of veterinary needs that includes strengthening local lab capabilities and improving hygiene on farms and in markets. All these measures are desirable no matter how H5N1 is being spread, he says. FAO has appealed to the international community for $100 million to fight avian influenza in Asia but has so far only raised $30 million—a small sum, Lubroth says, for trying to avert a human pandemic.

–DENNIS NORMILE

CREDIT: M. ENSERINK/*SCIENCE*

Preaching Against the Pandemic

He's a retired American living in the French countryside. So what makes David Fedson one of the most vocal advocates for pandemic preparedness?

Sergy Haut, France—On a clear day, you can see Mont Blanc, Europe's highest mountain, from David Fedson's study. His 320-year-old home, tastefully restored and decorated, is a haven of tranquility in a small French village.

But the relaxed atmosphere is deceptive. Working from his home, Fedson, 67, a former academic and pharma executive, is on a tireless crusade to help ready the world for what he believes could be a global catastrophe: the next influenza pandemic. After a career spent studying adult vaccination, he's convinced that only billions of flu shots, deployed worldwide soon after a pandemic strikes, could avert global mayhem. And the world still isn't moving fast enough to make that possible, he says.

To change that, Fedson is constantly writing papers, talking to scientists, and lobbying policymakers. Colleagues say he's an influential voice in the debate on pandemic preparedness. From 1996 until his retirement in 2002, Fedson was director of medical affairs at Aventis Pasteur MSD (now Sanofi Pasteur MSD) in Lyon. Even then, he was known to speak his mind. Sanofi Pasteur, the world's biggest flu vaccine producer, pays Fedson's expenses to speak about the pandemic danger, but he has no formal ties to this or any other company or organization, which allows him to speak freely, says Harvard epidemiologist Marc Lipsitch: "I'm kind of a fan."

Fedson frequently tries to cajole reporters into covering the subject he worries about. In an e-mail to a *New York Times* reporter last year, he praised a particular story but said that overall, the paper had "barely scratched the surface," adding, "You have work to do."

Fedson studied medicine at Yale and worked at the University of Chicago before joining the University of Virginia School of Medicine in Charlottesville in 1982, where he became an expert in the clinical effectiveness, cost-effectiveness, and distribution of flu and pneumococcal vaccines. He was a member of the Advisory Committee on Immunization Practices and the National Vaccine Advisory Committee; at Aventis, he founded the Influenza Vaccine Supply International Task Force, an industry group working to prepare for pandemic vaccination. After retiring, he set up a study group to monitor the use of flu vaccines around the world.

Fedson's ideas about pandemic vaccines are based on simple arithmetic. In a pandemic, antiviral drugs like Tamiflu can't be more than a stopgap; only vaccines offer long-term protection. As for supply, for the next 5 years at least, the world is stuck with the nine major flu vaccine companies, which produce just 300 million doses annually using chicken eggs, a process that's difficult to scale up quickly. They could all switch to making pandemic vaccine in an emergency—but they would need to produce billions of doses instead of 300 million.

The only way to increase supply dramatically, Fedson says, is to produce vaccines that use far less antigen, or viral proteins, per dose. For the annual influenza vaccine, which protects against three different strains, manufacturers use 45 micrograms of antigen, 15 for each strain. To vaccinate 3 billion people during a pandemic—and assuming everyone will need two shots—the amount of antigen per shot would have to come down 20-fold, to about 2 micrograms. Studies have suggested that such small doses may be effective when coupled with a so-called adjuvant, such as alum, to rev up the immune system.

Work to do. David Fedson says the world needs a global plan to develop, produce, and distribute pandemic vaccines.

Trials using such vaccines have been slow to start. Adjuvants aren't needed in annual flu vaccines, and they create regulatory worries about side effects. For these reasons, the first pandemiclike H5N1 vaccine that the United States tested in humans did not contain an adjuvant. The vaccine triggered reasonable levels of antibodies, but only when two doses of 90 micrograms were given (*Science*, 12 August, p. 996). Rather than stretch global capacity, this approach would dramatically shrink it, says Fedson. Additional trials with dose-sparing strategies, including alum, are now planned in the United States. Still, says Fedson, "they wasted a year. That's unforgivable."

In Europe, adjuvants are widely accepted, but public funding has lagged. Sanofi Pasteur will soon complete one small study, and several more are planned. But in most studies, the lowest dose tested will be 7.5 micrograms of antigen. That's still too high, says Fedson, who recommends testing doses as low as 1.875 micrograms. The hesitation is "absurd," he says: "We know what needs to be done, but it's not being done."

Other hurdles need to be tackled urgently, he adds. To speed new vaccines to the market, Fedson calls for a global licensing protocol, rather than the current patchwork of national regulations. Governments should also shield companies from liability, he argues, because when large numbers of people take a vaccine, some will come down with health problems.

As an alternative strategy, Fedson has urged researchers to study patient databases to see whether statins, cholesterol-lowering drugs that also fight inflammation, might prevent the most severe complications from influenza. If so, he says, generic statins could offer poor countries a cheap alternative to Tamiflu. Two groups recently found encouraging data (*Science*, 23 September, p. 1976), and top flu teams in the United States have promised to test the idea in H5N1-infected mice and ferrets.

Coordinating a truly global plan for pandemic vaccine development, production, and distribution requires exceptional leadership, which Fedson says the underfunded World Health Organization in nearby Geneva can't provide. He advocates the creation of a new organization like the Global Fund to Fight AIDS, Tuberculosis, and Malaria, led by someone like the blunt and hard-driving General Leslie R. Groves, who built the Pentagon and went on to lead the Manhattan Project.

Meanwhile, Fedson has plenty of advice to give. He hands the reporter a letter urging the World Economic Forum to put the pandemic threat on the agenda of its annual elite gathering in Davos, Switzerland. (They should enlist people such as Bill Clinton, he suggests.) He produces a paper arguing for statin research and another about pandemic vaccine development. More will come by e-mail, he promises. Like General Groves, Fedson knows what needs to be done. **–MARTIN ENSERINK**

CREDIT: M. ENSERINK/*SCIENCE*

Published by AAAS

European Probe Returns to Our Neglected Neighbor

Venus may lack the appeal of Mars, with the possibility of life, but it has much to teach us. Venus Express is going to find out what is happening beneath the clouds

Over the past 15 years, 12 spacecraft have been launched toward Mars. In the same period, none went to Venus—even though Venus is larger, closer, and more mysterious than the Red Planet. Now the European Space Agency (ESA) is about to take a step toward evening things up. ESA's Venus Express spacecraft, scheduled for launch later this month and due to reach its destination next spring, may finally unveil some of the haze-enshrouded planet's many secrets. "In several important areas, such as atmospheric composition and variability, Venus Express will give us the best observations to date and will help us solve the puzzle that is Venus," says astrobiologist David Grinspoon of the Southwest Research Institute in Boulder, Colorado.

Until space probes shattered the illusion, Venus was sometimes imagined as a lush, tropical paradise. Now astronomers know it is the closest place in our solar system to hell. The greenhouse effect of its thick carbon dioxide atmosphere has heated the surface to a sweltering 500°C, and its atmospheric pressure is 90 times that at Earth's surface. Sulfuric acid rains down from the planet's high-altitude clouds, while crackling lightning and possibly erupting volcanoes complete the apocalyptic scene.

Eight armored Russian landers touched down on Venus during the 1970s and 1980s, but none lasted more than a couple of hours. Because orbiting cameras can't see through the clouds, planetary scientists have had to rely on radar to study the surface. NASA's Magellan radar mapper, which operated between October 1990 and December 1994, revealed impact craters, chasms, mountain ridges, shield volcanoes, and lavalike flows. But many important facts about Venus, including its geologic and climatic history, remain a blank.

"We need to study all aspects of Venus: surface, atmosphere, interior, and how they all work together over time," says geologist Stephen Saunders of NASA Headquarters in Washington, D.C., who was Magellan's project scientist. "Venus Express will provide many answers." The $260 million spacecraft will focus on the venusian atmosphere, using seven science instruments, five of which are spares from two earlier ESA missions, Mars Express and the Rosetta comet chaser.

Researchers hope to peer back into the planet's past. Venus probably started out very much like Earth, but for some reason its climate went awry. And no one yet knows when clouds first shrouded the planet. "It's not clear whether or not the atmosphere of Venus is in equilibrium with the surface and the interior," notes Jean-Loup Bertaux of France's Aeronomy Service in Verrières le Buisson, the principal investigator of one of the craft's three spectrometers. "We also want to know how much water has been around on Venus in the distant past." Mission scientists hope to learn more about the composition and dynamics of Venus's atmosphere. Unlike the planet itself, which turns on its axis only once every 243 days, the atmosphere rotates every 4 days, creating hurricane-force winds, and an unexplained double vortex whirls above the poles.

"There are many mysteries about the clouds and the atmosphere" of Venus, Grinspoon says. For instance, an enigmatic "unknown ultraviolet absorber" high in the clouds keeps huge amounts of solar energy from reaching the surface. "We don't know what it is, but it's possible that Venus Express will help us solve this mystery." Grinspoon thinks the clouds might even support some kind of life (*Science*, 29 November 2002, p. 1706). "It's an outlandish but entirely possible idea," he says.

Researchers are also eager to find out if any of Venus's volcanoes are still active. Larry Esposito of the University of Colorado, Boulder, who works on the mission's Venus Monitoring Camera, says it's very likely that Venus is volcanically active. "It's about the same size as the Earth, so it has to get rid of the same amount of internal heat," he says. Esposito thinks a temporary high abundance of atmospheric sulfur dioxide that NASA's Pioneer Venus Orbiter measured a quarter of a century ago could be evidence of a volcanic eruption back then. "By observing volcanic activity directly, Venus Express could settle this issue," he says.

The team is pinning its hopes on the Venus Monitoring Camera to do this. The wide-angle camera is both an ultraviolet cloud imager and an infrared detector at about 1-micrometer wavelength, where the atmosphere is transparent. During the venusian night, the team will be able to make a temperature map of the surface, which might reveal recent lava flows, says principal investigator Wojciech Markiewicz of the Max Planck Institute for Aeronomy in Katlenburg-Lindau, Germany. The spacecraft's infrared spectrometers will also search for volcanic activity by taking accurate temperature readings of the surface. "Everybody hopes to find an active volcano on Venus," says Markiewicz.

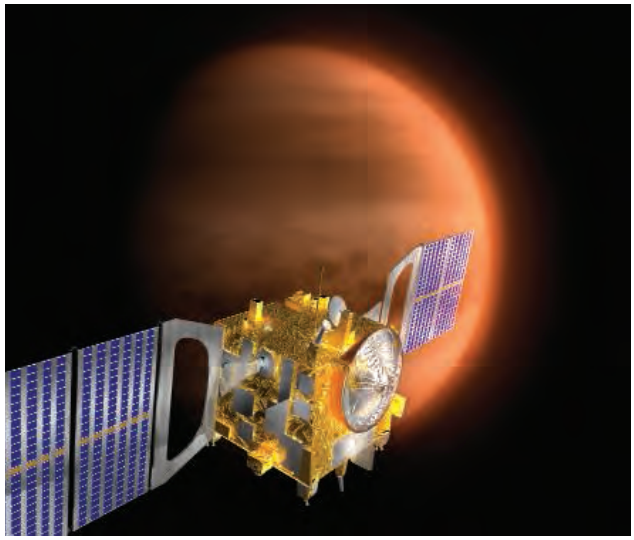

Lifting the veil. Venus Express will peer through the planet's dense clouds in search of volcanic activity.

CREDIT: ESA

Bertaux agrees. "There will be a friendly competition between the various instrument teams to find the first hot spot," he says.

Right now, the biggest worry is the launch, planned for the early morning of 26 October, with a Russian Soyuz rocket and a Fregat upper stage. Orbit insertion will be the next "very critical moment," says project scientist Håkan Svedhem of the European Space Research and Technology Centre in Noordwijk, the Netherlands. After 162 days in interplanetary space, Venus Express will settle into an extremely elongated polar orbit in which it will dip down to just 250 kilometers above Venus's surface every 24 hours. The planned mission lifetime is about 500 days, but Venus Express carries enough fuel to last twice that long.

Planetary scientists will be hoping for that and more. "Venus Express will whet our appetite for even more knowledge about our sister planet," says Saunders.

–GOVERT SCHILLING

Govert Schilling is an astronomy writer in Amersfoort, the Netherlands.

Published by AAAS

Confronting the Bogeyman of The Climate System

The threat from an abrupt circulation switch in the North Atlantic and resultant climatic chaos seems to be receding, but researchers are still worried

ASPEN, COLORADO—Scientists have been warning us for a quarter-century that the climate system has some surprises up its sleeve. By the 1990s, as paleoclimatologists discovered the whiplash history of recent climate, attention turned to the far North Atlantic. There, as the world emerged from the last ice age more than 8000 years ago, the supply of warm water to high Atlantic latitudes appeared to shut down in mere decades. The collapse of the warm circulation chilled and dried surrounding lands back to near-glacial conditions for centuries, skewing regional climate around the world.

A precipitous shift in climate could happen again, say researchers, 25 of whom gathered here last summer to discuss abrupt climate change.* But the prime menace no longer lies in the North Atlantic. Instead, a growing contingent of scientists now sees the North Atlantic as no more of a threat than accelerating sea level rise, megadroughts, and monsoon failures. "A few years ago, people thought the [Atlantic circulation] could collapse almost like *The Day After Tomorrow*," said paleoclimatologist Julia Hargreaves of the Frontier Research Center for Global Change in Yokohama, Japan. "But a very rapid collapse now seems fairly unlikely under global warming."

Shifty climate

Paleoclimatologists have certainly turned up worrisome examples of abrupt North Atlantic climate change. In ice cores retrieved from the Greenland ice cap, isotopic studies showed temperature shifts of 10°C during the last ice age and during the transition out of glacial times. Projections for greenhouse warming by the end of the century are running about 1.5°C to 2°C. And other ice-core studies showed that 10° shifts took only a few years—50 at most, which is abrupt by anybody's standard.

Some of these sudden events began to look disquietingly familiar from recent events. Apparently, melting ice sheets during the last glaciation had sent meltwater gushing into the far northern North Atlantic to form a surface layer of relatively fresh and, therefore, less dense seawater. That would have thrown a monkey wrench into the far end of the ocean "conveyor belt" that carries warm surface water northward, according to the story developed by paleoceanographers. The less-dense freshwater lid would have prevented surface water from sinking at the northern end of the conveyor and returning southward. That would have jammed the conveyor and shut it down. With no added warm water from the south, the North Atlantic and surrounding land would have chilled (*Science*, 10 July 1998, p. 156).

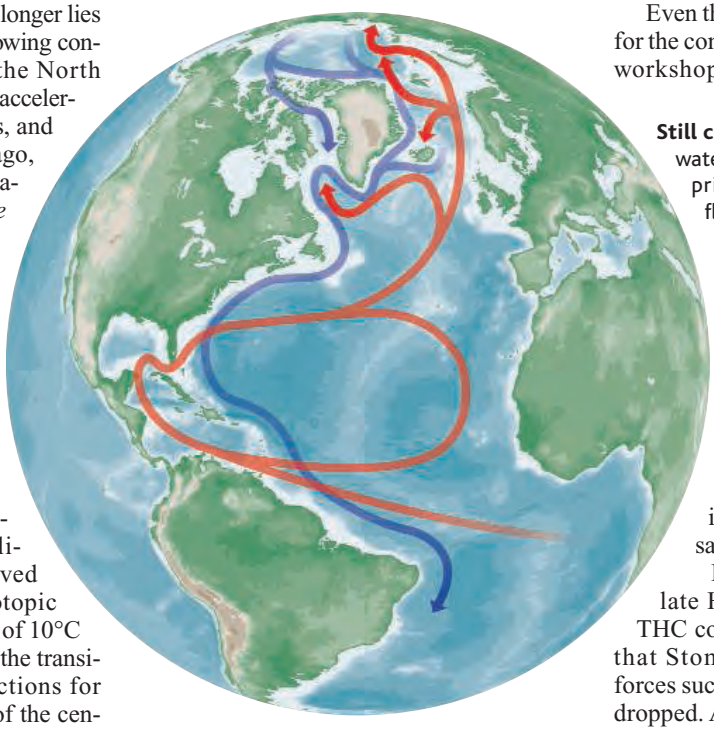

Still circulating, for now. Dumping fresh water on the far North Atlantic could, in principle, shut down the northward flow of warm surface waters (red) and the deep return of cold water (blue).

ILLUSTRATION: C. BICKEL/*SCIENCE*

In recent years, researchers have reported freshening seawater in the far north similar to that of the last ice age in pattern, if not in magnitude. Rivers have been dumping more fresh water into the Arctic Ocean, perhaps as the strengthening greenhouse increases high-latitude precipitation. At the same time, high-latitude Atlantic surface waters have been freshening (*Science*, 2 January 2004, p. 35). And at least one cog in the northbound conveyor—the subpolar gyre—has slowed of late (*Science*, 16 April 2004, p. 371). All the while, the conveyor circulations collapsed in one climate model after another when the North Atlantic was flooded with fresh water.

Not so simple

These discoveries commingled with the idea that humans tinkering with Earth's greenhouse could in theory drop temperatures around the North Atlantic. Some media found the result irresistible. European newspapers have carried dramatic headlines such as "Global Warming May Freeze Out British Isles," and even the sedate National Academy Press selected *Climate Crash* this year as the title of a journalist-written book on abrupt climate change. And although an alarmist headline or two might not seem far out of line, some scientists are beginning to doubt that a North Atlantic shutdown is looming. Physical oceanographer Carl Wunsch of the Massachusetts Institute of Technology, for one, contends that the North Atlantic Ocean simply can't determine climate single-handedly.

Even the commonly used technical name for the conveyor is misleading, he said at the workshop. "The ocean flow is a complicated beast," he said. Calling the ocean conveyor the thermohaline circulation (THC) has come to imply that only differences in temperature and salt content drive it. In fact, "the crucial element for knowing what the ocean is doing is knowing what the wind is doing," he said.

His graduate school adviser, the late Henry Stommel, introduced the THC concept in 1958. But Wunsch says that Stommel included crucial driving forces such as the wind that have since been dropped. As long as the wind blows, essential parts of the THC such as the warm Gulf Stream will continue to flow, Wunsch said, "and I don't know how to stop the wind." A safer label for the ocean conveyor might be the meridional (north-south) overturning circulation (MOC, pronounced "mock"), many at the workshop concluded.

Another complication is ice—in particular, the dearth of it around the North Atlantic. At the workshop, geophysicist Richard Peltier of the University of Toronto, Canada, argued

* "Abrupt Climate Change: Mechanisms, Early Warning Signs, Impacts, and Economic Analyses," held 9 to 15 July in Aspen, Colorado; organized by the Aspen Global Change Institute.

Published by AAAS

that abrupt shifts "have something to do with ice," noting that all of the Northern Hemisphere's glacial ice melted away shortly after the last abrupt climate event 8200 years ago. Ice might have done its work by producing fresh meltwater fast enough to put a lid on the North Atlantic. Or, as Wunsch suggests, the mountains of it sticking up into the prevailing winds at high latitudes could have skewed atmospheric circulation the way the Rockies do today. In either case, vast amounts of it seem to have been required.

Unmoved models

If the past is not a good analog for the future, computer models might serve as guides to global warming's effect on the MOC. Lately, the most sophisticated and realistic model simulations of a warmer world have failed to drive the MOC anywhere near collapse. For example, climate modeler Peter Gent of the National Center for Atmospheric Research (NCAR) in Boulder, Colorado, told the workshop how the latest version of the NCAR climate model responded to greenhouse gas increases like those expected in the next century or two. Over a range of rates of greenhouse strengthening, the model's MOC slowed by an average of 25% to 30%. "That is not a collapse," said Gent.

Modeler Jonathan Gregory of the University of Reading, U.K., and 17 colleagues got similar results in an international comparison of models. They ran 11 different models—six of the most sophisticated sort, including an earlier version of NCAR's, and five "intermediate complexity" models—for 140 simulation years, quadrupling the concentration of greenhouse gases in the process. None led to a collapse of the MOC; instead, they slowed it gradually by 10% to 50%.

Not that model MOCs can't collapse. "If you really hit the North Atlantic with fresh water," says Gent, "you can make it collapse." But the flow needs to be something like 10 times faster than current greenhouse simulations, says Gent. That's also the only way to chill Europe in greenhouse models. None of the models in Gregory's intercomparison showed a cooling anywhere; greenhouse warming always prevailed.

Not everyone is ready to consign the MOC collapse threat to the back burner, however. Climate modeler Michael Schlesinger of the University of Illinois, Urbana-Champaign, an organizer of the workshop, notes that model simulations are not entirely realistic. For one, they have yet to include meltwater from a warming Greenland. And, as geochemist Daniel Schrag of Harvard University has pointed out, models cannot yet simulate other climate extremes known from the geologic record, such as the extreme warming that occurred 55 million years ago.

By the end of the workshop, the threat of a MOC collapse seemed to have receded, at least relative to other climate threats. "The [scientific] community is way, way overfocused on the MOC," said ice core geochemist Jeffrey Severinghaus of the Scripps Institution of Oceanography (SIO) in San Diego, California. Tropical oceanographer George Philander of Princeton University agreed: "The last 6 months, every computer center has been tied up pouring fresh water on the North Atlantic. That's not good. How do we get off this bandwagon?"

A looming MOC collapse "has inspired a Hollywood movie and a lot of fear," said statistical economist Richard Tol of Hamburg University in Germany. "It's everyone's favorite bogeyman, but they may be barking up the wrong tree." Tol would direct more attention toward the prospect of rising sea levels, possibly sharply rising if the ice of West Antarctica accelerates its slipping into the sea (*Science*, 24 September 2004, p. 1897).

Others pointed to the possibility of sudden "regime shifts." In these, the slowly strengthening greenhouse could abruptly snap climate patterns into new configurations. Such climatic switches have happened in the past, Severinghaus noted. The central United States seems to go through centuries-long intervals of longer and more frequent droughts separated by periods of less drought-prone climate. And there are signs that the recent western U.S. drought was intensified by the warming of tropical waters (*Science*, 31 January 2003, p. 636). Other climate regimes, such as the monsoons, might be susceptible to greenhouse-triggered shifts as well, noted physical oceanographer Lynne Talley of SIO. Abrupt surprises, it seems, may yet be found far beyond the North Atlantic.

–RICHARD A. KERR

Hedging Your Climate-Change Bets

The prospects for sudden shifts in climate are highly uncertain. For some, that's justification for further study. But some economists disagree. To them, uncertainty is itself a reason to take action, and right away.

In a classic cost-benefit analysis, the immediate costs of dealing with profound uncertainty can be considerable. Unless decision-makers have a clear view of the future, economist Gary Yohe of Wesleyan University in Middletown, Connecticut, told workshop participants, the cost-benefit approach is likely to discourage any action.

But turned on its head, uncertainty can justify an alternative to cost-benefit analysis called risk management, an approach people take when they buy insurance. "Uncertainty is the reason you buy insurance," says Yohe. Insurance does nothing to reduce the chances that your house will catch fire, he notes, but "it decreases the consequences should the bad event occur. People are willing to pay premiums for insurance because that spreads the risk."

Under risk management, decision-makers would consider the range of possible outcomes and then try to avoid the worst by, for example, levying a tax on the carbon in fossil fuels that becomes the greenhouse gas carbon dioxide. The tax would reduce the urgency of making more sweeping decisions. At the same time, it would keep in play more ambitious goals such as holding greenhouse gases to even lower levels. All the while, scientists would be learning more about the risks of global warming.

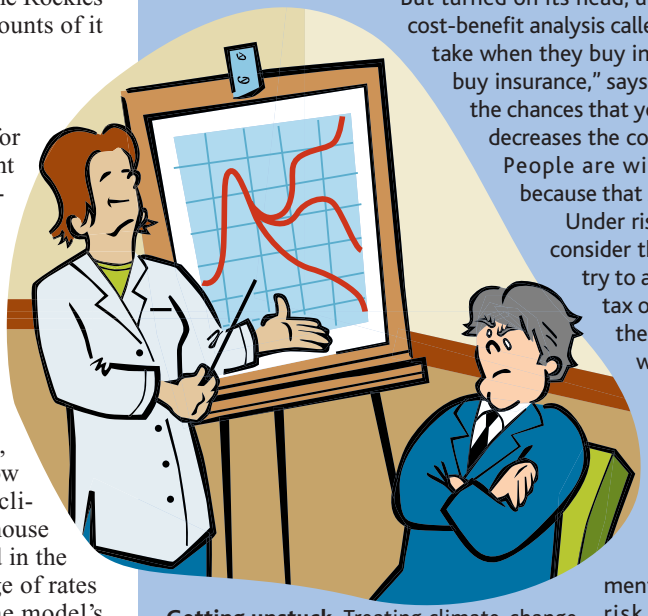

Getting unstuck. Treating climate-change mitigation as a form of insurance would buy time for scientists to sort out the risks.

Without much formal acknowledgement, decision-makers seem to be adopting risk management as they tackle global warming. Under the Kyoto Protocol, says Yohe, "the European approach to thinking about climate is based in large measure on risk management." And in announcing goals for reducing greenhouse-gas emissions, the governor of California and a consortium of New England states seem to be thinking along the same lines. Perhaps the answer to climate uncertainty is doing what comes naturally.

–R.A.K.

ILLUSTRATION: TIM SMITH

Published by AAAS

Random Samples

Edited by Constance Holden

What's Your Poison?

Alcoholism is running rampant in Russia, and a new study points out how dangerously people there satisfy their thirsts.

Russians drink a lot of moonshine, or samogen, which is much cheaper than vodka. Some also drink more dangerous substances including eau de cologne, industrial solvents, cleaning fluids, and fire starters. Indeed, Russian fighter pilots have reportedly crashed because mechanics had drunk their deicer fluid.

Scientists have for the first time tried to analyze what is going down the Russian gullet. Martin McKee of the London School of Hygiene and Tropical Medicine and Vladimir M. Shkolnikov of the Max Planck Institute for Demographic Research in Rostok, Germany, have been studying men aged 25 to 54 in the Siberian industrial city of Izhevsk. They report in the October issue of *Alcoholism: Clinical & Experimental Research* that a substantial proportion—perhaps 7%—are drinking stuff never meant for consumption, notably medicinal compounds, after-shaves, and cleaning fluids. "These substances are playing an important role in the high level of alcohol-related deaths in Russia," claims McKee. Life expectancy for Russian males has plummeted to below 59.

Among the researchers' findings: Samogen has less ethanol than does vodka but is contaminated with other alcohols toxic to hearts and livers. Medicinal compounds contain more alcohol than vodka does. And after-shave was almost pure ethanol. According to McKee, Russian after-shaves "are sold in brightly colored quarter-liter bottles, and it is difficult to avoid the conclusion that they are primarily produced for drinking."

MIT replay of alleged Greek trick.

Death-Ray Test

In 213 B.C.E., Archimedes made a "death ray," an ingenious set of mirrors that concentrated the sun's rays onto a Roman fleet, setting the ships aflame and staving off the siege of Syracuse—or so the story goes.

The Discovery Channel's show *Mythbusters* last year declared this story "busted" after an unsuccessful attempt to replicate the trick. But mechanical engineer David Wallace of the Massachusetts Institute of Technology in Cambridge thought it doable, so this month he assigned it as an exercise to his product-design class. Students built an oak replica of a Roman warship and carefully aligned 127 mirrored tiles, a total of 12 square meters, to focus light on one spot 30 meters away. Sure enough, after about 10 minutes of sunlight, the planks burst into flame.

Although successful, the experiment "demonstrated just how impractical the mirrors are," because they wouldn't work if the ships moved, says Chris Rorres, a mathematician and Archimedes scholar at the University of Pennsylvania, Kennett Square. Archimedes, famous for his weapons, would most likely have used oversized crossbows to rain pots of a flammable liquid called "Greek fire" onto the ships, he says.

Telescope Nest

A design has been selected for the building that will house Europe's next big telescope, one with a 50-meter mirror that will dwarf all existing optical scopes.

The winning design, to cost up to €300 million, is by a team from the Lund Institute of Technology in Sweden. "The building is also an instrument; it has to work in tandem with the telescope," says project director Göran Sandberg. To achieve this, supersensitive temperature controls, separate foundations for the building and the telescope to minimize vibration, and an aerodynamic shape to reduce wind effects are required, he explains.

The new mainly E.U.-funded instrument is still a decade or so away. Where it will be located—the Canary Islands or Chile—and just what it will be are still up in the air. Feasibility studies are being conducted by the European Southern Observatory and a five-country consortium on two designs: an Overwhelmingly Large Telescope called OWL, and an instrument dubbed the Euro50. Boosters say the new telescope will have a resolving power of 2.5 milli–arc seconds—15 times that of the Hubble Space Telescope and enough to discern a dime 1400 kilometers away.

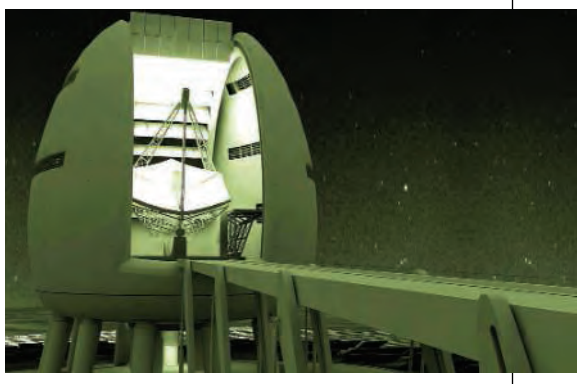

In Darwin's Hand

A reproduction of the first-known sketch by Charles Darwin of an evolutionary tree will be on display starting 19 November at the American Museum of Natural History in New York City in what the museum describes as "the most in-depth [Darwin] exhibition ever mounted." It will go on through next May.

CREDITS (TOP TO BOTTOM): MIT; AMERICAN MUSEUM OF NATURAL HISTORY

Published by AAAS

Edited by Yudhijit Bhattacharjee

JOBS

EPA bound. Toxicologist George Gray, an expert in risk assessment, won approval from a Senate panel last week to lead the Environmental Protection Agency's (EPA's) Office of Research and Development. Gray heads the industry-backed Center for Risk Analysis at Harvard School of Public Health in Boston; he succeeded John Graham in 2001 when Graham became the Bush Administration's chief regulatory cop at the Office of Management and Budget. Gray has said EPA's worst case scenarios can distort comparisons of hazards and mislead the public. "What we've learned at nearly every point over the last 30 years is that things like industrial chemicals and pollution were not as dangerous as we originally thought," Gray told the *Detroit News* in 2000.

His predecessor, Paul Gilman, praises Gray's knowledge of science and policy. Gilman says he'd like to see Gray build congressional support for EPA's $97 million extramural Science to Achieve Results grants program.

Wildlife post. H. Dale Hall, a controversial career administrator at the U.S. Fish and Wildlife Service (FWS), is in line to run the agency over the objections of several environmental groups that question his commitment to protecting threatened and endangered species. On 6 October, Hall's nomination was approved by the Senate Environment and Public Works Committee, leaving full Senate confirmation a formality. He would replace Steven Williams, who left in March to head the Wildlife Management Institute in Washington, D.C.

Critics, including the Center for Biological Diversity in Tucson, Arizona, cite a moratorium Hall placed on the release of Mexican gray wolves during his stint as head of the agency's southwest regional office. Earlier this year, Hall raised hackles when he limited the use of genetic research to protect particular lineages of endangered species. Hall's backers at the Department of Interior say he's fully qualified and point to an FWS award he received for a plan to reconcile conservation and logging in the U.S. northwest (*Science*, 29 July, p. 688).

DEATHS

Fatal fieldwork. Two geophysicists accustomed to the hazards of their profession died 4 October when a logging truck lost its load on a winding, scenic road on the Olympic Peninsula of coastal Washington state.

State seismologist Anthony Qamar (below, left), 62, of the University of Washington, Seattle, and geophysicist Daniel Johnson, age 46, of the University of Puget Sound, Tacoma, had both worked on the bulging slopes of Mount St. Helens in the spring of 1980 before it blew, killing a volcanologist. An undergraduate then, Johnson would spend much time taking the pulse of other unstable volcanoes around the world. But on the day their vehicle was hit by logs that rolled off a truck in front of them, he and Qamar were simply retrieving GPS equipment that had been monitoring an otherwise undetectable earthquake deep below the boundary of two tectonic plates.

AWARDS

Helping hands. The two winners of the 2005 New York Academy of Sciences Heinz R. Pagels human rights award have devoted themselves to speaking truth to repressive regimes and helping researchers who live under their thumbs. "Scientists have a special obligation in society," says Israel-born Zafra Lerman (top right), a chemist who shares the honor with physicist Herman Winick. Lerman, who leads a science education and policy institute at Columbia College Chicago in Illinois, is arranging a November conference in Malta to build on a similar meeting last year between Arab and Israeli scientists.

Winick, of the Stanford Linear Accelerator Center in Palo Alto, California, co-founded the Jordan-based SESAME synchrotron light source, which was relocated from Germany and is under construction in Jordan. He recently helped secure the release of Mohammed Hadi Hadizadeh, an Iranian physicist who had been jailed since 2001.

Biology prize. Dario Alessi of the University of Dundee, U.K., is the winner of the 2005 Gold Medal awarded by the European Molecular Biology Organization. Alessi receives the honor—and $10,000—for uncovering the role of kinases in hereditary diseases.

Got any tips for this page?
E-mail people@aaas.org

CREDITS (TOP TO BOTTOM): USFWS; COLUMBIA COLLEGE; DIANA ROGERS/SLAC; RICHARD CHASE; WES THELAN/PNSN; AL EGGERS

Published by AAAS

An Open Letter to Cancer Researchers

OVER THE PAST TWO YEARS, PANEL DISCUSSions have been held to propose recommendations to the National Cancer Institute (NCI) regarding critical initiatives in cancer biology. One outcome was a proposal for a new initiative, the Human Cancer Genome Project (HCGP) (*1*). This program involves systematically analyzing genomic alterations in large numbers of human tumors to determine both common genetic and epigenetic alterations and to identify changes that characterize different tumor subtypes. The price tag would be $1,500,000,000 over 10 years, the equivalent of 1000 R01 grants.

We have three questions concerning the project: (i) Would the project, as proposed, achieve its goals? (ii) Would it impact ongoing or future funding for investigator-initiated cancer research? (iii) Is this the best application of funds toward the objective of hastening the discovery of cures for cancer?

A major goal of the HCGP is the identification of new cancer genes through genome resequencing, specifically to find mutations that occur with 5% or greater frequency across a broad range of human tumors. The implication is that such mutations would lead to new therapeutic targets. In support of this strategy, much has been said about the recent identification of activating mutations in the EGF receptor, EGFR, in lung cancer and the ability of patients with such mutations to respond dramatically to certain kinase inhibitors, such as Iressa. Mutations in EGFR exist in approximately 7% of small cell lung cancer patients, and over 50% of patients carrying mutations are responsive to Iressa, but as yet there is no increase in survival in this population. This partial success is being used as an example of the information that will emerge from the HCGP, implying that identification of many new mutations would lead to rapid cures. However, the vast majority of mutations identified by sequencing tumors would be loss-of-function mutations, not gain-of-function mutations as in EGFR, and thus would not be candidates for drug inhibition. Additionally, much of the excitement surrounding the identification of EGFR mutations was due to their ability to predict responses of lung cancers to a pre-existing drug, a situation unlikely to exist for mutations in new genes.

A pilot project that provides clues to the potential information yield from the sequencing component of the HCGP was recently published by Stephens *et al.* (*2*). Out of 72 breast tumors and 9 cell lines, only six kinases out of 518 sequenced had two mutations resulting in amino acid changes. Thus, mutations identified in the kinases fall below the 5% cut-off level for significance proposed for the HCGP, an already low bar. Similar results were obtained for lung and testicular cancer (*3*, *4*). These studies addressed a family of key signaling molecules. As such, alterations in these proteins might be expected to affect cell physiology in a sufficiently broad sense to contribute to tumor development. They are also among the most easily "drugable" proteins and are a family about which we have extensive knowledge. If we cannot find interpretable information here, what gene families are likely to yield such information? These results call into question whether a massive sequencing effort, estimated to be 75% of the entire $1.5-billion price tag, is going to produce a harvest of useful information that matches its huge budget.

A key stated component of the HCGP is that the money to fund this initiative would not be taken from the funds currently available for ongoing cancer research. We are skeptical of the assertion that such "new" money would not impact current or future funding for investigator-initiated cancer research. Although it is possible that NCI would be able to persuade Congress to allocate this money, in the current fiscal climate, the HCGP would likely be weighed against future allocations, as NIH funding is likely to be a zero sum game for the foreseeable future. In view of current budget constraints, it seems responsible to plan a more conservative effort that balances the cost and potential yield of current sequencing technologies against future advances that promise to greatly reduce sequencing costs.

The unstated goal of the HCGP is to accelerate the discovery of cures for cancers. The question we need to answer is not whether the information generated will be useful, but whether, if given $1.5 billion in "new" cancer money, would the HCGP be the best application of that money toward the goal of cancer cures. Some elements of the proposed HCGP represent sensible and cost-effective steps toward the goal of managing cancer. Identification of regions amplified in tumors can be achieved at a fraction of the cost of sequencing. Such efforts yield not only potential drug targets but also diagnostic information. However, there are also important approaches that are completely missing. One is a systematic exploration of the genetic alterations that could kill cancer cells, a Genetic Cancer Genome Project. With RNAi, we can now systematically identify genes that interfere with the growth and survival of tumor cells—both in cell culture and in animal models. These functional screens seem a highly plausible method to identify potential anticancer drug targets and a more direct approach than those contemplated within the current framework of the HCGP. A second and more immediate way to enhance cancer therapy in the short term is the development of biomarkers for early detection.

As cancer researchers, we have a special responsibility with respect to guiding resource allocation to fight cancer. We need to be able to look cancer patients and their families in the eye and say, "We are spending your money in the best way we know to find a cure for you." We must apply this standard in judging any large-scale proposal for dedicated research funding allocations. As currently configured, the HCGP needs to be reconsidered and reprioritized to produce a program that gives us the best chance for

> **"As cancer researchers, we have a special responsibility with respect to guiding resource allocation to fight cancer.... [T]he [Human Cancer Genome Project] needs to be reconsidered and reprioritized to produce a program that gives us the best chance for fighting this disease."**
>
> –ELLEDGE AND HANNON

Published by AAAS

fighting this disease. Therefore, because the most productive direction of research is still a debatable question, we propose that (i) sequencing be delayed until advances in sequencing technology are achieved; (ii) objective criteria be established to allow a go/no go decision for continued DNA sequencing based on pilot studies; and (iii) large-scale genetic screening to identify targets whose inhibition kills cancer cells should be incorporated into the HCGP.

STEPHEN J. ELLEDGE[1,3] AND GREGORY J. HANNON[2,3]
[1]Department of Genetics, Center for Genetics and Genomics, Harvard Medical School, Boston, MA 02115, USA. [2]Cold Spring Harbor Laboratory, Cold Spring Harbor, NY 11724, USA. [3]Howard Hughes Medical Institute.

References

1. A portion of this overall report has now been presented publicly at the recent symposium "Molecular Approaches to Controlling Cancer" at Cold Spring Harbor in the format of a panel discussion to solicit input from the broader community of cancer biologists.
2. P. Stephens *et al.*, *Nat. Genet.* **37**, 590 (2005).
3. H. Davies *et al.*, *Cancer Res.* **65**, 7591 (2005).
4. G. Bignell *et al.*, *Genes Chrom. Cancer*, 20 Sept. 2005 (E-pub ahead of print).

Evaluating Evidence for Aging

IN THEIR REPORT "MITOCHONDRIAL DNA mutations, oxidative stress, and apoptosis in mammalian aging" (15 July, p. 481), G. C. Kujoth *et al.* present data showing that mice with a mutant form of mitochondrial DNA polymerase accumulate mitochondrial mutations, die at a very early age, and exhibit multiple forms of pathology that the authors interpret as "accelerated aging." The evidence for this last claim, however, needs to be evaluated more critically. The mutant mice show a dramatic anemia, with erythrocyte counts falling by more then 50% by 10 months of age. In normal aging mice, however, red blood cell counts fall only by about 10% (*1*), unless the mice become ill. The mutant mice show a dramatic loss of intestinal crypts, but in normal mice, crypt numbers of very old mice remain at levels of 80 to 90% of those seen in young mice (*2*). The mutants show hearing loss, but apparently without the loss in cochlear hair cells that underlies late-life hearing deficits in normal mice. The animals show many phenotypes, such as grey hair, spontaneous alopecia, kyphosis, and weight loss, that are uncommon in healthy aged mice, although the latter two are commonly seen in chronically ill mice of any age.

There are two ways to try to show that a mutant exhibits accelerated aging. The primrose path, selected by nearly all enthusiasts of "accelerated aging" models, is to list symptoms seen in a mutant, note that some of these are seen in normal aged mice [or aged humans; see (*3*)], and declare the case closed. The thornier approach, which is more convincing but seldom attempted, is to start with a set of traits shown by authentic aging mice and then determine how many of these are seen in the mutant.

Kujoth *et al.* have developed an exciting system for the analysis of how mitochondrial mutations can affect erythropoiesis, gastrointestinal homeostasis, and muscle function. Whether the rate of aging depends critically on mitochondrial mutations is still very much an open question.

RICHARD A. MILLER
Department of Pathology, University of Michigan and Ann Arbor VAMC, Geriatrics Center, 1500 East Medical Center Drive, Ann Arbor, MI 48109–0940, USA.

References

1. D. E. Harrison, *J. Gerontol.* **30**, 286 (1975).
2. K. Martin, T. B. Kirkwood, C. S. Potten, *Exp. Cell Res.* **241**, 316 (1998).
3. M. Kuro-o *et al.*, *Nature* **390**, 45 (1997).

THE REPORT "MITOCHONDRIAL DNA mutations, oxidative stress, and apoptosis in mammalian aging" by G. C. Kujoth *et al.* (15 July, p. 481) has flawed reasoning and conclusions. Basing conclusions regarding life-span–determining factors on a model of shortening the life-span of organisms rather than extending it is misleading. The authors achieved a technical feat in introducing genetic instability into mitochondria by reducing proofreading of the mitochondrial genome. By their own calculations, this uncontrolled, introduced mutability resulted in 4 to 10 mitochondrial mutations per mitochondrial genome. Considering that the mitochondrial genome contains only 37 genes, all essential, such a rate of mutation is highly detrimental. Much lower levels of mitochondrial mutations occur in cells of "normal" aging mice [e.g., (*1*)]. This catastrophic mutation rate can be discerned from the precipitous mortality of the engineered mice (see fig. 1C), which is rarely observed in wild-type mice. Also, the homozygous engineered mice are likely infertile because of severe problems in their germ cells caused by faulty mitochondria. It is a false premise that if a certain genotype containing detrimental alleles mimics some features found in aging organisms, such as hair graying, that it is a good model for studying biological aging.

DAVID GERSHON
Professor emeritus, Technion-Israel Institute of Technology, and Redox Pharmaceutical Corp., 3960 Broadway, New York, NY 10032, USA. E-mail: dgershon@redoxpharm.com

Reference

1. A. Chomyn, G. Attardi, *Biochem. Biophys. Res. Commun.* **304**, 519 (2003).

Response

MILLER DISPUTES OUR CONCLUSION THAT aging phenotypes in mice carrying a mutation in the exonuclease domain of POLG (D257A mice) are relevant to normal aging and also questions the validity of animal models of accelerated aging. Because multiple biological processes are likely to contribute to aging in complex organisms, interventions that significantly extend maximum life-span in mammals are likely to be rare. Large (over 50%) increases in life span in mice are only observed with caloric restriction or dwarfism (*1*), both of which result in overt metabolic and hormonal alterations and multiple secondary effects. In contrast, interventions that result in accelerated aging phenotypes have provided information on how the alteration of a given pathway or individual gene impacts aging (*2*, *3*). The accumulation of mitochondrial DNA (mtDNA) mutations is a hallmark of aging in multiple species, and we have clearly demonstrated that such mutations can lead to aging phenotypes. Many of these, such as hearing loss, graying, bone loss, and sarcopenia, are associated with aging in multiple species. Miller's argument is based on a misconception: The severity of phenotypes in D257A mice need not be present in aging of normal mice for this animal model to be relevant to our understanding of aging mechanisms. The severe phenotypes associated with mtDNA mutations in D257A mice can be explained by stem cell depletion through increased apoptosis, which is unlikely to occur to a similar extent in normal aging. However, progressive accumulation of mtDNA mutations is likely to lead to physiological impairments and a decline in tissue regenerative capacity. We believe that interventions that result in either accelerated aging phenotypes or extend life-span have contributed to our understanding of general aging mechanisms. This is clearly demonstrated by the analysis of the mouse klotho gene, first identified as resulting in accelerated aging when mutated and recently shown to extend survival when overexpressed (*4*).

Gershon questions the relevance of high mtDNA mutation rates observed in D257A mice to normal aging, but misrepresents our findings in the process. We observed high levels of mtDNA mutations in both wild-type and D257A mice by 5 months of age. Specifically, the quoted estimation of 4 to 10 mtDNA mutations/mtDNA was the number observed for wild-type mice. D257A mice show mutation frequency increases above this baseline on the order of three- to eight-fold, depending on the tissue under study. Thus, mtDNA mutations are surprisingly high in wild-type, relatively young animals.

Further age-related accumulation of mutations is likely to contribute to age-related declines in physiological function. Several features of aging in D257A mice, such as sarcopenia, bone loss, and hearing loss, are commonly observed in aging. More severe phenotypes, such as anemia and severe loss of intestinal crypts, are likely to be secondary to complete stem cell depletion, which is not observed in normal aging.

TOMAS A. PROLLA[1] AND R. H. WEINDRUCH[2]
[1]Department of Genetics and Medical Genetics, University of Wisconsin–Madison, 445 Henry Mall, Madison, WI 53706, USA. [2]Department of Medicine and Veterans Administration Hospital, University of Wisconsin–Madison, Madison, WI 53705–2286, USA.

References
1. J. L. Barger, R. L. Walford, R. Weindruch. *Exp. Gerontol.* **38**, 1343 (2003).
2. S. D. Tyner *et al.*, *Nature* **415**, 45 (2002).
3. S. Chang *et al.*, *Nat. Genet.* **36**, 877 (2004).
4. H. Kurosu *et al.*, *Science* **309**, 1829 (2005) (published online 25 Aug. 2005; 10.1126/science.1112766).

Tracing Contaminants with $\delta^{15}N$ Measurements

IN THEIR BREVIA "ARCTIC SEABIRDS TRANSport marine-derived contaminants" (15 July, p. 445), J. M. Blais *et al.* showed that contaminant concentrations increased exponentially with stable isotope ratio of nitrogen ($\delta^{15}N$) values in sediments of high Arctic pools associated with guano input from a seabird (fulmar) colony. However, this nice result may mask complexities associated with the use of $\delta^{15}N$ as a proxy for trophic level and as a direct tracer in contaminant studies. First, the $\delta^{15}N$ value of 20 per mil for fulmar guano far exceeds that expected from fulmar diet, tissue, and isotopic mass balance considerations (*1*). In fact, these values approximate those expected for polar bears from the same area (*2*). Rather, such elevated $\delta^{15}N$ values in guano derive, in part, from ammonia volatilization, as noted previously for soils in several Antarctic seabird rookeries, a factor fairly independent of the trophic level of the bird species involved (*3*–*5*). In addition, $\delta^{15}N$ values in foodwebs reflect not only baseline nutrient values, but also nutrient concentration and rate of growth of primary production. Plotting $\delta^{15}N$ values versus chlorophyll a, total phophorus, and dissolved organic carbon from the authors' data shows threshold responses involving high sensitivity of sediment $\delta^{15}N$ values at low nutrient concentrations and a plateau at higher concentrations. Future studies using stable isotopes to track ornithogenic origins of contaminants should consider nonlinear effects of nutrient concentrations and variable effects of ammonification on foodweb $\delta^{15}N$ values using multiple stable isotopes (*6*).

KEITH A. HOBSON
Canadian Wildlife Service, 115 Perimeter Road, Saskatoon, SK S7N 0X4, Canada.

References
1. K. A. Hobson, *Mar. Ecol. Progr. Ser.* **95**, 7 (1993).
2. K. A. Hobson, H. E. Welch, *Mar. Ecol. Progr. Ser.* **84**, 9 (1992).
3. H. Mizutani *et al.*, *Biogeochemistry* **2**, 221 (1986).
4. H. Mizutani *et al.*, *Auk* **108**, 960 (1991).
5. E. Wada, R. Shibata, *Nature* **292**, 327 (1981).
6. A. Evanset *et al.*, *Organohal. Comp.* **66**, 2415 (2004).

Response

WE THANK HOBSON FOR RAISING VALID points about the use of stable isotopes in contaminant studies, and we fully acknowledge these concerns. Stable isotopic composition of nitrogen can be altered by many external factors and thus is not a flawless tracer for nitrogen sources. For example, ammonification and denitrification are well known to increase $\delta^{15}N$ in dissolved inorganic nitrogen species and in dissolved and particulate organic nitrogen in water and sediment [e.g., (*1*), footnote number 14]. However, as we indicated in our study (see Fig. 1 caption), if we expressed our contaminant data relative to other indicators of guano input (e.g., total phophorus, total nitrogen, dissolved organic carbon and cadmium), we would see similar relationships with contaminant concentrations in sediments, as we showed with the isotope data. The purpose of these chemical tracers was to link contaminants to the guano produced from the seabirds, which could have been accomplished with any of the tracers mentioned above. Furthermore, we could have shown the same patterns simply using field observations. A simple ranking of bird influence from 1 to 11 for the 11 study ponds would have matched the same ranking we described with the isotope data (or the same general ranking we would achieve using our other proxies of bird influence). The fact that all tracers produced a similar pattern is further evidence that the source was adequately identified by the isotope data in our study.

Hobson is mistaken in saying that the contaminant concentrations increased exponentially with $\delta^{15}N$ values in all cases for the sediments of our study ponds. This interpretation is perhaps prompted by our logarithmic axis in Fig. 1. The distribution of these data was log-normal, so a transformation was considered necessary for regression analysis. There is also the implication that we used $\delta^{15}N$ measurements in sediments to directly infer trophic position. That was not our intention; nitrogen isotopes were used as one of several possible proxies to infer bird influence. We believed that the isotope data on our figure would be more easily interpreted by a general readership. Finally, we agree with Hobson's last point that, ideally, multiple stable isotopes should be used, if possible, in future food web studies.

JULES M. BLAIS,[1]* LYNDA E. KIMPE,[1] DOMINIQUE MCMAHON,[1] BRONWYN E. KEATLEY,[2] MARK L. MALLORY,[3] MARIANNE S. V. DOUGLAS,[4] JOHN P. SMOL[2]
[1]Centre for Advanced Research in Environmental Genomics, Department of Biology, University of Ottawa, Ottawa, ON K1N 6N5, Canada. [2]Paleoecological Environmental Assessment and Research Laboratory, Department of Biology, Queen's University, Kingston, ON K7L 3N6, Canada. [3]Canadian Wildlife Service, Environment Canada, Iqaluit, NU X0A 0H0, Canada. [4]Department of Geology, University of Toronto, Toronto, ON M5S 3B1, Canada.
*To whom correspondence should be addressed. E-mail: jblais@science.uottawa.ca

Reference
1. B. P. Finney *et al.*, *Science* **290**, 795 (2000).

Letters to the Editor

Letters (~300 words) discuss material published in *Science* in the previous 6 months or issues of general interest. They can be submitted through the Web (www.submit2science.org) or by regular mail (1200 New York Ave., NW, Washington, DC 20005, USA). Letters are not acknowledged upon receipt, nor are authors generally consulted before publication. Whether published in full or in part, letters are subject to editing for clarity and space.

CORRECTIONS AND CLARIFICATIONS

2005 Visualization Challenge: "Noninteractive media" by C. Gramling (23 Sept., p. 1992). The print version of this article contained the following errors: The winning entry, "Return of the 17-Year Cicadas," was credited in the subtitle to Roger Hangarter; it should have been credited to Roger Hangarter and Samuel Orr. In the subtitle for the honorable mention "Rip Currents: Nearshore Fundamentals," the name of credited contributor Dan Riter was misspelled. The honorable mention, "Forces of Nature," was credited in both the subtitle and the text to Leslie Ann Aldridge of National Geographic TV & Film, Washington, D.C.; it should have been credited to National Geographic TV & Film, Washington, D.C.; Evan Ricks, Pixel Play Studios, Los Angeles, California; and Tim Sassoon, Sassoon Film Design, Santa Monica, California. The honorable mention "Evolutionary Morphing" was credited in the subtitle to Nina Amenta, University of California, Davis; it should have been credited to Nina Amenta and David Wiley, University of California, Davis; Eric Delson, City University of New York; F. James Rohlf, State University of New York, Stony Brook; and colleagues. (These credits are all correct in the HTML version of the article on *Science* Online.)

2005 Visualization Challenge: "Interactive media" by C. Gramling (23 Sept., p. 1993). In the text, Tracy Sterling's first name was misspelled in the subtitle and she was described as an entomologist and plant pathologist; she is actually a weed pathologist.

INFECTIOUS DISEASES

Escaping an Epidemic

Larry J. Anderson

SARS
A Case Study in Emerging Infections
Angela R. McLean, Robert M. May, John Pattison, and Robin A. Weiss, Eds.
Oxford University Press, New York, 2005. 141 pp. $99.50, £55. ISBN 0-19-856818-5. Paper, $39.50, £24.95. ISBN 0-19-856819-3.

Twenty-First Century Plague
The Story of SARS
by Thomas Abraham
Johns Hopkins University Press, Baltimore, MD, 2005. 173 pp. $24.95. ISBN 0-8018-8124-2.

On 22 February 2003, an ill physician from Guangdong province, China, stayed overnight in a hotel in Hong Kong. During his brief stay he transmitted a coronavirus (CoV) to other guests, who then directly or indirectly initiated outbreaks of severe acute respiratory syndrome (SARS) throughout the world. The outbreaks created fear and concern, affected social and commercial activity worldwide, shut down entire cities, and led to a well-focused global scientific and public health response coordinated by the World Health Organization (WHO). In less than 4 months, the outbreaks were controlled. The speed, intensity, and level of cooperation and collaboration that the response effort engendered among governments, the public health and primary health care communities, academia, and private industry were unprecedented. The courage and unselfish effort by public health and health care staff in the affected areas were truly remarkable.

To fully describe the SARS epidemic of 2003 is a daunting task, but two recent books—*SARS: A Case Study in Emerging Infections*, edited by Angela McLean *et al.*, and Thomas Abraham's *Twenty-First Century Plague: The Story of SARS*—capture some aspects of the story. Reading the books and considering the complexities of the response to SARS brought John Godfrey Saxe's 19th-century poem "The Blind Men and the Elephant" to mind. The poem, which is based on a legend from India, describes six blind men who went to "see" an elephant for the first time. Each of the men encountered and felt a different part of the animal, and each came away with a very different version of what the elephant was like. In much the same way, the two books present distinct and interesting but incomplete pictures of the SARS story—which, given the story's complexity, is not surprising.

The edited volume *SARS: A Case Study in Emerging Infections* contains 13 chapters plus an introduction and a concluding summary of what we have learned from the outbreak. The book originated in a January 2004 Royal Society Discussion Meeting, the results of which were published in the July 2004 issue of the *Philosophical Transactions of the Royal Society B: Biological Sciences*. The chapters, authored by experts in their respective fields, primarily present SARS from an academic or laboratory standpoint rather than from the clinical or public health perspective. They are generally well written and usually have sufficient depth to be informative. However, two of the shorter chapters—"Management and Prevention of SARS in China" and "The Aetiology of SARS: Koch's Postulates Fulfilled"—provide only very cursory discussions of their topics. For example, that on the etiology of SARS describes studies of SARS-CoV disease in animal models but fails to mention the critical epidemiologic-based laboratory and pathologic studies that rapidly and conclusively established the link between SARS-CoV and the SARS outbreak in humans. The chapter on SARS in China sketches some features of the outbreak in Guangdong province and the postoutbreak community- and laboratory-acquired cases in Guangzhou and Beijing, respectively. It also outlines measures to control human-to-human and animal-to-human transmission but includes very few details to fill in the picture.

Although most contributors to the volume edited by McLean *et al.* focus on SARS, for some the disease is principally used as a starting point for discussing topics of particular interest to the authors. The chapter on environmental and social influences on the spread of infectious diseases discusses how such changes as increased contact among human populations, agricultural development, urbanization, population movement, loss of biodiversity, and road building have, over the millennia, increased the risks of humans contracting new diseases from other human populations or animals. The two chapters on evolution and cross-species transfer reconsider links inferred among SARS-CoV and among influenza viruses based on sequence data. This reconsideration nicely illustrates potential pitfalls in definitively establishing evolutionary relationships among viruses. The chapter on informed consent, however, seemed too academic to be helpful for outbreak-related investigations.

The chapter on international trade in small carnivores demonstrates the need to consider regional and global reservoirs of new viruses rather than focusing only on the site where the infection originated. The two chapters on mathematical models of outbreaks provide helpful insights into factors that affect transmission of infectious agents and control of community or global outbreaks. From where Roy Anderson *et al.* (the authors of the one of these chapters) seem to stand, models can be used to assess efficacy of control measures, such as contact tracing. From my perspective, studies using actual outbreak data are better suited to address this type of question. It should be noted that whatever measures are indicated for controlling an outbreak, their effectiveness is dependent on the public health workers who implement them and the primary health care workers who care for the infected patients. The chapter on traumatic stress among health care workers is an important reminder of the substantial and often unrecognized needs of those on the front lines who respond to outbreaks like SARS despite the risk to themselves and their own families.

Masked for protection. Hong Kong commuters wearing surgical masks pass a poster that promoted precautions against SARS and saluted medical workers (late April 2003).

CREDIT: ANAT GIVON/ASSOCIATED PRESS

The reviewer is in the Respiratory and Enteric Viruses Branch, National Center for Infectious Diseases, Centers for Disease Control and Prevention, 1600 Clifton Road, Atlanta, GA 30333, USA. E-mail: landerson@cdc.gov

BROWSINGS

The Smaller Majority. The Hidden World of the Animals That Dominate the Tropics. *Piotr Naskrecki.* Harvard University Press, Cambridge, MA, 2005. 288 pp. $35, £21.95, €32.30. ISBN 0-674-01915-6.

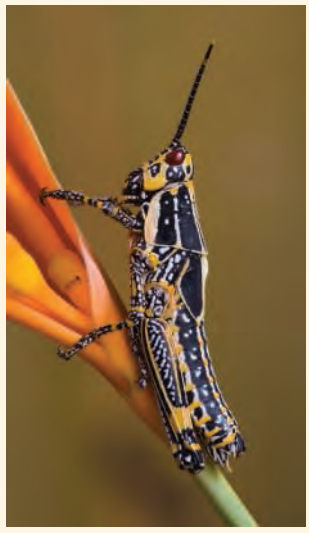

This volume celebrates the "noncharismatic" mesofauna of tropical terrestrial ecosystems. In place of the images of birds and mammals that fill most collections of natural history photography, the author offers portraits of insects, arachnids, flatworms, and amphibians. With a few exceptions—such as island-dwelling coconut crabs and caecilians (subterranean legless amphibians)—the featured organisms would fit within a matchbox. The images, captions, and accompanying text offer glimpses into the biology and behavior of the animals, all of which were photographed in their natural habitats. Despite the help of many specialists, some of the species portrayed—including this onychophoran ("velvet worm") from northern Queensland, Australia (**left**)—remain unidentified; as one might expect for these relatively neglected taxa, others have yet to be formally described. Naskrecki organizes his pictorial essays into three sets, representing humid forests, grasslands [the habitat of *Zonocerus variegatus*, a common grasshopper across much of sub-Saharan Africa (**right**)], and deserts. He hopes that the volume will help the public appreciate the beauty and importance of small animals because such appreciation is the first step toward conserving them and their environments.

CREDITS: PIOTR NASKRECKI/COURTESY HARVARD UNIVERSITY PRESS

Twenty-First Century Plague discusses SARS from a reporter's vantage point. Abraham, a science journalist based in Hong Kong, provides a fascinating picture of some of the events and people who played key roles in determining the course of the SARS outbreak in China and Hong Kong and around the world. The book is divided into six chapters, two appendices, and a list of resource materials by chapter. The introduction sets the stage for the book with a discussion of emerging infectious diseases in general and with specific descriptions of other recent outbreaks of emerging infectious diseases, such as Nipah virus in Malaysia and monkeypox and West Nile virus in the United States. The book's strength, however, comes from the way it sets forth the story behind the story: the impact that people and events had on the course of the SARS outbreak and the effect of steps that were or were not taken. The chapter on China describes in some detail the individuals, occurrences, and political forces that affected the early course of the outbreak in Guangzhou. A key feature of this chapter is the author's effort to document the people and factors that contributed to the delay in sharing information about the outbreak. Abraham delineates how that delay likely contributed to the spread of SARS within Guangzhou, within China, and worldwide.

The chapter on Hong Kong details the early course of the outbreak there, including the inside story on some of the superspreading events. Abraham adds to the personal nature of his account of SARS in Hong Kong by including descriptions from staff of how their involvement in the outbreak affected them and their families. In discussing the spread of the disease to become "a global emergency," he provides an in-depth description of the interplay between participants and events that molded WHO's response to SARS. Abraham aptly describes the courage, timeliness, complexity, intense effort, and success that characterized that response. As with the six blind men and the elephant, however, where the author stands can make all the difference. Whereas Abraham writes that the U.S. Centers for Disease Control and Prevention (CDC) was not as forthcoming as other laboratories in sharing its findings, the truth is that CDC promptly and willingly provided its discoveries to the WHO laboratory network. Had Abraham investigated more thoroughly, he would have found that electron microscopic evidence of a coronavirus isolate was reported by CDC during a SARS teleconference within 24 hours of the observation, CDC's PCR primers and its first SARS-CoV sequences were posted on the WHO laboratory network Web site on 24 March 2003 (less than 36 hours after the first sequence reactions were completed), and partial sequences (once validated) were provided to the WHO Web site the week before the full genome sequences were completed. The author's comments about CDC's approach to participation in the outbreak left me wondering about the accuracy of other details in the book.

In describing the hurried hunt for the causal virus, Abraham offers an interesting and very personal account of the events and laboratory findings that led to identification of SARS-CoV in Hong Kong. He also notes that a group at the Academy of Military Medical Sciences in Beijing may have been the first to isolate the virus. In late February 2003, this group isolated a virus with electron microscopic features suggestive of a coronavirus. But in order not to contradict a famous senior Chinese scientist who felt that SARS was caused by a *Chlamydia*-like agent, they chose not to report their findings.

As with the six blind men and their differing impressions of the elephant, the two books give multiple views of the virus and the outbreak. *SARS: A Case Study in Emerging Infections* presents academic views on very specific aspects of the virus and its spread. *Twenty-First Century Plague* describes many of the people, events, political settings, and other contributing factors in a fascinating view of the story behind the story of the outbreak. There are other important perspectives and stories, including the clinical and public health viewpoints, the social and economic impact of the outbreak, and the efforts to develop anti-viral drugs and vaccines. Nonetheless, both books contribute, in their own ways, to the complex, multilayered story of the SARS outbreak of 2003 and the lessons learned that, hopefully, will be applied to future outbreaks.

10.1126/science.1117649

NUCLEAR WASTE

Proof of Safety at Yucca Mountain

Luther J. Carter and Thomas H. Pigford

It has long been recognized that the physical and chemical interactions associated with placing heat-generating nuclear waste in a geo-hydrologic environment are complex and difficult to predict (*1*) and that proof of safety in an absolute sense is beyond reach. The fundamental problem of the Yucca Mountain nuclear waste repository project, for which the life-cycle cost was last put at over $57 billion (*2*), is its lack of a robust proof of safety for a period of hazard of a half-million years or longer. Proof of safety calls for a design of relative simplicity based on well-understood physical and chemical phenomena, careful testing and measurement, and adequate theory for extrapolations. The "proof" ultimately lies in performance assessments showing such low radiation doses as to indicate that throughout the period of hazard essentially all radioactive elements are contained near the point of waste emplacement. In our view, the present repository design cannot meet these tests.

To understand this, it is important to appreciate the Environmental Protection Agency's evolving radiation protection standards for the Yucca Mountain project. In June 2001, the EPA issued standards setting the maximum allowed dose at 15 millirems (mrem) per year but limiting compliance assessment to 10,000 years. These standards were invalidated by the U.S. Circuit Court of Appeals for the District of Columbia in its ruling of 9 July 2004. The court found that the EPA, by limiting compliance assessment to 10,000 years, had failed its statutory obligation to heed recommendations of the National Academy of Sciences. An academy panel (*3*) had found that "peak risks might occur tens to hundreds of thousands of years or even further into the future" and that performance assessments would be feasible.

In response to this court ruling, the EPA issued for public comment this past 9 August a proposed new standard that would establish a two-tiered radiation-protection regime, with a 15-mrem/year maximum dose for the first 10,000 years and a 350-mrem/year dose for up to 1 million years thereafter. If this proposed standard is adopted, licensing may become easier, but credibility of project performance assessments will continue to face serious challenge.

The Total System Performance Assessment (TSPA) issued by the project in December 2001 (*4*) was a key input to the documents supporting the formal selection of the Yucca Mountain site and the joint resolution by Congress upholding that selection after the state of Nevada exercised its right to veto it. The TSPA did not, however, promise virtually total containment of radioactive elements out to hundreds of thousands of years. The waste containers are to be protected by two major engineered features: first, a corrosion-resistant outer layer of the nickel-based alloy-22 and second, a massive and continuous "drip shield" of titanium to be installed over the containers just before closure of the repository, about a hundred years after emplacement of waste in the repository has begun (see figure below). The performance assessment showed the containers and the drip shield beginning to fail within the first several tens of thousands of years (*5*). How, then, could safety be assured over times vastly longer than that?

A plume of groundwater contaminated by radioactive elements would form beneath the repository and would migrate southward down the hydraulic gradient, passing, over time, through the shallow aquifers of Armagosa Valley, where there is currently irrigated farming. Radiation doses above the usual regulatory limit of 15 mrem/year would begin to occur after about 200,000 years (*6*).

Even a new TSPA could not get around the fact that the preferred design does not match characteristics crucial to establishing proof of safety. It is not a simple design: The titanium drip shield itself adds substantial complexity to repository design and construction. Consider the 100-year delay (*7*) in installation of the drip shield. Will decision-makers four generations hence, with priorities unlike our own, choose to install a feature which in year-2000 dollars would add several billion dollars to project costs?

The project's most complicating feature is its preferred "hot repository" option, whereby waste containers would be spaced closely enough for the heat from radioactive decay to bring the water in the nearby rock above the boiling point. The water would become water vapor and migrate outward, away from the waste emplace-

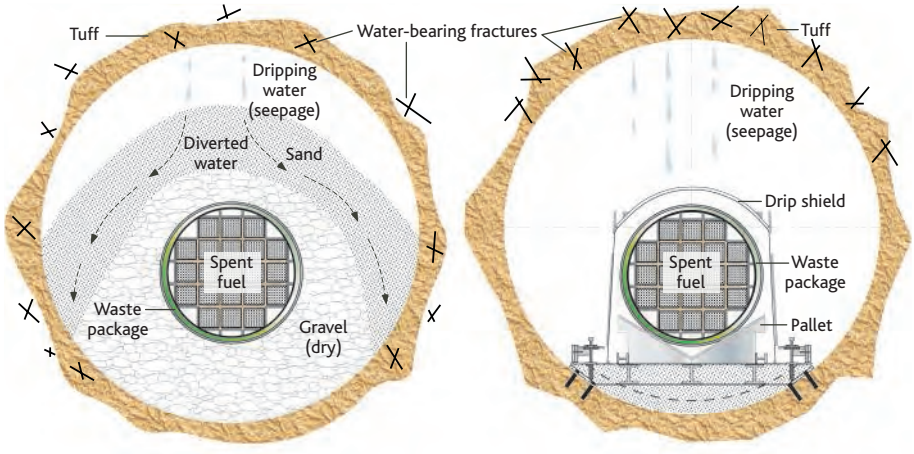

Proposed storage of nuclear waste at Yucca Mountain repository. (**Left**) Current DOE disposal design (*4*), including nuclear waste package and overlying titanium drip shield within an open tunnel. (**Right**) Capillary barrier design (*8*), in which the difference in permeability and capillary properties between two backfill materials assures diversion of groundwater flow around the waste packages (no drip shield needed).

CREDIT: MONITOR SCIENCE

L. J. Carter is an independent journalist in Washington, DC, and the author of *Nuclear Imperatives and Public Trust: Dealing with Radioactive Waste* (Resources for the Future, Washington, DC, 1987); e-mail: lcarter345@aol.com. T. H. Pigford is professor emeritus, Department of Nuclear Engineering, University of California, Berkeley, CA 94720, USA; e-mail: pigford@nuc.berkeley.edu

Published by AAAS

ment tunnels. But complicated flows of air, water vapor, and liquid water would be created, and chlorides and other corrosive chemicals would be mobilized by water reacting with the hot rock. This design feature is puzzling, because it could do nothing to prevent corrosion of waste containers beyond the first 10,000 years when the repository will have cooled from the declining levels of radioactivity.

Is the design based on well-understood physical and chemical phenomena? Does it allow reliable testing and measurement, and is there adequate theory for extrapolating far beyond real-time data? To these questions, too, the answer is no. The project design team has worked hard on safety, but the drip shield, the container's alloy-22 outer shell, and the preferred hot repository design appear to have been chosen in an ad hoc manner.

What would be a better repository design? First, the design must be carefully adapted to the specific characteristics of the site. At Yucca Mountain the repository would be built within a mountain ridge of volcanic tuff that is high above the water table in "unsaturated" rock where the water present, although there is plenty of it (100 liters per cubic meter), does not fill all the pores in the rock (*8*). In this unsaturated or vadose zone, water moves quickly through open fractures but its movement within pores in the rock is kept extremely slow by the capillary tension between air and water in a tightly confined space.

In this setting, the repository would be relatively dry and accessible by gentle ramps and tunnels from the flanks of the mountain ridge. But an accompanying disadvantage is that air moves freely through the mountain via interconnected open and dry fractures permeating the ridge. Thus, waste containers may corrode whenever they become wet or damp.

A design strategy (*9, 10*) that would appear to have an excellent chance of satisfying a robust proof of safety is based on a man-made capillary barrier (see figure, page 447). The waste containers would be covered first by a layer of coarse gravel, then by a layer of fine sand or finely ground tuff. This barrier would work by virtue of the strong capillary forces present in the sand layer and by their absence in the gravel layer. Water dripping from the tunnel ceiling onto the sand layer would be seized by capillary forces and caused to move very slowly away through the sand above the gravel. The gravel layer is the key to computing radiation safety over the long term.

All the waste containers beneath the gravel will corrode over time from the water vapor and oxygen present. Eventually, radioactive elements dissolved in water will emerge from the failed containers, diffuse along the gravel particle surfaces, and, as we infer from a performance assessment of 10 years ago, remain trapped there for hundreds of thousands of years. This assessment predicted that the radiation dose to future people from a repository using a capillary barrier would be lower at all times by a factor of one million than the dose from a repository similar to the one envisioned by the Yucca Mountain project today (*11*).

By comparison with the project's present reference design, the capillary barrier system would be far simpler. It would also be far cheaper, from a use of locally obtainable materials, without need for either the alloy-22 outer shell for the containers or a costly drip shield. The average cost for each of the 14,700 waste packages, with drip shield, would be about $900,000 (*7*). Given the intense radioactivity present, installing a drip shield or a capillary barrier would almost certainly entail remote handling, but the capillary barrier would be easier and cheaper. The capillary barrier concept remains untried for disposal of spent fuel or high-level waste, although there has been international experience with capillary barriers for disposal of low-level radioactive waste. There should also be tests of barrier integrity under earthquake forces, but ground shaking would be greatly attenuated deep in a geologic repository (*12*).

Another design concept worthy of serious exploration at Yucca Mountain is that of using depleted uranium in waste containers as a sacrificial material to protect the spent fuel. But finding a predictably enduring corrosion-resistant material could be critical, because proof of safety might turn on showing experimentally that failure of the container will not be by general corrosion but by pitting or pinholes. Oxidation of the depleted uranium should in that case occur slowly enough for the spent fuel to be protected from degradation for hundreds of thousands of years. The U.S. Department of Energy (DOE) has enormous stocks of depleted uranium from past uranium enrichment, and this material could be used in casks for storage and transport of spent fuel (*13*) but rigorous testing for its use in casks for final disposal has not been done.

If the Yucca Mountain project should be rejected or abandoned, continued storage of spent fuel in surface facilities is the default option. The most likely new place for such storage is in Utah where, on 9 September 2005, the U.S. Nuclear Regulatory Commission (NRC) denied the state of Utah's appeals to stop a nuclear industry initiative to store fuel on the Skull Valley Goshute Indian reservation (*14*). The availability of this new storage center, where older fuel from many of the 65 widely scattered reactor stations could go, should make for a better Yucca Mountain repository project by dampening legal and political pressures that might otherwise lead to undue haste in design work and the supporting experimentation.

Conditions similar to those at Yucca Mountain are found in rock types around the world wherever there is an arid climate, substantial topographic relief, and a deep-lying water table. Success at Yucca Mountain could powerfully suggest that hosting disposal of spent fuel and high-level waste can be a safe and profitable use for terrain previously deemed a wasteland, and that siting repositories in the future will be much less difficult than it has been in the past. The restraints on a global resurgence of nuclear power in response to growing energy demand and concerns about greenhouse warming are, to be sure, not limited to waste disposal. Nonetheless, a proof of safety for such disposal that is seen internationally as highly robust might relieve a matter of vexing and persistent concern.

References and Notes

1. J. D. Bredehoeft *et al.*, "Geologic disposal of high-level radioactive waste—Earth Science perspectives," *USGS Circular* (no. 779), 3 (1978).
2. "Monthly summary of program financial and budget information, as of November 30, 2004" (Office of Civilian Radioactive Waste Management, U.S. Department of Energy, Las Vegas, NV, 2004), pp. 1–4; (www.ocrwm.doe.gov/pm/budget/index.shtml).
3. R. W. Fri *et al.*, *Technical Bases for Yucca Mountain Standards* (National Academy Press, Washington, DC, 1995), pp. 2, 6, 9.
4. *Total System Performance Assessment—Analyses for Disposal of Commercial and DOE Waste Inventories at Yucca Mountain—Input to Final Environmental Impact Statement and Site Suitability Evaluation* (Rev 00, ICN 02, Bechtel SAIC Co., Las Vegas, NV, for DOE, Las Vegas, NV, December 2001).
5. *Yucca Mountain Science and Engineering Report* (DOE, Washington, DC, February 2002), pp. 11–16.
6. TSPA (*4*), Fig. 6-.
7. *Analysis of the Total System Life Cycle Cost of the Civilian Radioactive Waste Management Program* (DOE, Washington, DC, May 2001), pp. 2-2, 3-6.
8. J. C. S. Long, R. C. Ewing, *Annu. Rev. Earth Planet. Sci.* **32**, 363 (2004).
9. M. J. Apted, in *Proceedings of the Fifth Annual Conference on High-Level Radioactive Waste Management*, Las Vegas, NV, 22 to 26 May 1994, p. 485.
10. W. Zhou, J. Conca, R. Arthur, M. Apted, Analysis and confirmation of the robust performance for the flow-diversion barrier system within the Yucca Mountain site" (Tech. Rep. 107189, prepared by QuantiSci, for the Electric Power Research Institute, Palo Alto, CA, 1996).
11. TRW Environmental Safety Systems, "Total system performance assessment—1995: An evaluation of the potential Yucca Mountain repository" (B00000000-0717-2200-00136, Rev. 01, TRW, Las Vegas, NV, November 1995), pp. 9–84.
12. H. R. Pratt, in *Proceedings of the Workshop on Seismic Performance of Underground Facilities* (Savannah River Laboratory, Aiken, SC, 1981), pp. 74 and 370.
13. C. W. Forsberg, L. R. Dole, in *Proceedings of the Advances in Nuclear Cycle Management III* [CD-ROM], Hilton Head, SC, 3 to 8 October 2003 (American Nuclear Society, La Grange, IL, 2003), session 13–03, pp. 1–14.
14. S. Martin, Private Fuels Storage, LLC, personal communication and news release (www.privatefuelstorage.com/whatsnew/newsreleases/nr9-09-05.html).

10.1126/science.1112786

SYSTEMS BIOLOGY

Less Is More in Modeling Large Genetic Networks

Stefan Bornholdt

As the biology of information processing in the living cell shifts from the study of single signal transduction pathways to increasingly complex regulatory networks, mathematical models become indispensable tools. Detailed predictive models of large genetic networks could revolutionize how researchers study complex diseases, yet such models are not yet within reach. One reason is that experimental data for large genetic systems are incomplete; another is that large genetic systems are difficult to model. Extrapolating the standard differential equations model of a single gene (with its several kinetic parameters) to large systems would render the model prohibitively complicated. One possible way to simplify such models would be to find a "coarse-grained" level of description for genetic networks; that is, to focus on the system behavior of the network while neglecting molecular details wherever possible (see the figure). Such an approach exists for other fields of science—for example, the concept of molecular orbitals in organic chemistry, which mercifully spares us from the details of the underlying quantum physics. On page 496 in this issue, Brandman *et al.* (*1*) points to the possibility of simplifying large genetic network models. Using a standard differential equations approach, the authors find that the intricate internal dynamics of a frequent cellular subcircuit exhibits a simple bistable "ON/OFF" behavior, and thus could be modeled by something much simpler than differential equations—something as simple as a switch.

A first level of coarse-graining in genetic regulation already exists in the standard approach of modeling protein and RNA concentrations with specific equations called "ordinary" differential equations. These equations nicely summarize the molecular interactions that make up the cellular machinery that regulates the activity of a gene. When at least a few tens of molecules are involved in regulating a gene, details of the interactions can usually be neglected, and interaction rates can be used instead of tracking the single molecular binding events (*2*).

With large networks involving thousands of regulatory genes (genes that encode proteins that regulate other genes), the number of differential equations needed to describe the system can become huge. The sheer number of parameters (such as decay rates, production rates, and interaction strengths) in this mathematical model poses a chal-

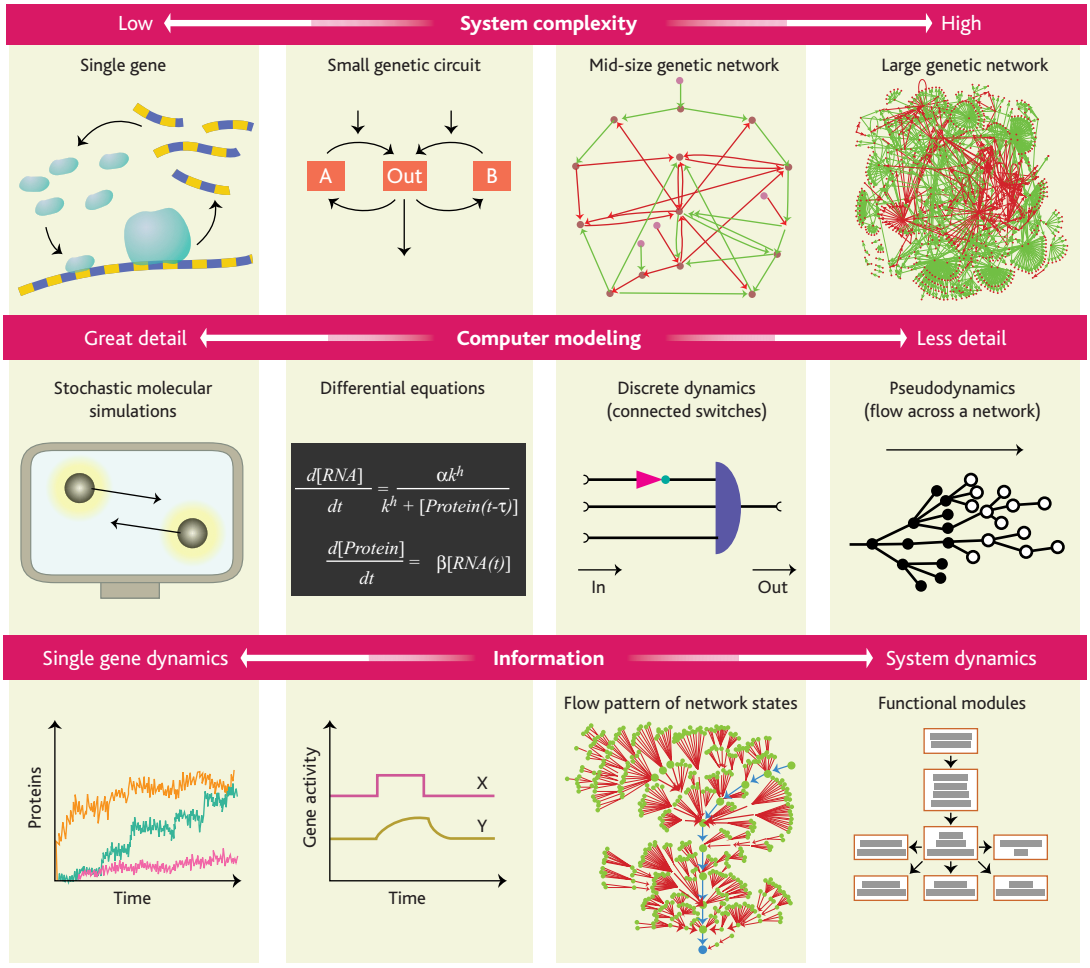

The different levels of description in models of genetic networks. Whereas single genes can be modeled in molecular detail with stochastic simulations (**left column**), a differential equation representation of gene dynamics is more practical when turning to circuits of genes (**center left column**). Approximating gene dynamics by switchlike ON/OFF behavior allows modeling of mid-sized genetic circuits (**center right column**) and still faithfully represents the overall dynamics of the biological system. Large genetic networks are currently out of reach for predictive simulations. However, more simplified dynamics, such as percolating flows across a network structure, can teach us about the functional structure of a large network (**right column**).

The author is with the Institute for Theoretical Physics, University of Bremen, Otto-Hahn-Allee, D-28359 Bremen, Germany. E-mail: bornholdt@itp.uni-bremen.de

Published by AAAS

lenge, both for experiment and theory. A central question is what the right level of description is when constructing quantitative models of large or even systemwide genetic networks (see the figure). Is coarse-graining of genetic network models possible?

A number of general building blocks identified in genetic networks at least indicate that robust simplified models are possible. Modules such as autoregulatory excitatory (positive) feedback loops (which can convert a transient signal into a sustained signal and thus serve as "storage" devices), inhibitory feedback loops (which suppress instability due to noise), or feed-forward loops (which may enhance responsiveness of a gene) represent different kinds of robust switching elements. Brandman *et al*. describe another such building block—the dual positive-feedback loop, which is frequently found in subnetworks of larger cellular and genetic networks. But why would cells have evolved two positive feedback loops when one is enough to create a switch? Brandman *et al*. find that the combination of the two loops can make genetic switching faster and, at the same time, reduce signal noise. A slow loop creates robustness in the signal, whereas a fast loop allows for switching speed. Given the quite complex cellular machinery that is needed to run this dual positive feedback circuit with biochemical means, its dynamic behavior is intriguingly simple. It functions as a particularly robust, yet fast switch that is reminiscent of the robustly designed electronic building blocks used to build modern computers.

This observation provides support for discrete models of genetic networks in which genes are modeled as switchlike dynamic elements that are either ON or OFF. The first such models, generated about 36 years ago, were random networks of discrete dynamical elements, as few data about regulatory genetic networks were available at the time (*3*). These models were long considered to be merely a speculative analogy. However, recent advances in modeling combined with the first opportunities to validate genetic network models with data from living cells show that simplified network models, such as those representing a regulatory gene as a binary (ON/OFF) switch, can indeed predict the overall dynamical trajectory of a biological genetic circuit. For example, the trajectory of the segment polarity network in the fly *Drosophila melanogaster* has been predicted solely on the basis of discrete binary model genes (*4*). Similarly, a dynamic binary model of the genetic network that controls the yeast cell cycle was constructed (*5*). In both systems, the dynamics converge to so-called attractors (states or sequences of states of the genes) and for these, the models match the biological dynamics. These dynamical attractors seem to depend not so much on the details of the kinetic constants, as on the circuit wiring. Insensitivity to biochemical kinetic parameters indicates that for understanding the dynamics of these circuits, it's their wiring that is most important (*6*). This seems to be why large genetic networks can be represented as networks of discrete dynamic elements, without the tuning of parameters. Simplified models on even larger scales are encouraged.

Modeling of large cellular networks is often hampered by incomplete knowledge of the full circuitry, despite a wealth of data. An example of how simplification of the dynamics of single elements enables us to gain valuable information about a system's function is presented in the recent article by Ma'ayam *et al*. (*7*). Here, discrete "pseudo-dynamics" of binary states simply percolate through the known part of a 1500-node mammalian cellular network and give a rough but informative estimate of the property of the regulatory information flow through the system. The thousands of parameters required to generate a standard differential equations model of all the relevant biochemical interactions has been neglected here in favor of a statistical perspective that provides valuable information about the global architecture of a cellular network. It is not a direct representation of the biochemical dynamics and does not allow a detailed dynamic simulation of the network. However, it is an analog of the potential propagation of a signal and therefore useful to determine the global signaling structure of an overall network. This approach is error tolerant and gives a robust picture of the overall global modular structure of a network.

The simple dynamics of the building blocks points to an interesting perspective for our further understanding of genetic networks. Distinguishing between the robust effective dynamics of a genetic or regulatory switch and the biochemical means to practically run it shows that, to understand the system, we do not have to retrace all the details of the biochemistry. Characterizing the circuit wiring seems to be the most important consideration, and when going "dynamic," a clever way to throw away details may be the most important part of model building.

References

1. O. Brandman, J. E. Ferrell Jr., R. Li, T. Meyer, *Science* **310**, 496 (2005).
2. H. H. McAdams, A. Arkin, *Proc. Natl. Acad. Sci. U.S.A.* **94**, 814 (1997).
3. S. A. Kauffman, *J. Theor. Biol.* **22**, 437 (1969).
4. R. Albert, H. G. Othmer, *J. Theor. Biol.* **223**, 1 (2003).
5. F. Li, T. Long, Y. Lu, Q. Ouyang, C. Tang, *Proc. Natl. Acad. Sci. U.S.A.* **101**, 4781 (2004).
6. A. Wagner, *Proc. Natl. Acad. Sci. U.S.A.* **102**, 11775 (2005).
7. A. Ma'ayan *et al*., *Science* **309**, 1078 (2005).

10.1126/science.1119959

CHEMISTRY

The Renaissance of Natural Products as Drug Candidates

Ian Paterson and Edward A. Anderson

Around half of the drugs currently in clinical use are of natural product origin (*1*, *2*). Despite this statistic, pharmaceutical companies have embraced the era of combinatorial chemistry, neglecting the development of natural products as potential drug candidates in favor of high-throughput synthesis of large compound libraries (*3*). Perhaps it is time to reassess this prevailing dogma for chasing quantity over quality.

Cancer chemotherapy, in particular, presents an ideal opportunity for natural product–inspired drug discovery and development. Unfortunately, many of the most promising natural lead compounds are available only in extremely small quantities, especially those from marine organisms such as sponges. The reluctance of industry to pursue such bioactive natural products as potential drugs lies primarily in the perceived supply problem. This leaves organic synthesis as a key option for sourcing these important drug candidates for preclinical and clinical studies. However, the academic-style approach to "hot target molecules" usually results in lengthy synthetic routes owing to their often exquisitely complicated architectures, with long development times, low overall yields, and impracticality of scale-up and provision of diverse structural analogs.

An alternative approach to drug discovery, which has been embraced by the phar-

The authors are in the Department of Chemistry, University of Cambridge, Lensfield Road, Cambridge CB2 1EW, UK. E-mail: ip100@cam.ac.uk

maceutical industry, lies in combinatorial chemistry and diversity-oriented synthesis (*4*). This method offers access to a preselected range of fairly structurally diverse molecules based around a common core, providing large compound libraries in a short time. These in turn fuel high-throughput biological assays, which have become possible through advances in biotechnology and automation. The problem with this approach lies in the relatively low hit rate of these libraries, relative to natural products, and the potential for undesired side effects due to the often less specific binding characteristics of many of these rather simple molecules.

Why do natural products possess such extraordinary specificity and potency compared to artificially designed molecules? The answer lies in evolutionary selection—nature's own high-throughput screening process for the optimization of biologically active compounds. Natural products tend to possess well-defined three-dimensional structures, embellished with functional groups (providing hydrogen bond acceptor/donors, etc.), which have been fine-tuned into a precise spatial orientation. Additionally, the structures of the biological targets of such natural products (e.g., protein binding sites) are often well conserved among proteins of markedly different genetic sequences (*5*, *6*), such that secondary metabolites that have evolved for a certain purpose and mode of action by a producing organism may exert different, yet equally potent, effects in other settings. This leaves open the question of whether further fine-tuning might increase the potency of what really corresponds to a highly advanced lead compound. The preparation of natural product analogs, which are themselves not naturally occurring, may allow humans to tailor and enhance the druglike properties (bioactivity, pharmacokinetics, solubility, etc.) of the medicines that nature has provided.

Structural modification of natural products can be approached in several ways. The first and possibly simplest (although least diverse) is to chemically modify the natural product itself by simple functional-group transformations. This semisynthetic approach has the benefit of providing analogs rapidly, but it is fairly limited in terms of variety. Another possibility is to use genetic engineering to reconstruct biosynthetic pathways (combinatorial biosynthesis) leading to natural product–like structures, but again this has limitations with respect to the extent of possible modification and diversity. Arguably the most versatile approach to analog preparation is the design of a synthetic path to a given natural product that allows for the introduction of deep-seated structural variations en route to the targeted molecule, so-called diverted total synthesis (*7*).

A fine example of a natural product–inspired drug candidate with its developmental roots in total synthesis is the potent oncolytic (cancer cell–killing) agent E7389 (see the figure), currently in phase I clinical trials. E7389 arose from extensive studies toward the total synthesis of halichondrin B (*8*), a highly cytotoxic and complex marine natural product. Zheng *et al.* modified the existing route to halichondrin B for analog synthesis (*9*) and discovered that deletion of a large region of the molecule did not adversely effect its antimitotic properties. Furthermore, increased stability in vivo was realized by replacing the readily cleaved lactone linkage with a ketone. The overall yield for the preparation of E7389 was around 1%; however, as with other highly potent and low-dosage drugs, multigram quantities should be sufficient for clinical development.

A key point from this exercise is that the analog is easier to synthesize than the parent natural product. In fact, this is one of the main aims of analog synthesis—the design of an unnatural relative that maintains or even improves biological activity, while removing unnecessary molecular complexity. The implications from a commercial and practical scale-up viewpoint are obvious. A further compelling illustration of the power of natural product–inspired drug design, embodying the concept of structural simplification, is the development of bryostatin analogs by Wender *et al.* (*10*). Consideration of the mode of action led to a hypothesis that a large part of the bryostatin structure acted as a framework to position three oxygen atoms (highlighted in blue in the figure), within the pharmacophore region, in a certain orientation for binding to the target protein. Simplification of the so-called scaffold region led to analog A, which was found to be more potent than bryostatin (currently in phase II clinical trials as an anticancer agent) in in vitro assays, yet could be prepared by a sufficiently practical route for consideration for large-scale synthesis, which would be extremely challenging for the natural bryostatin structure.

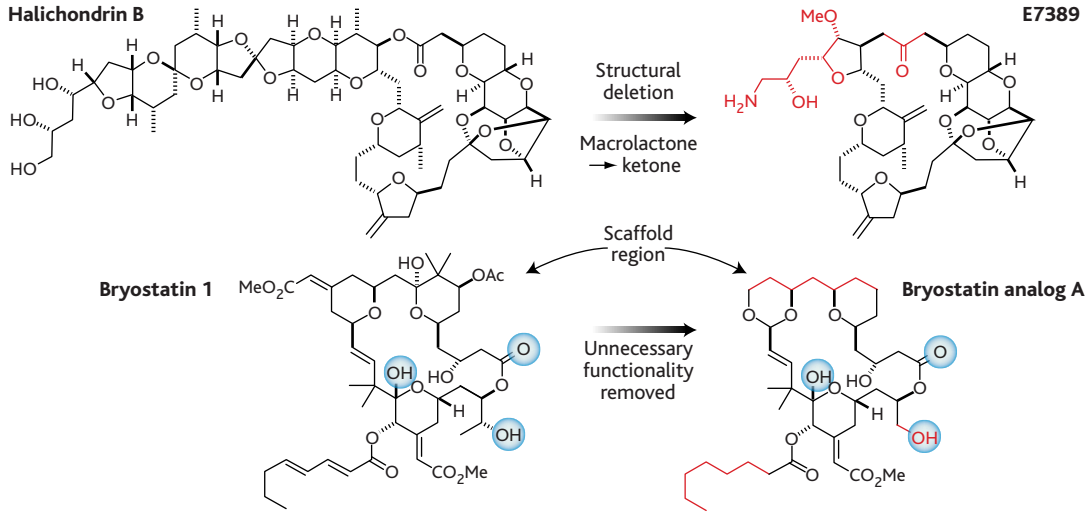

Nature's medicine cabinet. Structural modifications of natural product templates can lead to biologically effective drug candidates. Permutations include structural simplification with the removal of unneeded functional groups and stereochemistry, facilitating chemical synthesis. (Blue circles highlight proposed drug-target interaction sites.)

The microtubule-stabilizing agent discodermolide is available only in minute amounts from its natural origin (a marine sponge). Through the continued evolution and optimization of synthetic strategies, discodermolide has been prepared by increasingly practical routes (*11*, *12*). Moreover, recent reports highlight the ease with which certain analogs, which would not be accessible by direct modification of discodermolide (i.e., semisynthesis) but are again more potent than the parent natural product in preliminary biological assays, can be synthesized efficiently and rapidly (*13*). The ease of analog preparation relies entirely on a sound synthetic route toward the original natural product and underscores the importance of careful planning in total synthesis. Furthermore, an amalgamation of the best features of syn-

thetic routes from several academic groups (by Novartis process chemists) has resulted in an almost combinatorial-style synthesis of discodermolide, readily adaptable to analog preparation, that has provided more than 60 g of active pharmaceutical ingredient to enable its clinical development as an anticancer drug (*14*).

Of course, the opportunities for total synthesis are not restricted to the discovery of anticancer drug candidates. In the case of anti-infectives, analog design may allow us to circumvent drug resistance, in a manner that again cannot be matched by standard methods for antibiotic development. The recent report of a general synthetic route to tetracyclines and analogs shows the potential that lies in this area (*15*). From the outset, this synthesis was designed to access multiple analogs of tetracycline and could be achieved in consistently high overall yield (5 to 7% over 14 steps).

Synthetic developments have thus enabled the designed modification of natural product templates in ways that cannot be readily achieved by biosynthetic means, yet potentially allow large-scale and commercial syntheses. However, despite important advances in synthetic methodology, the typical time scale for the development of truly practical synthetic routes toward complex natural products, and therefore useful derivatives, is still rather lengthy. At present, the development of new drugs seems limited not by our ability to synthesize a given natural product, nor to make analogs, but rather to do so with efficiency and flexibility, and within the short time scale required to compete with high-throughput synthesis and combinatorial chemistry. Despite the challenges that researchers face in the development of such rapid and scalable natural product syntheses, the unbeatable potencies associated with natural molecules selected by evolution should secure their future as a mainstream source of therapeutic agents for many years to come. Furthermore, the continual isolation of an increasing range of novel bioactive secondary metabolites suggests that we have barely scratched the surface of nature's vast library of small-molecule ligands.

References

1. M. S. Butler, *Nat. Prod. Rep.* **22**, 162 (2005).
2. D. J. Newman, G. M. Cragg, K. M. Snader, *J. Nat. Prod.* **66**, 1022 (2003).
3. F. E. Koehn, G. T. Carter, *Nat. Rev. Drug Discov.* **4**, 206 (2005).
4. M. D. Burke, S. L. Schreiber, *Angew. Chem. Int. Ed.* **43**, 46 (2004).
5. C. Zhang, C. DeLisi, *J. Mol. Biol.* **284**, 1301 (1998).
6. V. Anantharaman, L. Aravind, E. V. Koonin, *Curr. Opin. Chem. Biol.* **7**, 12 (2003).
7. J. T. Njardarson *et al.*, *J. Am. Chem. Soc.* **126**, 1038 (2004).
8. T. D. Aicher *et al.*, *J. Am. Chem. Soc.* **114**, 3162 (1992).
9. W. Zheng *et al.*, *Bioorg. Med. Chem. Lett.* **14**, 5551 (2004).
10. P. A. Wender *et al.*, *Curr. Drug Discov. Technol.* **1**, 1 (2004).
11. I. Paterson, G. J. Florence, *Eur. J. Org. Chem.* **2003**, 2193 (2003).
12. A. B. Smith III *et al.*, *J. Am. Chem. Soc.* **122**, 8654 (2000).
13. S. J. Shaw *et al.*, *J. Am. Chem. Soc.* **127**, 6532 (2005).
14. S. J. Mickel *et al.*, *Org. Proc. Res. Dev.* **8**, 122 (2004).
15. M. G. Charest, C. D. Lerner, J. D. Brubaker, D. R. Siegel, A. G. Myers, *Science* **308**, 395 (2005).

10.1126/science.1116364

APPLIED PHYSICS

Molecular Orbitals Tell the Story

James N. O'Shea

To understand the rich physics of molecular nanostructures and solids, there are times when high-resolution photoemission data are all we need to build a detailed picture of the electronic structure. At other times, structural information from x-ray diffraction or scanning tunneling microscopy (STM) can reveal precisely what is going on at the molecular level. But the most intriguing questions often leave us wishing that we could simply get in there and take a good look at the single-molecule level. On page 468 of this issue, Wachowiak *et al.* describe how they have done precisely this in order to observe the molecular distortion in an insulating monolayer of K_4C_{60} by using a combination of topographic and spectroscopic STM at low temperature (*1*).

Enhanced online at www.sciencemag.org/cgi/content/full/310/5747/453

The particular distortion in question results from the Jahn-Teller (JT) effect, a phenomenon with a long history. JT distortions arise when a system is degenerate—that is, it exhibits two or more distinct states with exactly the same energy. Nature tries to avoid this situation if there is an energy saving to be made by a molecule undergoing a physical distortion so as to split the energy levels apart. JT distortions are thought to play a key role in the electronic properties of the alkali metal (A) fullerides A_nC_{60}, which range from insulating to metallic (*2*) and even high-temperature superconductivity (*3*).

There are technological considerations as well. C_{60} is an ideal building block for molecular devices because electrons can easily be donated to the fullerene cage from other molecules, atoms, and surfaces. In the case of A_nC_{60}, about one electron is transferred from each alkali-metal atom that sits in the interstitial sites of a C_{60} crystal or monolayer. So where do these electrons go?

Pure C_{60} is insulating. Its highest occupied molecular orbital (HOMO) is a fivefold degenerate band with a full complement of 10 electrons, whereas the lowest unoccupied molecular orbital (LUMO), some 2 eV above it, is a threefold degenerate band that could hold 6 electrons but is in fact completely empty. C_{60} is therefore a band insulator (see the figure). Additional electrons donated from the alkali-metal atoms are transferred into the LUMO, and on this basis we can intuitively understand why K_3C_{60} is metallic (because it has a half-filled conduction band). Perhaps the more compelling question, then,

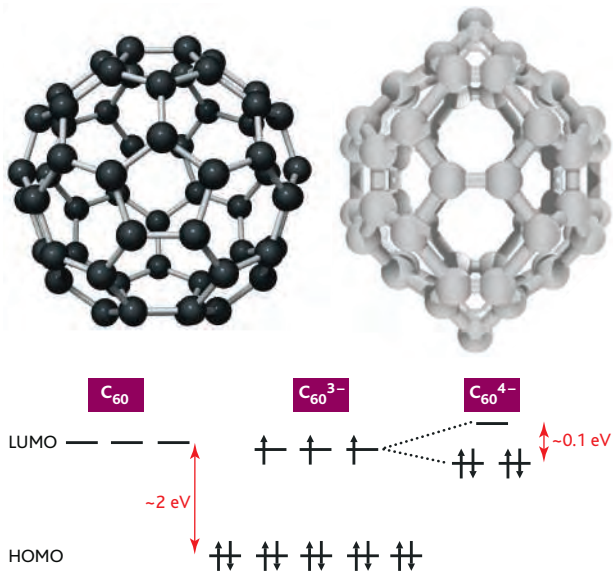

Squeezed fullerenes. Geometric and electronic structure of doped C_{60} molecules. (**Top left**) Undoped and undistorted insulating C_{60}. (**Top right**) JT distorted C_{60}^{4-}. (**Center**) The addition of electrons into the threefold degenerate LUMO of C_{60} and C_{60}^{3-} and (**center right**) the JT splitting of the LUMO for distorted C_{60}^{4-}.

The author is with the Nanoscience Group, School of Physics and Astronomy, University of Nottingham, Nottingham NG7 2RD, UK. E-mail: james.oshea@nottingham.ac.uk

is why K_4C_{60} and a host of other A_nC_{60} compounds are not metallic, despite having a partially filled LUMO band.

In fact, the underlying physics of both these compounds is intriguing because their strong interelectron repulsion should outweigh the energy gained by delocalizing the electrons in the crystal, thus driving these compounds to an insulating state. However, in A_3C_{60}, the orbital degeneracy of the LUMO lessens this effect by providing multiple hopping channels for an electron to reach a neighboring site (*4*, *5*). A_3C_{60} compounds, it seems, sit quite precariously on the metallic (and superconducting) side of a metal-insulator transition, so why not also A_4C_{60}?

The answer almost certainly lies in the lifting of the orbital degeneracy (*6*) of the LUMO in A_4C_{60} by the JT effect (*7*). In this case, it is a spontaneous molecular distortion arising from the coupling of degenerate electronic orbitals with certain vibrational modes of the molecule, leading to a lowering of the total energy. In A_4C_{60}, the JT distortion splits the LUMO into two lower (and now fully occupied) degenerate levels and an empty level some 0.1 eV higher in energy (see the figure).

The experiment of Wachowiak *et al.* reveals the story of the JT distortion in monolayer K_4C_{60} as told by the molecular orbitals involved. The researchers use a surface on which both the metallic K_3C_{60} and insulating K_4C_{60} phases exist simultaneously, which allows direct comparison between the two compounds from both topographic and spectroscopic points of view. Wachowiak *et al.* show clearly the metallic and insulating nature of the molecules directly beneath the STM tip by mapping the local density of states, of both occupied and unoccupied molecular orbitals, and observing the presence or absence of an energy gap at the Fermi level. When imaging the spatial distribution of the frontier molecular orbitals, they observe very different symmetries for the occupied and unoccupied states. This in itself is indicative of a JT distortion, which affects the two states in different ways, in contrast to the nondistorted molecules of the K_3C_{60} phase. However, a very powerful extension of this approach is the incorporation of detailed theoretical calculations of the expected molecular wavefunctions. Although there are three separate C_{60}^{4-} distortions consistent with a JT distortion (indistinguishable from an energetic perspective), only one of these was found to be consistent with the observed topographic images of the molecular orbitals. This combination of experiment and theory is becoming increasingly prevalent in many areas of science and has a very important role to play, especially in the study of molecular nanostructures with both imaging and spectroscopic techniques.

The work of Wachowiak *et al.* was carried out at low temperature, where infrared data for bulk K_4C_{60} have previously suggested a static JT distortion (*8*). Although structural evidence for the distortion has been observed for fully orientationally ordered Cs_4C_{60} at higher temperatures by neutron diffraction (*9*), the same cannot be said for K_4C_{60}. This has prompted suggestions that at these higher temperatures, molecular orientations in K_4C_{60} are either complex or disordered or that the JT distortion is not static at room temperature but rather exerts a dynamical effect (*10*). The molecules in the K_4C_{60} monolayers studied by Wachowiak *et al.* are certainly ordered and the JT distortion is clearly static, but is this driven to a dynamical JT effect at higher temperatures? Clearly, we have reached another question that is best answered at the single-molecule level. Indeed, there are a myriad of questions surrounding molecular interactions and the mechanisms of molecular electronics that need to be addressed. What is also clear is that the molecular orbitals of these and other systems can tell the story at the single-molecule level, and that by combining reliable calculations with high-resolution techniques that can probe these molecular orbitals, we can address many unanswered questions about the fundamental workings of molecular nanostructures.

References

1. A. Wachowiak *et al. Science* **310**, 468 (2005).
2. R. C. Haddon *et al. Nature* **350**, 320 (1991).
3. A. F. Hebard *et al. Nature* **350**, 600 (1991).
4. P. Durand *et al. Nat. Mater.* **2**, 605 (2003).
5. O. Gunnarsson *Rev. Mod. Phys.* **69**, 575 (1997).
6. N. Manini *et al Phys. Rev. B* **49**, 13008 (1994).
7. H. A. Jahn, E. Teller, *Proc. R. Soc. London Ser. A* **161**, 220 (1937).
8. K. Kamarás *et al., Phys. Rev. B* **65**, 052103 (2003).
9. P. Dahlke, M. J. Rosseinsky *Chem. Mater.* **14**, 1285 (2002).
10. M. Fabrizio, E. Tosatti *Phys. Rev. B* **55**, 13465 (1997).

10.1126/science.1119274

EVOLUTION

Changing the Cofactor Diet of an Enzyme

Andrew D. Ellington and J. J. Bull

Certain molecular processes are fundamental to all free-living organisms. The minimal set of genes necessary for life may be as small as a few hundred, as can be inferred from genome sequence comparisons across diverse organisms (*1*). Because this minimal set is so fundamental, it would be especially rewarding to understand the requirements for, and constraints on, a minimal metabolism. Understanding these parameters should also provide insights into how metabolism originally evolved. Yet such an endeavor seems fraught with one basic problem: If all life requires an essential function, how can we study life without that function?

On page 499 in this issue, Lunzer *et al.* (*2*) addresses a fundamental issue in metabolic evolution and gets around this dilemma. The authors choose a limited but relatively invariant feature of metabolism—biosynthesis of the amino acid leucine. All known forms of life need leucine. Those organisms that synthesize it use an enzyme called isopropylmalate dehydrogenase. In turn, this enzyme uses the coenzyme nicotinamide adenine dinucleotide (NAD^+) as a hydride acceptor during an oxidative decarboxylation. Not only is the use of NAD^+ by isopropylmalate dehydrogenase found in all three domains of life, but NAD^+ is the only cofactor so far found to be used by this enzyme. We can thus presume that this property of leucine biosynthesis is at least as old as the last common ancestor of modern life.

This invariant use of NAD^+ might be less puzzling were it not that a related tricarboxylic acid cycle enzyme, isocitrate dehydrogenase, uses NAD^+ as a cofactor in some species but uses nicotinamide adenine dinucleotide phosphate ($NADP^+$) in others. Why, then, does isopropylmalate dehydrogenase use only NAD^+? Although there are apparently no extant natural enzymes that could help answer this question, it can nonetheless be addressed by enzyme engineering. Studies of the reaction kinetics and mechanism of isocitrate dehydrogenase, combined with crystal structures and phylogenetic

The authors are in the Departments of Chemistry and Integrative Biology, Institute for Cell and Molecular Biology, University of Texas at Austin, Austin, TX 78712, USA. E-mail: bull@bull.biosci.utexas.edu, andy.ellington@mail.utexas.edu

analyses of isopropylmalate dehydrogenase (*3*), allowed Lunzer *et al*. to design a form of isopropylmalate dehydrogenase that would use $NADP^+$ instead of NAD^+. In all, they designed and analyzed 164 variants of isopropylmalate dehydrogenase, one of which was predicted to be the best for $NADP^+$ use and the others which would allow them to explore the fitness landscape and develop a predictive model of the switch. One of the striking results of this analysis is the tight coupling of empirical results with a highly accurate, predictive model of enzyme performance based on amino acid identities at just six sites in the molecule. Surprisingly, an additive model of amino acid effects across the six sites explains over 90% of the variance, whether enzyme performance and preference with NAD^+, with $NADP^+$, or their ratio is considered.

The rationally designed molecule worked in vitro with $NADP^+$; indeed, it performed essentially as well as the parent molecule performed with NAD^+. This experimental success raised a puzzle. If isopropylmalate dehydrogenase could work with $NADP^+$, why was life confined to using NAD^+ for this step of leucine biosynthesis? This question is particularly relevant given that many dehydrogenases involved in biosynthesis (including amino acid biosynthesis) use the chemically segregated pool of $NADP^+$ rather than NAD^+. The obvious answer to the question, as any evolutionary biologist knows, is the historical accident model: The last common ancestor had an isopropylmalate dehydrogenase that used NAD^+, and NAD^+ use became entrenched so that the switch to $NADP^+$ was not possible without several mutations at once. However, this answer proves untenable. Changes in $NAD^+/NADP^+$ cofactor specificity have been effected in dehydrogenases on numerous occasions, and typically (and surprisingly) require relatively small numbers of amino acid changes (*4*, *5*). On this occasion, only five substitutions were required, and fewer substitutions resulted in partial changes in specificity. Thus, there is no inherent or historical reason why isopropylmalate dehydrogenase could not use $NADP^+$ as a cofactor.

The authors offer an alternative explanation, based partly on an in vivo experiment. They also reintroduced the engineered isopropylmalate dehydrogenase into bacteria in place of the normal enzyme and measured fitness in culture. Even though the cofactor swap had no effect in vitro, the engineered isopropylmalate dehydrogenase did not work so well in vivo, growing at approximately 90% of the wild-type rate. The explanation proffered, and still awaiting tests, is that the new enzyme has a high affinity for both $NADP^+$ and its reaction product NADPH. The affinity for NADPH was not a problem in vitro, because NADPH was not present in the reaction mix. But NADPH is present at high concentrations in a growing cell and would therefore partially inhibit the enzyme. The isopropylmalate dehydrogenase has evolved or maintains the ability to use the NAD^+ pool of oxidized cofactor rather than the NADPH pool of reduced cofactor because this step in leucine biosynthesis is oxidative, not reductive. Of course, this begs the question of why isocitrate dehydrogenase can use both cofactors, until it is realized that the NADP-dependent enzyme occurs in organisms that have an associated isocitrate lyase and can use the pair of enzymes for growth on acetate and the production of NADPH for biosynthesis.

This is not the first time that the evolution and utility of NAD^+ have been considered. For example, Benner and co-workers have suggested that the use of the R- versus S-hydrides of NADH is under selective pressure to match the redox potential of natural substrates (*6*). However, what is new here is actually coupling enzyme and metabolic engineering with fitness measures that can provide substance for the "just-so" speculative stories that are typically crafted to explain enzyme evolution. Given the increasing number of unnatural enzymes and pathways that are being created, such as kinases that use N6-benzyl-ATP (*7*) and organisms that use unnatural amino acids (*8*), there should be increasing opportunities to measure the fitness and evolution of these unnatural organisms and thereby better understand the long-gone history of natural selection.

Another unexpected benefit of the story told by Lunzer *et al*. is that it provides proof for a fundamental issue relating to the origin and evolution of life (see the figure). It has been suggested that an RNA world preceded modern biochemistry, in part because of the prevalence of nucleotide-based cofactors such as NAD^+. This prevalence has in turn been suggested to be driven by the nature of metabolism at the time cofactors evolved: A metabolism organized around nucleotides and ribozymes would have evolved nicotinamide adenine dinucleotide rather than an equally plausible nicotinamide amino acid. Ribo-cofactors may have been conserved past the transition from an RNA world to the modern, protein-based world because changing a well-established cofactor would result in an evolutionary nadir. Any possible benefit of evolving and using a nicotinamide amino acid at this point would be overshadowed by the selective disadvantage of suddenly having thousands of dehydrogenases and other enzymes that could not possibly use the new compound without vast changes in their active sites and sequences. By showing that even a single dehydrogenase is subject to selection against a change as simple as using a different pool of an otherwise natural cofactor, the work with isopropylmalate dehydrogenase substantively bolsters conjectures about why we still are using the same ribocofactors that were present during the heyday of the RNA world, likely more than 3 billion years ago.

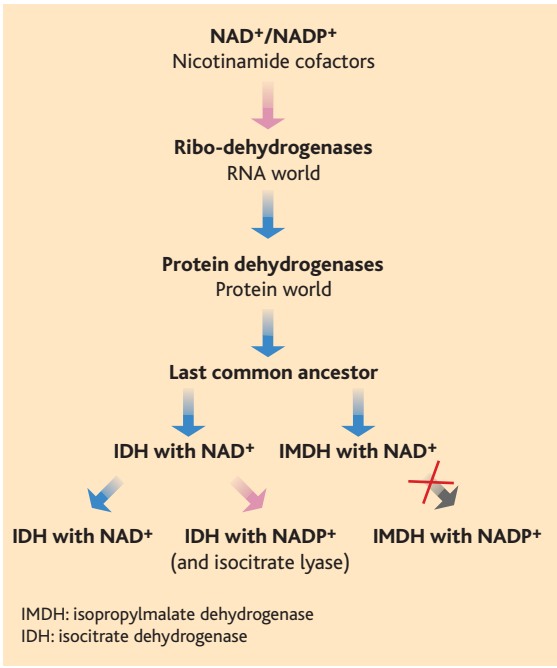

Putative descent of nicotinamide cofactors from the RNA world to the present. NAD^+ and perhaps $NADP^+$ were adopted in the RNA world as redox cofactors suited to ribozymes. With the advent of translation, ribozymes were replaced by protein enzymes of similar function and likely with similar cofactor specificities (*9*). Evolutionary constraints on cofactor choice (blue arrows); evolutionary adaptations to utilize new cofactors (red arrows). The experiment in Lunzer *et al*. (x) indicates a fitness nadir.

References

1. A. Mushegian, *Curr. Opin. Genet. Dev.* **9**, 709 (1999).
2. M. Lunzer, S. P. Miller, R. Felsheim, A. M. Dean, *Science* **310**, 499 (2005).
3. G. Zhu, G. B. Golding, A. M. Dean, *Science* **307**, 1279 (2005).
4. N. Holmberg, U. Ryde, L. Bulow, *Protein Eng.* **12**, 851 (1999).
5. H. Flores, A. D. Ellington, *Protein Eng. Des. Sel.* **18**, 369 (2005).
6. S. A. Benner, *Experientia* **38**, 633 (1982).
7. Y. Liu, K. Shah, F. Yang, L. Witucki, K. M. Shokat, *Chem. Biol.* **5**, 91 (1998).
8. J. W. Chin *et al*., *Science* **301**, 964 (2003).
9. H. B. White. *J. Mol. Evol.* **7**, 101 (1976).

10.1126/science.1120279

Ice-Sheet and Sea-Level Changes

Richard B. Alley,[1*†] Peter U. Clark,[2*] Philippe Huybrechts,[3,4*] Ian Joughin[5*]

Future sea-level rise is an important issue related to the continuing buildup of atmospheric greenhouse gas concentrations. The Greenland and Antarctic ice sheets, with the potential to raise sea level ~70 meters if completely melted, dominate uncertainties in projected sea-level change. Freshwater fluxes from these ice sheets also may affect oceanic circulation, contributing to climate change. Observational and modeling advances have reduced many uncertainties related to ice-sheet behavior, but recently detected, rapid ice-marginal changes contributing to sea-level rise may indicate greater ice-sheet sensitivity to warming than previously considered.

Because a heavy concentration of the population lives along coastlines, even small amounts of sea-level rise would have substantial societal and economic impacts through coastal erosion, increased susceptibility to storm surges, groundwater contamination by salt intrusion, and other effects. Over the last century, sea level rose ~1.0 to 2.0 mm/year, with water expansion from warming contributing 0.5 ± 0.2 mm (steric change) (*1*, *2*) and the rest from the addition of water to the oceans (eustatic change) due mostly to melting of land ice (*2*). By the end of the 21st century, sea level is projected to rise by 0.5 ± 0.4 m in response to additional global warming (*2*), with potential contributions from the Greenland and Antarctic ice sheets dominating the uncertainty of that estimate.

These projections emphasize surface melting and accumulation in controlling ice-sheet mass balance, with different relative contributions for warmer Greenland and colder Antarctica (*3*). The Greenland Ice Sheet may melt entirely from future global warming (*4*), whereas the East Antarctic Ice Sheet (EAIS) is likely to grow through increased accumulation for warmings not exceeding ~5°C (*5*). The future of the West Antarctic Ice Sheet (WAIS) remains uncertain, with its marine-based configuration raising the possibility of important losses in the coming centuries (*2*). Despite these uncertainties, the geologic record clearly indicates that past changes in atmospheric CO_2 were correlated with substantial changes in ice volume and global sea level (Fig. 1).

Recent observations of startling changes at the margins of the Greenland and Antarctic ice sheets indicate that dynamical responses to warming may play a much greater role in the future mass balance of ice sheets than previously considered. Models are just beginning to include these responses, but if they prove to be important, sea-level projections may need to be revised upward. Also, because sites of global deepwater formation occur immediately adjacent to the Greenland and Antarctic ice sheets, any notable increase in freshwater fluxes from these ice sheets may induce changes in ocean heat transport and thus climate. Here, we review these new developments in understanding ice-sheet mass balance and discuss their possible implications to future sea level and climate.

Paleoglaciology

The record of past glacial changes provides important insight to the behavior of large ice sheets during warming. At the last glacial maximum about 21,000 years ago, ice volume and area were more than twice modern values (*6*). Deglaciation was forced by warming from changes in Earth's orbital parameters, increasing greenhouse gas concentrations, and other attendant feedbacks. Deglacial sea-level rise averaged 10 mm/year, but with variations including two extraordinary episodes at 19,000 years before present (19 kyr B.P.) and 14.5 kyr B.P. (Fig. 2), when peak rates potentially exceeded 50 mm/year (*7*–*9*). Each of these "meltwater pulses" added the equivalent of 1.5 to 3 Greenland Ice Sheets to the oceans over a period of one to five centuries.

The freshwater fluxes associated with these events apparently induced large changes in ocean circulation and attendant heat transport. An important component of the ocean's overturning circulation involves deepwater formation in the North Atlantic Ocean and around the Antarctic continent, particularly in the Weddell and Ross Seas. Accordingly, partial collapse of northern ice into the North Atlantic Ocean at 19 kyr B.P. may have weakened North Atlantic deepwater formation, causing widespread cooling (*9*). In contrast, a large contribution of Antarctic ice to the event of 14.5 kyr B.P. (*10*) would have freshened the Southern Ocean, perhaps strengthening the Atlantic meridional overturning circulation (AMOC) and causing widespread warming (*11*).

Ice-Sheet Mass Balance

Ice-sheet mass balance can be estimated by taking the difference between ice input and output fluxes or by monitoring changes in ice-sheet elevation as a proxy for volume changes. Input, primarily from precipitation, can be estimated from field measurements and by atmospheric modeling. Output, primarily from surface melt, sub–ice-shelf melt, or iceberg calving, can be calculated from melt models or ice-velocity measurements from interfero-

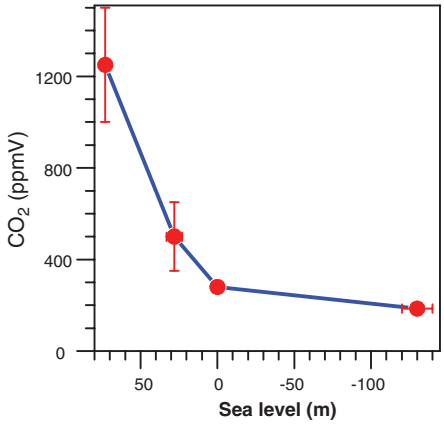

Fig. 1. Relation between estimated atmospheric CO_2 and the ice contribution to eustatic sea level indicated by geological archives and referenced to modern (pre-Industrial Era) conditions [CO_2 = 280 parts per million by volume (ppmV), eustatic sea level = 0 m]. The most recent time when no permanent ice existed on the planet (sea level = +73 m) occurred >35 million years ago when atmospheric CO_2 was 1250 ± 250 ppmV (*54*). In the early Oligocene (~32 million years ago), atmospheric CO_2 decreased to 500 ± 150 ppmV (*54*), which was accompanied by the first growth of permanent ice on the Antarctic continent, with an attendant eustatic sea-level lowering 45 ± 5 m (*55*). The most recent time of low atmospheric CO_2 (185 ppmV) (*56*) corresponds to the Last Glacial Maximum 21,000 years ago, when eustatic sea level was –130 ± 10 m (*8*). Error bars show means ± SD.

[1]Department of Geosciences and Earth and Environmental Systems Institute, Pennsylvania State University, Deike Building, University Park, PA 16802, USA. [2]Department of Geosciences, Oregon State University, Corvallis, OR 97331, USA. [3]Alfred-Wegener-Institut für Polar- und Meeresforschung, Postfach 120161, D-27515 Bremerhaven, Germany. [4]Departement Geografie, Vrije Universiteit Brussel, Pleinlaan 2, B-1050 Brussel, Belgium. [5]Polar Science Center, Applied Physics Lab, University of Washington, 1013 NE 40th Street, Seattle, WA 98105, USA.

*These authors contributed equally to this work.
†To whom correspondence should be addressed. E-mail: rba6@psu.edu

metric synthetic-aperture radar (InSAR). Monitoring changing ice volume by repeat altimetry from aircraft or satellite is increasingly important, after correction for any isostatic adjustments of bedrock elevation in response to past ice-load changes and for changing density of the snow and ice column in response to changing climate. Although some altimetry data were collected in the 1970s, comprehensive mass-balance observations did not begin until the early 1990s, precluding separation of decadal or subdecadal variability from longer term trends. Nevertheless, observations have documented changes in Greenland and Antarctica including notable increases in ice discharge, especially since the mid- to late 1990s (*12*, *13*).

For Greenland, updated estimates based on repeat altimetry, and the incorporation of atmospheric and runoff modeling, indicate increased net mass loss, with most change toward the coasts (*13*). Between 1993 to 1994 and 1998 to 1999, the ice sheet was losing 54 ± 14 gigatons per year (Gt/year) of ice, equivalent to a sea-level rise of ~0.15 mm/year (where 360 Gt of ice = 1 mm sea level). The excess of meltwater runoff over surface accumulation was about 32 ± 5 Gt/year, leaving ice-flow acceleration responsible for loss of ~22 Gt/year. Despite highly anomalous excess snowfall in the southeast in 2002 to 2003, net mass loss over the 1997-to-2003 interval was higher than the loss between 1993 and 1999, averaging 74 ± 11 Gt/year or ~0.21 mm/year sea-level rise, with increases in both the excess of surface melt over snow accumulation (42 ± 6 Gt/year) and the ice-flow loss. Summers were warmer from 1997 to 2003 than from 1993 to 1999, which likely explains the increased surface melt (*13*). These results are broadly similar to those from a mesoscale atmospheric model used to simulate the surface mass balance of the Greenland Ice Sheet from 1991 to 2000 (*14*). Accounting for additional mass loss from iceberg discharge and basal melting (assumed constant) yielded an estimated net mass loss of 78 Gt/year. Large interannual variability did not obscure significant simulated trends toward increased melting and snowfall consistent with reconstructed warming, especially in west Greenland.

In Antarctica, altimetry-derived estimates show thickening in EAIS (*15*) but thinning along the Amundsen Coast of WAIS (*15*–*17*). From 1992 to 2003, measured thickening (1.8 ± 0.3 cm/year) of the larger EAIS more than balances measured WAIS thinning (0.9 ± 0.3 cm/year); assigning snow density to the changes in EAIS owing to correlation with rising accumulation rate, but ice density to WAIS changes in light of probable dynamic contributions, yields a combined mass gain of ~33 ± 8 Gt/year (*15*). However, data gaps remain, including on the Antarctic Peninsula and near the South Pole, and additional uncertainty arises from lack of knowledge of changing density in upper layers. Mass-balance estimates covering an overlapping subset of drainage basins and times also suggest EAIS growth (20 ± 21 Gt/year) and show WAIS loss (44 ± 13 Gt/year) (*12*). Atmospheric modeling indicates that increasing snow accumulation has been important over the last decades (*15*, *18*), perhaps in response to weak warming, especially in coastal regions (*19*).

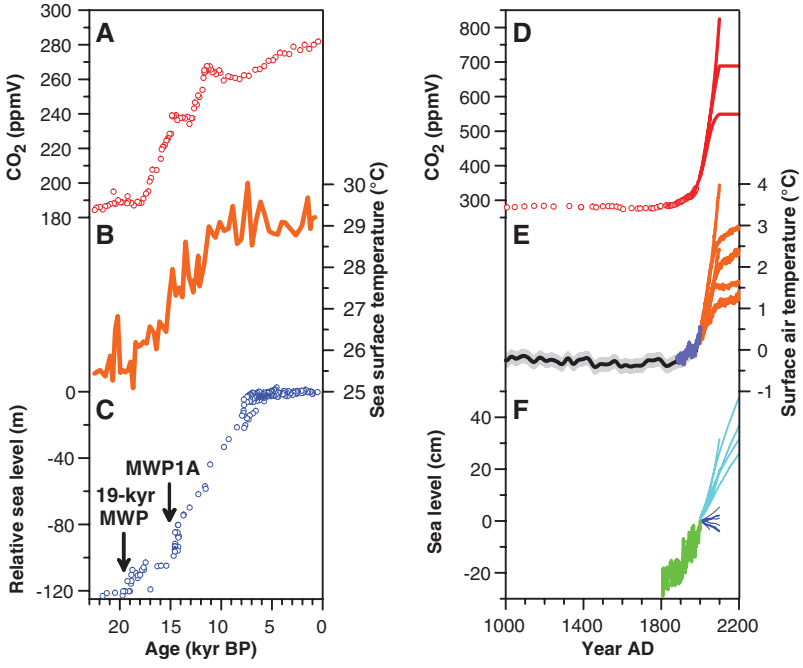

Fig. 2. Time series of key variables encompassing the last interval of significant global warming (last deglaciation) (left) compared with the same variables projected for various scenarios of future global warming (right). (**A**) Atmospheric CO_2 from Antarctic ice cores (*56*). (**B**) Sea surface temperature in the western equatorial Pacific based on Mg/Ca measured in planktonic foraminifera (*57*). (**C**) Relative sea level as derived from several sites far removed from the influence of former ice-sheet loading (*8*, *58*–*60*). MWP, meltwater pulse. (**D**) Atmospheric CO_2 over the past millennium (circles) and projections for future increases (solid lines). Records of atmospheric CO_2 are from Law Dome, Antarctica (*61*), and direct measurements since 1958 are from Mauna Loa, Hawaii (*62*). Also shown are three emission scenarios for time evolution of atmospheric CO_2 over the course of the 21st century and subsequent stabilization through the 22nd century (*63*). (**E**) Temperature reconstruction for Northern Hemisphere from 1000 to 2000 AD (*64*) (gray time series), global temperature based on historic measurements, 1880 to 2004 (*65*) (blue time series), and projected warming based on simulations with two global coupled three-dimensional (3D) climate models with the use of three emission scenarios (*66*) (orange time series). (**F**) Relative sea-level rise during the 19th and 20th centuries from tide gauge record at Brest, France (*67*) (green time series), projections for contributions from combined Greenland and Antarctic ice sheets (*3*) (dark blue time series), and projections for sea-level rise from thermal expansion based on climate simulations shown in (E) (light blue time series) (*66*).

Modeling

Interpretation of past changes and projection of future changes requires modeling. Two major traditions of ice-deformation modeling have developed, reflecting the very different stress regimes for inland ice versus ice shelves. Current comprehensive ice-sheet models typically treat inland ice and ice shelves separately, with regime coupling, but this approach does not fully capture the transitional behavior of ice streams and outlet glaciers (*5*). Use of this approach is motivated in part by poor understanding of the basal boundary condition in transition zones. Computational limitations also dictate rather coarse grid spacings, numerically widening and slowing fast-flowing ice streams. Because slower flowing ice cannot contribute as rapidly to sea-level change, this grid coarsening can cause models to respond more slowly than actual ice sheets. Furthermore, actual ice sheets transmit longitudinal stress perturbations almost instantaneously, but inland-ice models do not. Accordingly, these ice-sheet models may underestimate rates of change.

Despite their limitations, coupled-regime models show substantial skill in simulating ongoing changes, except in the rapidly changing marginal regions. Recent coupled-regime simulations (*3*) with mass balance driven by climate-model output suggest that 20th-century surface forcing should have caused slight inland thickening in Antarctica and Greenland, and coastal thinning in Greenland. These results show relatively little long-term trend in Greenland, but a long-term Antarctic thinning trend from the end of the last ice age, especially for WAIS. The modeled behavior in Greenland agrees with available data within stated errors (*13*), except for the highly variable ice-marginal changes discussed below. The modeled long-term Antarctic trend shows

poorer agreement with the limited data (*16*); this may reflect the short time span of the data or uncertainty in timing of ice-age forcing. The simulated Antarctic response to 20th-century forcing matches many observations in areas controlled mainly by changes in accumulation rate. However, rapid changes in some regions such as the Amundsen Coast are not simulated, in part because the oceanic forcing thought responsible for these shifts was not included.

Rapid Ice-Marginal Changes

The theory that ice shelves or ice tongues buttress fast-flowing ice streams and outlet glaciers, preventing faster flow and ice-sheet shrinkage or collapse (*20*), was disputed by subsequent work [such as (*21*)] but is again supported by recent observations and modeling.

On Greenland's west coast, Jakobshavn Isbrae, which drains about 6% of the ice-sheet area, experienced slight slowing from 1985 to 1992 but remained among the fastest glaciers on Earth. Jakobshavn has subsequently nearly doubled its flow speed and thinned rapidly, with the speedup extending ~30 km inland (*22*, *23*). Increased surface melting alone cannot explain this thinning. Instead, Jakobshavn Isbrae's acceleration in association with the loss of its floating ice tongue suggests a dynamic thinning following loss of restraint to flow provided by the ice tongue (Fig. 3) (*22*–*24*).

Although Jakobshavn Isbrae is the most notable example, laser altimeter surveys over a 5-year interval document that the lower sections of many other Greenland outlet glaciers also thinned (*25*). As for Jakobshavn Isbrae, surface melting cannot account for much of this thinning. The largest changes are found near the fronts of fast-moving outlet glaciers that feed small ice shelves or tongues that have retreated in response to atmospheric or ocean warming, suggesting that warming-induced reduction of ice-shelf restraint triggered flow acceleration. Taken together, accelerated discharge of documented Greenland outlet glaciers may have contributed up to ~0.09 mm/year to sea level since the mid-1990s (*13*, *23*).

Altimetry surveys and InSAR data document recent acceleration of the WAIS contribution to sea-level rise as a result of rapid ice-marginal changes. Along the Antarctic Peninsula, warming over the last few decades has caused retreat or near-total loss of several ice shelves, at least some of which had persisted for millennia (*26*). Ice shelves are susceptible to attack by warming-induced increases of meltwater ponding in crevasses that cause hydrologically driven fracturing (*27*) and by warmer subshelf waters that increase basal melting (*28*). Responses to ice-shelf breakup have been noteworthy. Collapse of the Larsen B Ice Shelf in 2002 was followed by speedup of its major tributary glaciers, by twofold to eightfold where they entered the former ice shelf; speedup decreased inland but was recognizable for roughly 10 km inland and contributed about 0.07 mm/year to sea-level rise; adjacent glaciers still buttressed by shelf ice changed little (*29*, *30*). Loss of the Larsen A Ice Shelf, north of the Larsen B, seems to have caused acceleration of tributary glaciers (*30*), and observed acceleration of tributary flow to the former Wordie Ice Shelf on the other side of the Antarctic Peninsula may have been linked to loss of that ice shelf as well (*31*). Models indicate that geometric and other factors contribute to the magnitude and speed of tributary-glacier response to ice-shelf reduction (*32*), so the range of observed responses is not surprising.

Recent changes in glaciers along the Amundsen Coast of WAIS are also contributing to sea-level rise, with discharge in excess of accumulation accounting for 0.13 ± 0.02 mm/year (*33*) to 0.24 mm/year (*34*). In Pine Island Bay of this coast, ice-shelf thinning at rates locally exceeding 5 m/year (*33*) was accompanied by grounding-line retreat of 1.2 km/year in the early 1990s (*35*). Apparently in response, large glaciers feeding Amundsen Coast ice shelves have thinned and accelerated by up to 26% over the last three decades, with perturbations extending more than 200 km inland (*17*, *34*, *36*). Although acceleration of Amundsen Coast glaciers increased mass flux to ice shelves, the shelves have thinned, suggesting increased basal melting likely from increased penetration of relatively warm Circumpolar Deep Water (*37*).

Not all ice-dynamical anomalies are causing thinning. On the Siple Coast of WAIS, thinning has switched to thickening as Whillans ice stream (ice stream B) slowed between 1974 and 1997, causing the ice-sheet contribution to sea-level rise in 1997 to be 0.03 mm/year smaller than if 1974 velocities had been maintained (*38*). Large dynamical changes of opposing signs have affected this region over the last millennium (*39*), however, and features of the region may predispose it to ice-flow "noise" (*40*).

The association of outlet-glacier acceleration, dynamical thinning, and ice-shelf changes affecting several ice streams implicates a response to ice-shelf changes rather than individual dynamical explanations such as periodic surging. An ice-sheet model including lateral drag and longitudinal stress gradients applied to Pine Island Glacier simulates instantaneous acceleration extending ~100 km inland in response to ice-shelf reduction, followed by diffusive-advective thinning up to 200 km inland, in good agreement with observations (*41*) and with results from other models that include nonlocal stresses (Fig. 4) (*32*, *42*). Similarly detailed

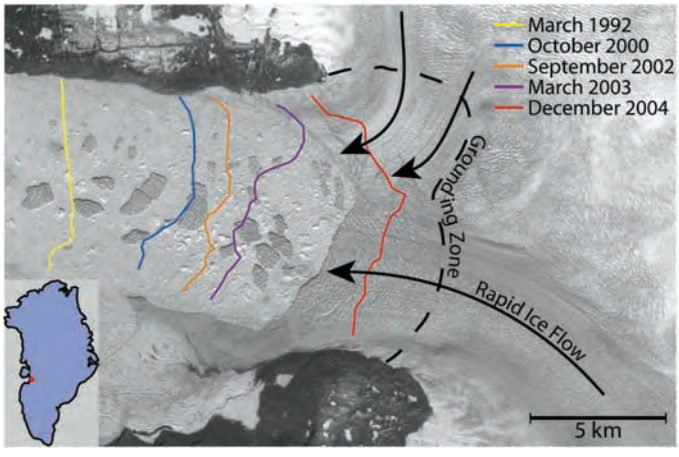

Fig. 3. Section of a May 2003 Landsat image acquired after the nearly complete disintegration of the floating ice tongue of Jakobshavn Isbrae, Greenland's largest outlet glacier. The black dashed line shows the approximate grounding zone (*68*). The color lines show the location of the ice tongue's front at several times. Short-term oscillations (not shown) were superimposed on the general trend. The ice tongue's breakup coincided with rapid thinning upstream of the floating ice (up to 15 m/year) and with a near doubling of the glacier's speed (up to ~13 km/year) (*22*, *23*).

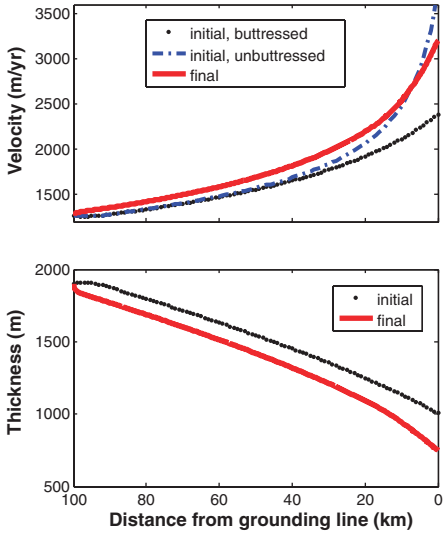

Fig. 4. Modeled response of an idealized version of Pine Island Glacier, West Antarctica, to loss of a small ice shelf (one resisting half of the tendency for ice spreading at the grounding line), following (*32*). In this model, response is limited to the ice stream itself and cannot propagate into the ice sheet beyond the ice stream. The near-instantaneous increase in velocity following ice-shelf loss is physical but is not simulated in older models lacking longitudinal stresses. The subsequent velocity evolution is largely a result of the thinning and stress reduction in response to that near-instantaneous speedup.

modeling has not been conducted for the recent changes of Jakobshavn Isbrae and the tributaries to the former Larsen B ice shelf, but all appear to be changing at rates not fully captured by models that exclude longitudinal stress gradients.

The data summarized above indicate a contribution to sea-level rise from ice-flow changes in marginal regions of roughly ⅓ mm/year, with evidence of increased discharge since the mid-1970s and especially since the mid-1990s. This dynamic imbalance is of comparable magnitude to the direct effect of recent surface mass-balance changes, of the same sign for Greenland but of opposite sign for Antarctica (*13*, *14*, *18*, *43*). The recently detected glacier accelerations are too young, however, and the observational record is too short to evaluate whether they represent short-term fluctuations or are part of a longer term trend that might scale with future climatic warming. Slight deceleration of portions of the fastest glaciers flowing into the former Larsen B ice shelf only 1 year after the ice shelf broke up (*29*) and a known record of variability of Jakobshavn Isbrae with slight thickening occurring only a decade ago (*22*, *23*, *44*) suggest that these events may just represent fast adjustments to marginal fluctuations. Alternatively, oceanic erosion of ice margins, especially in the Antarctic, may well continue in the future, in which case the eventual response could be far greater (*34*, *41*). Ice-flow perturbations may also affect basal conditions in poorly understood ways, with both positive and negative feedbacks possible and potentially large (*40*).

Whereas we have focused on inland response to changes in floating ice, an additional process that may prove important in Greenland is meltwater penetration to the bed, providing near-instantaneous communication between surface forcing and basal-ice dynamics. This is known to occur through ~1 km of cold ice in western Greenland, with modest (order of 10%) increase in speed from enhanced basal lubrication (*45*). In addition, one case of meltwater penetration through Ryder Glacier in northern Greenland was observed to cause a speed-up of more than threefold persisting several weeks (*46*). Meltwater penetration likely occurs through water-filled fractures, especially if fed by surface lakes (*47*). If meltwater access to the bed moves inland with warming, as seems likely, fracture penetration to and along the bed may cause rapid thawing and ice-flow speedup, thus shortening the ice-sheet response time to global warming and accelerating sea-level rise (*48*).

Future Behavior

Predictions of ice-sheet contributions to sea-level rise have relied on long integrations of ice-sheet models that extend well into the 21st century and beyond (*2*, *4*). These predict that up to the year 2100, warming-induced ice-sheet

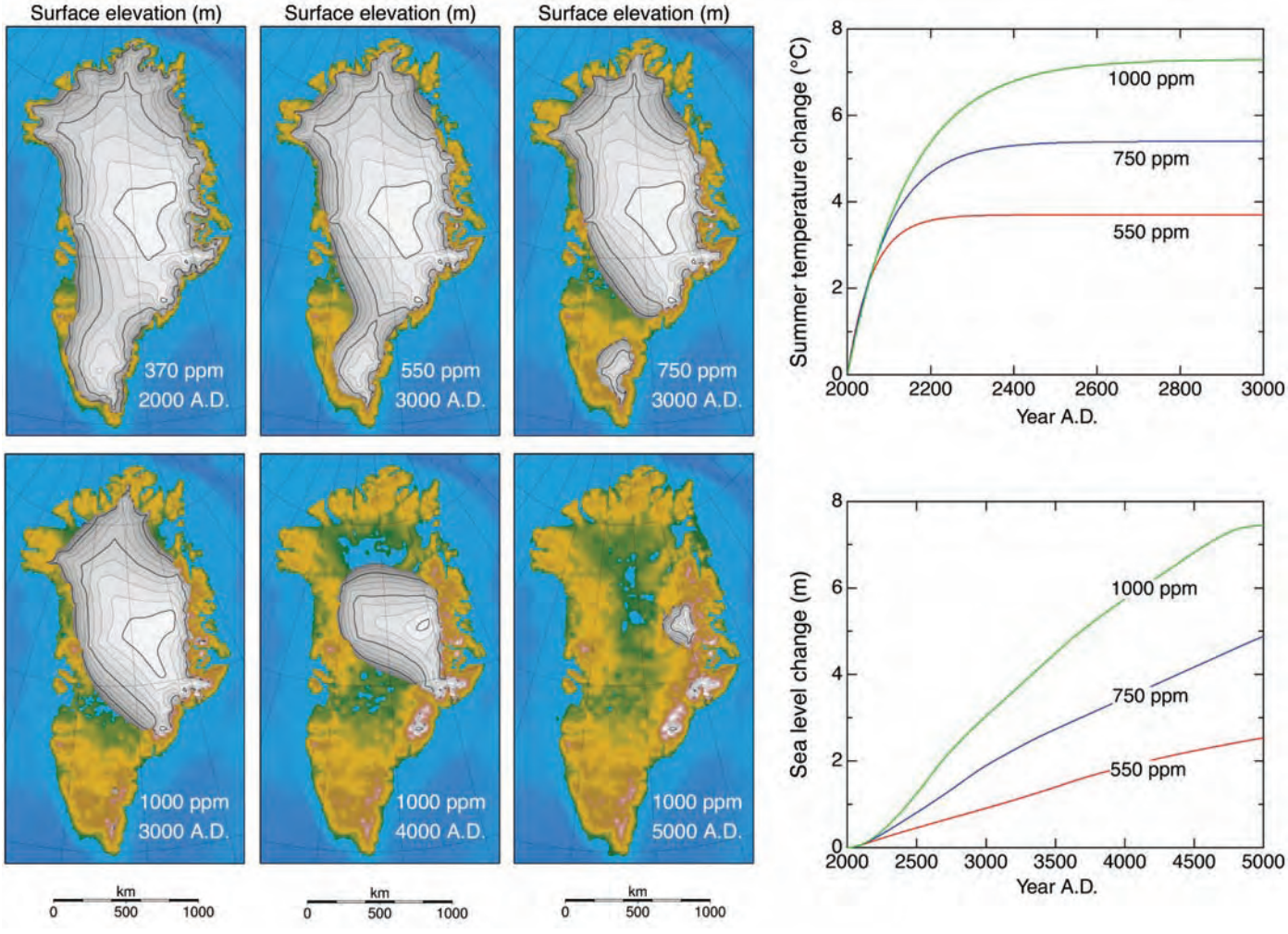

Fig. 5. Future evolution of the Greenland Ice Sheet calculated from a 3D ice-sheet model forced by three greenhouse gas stabilization scenarios. The warming scenarios correspond to the average of seven IPCC models in which the atmospheric carbon dioxide concentration stabilizes at levels between 550 and 1000 ppm after a few centuries (*4*) and is kept constant after that. For a sustained average summer warming of 7.3°C (1000 ppm), the Greenland Ice Sheet is shown to disappear within 3000 years, raising sea level by about 7.5 m. For lower carbon dioxide concentrations, melting proceeds at a slower rate, but even in a world with twice as much CO_2 (550 ppm or a 3.7°C summer warming) the ice sheet will eventually melt away apart from some residual glaciation over the eastern mountains. The figure is based on the models discussed in (*5*).

growth in Antarctica will offset enhanced melting in Greenland (*3*). For the full range of climate scenarios and model uncertainties, average 21st-century sea-level contributions are –0.6 ± 0.6 mm/year from Antarctica and +0.5 ± 0.4 mm/year from Greenland, resulting in a net contribution not significantly different from zero, but with uncertainties larger than the peak rates from outlet glacier acceleration during the past 5 to 10 years.

Looking further into the future, inland-ice models raise concerns about the Greenland Ice Sheet (Fig. 5). At present, mass loss by surface-meltwater runoff is similar to iceberg-calving loss plus sub–ice-shelf melting, with total loss only slightly larger than snow accumulation. For warming of more than about 3°C over Greenland, surface melting is modeled to exceed snow accumulation (*4*), and the ice sheet would shrink or disappear. For the most extreme Intergovernmental Panel on Climate Change (IPCC) warming scenario, one modeling study found 7 m of sea-level rise from Greenland in about 1000 years (*4*, *49*). This loss of the Greenland Ice Sheet would be irreversible without major cooling (*50*). However, increased Greenland meltwater may suppress the AMOC (*51*), causing regional cooling and an attendant decrease in Greenland melting. In contrast, important mass loss from surface melting of Antarctic ice is not expected in existing scenarios, although grounding-line retreat along the major ice shelves is modeled for basal melting rates >5 to 10 m/year, causing the demise of WAIS ice shelves after a few centuries and retreat of coastal ice toward more firmly grounded regions after a few millennia (*5*, *52*), with implied rates of sea-level rise of up to 3 mm/year. If large and rapid mass losses from WAIS occurred, any attendant freshening of Antarctic Intermediate Water may strengthen the AMOC (*11*).

Because the models used in these projections lack some of the physical processes that might explain the rapid rates of ongoing coastal changes and lack the oceanic forcing responsible for inducing these changes, previous estimates of sea-level change may become lower limits if ongoing speedups are sustained and eventually become more widespread. Progress is being made in ice-flow models (*32*, *41*, *53*), but no model including all relevant forces has yet been produced, and comprehensive ice-sheet integrations with such a model do not seem imminent. Nonetheless, the recent observations discussed here reveal that rapid dynamic changes can be important, contributing a notable fraction of ongoing sea-level rise and potentially becoming dominant over ice-sheet surface mass-balance changes in the future.

Summary

Ice sheets now appear to be contributing modestly to sea-level rise because warming has increased mass loss from coastal areas more than warming has increased mass gain from enhanced snowfall in cold central regions. At present, thickening on the EAIS appears to be nearly balanced by WAIS thinning along the Amundsen Coast, much of which reflects recent changes. With an Antarctic Ice Sheet not far from balance despite large regional imbalances, Greenland presently makes the largest contribution to sea-level rise. Ice-sheet models that have supported the IPCC effort do not include the full suite of physical processes implicated in the ongoing changes, however, and so are not able to assess whether these ongoing changes represent minor perturbations before stabilization or a major change that may affect sea level notably. Fundamental shortcomings in available data sets as well as models preclude confident projection of rapid future changes, and this difficulty is compounded by possible interactions between freshwater fluxes from ice sheets, ocean circulation, and climate. The major challenges then are to acquire the observations necessary to characterize rapid dynamic changes, and to incorporate those data into improved models, allowing more reliable predictions of ice contributions to sea-level change over the coming decades and centuries.

References and Notes

1. W. Munk, *Science* **300**, 2041 (2003).
2. J. Church *et al.*, in *Climate Change 2001: The Scientific Basis: Contribution of Working Group I to the Third Assessment Report of the Intergovernmental Panel on Climate Change*, J. T. Houghton *et al.*, Eds. (Cambridge Univ. Press, Cambridge, 2001), pp. 639–693.
3. P. Huybrechts, J. Gregory, I. Janssens, M. Wild, *Global Planet. Change* **42**, 83 (2004).
4. J. M. Gregory, P. Huybrechts, S. C. B. Raper, *Nature* **428**, 616 (2004).
5. P. Huybrechts, J. de Wolde, *J. Clim.* **12**, 2169 (1999).
6. P. U. Clark, A. C. Mix, *Quat. Sci. Rev.* **21**, 1 (2002).
7. R. G. Fairbanks, *Nature* **342**, 637 (1989).
8. Y. Yokoyama, K. Lambeck, P. De Deckker, P. Johnston, L. K. Fifield, *Nature* **406**, 713 (2000).
9. P. U. Clark, A. M. McCabe, A. C. Mix, A. J. Weaver, *Science* **304**, 1141 (2004).
10. P. U. Clark, J. X. Mitrovica, G. A. Milne, M. E. Tamisiea, *Science* **295**, 2438 (2002).
11. A. J. Weaver, O. A. Saenko, P. U. Clark, J. X. Mitrovica, *Science* **299**, 1709 (2003).
12. E. Rignot, R. H. Thomas, *Science* **297**, 1502 (2002).
13. W. Krabill *et al.*, *Geophys. Res. Lett.* **31**, L24402 (2004).
14. J. E. Box, D. H. Bromwich, L. S. Bai, *J. Geophys. Res.* **109**, D16105 (2004).
15. C. H. Davis, Y. Li, J. R. McConnell, M. M. Frey, E. Hanna, *Science* **308**, 1898 (2005).
16. D. J. Wingham, A. J. Ridout, R. Scharroo, R. J. Arthern, C. K. Shum, *Science* **282**, 456 (1998).
17. A. Shepherd, D. J. Wingham, J. A. D. Mansley, *Geophys. Res. Lett.* **29**, 1364 (2002).
18. D. H. Bromwich, Z. C. Guo, L. S. Bai, Q. S. Chen, *J. Clim.* **17**, 427 (2004).
19. J. Turner, J. C. King, T. A. Lachlan-Cope, P. D. Jones, *Nature* **418**, 291 (2002).
20. T. J. Hughes, *J. Glaciol* **27**, 518 (1981).
21. R. C. A. Hindmarsh, E. Le Meur, *J. Glaciol.* **47**, 271 (2001).
22. R. H. Thomas *et al.*, *J. Glaciol.* **49**, 231 (2003).
23. I. Joughin, W. Abdalati, M. Fahnestock, *Nature* **432**, 608 (2004).
24. R. H. Thomas, *J. Glaciol.* **50**, 57 (2004).
25. W. Abdalati *et al.*, *J. Geophys. Res.* **106**, 33729 (2001).
26. S. Brachfeld *et al.*, *Geology* **31**, 749 (2003).
27. D. R. MacAyeal, T. A. Scambos, C. L. Hulbe, M. A. Fahnestock, *J. Glaciol.* **49**, 22 (2003).
28. A. Shepherd, D. Wingham, T. Payne, P. Skvarca, *Science* **302**, 856 (2003).
29. E. Rignot *et al.*, *Geophys. Res. Lett.* **31**, L18401 (2004).
30. T. A. Scambos, J. A. Bohlander, C. A. Shuman, P. Skvarca, *Geophys. Res. Lett.* **31**, L18402 (2004).
31. E. Rignot *et al.*, *Geophys. Res. Lett.* **32**, L07502 10.1029/2004GL021947 (2005).
32. T. K. Dupont, R. B. Alley, *Geophys. Res. Lett.* **32**, 10.1029/2004GL022024 (2005).
33. A. Shepherd, D. Wingham, E. Rignot, *Geophys. Res. Lett.* **31**, L23402 (2004).
34. R. Thomas *et al.*, *Science* **306**, 255 (2004).
35. E. J. Rignot, *Science* **281**, 549 (1998).
36. I. Joughin, E. Rignot, C. E. Rosanova, B. K. Lucchitta, J. Bohlander, *Geophys. Res. Lett.* **30**, 1706 (2003).
37. E. Rignot, S. S. Jacobs, *Science* **296**, 2020 (2002).
38. I. Joughin, S. Tulaczyk, *Science* **295**, 476 (2002).
39. M. A. Fahnestock, T. A. Scambos, R. A. Bindschadler, G. Kvaran, *J. Glaciol.* **46**, 652 (2000).
40. B. R. Parizek, R. B. Alley, C. L. Hulbe, *Ann. Glaciol.* **36**, 251 (2003).
41. A. J. Payne, A. Vieli, A. P. Shepherd, D. J. Wingham, E. Rignot, *Geophys. Res. Lett.* **31**, L23401 (2004).
42. M. Schmeltz, E. Rignot, T. K. Dupont, D. R. MacAyeal, *J. Glaciol.* **48**, 552 (2002).
43. E. Hanna *et al.*, *J. Geophys. Res.* **110**, D13108 (2005).
44. S. Podlech, A. Weidick, *J. Glaciol.* **50**, 153 (2004).
45. H. J. Zwally *et al.*, *Science* **297**, 218 (2002).
46. I. Joughin, S. Tulaczyk, M. Fahnestock, R. Kwok, *Science* **274**, 228 (1996).
47. R. B. Alley, T. K. Dupont, B. R. Parizek, *Ann. Glaciol,* in press.
48. B. R. Parizek, R. Alley, *Quat. Sci. Rev.* **23**, 1013 (2004).
49. R. Greve, *Clim. Change* **46**, 289 (2000).
50. T. Toniazzo, J. M. Gregory, P. Huybrechts, *J. Clim.* **17**, 21 (2004).
51. T. Fichefet *et al.*, *Geophys. Res. Lett.* **30**, 1911 (2003).
52. R. Warner, W. F. Budd, *Ann. Glaciol.* **27**, 161 (1998).
53. F. Pattyn, *J. Geophys. Res.* **108**, 2382 10.1029/2002JB002329 (2003).
54. M. Pagani, J. C. Zachos, K. H. Freeman, B. Tipple, S. Bohaty, *Science* **309**, 600 (2005); published online 16 June 2005 (10.1126/science.1110063).
55. R. M. DeConto, D. Pollard, *Nature* **421**, 245 (2003).
56. J. Ahn *et al.*, *J. Geophys. Res.* **109**, 10.1029/2003JD004415 (2004).
57. K. Visser, R. Thunell, L. Stott, *Nature* **421**, 152 (2003).
58. E. Bard, B. Hamelin, R. G. Fairbanks, A. Zindler, *Nature* **345**, 405 (1990).
59. K. Fleming *et al.*, *Earth Planet. Sci. Lett.* **163**, 327 (1998).
60. T. Hanebuth, K. Statteger, P. M. Grootes, *Science* **288**, 1033 (2000).
61. D. H. Etheridge *et al.*, *J. Geophys. Res.* **101**, 4115 (1996).
62. C. D. Keeling, J. F. S. Chin, T. P. Whorf, *Nature* **382**, 146 (1996).
63. N. Nakicenovic, R. Swart, Eds., *Special Report on Emissions Scenarios* (Intergovernmental Panel on Climate Change, Cambridge Univ. Press, Cambridge, 2000).
64. M. E. Mann, P. D. Jones, *Geophys. Res. Lett.* **30**, 1820 (2003).
65. NASA Goddard Institute for Space Studies surface temperature analysis (www.giss.nasa.gov/data/update/gistemp).
66. G. A. Meehl *et al.*, *Science* **307**, 1769 (2005).
67. Permanent Service for Mean Sea Level, Proudman Oceanographic Laboratory (www.pol.ac.uk/psmsl/).
68. K. Echelmeyer, T. S. Clarke, W. D. Harrison, *J. Glaciol.* **37**, 368 (1991).

69. We thank G. Meehl for providing data used in Fig. 2. R.A. acknowledges support from the NSF Office of Polar Programs (including 0440899, 0229609, and 0229629). P.C. acknowledges support from the NSF Earth System History Program. P.H. acknowledges support through the German Helmholtz-Gemeinschaft (HGF)–Stategiefonds Projekt 2000/13 SEAL (Sea Level Change) and the Belgian Science Policy Office Second Programme on Global Change and Sustainable Development under contract EV/10/9B. I.J. acknowledges support from NASA.

10.1126/science.1114613

Glycine-Rich Antifreeze Proteins from Snow Fleas

Laurie A. Graham[1] and Peter L. Davies[1,2]*

Snow fleas are primitive arthropods with six legs and no wings (*1*). Some species produce antifreeze proteins (AFPs) to help resist freezing (*2*). We collected active *Hypogastrura harveyi* Folsom (Fig. 1A) from snowbanks or meltwater in late February and early March of 2001 at Chaffey's Locks, Ontario, Canada (*3*). An extract of fleas crushed in buffer inhibited the growth of a small ice crystal to 5.8 C° below the melting point of the solution. The extract also produced rice grain–shaped ice crystals with a hexagonal cross section (Fig. 1B) that were distinct from those produced by other AFPs tested.

AFPs were purified from snow flea homogenate by two cycles of ice affinity purification, in which AFPs, which bind to the surface of ice, become incorporated into a slowly grown ice hemisphere (*4*). The homogenate produced an ice hemisphere that was cloudy and showed shaping of the ice crystals (Fig. 1C), whereas a hemisphere grown in buffer did not (Fig. 1D). The purified fraction was resolved into two peaks by reversed-phase high-performance liquid chromatography (HPLC) at pH 7.0. We observed a single mass, by matrix-assisted laser desorption/ionization mass spectrometry, for each of these peaks. The larger peak contained a smaller (6.5-kD) but less active AFP, whereas the smaller peak contained a larger (15.7-kD), more active AFP (Fig. 1E).

Snow flea AFPs were more active than a typical fish AFP (Fig. 1F), and the 6.5-kD AFP had activity comparable to that of an 8.4-kD beetle AFP. Crystals formed with the 15.7-kD AFP were indistinguishable from those made in a crude homogenate, whereas those formed with the 6.5-kD AFP were similar but less elongated (Fig. 1, B and F).

The two AFPs had similar amino acid compositions, in which glycine made up >45 mole percent (mol%) and alanine was the next most abundant amino acid (15 mol%) (Fig. 1G). The smaller AFP contained no aromatic or long-chain aliphatic amino acids, and there were few of these residues in the larger one. The increase in mass after reduction and alkylation of cysteine residues indicated that there were four cysteines forming intramolecular disulfide bonds in the 6.5-kD AFP and two forming a bond in the 15.7-kD AFP. Reduction of these bonds eliminated antifreeze activity. Circular dichroism spectroscopy indicated that the 6.5-kD AFP has a defined three-dimensional structure required for antifreeze activity.

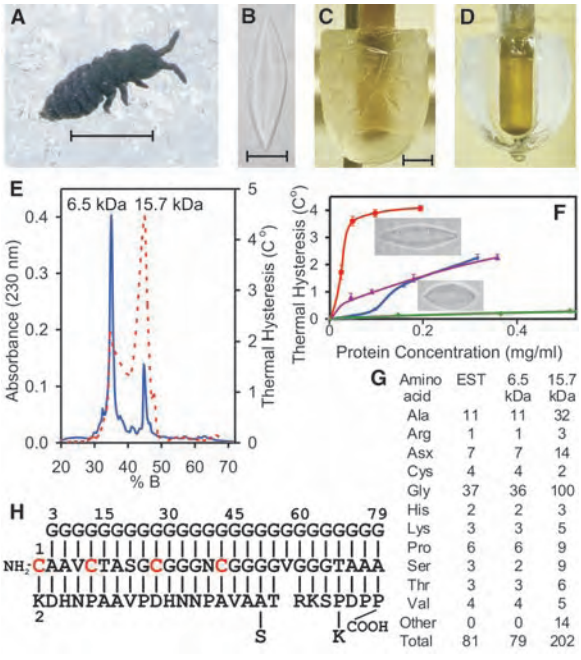

Fig. 1. (**A**) Specimen of *H. harveyi*. Scale bar, 1 mm. (**B**) Morphology of ice crystals in the presence of snow flea homogenate. Scale bar, 20 μm. (**C**) Ice hemisphere grown from snow flea homogenate and (**D**) from buffer alone. Scale bar, 1 cm. (**E**) Reversed-phase HPLC separation of AFP isoforms. Absorbance at 230 nm is indicated by the blue line, and the dashed red line shows antifreeze activity in C° of freezing point depression below the melting point (thermal hysteresis). B, buffer B (*3*). (**F**) Activity of 15.7-kD (red) and 6.5-kD (blue) AFPs compared to beetle (4-9 isoform, purple) and fish (type III QAE, green) AFPs. An ice crystal from the second-highest concentration of snow flea AFPs is shown just below their activity curves. (**G**) Amino acid composition of the two AFP isoforms alongside that deduced from the cDNA. EST, expressed sequence tag. "Other" includes Glx, Ile, Leu, Met, and Phe. (**H**) Amino acid sequence of the 81-residue small AFP isoform (minus the signal sequence), derived from the cDNA and displayed to reveal the tripeptide repeating pattern. The sequence reads from top to bottom, then left to right, beginning NH_2-CKGADGAH….

We obtained a sequence that appears to correspond to the 6.5-kD AFP (Fig. 1H) by randomly sequencing clones from a snow flea cDNA library. Four out of 57 clones (7%) encoded a sequence that matched the amino acid composition and mass of the purified sample (Fig. 1G). The sequence has a tripeptide repeat with glycine in the first position and a small side-chain amino acid in the second, whereas the third position is more variable. Size heterogeneity is common in AFPs with repetitive sequences (*5*, *6*), so the 15.7-kD AFP is likely a longer isoform of the 6.5-kD AFP. When the cDNA was cloned and expressed in *Escherichia coli*, the bacterial extracts inhibited ice growth, whereas control bacterial extracts did not.

These glycine-rich proteins do not resemble any of the AFPs described in fishes, plants, bacteria, or insects, including the two unrelated threonine-rich AFPs of moths and beetles (*5*, *6*). Thus, the emerging pattern of AFP evolution in arthropods seems similar to that in teleost fishes, whereby the initial radiation (speciation) may have occurred in a warm climate, after which multiple AFPs evolved from different progenitors (*7*, *8*). Fish may have acquired AFPs during the recent Cenozoic glaciations in the polar regions (*5*), but the events that drove antifreeze production in arthropods are uncertain. Because AFPs may have evolved in arthropods after speciation, we anticipate other unrelated AFPs will be found in insects and other arthropods.

References and Notes

1. P. F. Bellinger, K. A. Christiansen, F. Janssens, "Checklist of the Collembola of the World," available at www.collembola.org (1996–2005).
2. J. Zettel, *Rev. Ecol. Biol. Sol.* **21**, 189 (1984).
3. Materials and methods are available as supporting material on *Science* Online.
4. M. J. Kuiper, C. Lankin, S. Y. Gauthier, V. K. Walker, P. L. Davies, *Biochem. Biophys. Res. Commun.* **300**, 645 (2003).
5. Z. Jia, P. L. Davies, *Trends Biochem. Sci.* **27**, 101 (2002).
6. K. V. Ewart, Q. Lin, C. L. Hew, *Cell. Mol. Life Sci.* **55**, 271 (1999).
7. C. H. Cheng, L. Chen, *Nature* **401**, 443 (1999).
8. J. Baardsnes, P. L. Davies, *Trends Biochem. Sci.* **26**, 468 (2001).
9. Supported by grant no. MOP 6199 from the Canadian Institutes of Health Research (P.L.D.). Protein structure coordinates have been deposited with GenBank accession no. DQ177322.

Supporting Online Material
www.sciencemag.org/cgi/content/full/310/5747/461/DC1
Materials and Methods
Fig. S1
Tables S1 to S3
References and Notes

23 May 2005; accepted 7 September 2005
10.1126/science.1115145

[1]Department of Biochemistry, [2]Protein Function Discovery Group, Queen's University, Kingston, ON K7L 3N6, Canada.

*To whom correspondence should be addressed. E-mail: daviesp@post.queensu.ca

Air-Stable All-Inorganic Nanocrystal Solar Cells Processed from Solution

Ilan Gur,[1,3] Neil A. Fromer,[1] Michael L. Geier,[3] A. Paul Alivisatos[1,2]*

We introduce an ultrathin donor-acceptor solar cell composed entirely of inorganic nanocrystals spin-cast from solution. These devices are stable in air, and post-fabrication processing allows for power conversion efficiencies approaching 3% in initial tests. This demonstration elucidates a class of photovoltaic devices with potential for stable, low-cost power generation.

Organic materials offer strong potential for cost reduction vis-à-vis conventional solar cells, but their spectrally limited absorption and low carrier mobilities impose limitations on achieving commercially viable device efficiencies (*1*). Colloidal inorganic nanocrystals share all of the primary advantages of organics—scalable and controlled synthesis, an ability to be processed in solution, and a decreased sensitivity to substitutional doping—while retaining the broadband absorption and superior transport properties of traditional photovoltaic (PV) semiconductors (*2*–*4*). Using inorganic nanocrystals (NCs) for electron transport can enhance the performance of semiconductor polymer solar cells (*5*, *6*), but the ultimate limitations of these hybrid systems may still be dictated by the low mobility and environmental sensitivity of their organic phase. A solar cell that relies exclusively on colloidal NCs has been anticipated theoretically in recent years (*7*, *8*). We now demonstrate such a device and present a mechanism for its operation in the context of organic donor-acceptor (D-A) and conventional p-n junction solar cells.

A well-accepted model has emerged that describes the operation of organic-based solar cells relative to their conventional inorganic counterparts (*7*, *9*). The organic D-A solar cell relies on a type II heterojunction, which serves to dissociate the strongly bound excitons characteristic of organic systems. Materials design for this type of PV system thus requires proper energy band alignment of active materials to facilitate charge transfer. Examples to date have been limited to systems with at least one active organic component (*5*, *10*–*14*). However, studies of type II semiconductor NC heterostructures show that efficient charge transfer may also occur between two such inorganic components with staggered energy levels (*15*, *16*). In addition, recent research has revealed a growing number of similarities between NC films and organic molecular semiconductors. Like organic systems, NC films exhibit extremely low carrier concentrations and high trap densities (*17*, *18*), as well as confined excitations that may migrate between crystals (*19*). All of these properties are sufficient, and some are requisite, for solar energy conversion based on the D-A model (*7*, *9*).

The PV devices described here use rod-shaped CdSe (Fig. 1A) and CdTe (Fig. 1B) NCs that we synthesized and prepared separately (*20*). A schematic energy diagram (Fig. 1C) illustrates the staggered band alignment of this prototypical D-A pair. In fabricating devices, NCs were spin-cast from a filtered pyridine solution, which created ultrathin, flexible films of densely packed NCs on virtually any substrate. Typical films are homogeneous and pinhole-free over large areas (Fig. 1D).

We fabricated planar D-A heterojunctions by sequentially spin-casting films of CdTe and then CdSe on indium tin oxide (ITO) glass coated with 2 Å alumina. Thermally deposited aluminum was used as a reflective top contact. Brief annealing of the CdTe film for 15 min at 200°C removed residual solvent and allowed for subsequent deposition of the CdSe film. In this way, high-quality bilayer structures were formed with minimal intermixing at the interface (*20*).

The photoaction spectrum of a typical bilayer cell (Fig. 2A) reveals features from both the CdSe and CdTe absorption spectra. Thus, both components contribute to the photocurrent. Current-voltage (I-V) characteristics of this device in the dark and at simulated Air Mass 1.5 Global (AM1.5G) full-sun illumination are presented in Fig. 2B. The device exhibits strong photoresponse and diode rectification in the dark and light. In addition, this representative cell exhibits a notable PV effect, with a short-circuit current (I_{sc}) of 0.58 mA/cm^2, open-circuit voltage (V_{oc}) of 0.41 V, and fill factor (*FF*) of 0.40 (*21*).

We can distinguish the solar cells presented here from conventional thin film heterojunction cells. Conventional cells depend on a junction between bulk p- and n- doped materials to form a built-in field, which then acts as the primary driving force for minority carrier extraction (*22*, *23*). Similar to organic semiconductors, colloidal NCs are characterized by extremely limited free-carrier concentrations (*4*). In fact, three-dimensional CdSe colloid arrays have been found to contain essentially no free carriers without illumination (*18*). As such, the creation of a depleted junction in these NC cells is highly unlikely.

In accordance with these prior studies, the CdSe and CdTe films presented here are electrically insulating in the dark. Measuring surface conduction across a 1-mm gap between two aluminum electrodes yields linear IV curves, from which sheet resistances exceeding 500 G-ohms per square, a value

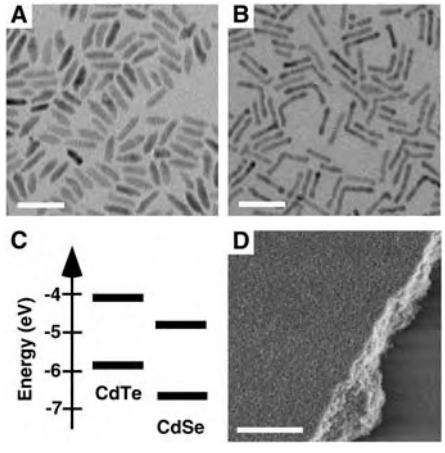

Fig. 1. Transmission electron micrographs of (**A**) CdSe and (**B**) CdTe NCs used in this investigation. Scale bar, 40 nm. (**C**) An energy diagram of valence and conduction band levels for CdTe and CdSe illustrates the type II charge-transfer junction formed between the two materials. Employing the effective mass approximation, bulk energy levels were modified to account for quantum confinement. Valence band edges for CdSe and CdTe rods were calculated to be –4.79 eV and –4.12 eV, respectively. Conduction band edges for CdSe and CdTe rods were calculated to be –6.64 eV and –5.85 eV, respectively. (**D**) A typical spin-cast film of colloidal NCs imaged by scanning electron micrography is homogeneous and defect-free; the film edge of this ~100-nm film is shown for contrast with the silicon substrate. Scale bar, 1 μm.

[1]Materials Science Division, Lawrence Berkeley National Laboratory, Berkeley, CA 94720, USA. [2]Department of Chemistry, [3]Department of Materials Science and Engineering, University of California, Berkeley, CA 94720, USA.

*To whom correspondence should be addressed. E-mail: alivis@berkeley.edu

limited by the measurement apparatus, can be extracted for films of either material on glass substrates. Exposing the films to 100 mW/cm^2 full-sun irradiation effected a marked rise in conductivity. Sheet resistances, now measurable, dropped at least one order of magnitude under illumination. Likewise, illumination afforded a greater than three orders of magnitude enhancement in conductivity of the device itself (Fig. 2B). This strong photoconductive effect suggests that these materials, like their organic counterparts, have an extremely limited number of untrapped carriers in the dark and are better characterized by a rigid band model than by one that employs band bending.

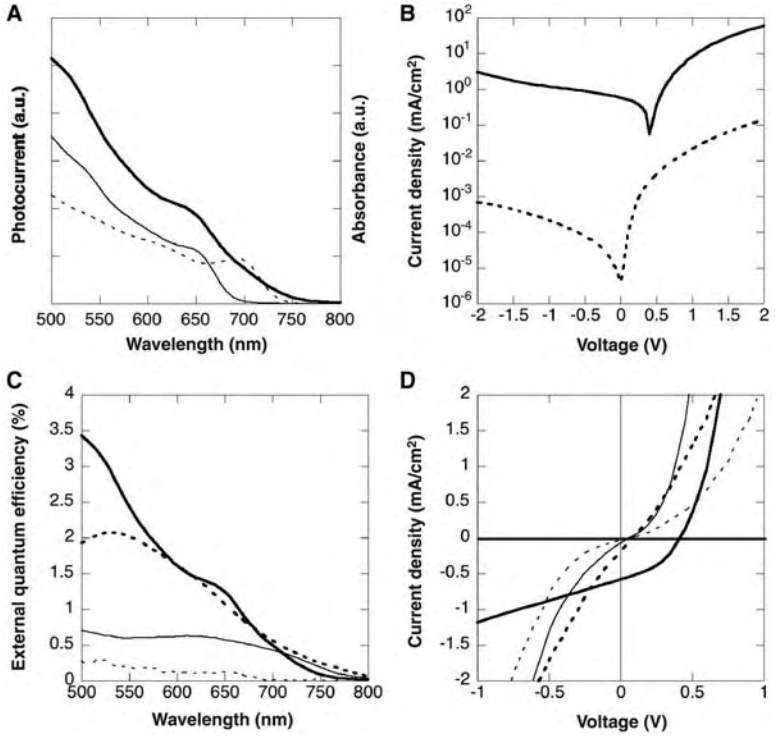

Fig. 2. (**A**) The normalized photocurrent spectral response of a typical ITO/100-nm CdTe/100-nm CdSe/Al bilayer device (bold) is illustrated alongside solution-phase absorption spectra for the CdTe (dotted) and CdSe (solid) NCs from which the device was fabricated. The photoaction spectrum reflects the red CdTe absorption edge and the prominent CdSe exciton peak, indicating that both components are active. a.u., arbitrary units. (**B**) I-V characteristics for this device in the dark (dotted) and under simulated one-sun AM1.5G illumination (solid). The device behaves as a rectifying diode with a notable photovoltaic response. The strong photoconductive response of the device is also illustrated. (**C**) A comparison of external quantum efficiency spectra collected under low-intensity illumination ($\sim 5 \times 10^{-2}$ mW/cm^2). We see significant enhancement in bilayer (bold, solid) and blend (bold, dotted) devices versus a CdTe single-material device (solid) and a CdSe single-material device (dotted), all of comparable optical density. The comparison serves to illustrate the role of charge transfer in photocurrent generation. (**D**) A comparison of I-V characteristics between the set of devices in (C) under simulated AM1.5G illumination. Nearly symmetric I-V behavior in the single-material devices suggests that diode behavior in the bilayer is not simply the result of a Schottky junction with either material. With no contact selectivity, blend cells show negligible rectification and photovoltage.

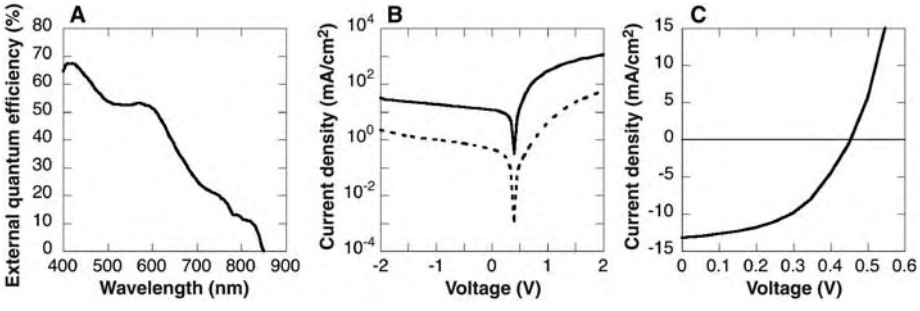

Fig. 3. (**A**) The normalized photoaction spectrum of a typical bilayer device after sintering reveals the broadened spectral response and enhanced quantum efficiency that result from sintering. (**B**) I-V characteristics of a typical bilayer device before sintering (dotted) and after sintering (solid), measured at simulated one-sun AM1.5G illumination. The sintered cell shows over an order of magnitude enhancement in photocurrent whereas the open-circuit voltage remains virtually unchanged. (**C**) The use of a Ca 20-nm/Al 80-nm top contact allows for fabrication of devices with AM1.5G power conversion efficiencies as high as 2.9%.

In order to assess the role of charge transfer in facilitating PV energy conversion, devices composed of a thin film of only one NC material were juxtaposed with cells containing charge transfer junctions between the two types of crystals. All devices had comparable thicknesses of active materials on the order of 200 nm and comparable optical densities across the spectrum. A direct comparison of external quantum efficiencies in the CdTe-only, CdSe-only, and bilayer CdTe/CdSe devices (Fig. 2C) shows a significant enhancement in creation and extraction of carriers due solely to the presence of a charge transfer interface within the device. As is the case in organic systems, separation of electrons and holes across the interface enhances the diffusional driving force for charge extraction while reducing the likelihood of exciton recombination. Devices composed of intimately mixed blends of CdSe and CdTe nanocrystals similarly exhibit enhanced quantum efficiencies over single-material cells (Fig. 2C), offering further evidence that the photoaction of these devices is based on a D-A junction rather than a conventional planar p-n junction.

We also compared the I-V characteristics of these various devices under simulated AM1.5G illumination. As noted above, cells based on heterojunction bilayers exhibit good diode behavior with strong rectification. By comparison, I-V characterization of devices composed of only CdTe or only CdSe showed no

significant rectification (Fig. 2D) (*24*). We can thus deduce that the observed PV effect in the bilayer is not a result of Schottky contacts to either material but rather is due to the intended heterojunction.

Having ruled out the presence of conventional p-n or Schottky junctions, it appears that the bilayer NC cell operates by means of the diffusion-assisted D-A heterojunction typical of organic devices. However, several characteristics of the NC solar cell set it apart from its organic-based counter parts. The most efficient organic solar cells are based on distributed heterojunctions, but devices based on simple blends of donor and acceptor NCs (Fig. 2D) neither rectify nor produce a significant photovoltage. In contrast to organic systems, common electrodes do not readily form selective contacts to either the donor or acceptor NCs. Electrons and holes can be injected into either material, such that blend cells pass current in both forward and reverse bias. Incorporation of blocking layers in future cell designs may allow for further investigation of the blend system.

Another fundamental distinction of the NC system has direct consequences on the performance of these devices. Although a heterojunction is nearly always required to efficiently produce free charges from excitons in organic systems, this is not the case for the NCs used in this study. Rod-shaped nanocrystals with high aspect ratios exhibit little confinement along the length of the rod (*25*). Excitons can thus dissociate over this dimension, creating free carriers throughout the NC film. In organic systems, free carriers are created only when otherwise tightly bound excitons are separated across the D-A junction.

With both free electrons and holes residing in the donor and acceptor materials, carriers are more susceptible to recombination in the NC system. This recombination is compounded by the large presence of surface states on the NCs, which act to trap carriers as they move through the film. Indeed, detrimental recombination losses are apparent in the low quantum efficiency of the NC cell compared with similar devices made from organic semiconductors.

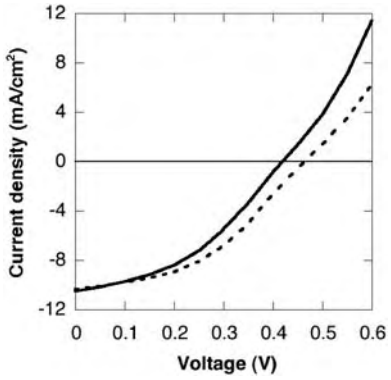

Fig. 4. I-V behavior at simulated one-sun AM1.5G illumination for a typical sintered bilayer device upon first exposure to air (solid) and after 13,000 hours of exposure to ambient atmosphere and light at open circuit. Idle exposure to air and ambient light results in minimal degradation of photocurrent and ultimately affords a 13.6% improvement in overall power conversion efficiency.

We can minimize the high surface trap area inherent in a densely packed array of NCs and concurrently improve carrier transport in the device by annealing and sintering the crystals. Following a well-known technique to facilitate sintering of CdTe thin films (*26*), we exposed NC films to a saturated solution of $CdCl_2$ in methanol and annealed them at 400°C in air for 15 min. After sintering, films of CdSe and CdTe remain insulating in the dark but show about two orders of magnitude enhancement in photoconductivity. The sintering process markedly improves carrier transport but does not appear to result in significant doping.

The photoresponse of sintered CdTe/CdSe bilayer cells mirrors the drastic rise in photoconductivity exhibited by the active layers. A typical photoaction spectrum (Fig. 3A) shows external quantum efficiencies approaching 70% (*27*). As expected, the spectrum reflects a strong red-shift in the onset of photocurrent to the bulk absorption edge. With I_{sc} of 11.6 mA/cm^2, V_{oc} of 0.40 V, and *FF* of 0.45, the resulting solar cell demonstrates a power conversion efficiency of 2.1% under simulated AM1.5G illumination (*28*). The enhancement in efficiency arises solely from the marked increase in photoresponse, whereas cells exhibited a nearly unchanged open-circuit voltage after sintering (Fig. 3B). This result is strong evidence that the driving force for charge extraction is the same in sintered and unsintered devices.

By varying simple system parameters such as electrode material, even higher efficiencies have already been achieved in sintered nanocrystal cells. Figure 3C shows I-V characteristics for the best device fabricated to date, which employs a Ca top contact capped with Al. This cell has an AM1.5G power conversion efficiency of 2.9%, with I_{sc} of 13.2 mA/cm^2, V_{oc} of 0.45 V, and *FF* of 0.49.

None of the solar cells presented here, whether sintered or not, exhibited the strong sensitivity to photo-oxidation characteristic of organic-based devices; in fact, aging seems to improve rather than deteriorate their performance. Figure 4 shows the AM1.5G full-sun behavior of a typical sintered device characterized in air before and after 13,000 hours' open-circuit exposure to ambient atmosphere and lighting. The cell shows only a 1.4% decrease in short-circuit current, whereas the fill factor rose 4.4% and the open-circuit voltage increased by more than 10%. Overall, the atmospheric aging resulted in a 13.6% increase in efficiency. Light-soaking experiments revealed less than 2% degradation in photocurrent after 14 hours at short circuit under simulated AM1.5G illumination with no encapsulation. These phenomena serve to illustrate the robustness of this system over its organic counterparts.

This demonstration introduces solar cells based entirely on colloidal semiconductor nanocrystals. They are ultrathin, solution-processed, and stable in ambient environments. Composed of dense nanocrystal films that mirror the basic properties of semiconducting polymers, these cells function as a class of diffusion-assisted, donor-acceptor heterojunctions. Sintering is found to enhance the performance of these devices, allowing for air-stable power conversion efficiencies up to 2.9%. The nanocrystal solar cells presented here offer an exciting research direction and serve as a key development toward achieving stable and low-cost solar energy conversion.

References and Notes

1. S. E. Shaheen, D. S. Ginley, G. E. Jabbour, *MRS Bull.* **30**, 10 (2005).
2. A. P. Alivisatos, *J. Phys. Chem.* **100**, 13226 (1996).
3. C. B. Murray, C. R. Kagan, M. G. Bawendi, *Annu. Rev. Mater. Sci.* **30**, 545 (2000).
4. M. Shim, C. J. Wang, D. J. Norris, P. Guyot-Sionnest, *MRS Bull.* **26**, 1005 (2001).
5. W. U. Huynh, J. J. Dittmer, A. P. Alivisatos, *Science* **295**, 2425 (2002).
6. B. Q. Sun, H. J. Snaith, A. S. Dhoot, S. Westenhoff, N. C. Greenham, *J. Appl. Phys.* **97**, 014914 (2005).
7. B. A. Gregg, M. C. Hanna, *J. Appl. Phys.* **93**, 3605 (2003).
8. A. J. Nozik, *Phys. E* **14**, 115 (2002).
9. J. A. Barker, C. M. Ramsdale, N. C. Greenham, *Phys. Rev. B* **67**, 075205 (2003).
10. J. J. M. Halls *et al.*, *Nature* **376**, 498 (1995).
11. G. Yu, J. Gao, J. C. Hummelen, F. Wudl, A. J. Heeger, *Science* **270**, 1789 (1995).
12. P. Peumans, V. Bulovic, S. R. Forrest, *Appl. Phys. Lett.* **76**, 2650 (2000).
13. S. E. Shaheen *et al.*, *Appl. Phys. Lett.* **78**, 841 (2001).
14. K. M. Coakley, M. D. McGehee, *Appl. Phys. Lett.* **83**, 3380 (2003).
15. S. Kim, B. Fisher, H. J. Eisler, M. Bawendi, *J. Am. Chem. Soc.* **125**, 11466 (2003).
16. D. J. Milliron *et al.*, *Nature* **430**, 190 (2004).
17. D. S. Ginger, N. C. Greenham, *J. Appl. Phys.* **87**, 1361 (2000).
18. N. Y. Morgan *et al.*, *Phys. Rev. B* **66**, 075339 (2002).
19. J. Heitmann *et al.*, *Phys. Rev. B* **69**, 195309 (2004).
20. Materials and methods are available as supporting material on *Science* Online.
21. Results presented are based on devices that use the standardized syntheses of CdTe and CdSe described above. Other syntheses have yielded slightly different results. For instance, devices with open-circuit voltages as high as 0.6 have been achieved by varying NC diameter; a thorough description of this dependence will be described elsewhere.
22. S. M. Sze, *Physics of Semiconductor Devices* (Wiley, New York, 1981).
23. A. L. Fahrenbruch, R. H. Bube, *Fundamentals of Solar Cells* (Academic Press, New York, 1983).
24. Devices composed of intimately mixed blends of CdSe and CdTe NCs show lower short-circuit currents than bilayer devices, despite comparable external quantum efficiencies (Fig. 2C). This can be attributed to the difference in illumination conditions between these two measurements. Because of instrument limitations, spectral response curves were measured at nearly four orders of magnitude lower illumination intensity than the simulated 100-mW/cm^2 AM1.5G conditions used in I-V comparisons. Increased leakage and recombination in the

blend devices are likely responsible for this discrepancy, but further investigation is needed to fully understand this effect.
25. L. S. Li, J. T. Hu, W. D. Yang, A. P. Alivisatos, *Nano Lett.* **1**, 349 (2001).
26. B. E. McCandless, L. V. Moulton, R. W. Birkmire, *Prog. Photovoltaics* **5**, 249 (1997).
27. These ultrathin cells exhibit suboptimal absorptivity, with average optical density of ~0.7. This assumes full back contact reflection such that incident light passes through the film twice.
28. Short-circuit currents obtained under simulated AM1.5G illumination were well matched with those obtained by integrating external quantum efficiency data with the true AM1.5G solar emission spectrum (*20*).
29. We thank A. Radenovic, K. Sivula, U. Bach, D. Milliron, J. Wang, and S. Laubach for research support and valuable discussion. Supported by the Director, Office of Energy Research, Office of Science, Division of Materials Sciences, of the U.S. Department of Energy under contract no. DE-AC02-05CH11231. I.G. further acknowledges the National Science Foundation for support under a Graduate Research Fellowship. Dedicated in loving memory to Benjamin Boussert, Giulia Adesso, and Jason Choy.

Supporting Online Material
www.sciencemag.org/cgi/content/full/310/5747/462/DC1
Materials and Methods

25 July 2005; accepted 20 September 2005
10.1126/science.1117908

Bridging Dimensions: Demultiplexing Ultrahigh-Density Nanowire Circuits

Robert Beckman, Ezekiel Johnston-Halperin, Yi Luo, Jonathan E. Green, James R. Heath*

A demultiplexer is an electronic circuit designed to separate two or more combined signals. We report on a demultiplexer architecture for bridging from the submicrometer dimensions of lithographic patterning to the nanometer-scale dimensions that can be achieved through nanofabrication methods for the selective addressing of ultrahigh-density nanowire circuits. Order $\log_2(N)$ large wires are required to address N nanowires, and the demultiplexer architecture is tolerant of low-precision manufacturing. This concept is experimentally demonstrated on submicrometer wires and on an array of 150 silicon nanowires patterned at nanowire widths of 13 nanometers and a pitch of 34 nanometers.

One of the central challenges of nanotechnology is the selective addressing of and interaction with individual nanostructures at high densities (i.e., densities limited only by the intrinsic size and packing of the nanostructures). Specifically, this challenge manifests over a range of problems, including coupling of conventional electronics to novel nanoelectronic devices (*1*), addressing of single nanoparticles for applications in quantum computing (*2*), and construction of high-density biomolecular sensor (*3*, *4*) circuits. For nanoelectronics, this challenge relates to the ability to address circuits that have characteristic wire dimensions and pitches that are smaller than the resolution achievable through lithographic patterning. Several groups have reported on methods for fabricating ultrahigh-density nanowire arrays (*4*–*9*).

Architectural concepts for meeting the challenge of electrically addressing (demultiplexing) individual nanowires that are patterned at sublithographic densities should satisfy three criteria. First, the demultiplexer architecture must bridge from the micrometer or submicrometer dimensions achievable through lithography to the few-nanometer dimensions achievable through alternative patterning methods. Second, the architecture should allow for the addressing of many nanowires with a few large wires. Third, the manufacture of the demultiplexer should be tolerant of fabrication defects.

Proposed demultiplexer architectures (*10*, *11*) have been based on combining crossbars (*12*) (lithographically patterned demultiplexing address wires crossing the nanowires) with multi-input binary tree demultiplexers (*13*). Binary trees, by their very nature, exhibit order $2[\log_2(N)]$ scaling, where N is the number of nanowires and $2[\log_2(N)]$ is the number of the large demultiplexing wires used to address the nanowires. Nanowire assemblies are often characterized by some randomness in organization, as well as by defects such as broken or nonconducting nanowires. To compensate, the proposed schemes contain a certain amount of redundancy (extra wires). The major cost of this redundancy is that the use of additional address wires implies that certain nanowire addresses will be redundant or nonactive; circuit testing must then be carried out to determine the good addresses, and memory must be devoted to storing those addresses (*14*). Kuekes and Williams (*10*) described a diode- or resistor-based decoder that uses $5[\log_2(N)]$ large microscale address wires crossing an array of N nanowires. DeHon *et al.* (*11*) described an architecture that uses no more than $2.2[\log_2(N)] + 11$ address wires. Their scheme is based on the field-effect gating of nanowires by the demultiplexer, and it requires control over the doping profile along the axial dimension of the nanowires. Such nanowires have been realized experimentally (*15*–*17*), and Lieber's group has used them to demonstrate a demultiplexer that bridges fabrication methods (i.e., self-assembly versus lithographic patterning) but not length scales (*18*). Both schemes are based on placing controllable regions on the surface of the nanowires. An individual nanowire, which is initially in the nonconducting state, will conduct only when all of the control regions are field- or voltage-addressed; that is, it is the logical equivalent of a multi-input AND gate.

Here, we describe an electric field effect–based demultiplexing scheme that is tolerant of manufacturing defects, is not seriously limited in terms of the wire size and pitch of the demultiplexer structure, and uses $2[\log_2(N)] + R$ microwires to address N nanowires, where R (for redundant address lines) is zero or a small integer (*14*). This scheme does not require control over the axial doping profile of the underlying nanowires but can take advantage of readily achieved vertical doping profiles, and it is designed to bridge length scales. It is optimized (i.e., R is small) for nanowires for which the pitch and width of the nanowire array are precisely controlled. The scheme is based on NOR logic; that is, the only nanowire that is not field-addressed is the one selected. We first illustrate the feasibility of this concept by demultiplexing an array of Si wires 200 nm wide, patterned at a pitch of 1 μm. We then extend this approach to demultiplexing an array of 150 nanowires at a pitch of 34 nm with individual wire widths of 13 nm. Finally, we identify specific materials development pathways that should allow the full and robust realization of this architecture.

The multiplexer concept is shown in Fig. 1. Here, 2^5 (= 32) nanowires are addressed with five pairs of (drawn) large wires. Note that the binary tree pattern extends above and below the nanowire array. This eases the vertical alignment requirements: As long as the multiplexer pattern is oriented perpendicular to the nanowire array and the nanowire pitch and width dimensions are well defined, the circuit will function (*14*). This aspect of the architecture makes it particularly amenable to patterning methods such as nanoimprint molding (*19*, *20*). The major cost associated with giving up vertical alignment precision is the knowledge of exactly which nanowire is selected by a given input address. For example, the binary address "1 0 1 0 1" used in Fig. 1 corresponds

Division of Chemistry and Chemical Engineering, California Institute of Technology, MC 127-72, 1200 East California Boulevard, Pasadena, CA 91125, USA.

*To whom correspondence should be addressed. E-mail: heath@caltech.edu

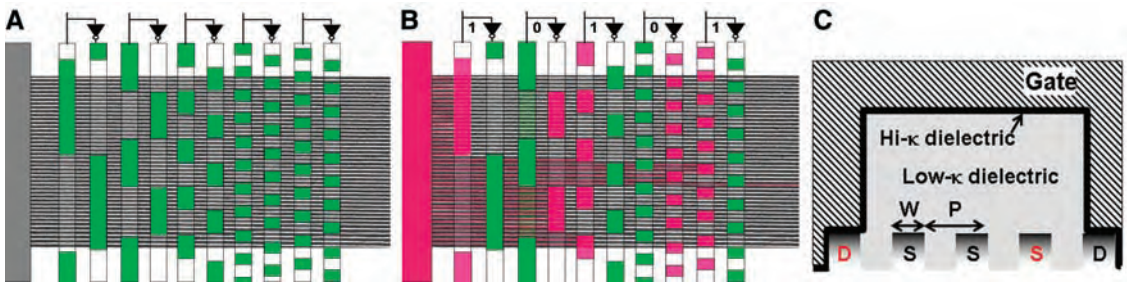

Fig. 1. (A and B) The demultiplexer concept, drawn over an electron micrograph of 32 (= 2^5) silicon nanowires. (A) All nanowires are ohmically contacted to the electrode at left. A binary tree pattern consisting of five complementary pairs of large wires is shown. The green regions correspond to areas in which a voltage applied to the top (metal) wires can reduce the conductivity of the nanowires through field-effect gating. All multiplexer features are larger than the nanowire features. (B) A voltage applied to the left electrode raises all nanowires to that voltage level. A single nanowire is selected by applying the input address "1 0 1 0 1." Application of a voltage onto a given wire pair sends one wire high and the other low. The resistance of nanowires that pass under a voltage-gated (red) region is increased. Only a single wire (colored red across the entire structure) remains in the high-conducting state. (C) Implementation of the multiplexer. Five nanowires, labeled D (deselected) or S (selected), are shown in an end-on view. W and P are the width and pitch of the nanowires. For small values of P, the pitch determines the distance of at least some of the selected nanowires from the gate electrode, and hence the gating selectivity. By probing the two red-labeled nanowires, the gating selectivity may be quantified without interrogating adjacent nanowires. The shading of the nanowires represents the doping profile, with heavier doping at the top surface of the nanowires (*14*).

to the decimal address 21, but it is the 28th wire from the top that is selected. In practice, there is usually no need to know the physical location of the nanowire—just its address—and so this "cost" is not substantial for most applications. Also notice that the smallest patterned binary tree feature sizes and pitches are considerably larger than the smallest corresponding dimensions within the nanowire array. Indeed, the patterned dimensions of the multiplexer can be made considerably larger than what is shown; the additional requirements are the need for additional wire pairs within the multiplexer (*14*). Note that $R = 0$ for the example of Fig. 1.

For both demultiplexers described here, some important fabrication and testing concepts are illustrated in Fig. 1C. A key performance metric of this circuit is its capability for deselecting one nanowire (labeled D) through voltage gating while simultaneously minimizing voltage gating of (and thus selecting) an adjacent nanowire (S). This requires careful choice of both the low-κ and high-κ dielectrics. HfO_2 (κ = 25) was chosen as the high-κ dielectric because it forms a stable insulator on Si (*21*), it exhibits little leakage current (*22*), interdiffusion between Si and Hf is not observed (*23*), and methods for growing very thin films of HfO_2 exist (*24*). Additionally, HfO_2 has been shown to be an effective gate dielectric for nanotube (*25*, *26*) and nanowire (*27*) field-effect transistors. For the low-κ dielectric we chose SiO_2 because of the ease of fabricating such films.

In Fig. 2 we present the results from the demonstration circuit for demultiplexing relatively large Si wires (doping: $n = 5 \times 10^{18}$ cm^{-3}). These data validate the architecture for the selection of individual wires with high fidelity, but the capability to bridge length scales is not demonstrated here. The thickness of the SiO_2 low-κ dielectric (100 nm) largely determines the selectivity (i.e., the selected nanowire/deselected nanowire current ratio), which is about 40.

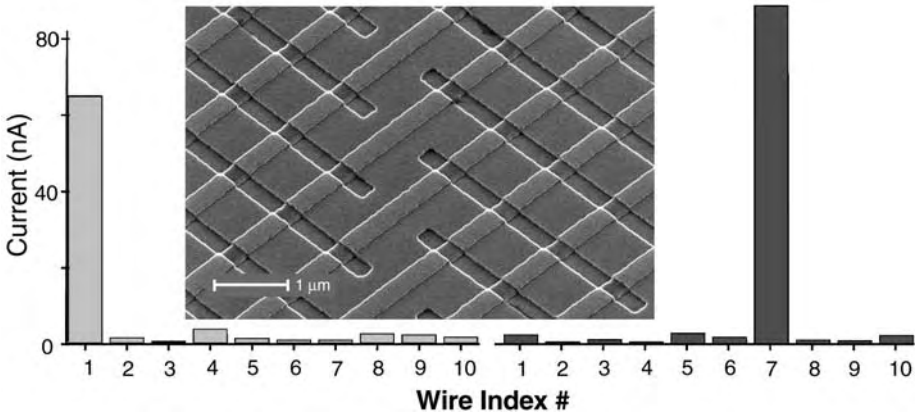

Fig. 2. A demultiplexer constructed on a test circuit of 10 Si wires, each 200 nm wide, patterned at 1-μm pitch. The inset shows the gating electrode structure (before deposition of the gate electrodes) that was patterned on top of the underlying wire array. Results illustrating the operation of this circuit are shown in the two bar graphs, in which individual wires were maintained in the high-conductivity state while all other wires were deselected through appropriate input addressing.

We now consider the application of this demultiplexer to a nanowire array characterized by a nanowire width of 13 nm and a pitch of 34 nm. In Fig. 3 we present images of the demultiplexer fabrication process for this circuit (*14*). We used the superlattice nanowire pattern transfer (SNAP) method (*9*) to fabricate 150 silicon nanowires. SNAP produces well-aligned arrays of high–aspect ratio metal and semiconductor nanowires with bulk-like and controllable conductivity characteristics (*28*) at dimensions that are not achievable through alternative methods. The demultiplexer itself was patterned using electron beam lithography. Highly conducting p^+ (10^{19} cm^{-3}) nanowires were used. Highly doped silicon nanowires do not exhibit a strong gating response. However, the doping profile through the nanowires was graded (*14*), and so the nanowires were thinned by about 10 nm in the regions where the gate electrodes were deposited. In those thinned regions, the effective doping was reduced to ~10^{18} cm^{-3}. This allowed us to maximize the gating response while maintaining highly conductive nanowires (*14*).

The metal gate electrode is separated from a deselected wire by about 5 nm of HfO_2 and 1 to 2 nm of SiO_2 (the native oxide on the nanowire surface). It is separated from a selected nanowire by 5 nm of HfO_2 and about 20 nm (= pitch – width) of SiO_2. Thus, in contrast to the demonstration circuit of Fig. 2, it is the nanowire circuit dimensions rather than the thickness of the low-κ dielectric that determines the gating selectivity of adjacent and very closely spaced nanowires. The result is that for a perfectly fabricated circuit, a gating field felt by a deselected nanowire is approximately 10 times that felt by an adjacent selected nanowire. For realistic fabrication tolerances, the field ratio will be reduced (*14*).

There is a chicken-and-egg challenge associated with testing this demultiplexer: How does one test whether the demultiplexer can address individual nanowires, when the individual nanowires themselves are too closely spaced to separately wire up for the test? Our approach

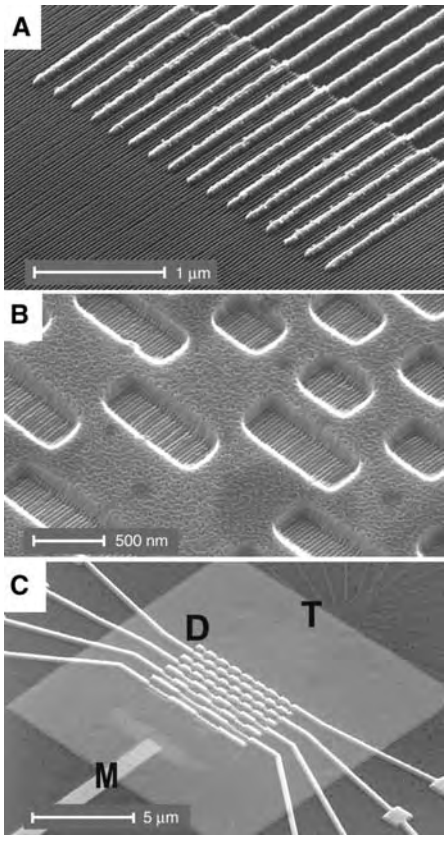

Fig. 3. Scanning electron micrographs of the nanowire demultiplexer assembly process. **(A)** Sixteen electrical contacts are established, each to two or three nanowires from an array of silicon nanowires. **(B)** The binary gate demultiplexer pattern, after deposition of the low-κ SiO_2 dielectric and before deposition of the HfO_2 dielectric. **(C)** Assembled demultiplexer circuit. M refers to the multiplexer electrode used to apply a voltage to all of the nanowires. D is the demultiplexer structure, shown with metal electrodes deposited on the HfO_2 gate insulator. T refers to test electrodes. Individual nanowires are measured by applying a voltage to M and grounding the test connections through an ammeter.

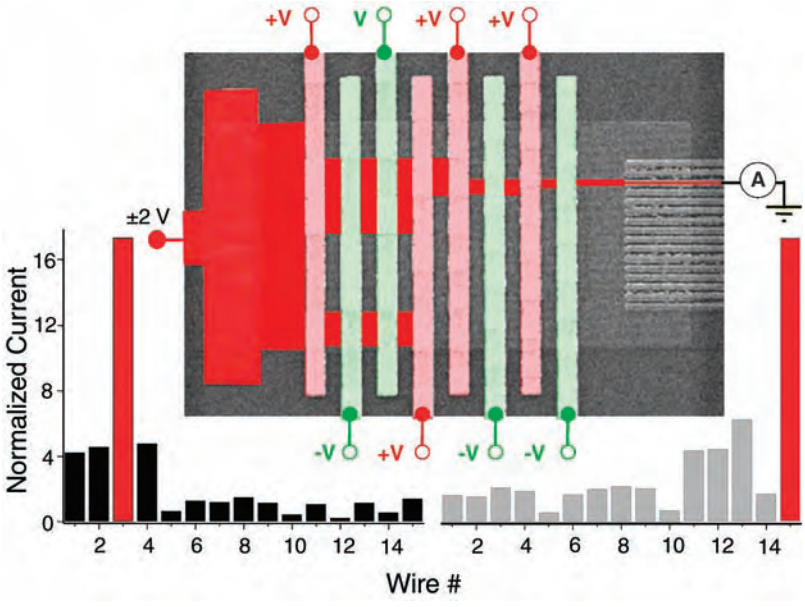

Fig. 4. Characteristic operation of the nanowire demultiplexer for two different input addresses. The central picture illustrates the address that was used to select out wire 3 in the bottom left bar graph. Gate voltages of +10 V and −10 V were applied to the red and green wires, respectively. The normalized current is the ratio of wire current measured under an addressing gate configuration to the current of the wire when +10 V is applied to all gates.

was twofold. First, we established 2^4 (= 16) electrical contacts, each to two or three nanowires, at a 150-nm pitch for testing (Fig. 3A). Second, a binary gating tree of four pairs of wires was fabricated to allow for the separate addressing of these 16 individual groups (Fig. 3B). The most closely spaced wire pairs were patterned at a 600-nm pitch, and these pairs were repeated twice, with the second wire pair phase-shifted 300 nm from the first. The gate width was also twice the intergate spacing. The result was that relatively large binary tree features could select out the two or three nanowires addressed by a given test electrode (*14*). Note that the selectivity of the demultiplexer for individual nanowires can be tested by probing the red-labeled nonadjacent nanowires (Fig. 1C). In other words, nanowires with adjacent addresses can be equivalent, in terms of electronic properties, to physically adjacent nanowires.

In Fig. 4 we present the results from the SNAP nanowire demultiplexer, in which, for two different address combinations, different sets of nanowires were selected at a signal-to-background level of about 4 for the worst-case comparison (*29*). We fabricated two such demultiplexers, with comparable results.

The results of Fig. 4 validate the demultiplexing concept for addressing ultradense nanowire circuits, although a robust and general pathway toward bridging the dimensions between micro- and nanoelectronic circuits will require additional modifications. For example, the relatively large gate voltages used here can be reduced by optimizing the doping levels and profiles of the Si nanowires, as well as by engineering the dielectric interfaces. For example, the HfO_2 dielectric can be reduced to about 2 nm and thermodynamically stabilized through the use of atomic layer deposition methods (*24*) and other treatments (*30*). Furthermore, the 1 to 2 nm of native oxide on the Si nanowires greatly reduces the effective dielectric constant of the gate insulator (i.e., it is a combination of HfO_2 and SiO_2). Replacing that native oxide with a methyl termination of the silicon surface (*31*) should yield important benefits in terms of increasing the mobility (*32*) (and hence the field gating response) of the charge carriers within the Si and for increasing the dielectric constant of the thin-film gate insulator. The incorporation of ultralow-κ (< 2.0) materials, such as nanoporous silica films (κ = 1.3 to 2.5), porous polymers, or polytetrafluoroethylene (κ = 1.9), in place of the present SiO_2 layer would also help (*33*). A challenge will be to incorporate these changes while maintaining a low-leakage current through the gate electrodes (currently 6 pA into a signal channel, or 300 μA cm^{-2}). For nanowires much smaller than those used here, statistical fluctuations in dopant density may ultimately prove limiting to this and other field-effect approaches.

This demultiplexer architecture allows for the selective addressing of nanowires within a dense array, using order $2[\log_2(N)]$ large wires to address N nanowires. Full validation of this concept is limited only by our ability to establish contacts to individual nanowires. In principle, this might be accomplished by constructing and testing a crosspoint memory circuit. Within a broader context, the development of a selectively addressable nanoelectrode array may provide leverage for other areas of nanotechnology. For example, when coupled with a suitable electrochemical attachment scheme (*34*), the nanowire array may be transformed into an array of label-free biomolecular sensors (*3*), allowing imaging of cellular processes with resolution in the tens of nanometers (*35*). It could also be used to demonstrate logic or memory circuits that are patterned at substantially higher densities than are currently envisioned with existing fabrication technologies.

References and Notes

1. J. R. Heath, M. A. Ratner, *Phys. Today* **56**, 43 (May 2003).
2. D. Loss, D. P. DiVincenzo, *Phys. Rev. A* **57**, 120 (1998).
3. Y. Cui, C. M. Lieber, *Science* **291**, 851 (2001).
4. S. W. Chung, G. Markovich, J. R. Heath, *J. Phys. Chem. B* **102**, 6685 (1998).
5. P. D. Yang, F. Kim, *ChemPhysChem* **3**, 503 (2002).

6. S. Jin *et al.*, *Nano Lett.* **4**, 915 (2004).
7. R. P. Sear *et al.*, *Phys. Rev. E* **59**, R6255 (1999).
8. M. Diehl *et al.*, *Angew. Chem. Int. Ed. Engl.* **41**, 353 (2002).
9. N. A. Melosh *et al.*, *Science* **300**, 112 (2003); published online 13 March 2003 (10.1126/science.1081940).
10. P. J. Kuekes, R. S. Williams, U.S. Patent 6,256,767 (3 July 2001).
11. A. DeHon, P. Lincoln, J. Savage, *IEEE Trans. Nanotechnol.* **2**, 165 (2003).
12. J. Heath, P. Kuekes, G. Snider, R. S. Williams, *Science* **280**, 1716 (1998).
13. R. P. Feynman, *Lectures in Computation*, A. J. G. Hey, R. W. Allen, Eds. (Addison-Wesley, Menlo Park, CA, 1996).
14. See supporting data on *Science* Online.
15. M. S. Gudiksen *et al.*, *Nature* **415**, 617 (2002).
16. Y. Wu, R. Fan, P. Yang, *Nano Lett.* **2**, 83 (2002).
17. M. T. Bjork *et al.*, *Nano Lett.* **2**, 87 (2002).
18. Z. Zhong *et al.*, *Science* **302**, 1377 (2003).
19. S. Y. Chou, P. R. Krauss, P. J. Renstrom, *Science* **272**, 85 (1996).
20. Y. Chen *et al.*, *Appl. Phys. Lett.* **82**, 1610 (2003).
21. G. D. Wilk, R. M. Wallace, *Appl. Phys. Lett.* **74**, 2854 (1999).
22. J. Hergenrother *et al.*, in *Electron Devices Meeting, 2001. IEDM Technical Digest International* (IEEE, Piscataway, NJ, 2001), pp. 3.1.1–3.1.4.
23. M. Quevedo-Lopez *et al.*, *Appl. Phys. Lett.* **79**, 4192 (2001).
24. D. M. Hausmann, E. Kim, J. Becker, R. G. Gordon, *Chem. Mater.* **14**, 4350 (2002).
25. A. Javey *et al.*, *Nat. Mater.* **1**, 241 (2002).
26. A. Javey *et al.*, *Nano Lett.* **4**, 447 (2004).
27. D. Wang *et al.*, *Appl. Phys. Lett.* **83**, 2432 (2003).
28. R. Beckman *et al.*, *J. Appl. Phys.* **96**, 5921 (2004).
29. These comparisons are based on measurements of the normalized current through the selected and deselected nanowires, rather than absolute current values.
30. R. Puthenkoviliakam, M. Sawker, J. P. Chang, *Appl. Phys. Lett.* **86**, 202902 (2005).
31. H. Yu *et al.*, *J. Phys. Chem. B* **109**, 671 (2005).
32. W. J. Royea, A. Juang, N. S. Lewis, *Appl. Phys. Lett.* **77**, 1988 (2000).
33. L. Peters, *Semiconductor International*, September 1998 (available at www.reed-electronics.com/semiconductor/archive/1998).
34. Y. Bunimovich *et al.*, *Langmuir* **20**, 10630 (2004).
35. L. Hood, J. R. Heath, M. E. Phelps, B. Lin, *Science* **306**, 640 (2004).

36. Supported by the Defense Advanced Research Projects Agency (DARPA) Moletronics Program and by the MARCO Center for Advanced Materials and Devices.

Supporting Online Material

www.sciencemag.org/cgi/content/full/1114757/DC1
Materials and Methods
SOM Text
Figs. S1 to S6
References

12 May 2005; accepted 21 September 2005
Published online 29 September 2005
10.1126/science.1114757
Include this information when citing this paper.

Visualization of the Molecular Jahn-Teller Effect in an Insulating K_4C_{60} Monolayer

A. Wachowiak, R. Yamachika, K. H. Khoo, Y. Wang, M. Grobis, D.-H. Lee, Steven G. Louie, M. F. Crommie*

We present a low-temperature scanning tunneling microscopy (STM) study of K_xC_{60} monolayers on Au(111) for $3 \leq x \leq 4$. The STM spectrum evolves from one that is characteristic of a metal at $x = 3$ to one that is characteristic of an insulator at $x = 4$. This electronic transition is accompanied by a dramatic structural rearrangement of the C_{60} molecules. The Jahn-Teller effect, a charge-induced mechanical deformation of molecular structure, is directly visualized in the K_4C_{60} monolayer at the single-molecule level. These results, along with theoretical analyses, provide strong evidence that the transition from metal to insulator in K_xC_{60} monolayers is caused by the Jahn-Teller effect.

Unlike atoms in an elemental solid, the building blocks of a molecular solid are more susceptible to tuning. C_{60}-based bulk solids, for example, can be tuned between metallic (*1*), insulating (*2*, *3*), and superconducting (*4*) states by changing the charge state and/or local environment of the constituent molecules. The cooperative interplay between molecular electronic and lattice degrees of freedom (the latter referring to intramolecular and intermolecular atomic displacements) is particularly important in fullerenes, because the energy scale of their electron-lattice interaction is comparable to their electronic bandwidths (*5*, *6*). As a result, small changes in properties such as intermolecular hybridization, intramolecular charging energy, and Jahn-Teller (JT) distortions (*7*) can tip these systems from one side of the metal-insulator divide to the other. This behavior has been studied extensively in C_{60}-based systems (*8*–*11*), but the role played by the JT effect, in which degenerate molecular electronic levels are split due to a spontaneous charge-induced structural deformation (*7*), is still under debate (*11*–*18*).

We report a cryogenic (temperature $T = 7$ K) scanning tunneling microscopy (STM) study of a single monolayer (ML) of potassium-doped C_{60} (K_xC_{60}) on Au(111), which shows that the JT effect plays a central role in driving the K_xC_{60} ML from a metal at $x = 3$ to an insulator at $x = 4$. This progress is made possible by our ability to directly image the influence of a JT distortion on intramolecular electronic wave functions.

The driving force for the JT effect is a lowering of occupied electronic levels coincident with a raising of empty ones, which reduces the total energy. The symmetry of electronic wave functions in a JT distorted molecule bears the imprint of the distortion itself and is very different for occupied and empty levels, in contrast with undistorted molecules. By comparing STM images of the intramolecular local density of states (LDOS) above and below the Fermi energy (E_F), we can determine the presence or absence of a JT distortion.

The charge state of C_{60} molecules in the K_xC_{60} ML was controlled through the local K concentration (each K atom donates approximately one electron to the physisorbed C_{60} molecules) (*5*, *19*, *20*). Upon bias reversal, the LDOS images changed dramatically for the $x = 4$ system but remained the same for $x = 3$, suggesting that a substantial JT distortion was present in the former and absent in the latter. We back this conclusion with ab initio electronic structure calculations that show our STM images are well-matched by the theoretical LDOS of a molecule undergoing a JT distortion. This combined evidence not only prompts us to conclude that a static JT distortion is the trigger of the insulating behavior in K_4C_{60} MLs but also allows us to determine the nature of the distortion.

The local structure of K-doped C_{60} MLs can be seen in the STM data of Fig. 1 (*21*). At $x = 3$, K_xC_{60} exhibits a triangular lattice backbone with a "bright molecule" supermodulation (Fig. 1A), reflecting a K-induced surface reconstruction. The exact form of the supermodulation varies across the K_3C_{60} surface and exhibits pronounced disorder in some regions, whereas it disappears altogether in others. Metallic dI/dV spectra, where I is current and V is voltage (Fig. 1D), are observed regardless of the details of the supermodulation. At $x = 4$, the K_xC_{60} ML undergoes a dramatic restructuring that transforms the underlying triangular backbone into a nearly rectangular structure with four molecules per unit cell (Fig. 1C). This structure is free of supermodulation and is far more ordered than are the $x = 3$ structures. The dI/dV spectrum for the $x = 4$ phase exhibits an energy gap of 200 ± 20 mV that is roughly symmetrical about E_F (see Fig. 1E). When the average K content (x) falls between 3 and 4, the system is an inhomogeneous mixture of the two phases (Fig. 1B). The spatial inhomogeneity is reflected both in the dI/dV spectra and structurally.

Department of Physics, University of California at Berkeley, Berkeley, CA 94720–7300, USA, and Material Sciences Division, Lawrence Berkeley Laboratory, Berkeley, CA 94720–7300, USA.

*To whom correspondence should be addressed. E-mail: crommie@berkeley.edu

The difference in electronic properties between the $x = 3$ and $x = 4$ phases can be seen by comparing real-space images of the filled and empty states straddling E_F (Figs. 2 and 3). A collection of *dI*/*dV* spectra measured at different points within a 3 nm × 3 nm region of the K_3C_{60} ML (Fig. 2C) shows some variability, but all of the spectra reveal a similar peak near E_F ($V = 0$). Topographic images at $V = -100$ mV (filled states) and $V = +100$ mV (empty states) for the same patch of K_3C_{60} surface (Fig. 2, A and B) show little change upon bias reversal, which is indicative of undistorted molecules and a continuous metallic LDOS. Data for the K_4C_{60} phase (Fig. 3C) show that instead of a peak at E_F, a 200-mV energy gap exists. Most striking, however, is the difference in the topographic images associated with filled and empty states (measured at $V = -100$ mV and $+100$ mV, respectively). Filled-state images (Fig. 3A) show that each C_{60} molecule is bisected by a single nodal line (i.e., a dark stripe), which implies the presence of a similar feature in the molecular LDOS. Empty-state images (Fig. 3B), however, display an additional nodal line on each molecule that is rotated by 90° with respect to the node seen in the filled-state image.

We argue that the dramatic difference in the filled- and empty-state topography of Fig. 3 is a manifestation of the JT distortion. When four extra electrons are added, a C_{60} molecule is expected to undergo a JT distortion whereby the three degenerate lowest unoccupied molecular orbital (LUMO) levels split into a group of twofold degenerate levels (excluding spin mutiplicity) at lower energy and one nondegenerate level at higher energy (*22*–*24*). The four extra electrons are accommodated by the two lowered energy levels, making the distortion energetically favorable. The shifting of the electronic levels by the molecular distortion implies an intimate relation between the electronic wave functions and the symmetry of the JT distortion.

To determine that relation, we compared our STM topographic images with calculated molecular LDOS by using density functional theory (DFT) with ab initio pseudopotential in a local orbital basis. Different locally stable distorted structures for isolated C_{60}^{4-} were found by total energy minimization. Their electronic LDOSs were then compared to our STM results and the best-fit structure selected. Apart from using an improved basis set (*25*), a finer real space grid (0.1 Å mesh), and excluding the surface, details of the calculation method are similar to those in (*26*). Guided by symmetry considerations (*22*–*24*), the molecule was given a small initial distortion having either D_{2h}, D_{3d}, or D_{5d} symmetry, and then allowed to relax to minimize the energy. The resulting displacements can be resolved in terms of the H_g and A_g phonon modes (H_g and A_g are symmetry classes that have even symmetry). The lowest-energy deformation for each of these symmetry channels shows an essentially identical total-energy reduction from the undistorted structure of 0.3 eV per molecule. In all three cases, the molecular JT distortion splits the LUMO manifold by 0.11 eV into doubly degenerate occupied levels and a single unoccupied level. However, only the D_{2h} distortion results in electronic wave functions that match the STM data (supporting online text). Therefore, we believe that this particular distortion is stabilized in the K_4C_{60} ML.

The calculated D_{2h} distortion of the C_{60} cage (Fig. 4, A and B) creates an oblate spheroid, with the short axis along the y direction of the figure. Most of the bond dis-

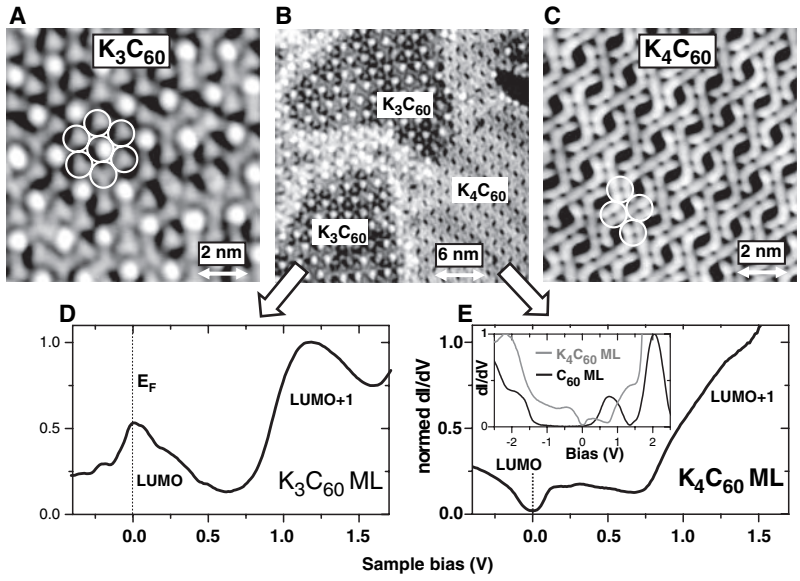

Fig. 1. STM images for K_xC_{60} ML on Au(111), $3 \leq x \leq 4$. (**A**) $x = 3$, single phase ($V = 0.1$ V, $I = 20$ pA, 10 × 10 nm²). (**B**) $x = 3.5$, mixed phase ($V = 0.5$ V, $I = 10$ pA, 25 × 25 nm²). (**C**) $x = 4$, single phase ($V = 0.2$ V, $I = 10$ pA, 10 × 10 nm²). Single molecules are marked by circles. (**D**) Spatially averaged *dI*/*dV* spectrum measured for K_3C_{60} shows metallic behavior. (**E**) Spatially averaged *dI*/*dV* spectrum measured for K_4C_{60} shows energy gap at E_F. The inset shows spatially averaged *dI*/*dV* spectra for a bare C_{60} ML and a K_4C_{60} ML over wider energy range. The spectra shown in (D) and (E) were obtained by spatially averaging over an area of 5 × 5 nm². [All spectra are normalized to the peak value of the LUMO+1 or the highest unoccupied molecular orbital (HOMO).]

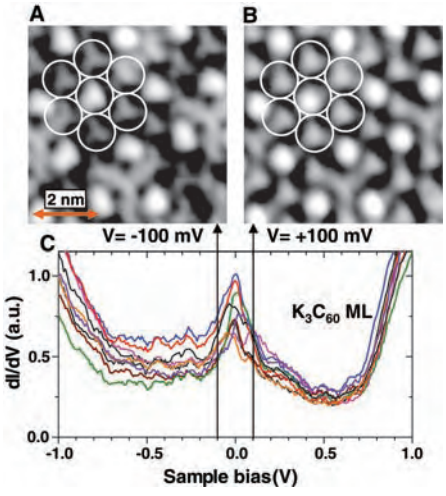

Fig. 2. Energy-dependent STM topographs of same region of K_3C_{60} ML. (**A**) Filled states ($V = -0.10$ V, $I = 20$ pA, 6 × 6 nm²). (**B**) Empty states ($V = +0.10$ V, $I = 20$ pA). Single molecules are marked by circles. (**C**) Spatial variation of *dI*/*dV* spectra measured at different positions in K_3C_{60} ML.

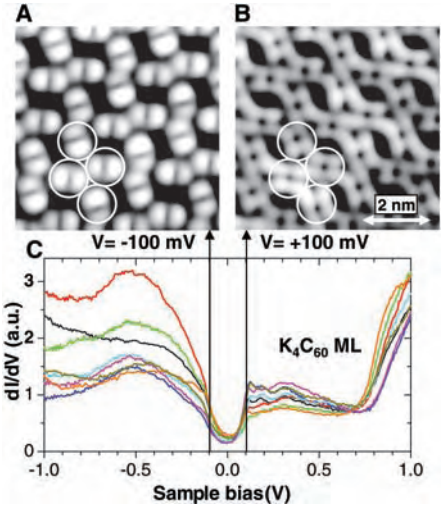

Fig. 3. Energy-dependent STM topographs of same region of K_4C_{60} ML. (**A**) Filled states ($V = -0.10$ V, $I = 10$ pA, 6 × 6 nm²). (**B**) Empty states ($V = +0.10$ V, $I = 10$ pA). The characteristic molecular structure above E_F does not change over the bias range $+0.10$ V to $+0.6$ V, whereas the one below E_F does not change over the bias range -0.10 V to -0.7 V. Single molecules are marked by circles. (**C**) Spatial variation of *dI*/*dV* spectra measured at different positions in K_4C_{60} ML. a.u., arbitrary units.

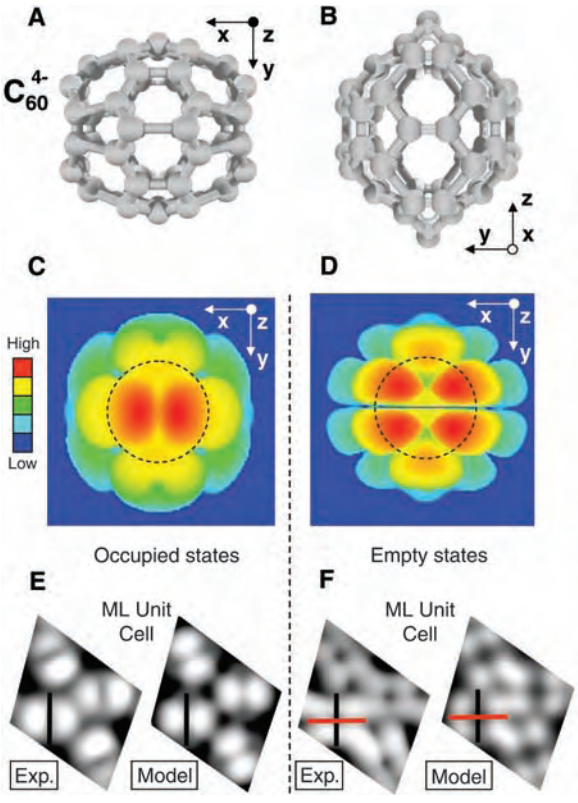

Fig. 4. Results of DFT calculation of isolated C_{60}^{4-} molecule. (**A**) Top view and (**B**) side view of the JT distorted C_{60}^{4-} configuration having D_{2h} symmetry (nuclear displacements are exaggerated by a factor of 30 for viewing). The proposed orientation corresponds to the Au surface parallel to the *xy* plane of the figure. (**C** and **D**) Two-dimensional projection of C_{60}^{4-} isosurface showing highest filled-state and lowest empty-state LDOS for JT split levels at ~3 Å outward from carbon centers. Regions within the dashed circles are preferentially imaged in ML topographs because of finite tip size. (**E** and **F**) STM data for a K_4C_{60} ML unit cell compared with a simulated unit cell obtained from the circled regions of (C) and (D) arranged in ML configuration for filled and empty states. Locations of nodal lines are marked in black and red. Exp., experimental.

tortion occurs in the equatorial *xz* plane. The resulting "isosurfaces" of the LDOS of the energy-split states (plot of $\{\mathbf{x}\}$ with $\Sigma_i \Psi_i(\mathbf{x})\Psi_i(\mathbf{x})^* = C$, where $\mathbf{x}$ is the position vector, Ψ is the wave function, i ranges over degenerate eigenstates at a particular energy, and C is a constant) can be seen in Fig. 4, C and D, for the unique orientation that fits our experimental data (here the Au surface lies in the *xy* plane of the figure). The most pronounced feature in the calculated LDOS of the highest occupied C_{60}^{4-} level (Fig. 4C) is a strong linear depression that bisects the topmost region of the LDOS into two bright areas. The lowest empty state LDOS (Fig. 4D) is similar to the occupied LDOS, except for the addition of a pronounced nodal plane that lies at an angle of 90° from the linear depression seen in the occupied LDOS. This new node lies exactly in the *xz* equatorial plane, where the greatest JT-induced changes in bond length occur, thus marking the spatial location of the JT distortion in the molecular local-electron spectral function. Simulated ML topographs (Fig. 4, E and F) using the results of Fig. 4, C and D, are in good agreement with experimentally observed energy-resolved K_4C_{60} topography. Empty-state imaging of the K_4C_{60} ML thus allows us to directly determine the spatial location of the JT distorted equatorial plane for each individual C_{60} molecule.

Our results provide strong evidence that JT distortion plays a central role in causing the strikingly different electronic properties of $x = 3$ and $x = 4$ K-doped C_{60} MLs. In particular, we believe that the JT effect and the intermolecular Coulomb interaction act cooperatively. For an even number of electrons, the JT effect suppresses intermolecular electron itinerancy (via Pauli exclusion) and hence reduces metallic screening. Worsened screening then enhances intramolecular charging energy (*6*, *26*, *27*) and thus enhances electron localization. Increased electronic localization, in turn, favors JT distortion (by reducing electron-number fluctuation on each molecule), causing a feedback cascade that results in an insulating K_4C_{60} ML ground state.

Two possible mechanisms might lead to the rearrangement of orientation seen in the insulating K_4C_{60} ML. The first involves quadrupole-quadrupole interactions between charged C_{60} molecules. Our DFT calculation indicates that JT distorted C_{60}^{4-} has a quadrupole moment of order $1|e|$ Å^2, where e is the electron charge. The ordering of C_{60} orientation seen in Fig. 3 is indeed favored by the quadrupolar interaction, but the energy difference between the observed structure and other metastable structures is small (on the order of 1 meV per molecule). Another possible mechanism for the order of orientation seen in Fig. 3 results from the anisotropic electronic overlap integral between molecules (*6*, *28*). Because the highest occupied molecular orbitals peak near the C_{60} pentagons, one intuitively expects direct pentagon-pentagon intermolecular alignment to enhance intermolecular overlap and reduce electronic kinetic energy. Indeed, for the order of orientation seen in Fig. 3, three of four equatorial pentagons per molecule face a pentagon from a neighboring molecule. A better understanding of the observed C_{60} arrangement and detailed spectroscopic features will likely have to include interaction of the molecules with the K ions and with the Au substrate, as well as quasiparticle effects that go beyond DFT in the standard local-density approximation.

References and Notes

1. R. C. Haddon *et al.*, *Nature* **350**, 320 (1991).
2. R. F. Kiefl *et al.*, *Phys. Rev. Lett.* **69**, 2005 (1992).
3. F. Stepniak, P. J. Benning, D. M. Poirier, J. H. Weaver, *Phys. Rev. B* **48**, 1899 (1993).
4. A. F. Hebard *et al.*, *Nature* **350**, 600 (1991).
5. W. L. Yang *et al.*, *Science* **300**, 303 (2003).
6. O. Gunnarsson, *Alkali-Doped Fullerides: Narrow-Band Solids with Unusual Properties* (World Scientific, River Edge, NJ, 2004).
7. H. A. Jahn, E. Teller, *Proc. R. Soc. London Ser. A* **161**, 220 (1937).
8. R. Kerkoud *et al.*, *J. Phys. Chem. Solids* **57**, 143 (1996).
9. P. Durand, G. R. Darling, Y. Dubitsky, A. Zaopo, M. J. Rosseinsky, *Nat. Mater.* **2**, 605 (2003).
10. Y. Iwasa, T. Takenobu, *J. Phys. Cond. Matter* **15**, R495 (2003).
11. V. Brouet, H. Alloul, S. Garaj, L. Forro, *Struct. Bonding* (*Berlin*) **109**, 165 (2004).
12. P. Paul, Z. W. Xie, R. Bau, P. D. W. Boyd, C. A. Reed, *J. Am. Chem. Soc.* **116**, 4145 (1994).
13. M. Fabrizio, E. Tosatti, *Phys. Rev. B* **55**, 13465 (1997).
14. L. F. Chibotaru, A. Ceulemans, S. P. Cojocaru, *Phys. Rev. B* **59**, R12728 (1999).
15. J. E. Han, E. Koch, O. Gunnarsson, *Phys. Rev. Lett.* **84**, 1276 (2000).
16. M. Capone, M. Fabrizio, P. Giannozzi, E. Tosatti, *Phys. Rev. B* **62**, 7619 (2000).
17. P. Dahlke, M. J. Rosseinsky, *Chem. Mater.* **14**, 1285 (2002).
18. K. Kamaras *et al.*, *Phys. Rev. B* **65**, 052103 (2002).
19. L. H. Tjeng *et al.*, *Solid State Commun.* **103**, 31 (1997).
20. C. Cepek, M. Sancrotti, T. Greber, J. Osterwalder, *Surf. Sci.* **454**, 467 (2000).
21. Our experiments were performed using a home-built ultrahigh vacuum STM cooled to 7 K. A polycrystalline PtIr tip was used for all measurements. C_{60} was dosed at coverages between 80% ML and 90% ML onto a clean Au(111) substrate cooled to 80 K. C_{60} coverages were determined from STM images. K was deposited progressively from a calibrated K getter onto the cooled C_{60} sample, followed each time by an anneal at 490 ± 10 K for 15 min. K getters were manufactured by SAES Getters (Milan, Italy), and calibrated by deposition of K on a clean Ag(100) substrate cooled to 80 K and counting single K atoms in topographic STM images acquired at 7 K. Local electronic structure was measured through STM *dI/dV* spectra acquired using standard lock-in techniques under open-loop conditions.
22. A. Ceulemans, *J. Chem. Phys.* **87**, 5374 (1987).
23. N. Koga, K. Morokuma, *Chem. Phys. Lett.* **196**, 191 (1992).
24. N. Manini, E. Tosatti, A. Auerbach, *Phys. Rev. B* **49**, 13008 (1994).
25. J. Junquera, Ó. Paz, D. Sánchez-Portal, E. Artacho, *Phys. Rev. B* **64**, 235111 (2001).
26. X. H. Lu, M. Grobis, K. H. Khoo, S. G. Louie, M. F. Crommie, *Phys. Rev. B* **70**, 115418 (2004).
27. R. Hesper, L. H. Tjeng, G. A. Sawatzky, *Europhys. Lett.* **40**, 177 (1997).
28. O. Gunnarsson, S. Satpathy, O. Jepsen, O. K. Andersen, *Phys. Rev. Lett.* **67**, 3002 (1991).

29. This work was supported in part by the Director of the Office of Energy Research, Office of Basic Energy Science, Division of Material Sciences and Engineering, U.S. Department of Energy under contract no. DE-AC03-76SF0098 and by NSF grant no. DMR04-39768. Y.W. thanks the Miller Institute for a research fellowship.

Supporting Online Material

www.sciencemag.org/cgi/content/full/310/5747/468/DC1
SOM Text
Fig. S1

12 July 2005; accepted 9 September 2005
10.1126/science.1117303

Biomarker Evidence for Photosynthesis During Neoproterozoic Glaciation

Alison N. Olcott,[1]* Alex L. Sessions,[2] Frank A. Corsetti,[1] Alan J. Kaufman,[3] Tolentino Flavio de Oliviera[4]

Laterally extensive black shales were deposited on the São Francisco craton in southeastern Brazil during low-latitude Neoproterozoic glaciation ~740 to 700 million years ago. These rocks contain up to 3.0 weight % organic carbon, which we interpret as representing the preserved record of abundant marine primary productivity from glacial times. Extractable biomarkers reflect a complex and productive microbial ecosystem, including both phototrophic bacteria and eukaryotes, living in a stratified ocean with thin or absent sea ice, oxic surface waters, and euxinic conditions within the photic zone. Such an environment provides important constraints for parts of the "Snowball Earth" hypothesis.

The impacts of low-latitude Neoproterozoic glaciation on the biosphere are widely debated (*1*–*6*). On one hand, one conception of "Snowball Earth" envisions sea-ice cover thick enough to preclude photosynthesis over most of the Earth, creating an "intense environmental filter" for the survival of photosynthetic organisms (*2*). Thick ice cover would also lead to anoxic oceans, threatening the existence of all eukaryotes. In this model, photosynthetic and eukaryotic clades survived in rare refugia, perhaps sustained by hydrothermal or volcanic activity or in transient equatorial polynya. Thus, the Neoproterozoic glaciations would have represented major evolutionary bottlenecks that influenced the subsequent radiation of multicellular life (*2*, *5*, *7*–*9*). Large ^{13}C depletions in the carbonate rocks that cap the glacial deposits have been attributed to the collapse of biologic productivity (and its consequent isotopic fractionation) during these glaciations (*2*, *9*). On the other hand, some climate models indicate that tropical oceans could have persisted through the glaciations with thin or no sea ice, allowing enough sunlight to reach the oceans to sustain diverse marine ecosystems and providing less extreme evolutionary pressure (*10*, *11*). Unfortunately, the results of these climate models are sensitive to several parameters that are difficult to estimate, including CO_2 concentration, oceanic heat transport, the flux of windborne dust, snow thickness and distribution, and ice optical properties (*11*). Both hypotheses remain speculative, because no unambiguous proxy for sea ice thickness is available. Here, we describe organic-rich shales deposited in southeastern Brazil during a Neoproterozoic glaciation. Given their lateral extent [>1000 km^2 (*12*)], substantial organic content (up to 3.0%), and stratigraphic position within the midst of glacial diamictites, these rocks provide evidence that life continued to flourish, at least in this location, during low-latitude Neoproterozoic glaciation.

Samples were collected from a subsurface core drilled near Paracatú, Brazil (Fig. 1A), in the Neoproterozoic Vazante Group by the Companhia Mineira de Metais (*13*). The succession (Fig. 2) includes the Serra do Garrote Formation, the glacial Poço Verde and Morro do Calcario formations, and the Lapa Formation, recently recognized as a postglacial succession from carbon- and sulfur-isotopic anomalies at its base (*14*). In the Paracatú region, the Poço Verde Formation includes diamictite, rhythmic marl, carbonate, and thinly laminated organic-rich black shale, deposited below storm wave base. Although radiometric age constraints for the succession are unavailable, the strontium isotope composition of carbonate above the studied shale horizon (*15*) is consistent with an age of 740 to 700 million years (Ma) (*1*, *16*).

[1]Department of Earth Sciences, University of Southern California, Los Angeles, CA 90089, USA. [2]California Institute of Technology, Pasadena, CA 91125, USA. [3]University of Maryland, College Park, MD 20742, USA. [4]Companhia Mineira de Metais, Brazil.

*To whom correspondence should be addressed. E-mail: olcott@usc.edu

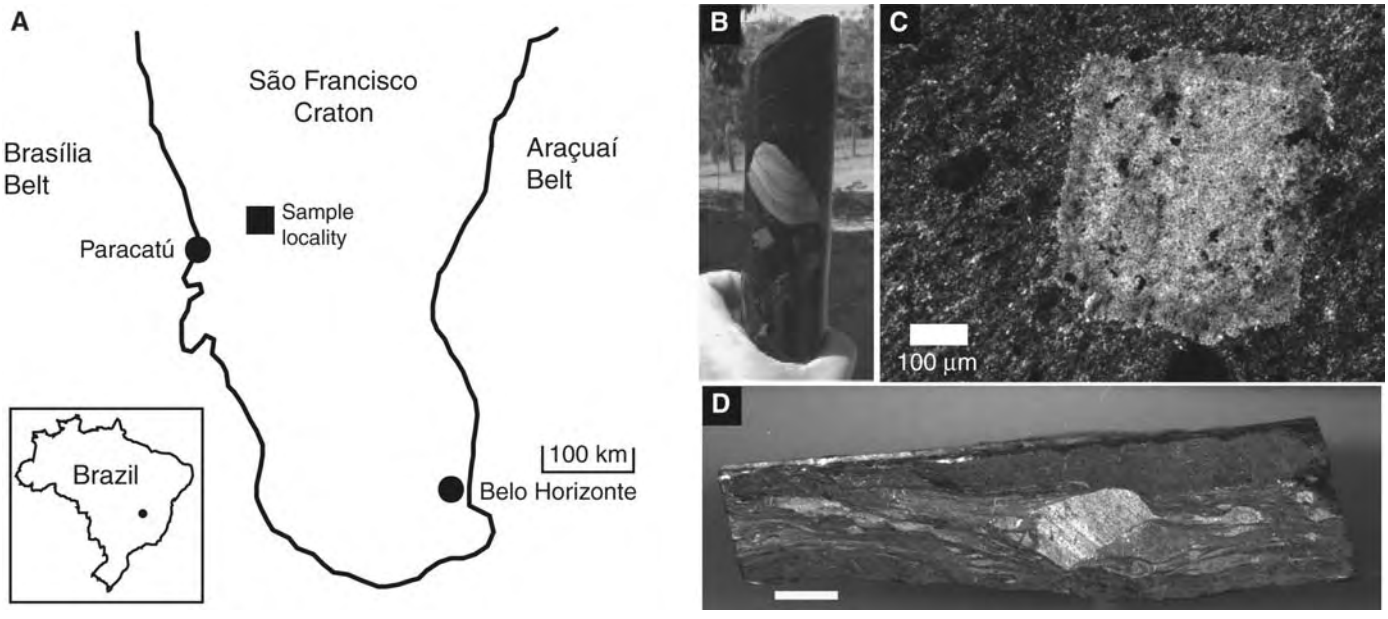

Fig. 1. (**A**) Locality map [modified after (*47*)] indicating the position of largely undeformed Vazante Group strata on the São Francisco craton between the Brasília and Araçuaí fold belts. (Inset) Brazil; dot marks region of interest. (**B**) Dropstone in core MAF 42-88 from the Neoproterozoic Poço Verde Formation. (**C**) Photomicrograph of carbonate nodule with squared crystal terminations formed before substantial compaction interpreted to be glendonite, a pseudomorph of ikaite formed in frigid, organic-rich sediments. (**D**) Faceted dropstone in core penetrating underlying laminae; scale bar is 5 mm.

Evidence for glacial processes exists throughout the Poço Verde Formation. Thinly laminated shale is sandwiched between thick carbonate diamictites, and lonestones, interpreted as ice rafted debris (dropstones), are present within it, indicating the presence of overlying ice at the time of deposition (Fig. 1, B and D). Shale samples also contain small nodules with squared prismatic crystal terminations formed before substantial compaction, which we identify as glendonite (Fig. 1C). Glendonite is a pseudomorph after ikaite, a carbonate mineral that most commonly forms between –1.9° and 7°C in organic-rich muds and that has been previously reported in a Neoproterozoic glacial succession from Svalbard containing "wispy" organic matter (*17*). It is probable that Poço Verde Formation strata were deposited at relatively low latitudes. The São Francisco craton, upon which the Poço Verde strata were deposited, was contiguous with the Congo craton in southern Africa, which contains broadly equivalent glacial deposits with near-equatorial paleolatitudes (*3*). In sum, the features recorded in the Poço Verde Formation of the Vazante Group are consistent with deposition at relatively low latitudes during Neoproterozoic glaciation.

We consider first the possibility that the organic-rich shale might represent recycled sediments that were eroded and redeposited via glacial processes. Several lines of evidence argue against this interpretation. Dropstones in the black shale are almost exclusively composed of organic-poor carbonate, indicating that the terrain eroded by the glaciers was not rich in black shale. Ikaite (the precursor to observed glendonite) forms in cold, anoxic sediments where rapid microbial remineralization of organic matter dramatically boosts porewater concentrations of both alkalinity and orthophosphate, a calcite inhibitor (*18*). Finely disseminated pyrite is also abundant in the matrix of the black shales, presumably resulting from extensive remineralization of organic matter by sulfate-reducing bacteria. Organic matter in eroded black shales is widely observed to be recalcitrant to microbial degradation (*19*) and thus would not have supported conditions necessary for either ikaite or sulfide formation. Therefore, we conclude that the preserved organic matter is the remains of abundant primary productivity occurring during the glacial interval.

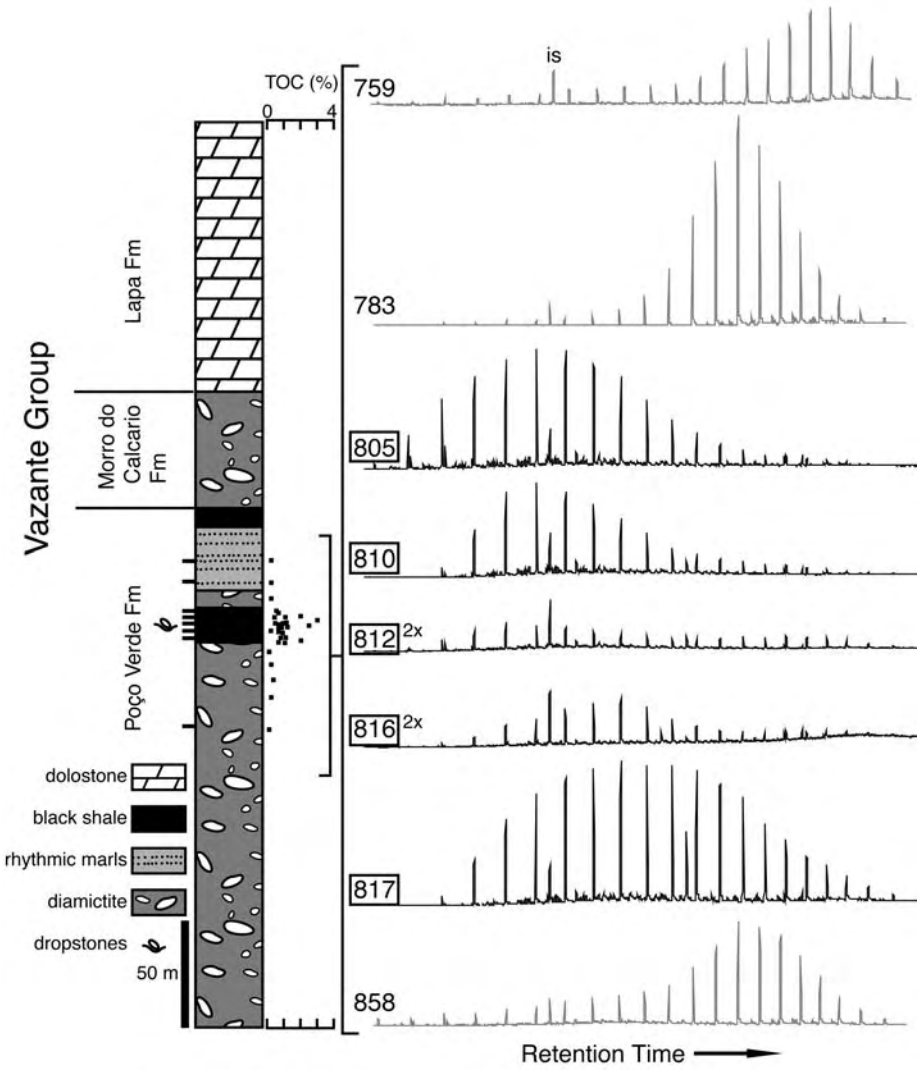

Fig. 2. Stratigraphic log of the core, TOC through the Poço Verde Formation (Fm), and GC-MS total ion chromatograms for saturate fractions of extracted samples. The underlying Serra do Garrote Formation was not sampled by this drill core, but in other cores the Poço Verde Formation is over 200 m thick. Tick marks to the left of the core log show location of samples used for biomarker analysis, and the numbers to the left of the chromatograms show the depth from which these samples were taken. The five boxed depths indicate samples from the organic-rich interval, which were also used to determine the biomarker ratios in table S2. IS is internal standard (hexadecanoic acid isobutylester), present in all chromatograms. Chromatograms for meters 812 and 816 are shown at 2× vertical scale.

To further evaluate environmental conditions during deposition of the Poço Verde Formation, we examined extractable biomarkers in the organic-rich shale by standard techniques (*20*). This interval is located 100 m below the postglacial unit and bounded above and below by diamictite units, and was thus deposited during the glaciation. Although these rocks are well preserved in comparison to other syn-glacial deposits of similar age, they are thermally mature and contain very small quantities of bitumen. They are thus susceptible to interference from migrating hydrocarbons, drill-core collection and handling, and extant biota. Although these sources of contamination would not contribute substantially to measured total organic carbon (TOC, which is >99% insoluble kerogen), they could affect biomarker distributions.

Multiple lines of evidence support the interpretation that extractable biomarkers in these rocks are indigenous. (i) Samples were repeatedly crushed and extracted, and the highest yields of biomarkers were obtained from the finest-grained powders (i.e., the final extraction). (ii) TOC contents and carbon-isotope ratios of kerogen and bitumen covary with lithology. Extract yields from different rocks correlate with measured TOC and constitute <0.05% of the TOC (table S1). (iii) Extracts from carbonate rocks above the organic-rich intervals and from diamictites below contain different biomarker distributions than those within organic-rich rocks (Fig. 2 and fig. S1), whereas laboratory blanks contained no detectable biomarkers. (iv) No petroleum source rocks or reservoirs are known from the Paracatú region, and no biomarkers indicative of exclusively Phanerozoic biota (such as higher plants) were detected. (v) Biomarker ratios that are controlled by depositional source conditions vary between rock types (table S2). (vi) Biomarker

ratios controlled by heating (table S2) predict moderate thermal maturity in these rocks, in agreement with petrologic assessments of thermal history including amber-colored blebs of organic matter. (vii) Polar lipids indicative of living microorganisms were not detected in the extracts.

Biomarker abundance is higher in the black shale than in the marl and the carbonate-matrix diamictite (fig S1). Taxa-specific biomarkers (table S3) extracted from the syn-glacial organic-rich shale include 2-α-methylhopanes, derived from cyanobacteria (*21*), and alkylated 2,3,6-trimethylbenzenes, which we interpret as molecular fossils of the isoprenoid pigment isorenieratene from green sulfur bacteria (*22*, *23*). The green sulfur bacteria are anaerobic organisms that use H_2S as the electron donor for photosynthesis and are strongly inhibited by the presence of O_2. Their presence is generally interpreted as evidence for an anoxic, sulfidic, photic zone (*22*). These biomarkers provide good evidence for the presence of photosynthetic organisms and, by extension, the penetration of sunlight to the sea surface. Other extractable biomarkers include 3-β-methylhopanes, known only from microaerophilic proteobacteria including the aerobic methanotrophs (*24*). Gammacerane, a C_{30} triterpane, is thought to derive from protozoan tetrahymanol (*25*). Although the organisms that produce tetrahymanol are heterotrophic aerobes, gammacerane is often prevalent in sediments formed under a stratified water column. Stable carbon-isotope studies of gammacerane have shown that the bacteriovores that produce tetrahymanol consume green and purple sulfur bacteria, so the protozoa live at or below the chemocline (*26*). C_{27} and C_{28} di- and trinorhopanes tend to be found in high concentration in sulfidic sediments, although the precursor organism is not yet known (*27*). Steranes not methylated at C-4, also found in the core, are produced exclusively by aerobic eukaryotes and may represent algal contributions.

Taken together, the biomarker data portray a diverse microbial community based upon photosynthetic primary production, consistent with sunlight availability and thus with relatively thin sea ice or an ice-free environment. Residents included anaerobic and aerobic bacteria, photoautotrophs and heterotrophs, eukaryotes, and perhaps even protists. Although our description of such a community via molecular fossils is necessarily incomplete and has very limited ability to discern eukaryotic diversity, the assemblage is nevertheless indistinguishable from those recorded in rocks both before and after this low-latitude Neoproterozoic glaciation (*27–32*). There is thus no evidence of a biotic crisis among prokaryotes at this location, and the inferred oxic, sunlit waters would have provided ample habitat for eukaryotes. Recent investigations of syn-glacial microfossil assemblages have reached similar conclusions (*33*, *34*).

Although the Poço Verde Formation rocks are consistent with local ice-free conditions, they are also compatible with the possibility that a complex ecosystem persisted within or immediately beneath relatively thin sea ice. Both modern and ancient examples of productive sea ice are known. Permian glacial strata in Tasmania provide a Paleozoic analog and contain up to 60% organic carbon interbedded with abundant ice-rafted debris (*35*). Perhaps the most striking modern analog originates in the highly productive ice margin environments surrounding Antarctica today, where complex communities of microbial eukaryotes (including metazoa) and photosynthetic and heterotrophic bacteria thrive (*36–39*). Annual net primary productivity in the Ross Sea is estimated at 200 g C m^{-2} $year^{-1}$ (*40*), comparable to estimates for coastal oceans of 250 g C m^{-2} $year^{-1}$ (*41*). Such environments have been previously proposed as analogs to Snowball Earth (*39*, *42*). The Poço Verde strata described here provide some support for this proposal.

Whether the environment represented by the Poço Verde rocks represents a singular, albeit large, refugium or a widespread phenomenon remains an open question to be settled by discovery and analysis of other rocks. The Poço Verde strata suggest limited ice thickness at low latitudes during at least part of the glacial interval, although the data are compatible with periods of more complete ice cover at other times. However, if the Poço Verde strata are representative of more widespread conditions, then the hypothesis of thick, global sea ice—and dependent mechanisms for carbon-isotopic anomalies during this period—will need to be reexamined. Regardless of the extent to which the Earth was icebound, the presence of this deposit indicates that diverse life, including eukaryotes and photosynthetic bacteria, apparently continued in abundance during this Neoproterozoic glaciation.

References and Notes

1. A. J. Kaufman, A. H. Knoll, G. M. Narbonne, *Proc. Natl. Acad. Sci. U.S.A.* **94**, 6600 (1997).
2. P. F. Hoffman, A. J. Kaufman, G. P. Halverson, D. P. Schrag, *Science* **281**, 1342 (1998).
3. M. J. Kennedy, N. Christie-Blick, L. E. Sohl, *Geology* **29**, 443 (2001).
4. M. J. Kennedy, N. Christie-Blick, A. R. Prave, *Geology* **29**, 1135 (2001).
5. P. F. Hoffman, D. P. Schrag, *Terra Nova* **14**, 129 (2002).
6. F. A. Corsetti, A. J. Kaufman, *Geol. Soc. Am. Bull.* **115**, 916 (2003).
7. S. Xiao, in *The Extreme Proterozoic: Geology, Geochemistry, and Climate*, G. Jenkins, M. McMenamin, L. Sohl, Eds. [*Geophys. Monogr. Am. Geophys. Union* 146 (2004)], pp. 199–214.
8. J. L. Kirschvink, in *The Proterozoic Biosphere: A Multidisciplinary Study*, J. W. Schopf, C. Klein, Eds. (Cambridge Univ. Press, Cambridge, 1992), p. 1348.
9. B. Runnegar, *Nature* **405**, 403 (2000).
10. W. T. Hyde, T. J. Crowley, S. K. Baum, W. R. Peltier, *Nature* **405**, 425 (2000).
11. D. Pollard, J. F. Kasting, *J. Geophys. Res.* **110**, C07010 (2005).
12. M. Babinski, L. V. S. Monteiro, A. H. Fetter, J. S. Bettencourt, T. F. Oliveira, *J. S. Am. Earth Sci.* **2005**, 293 (2005).
13. Six cores were examined in the field, four of which were collected. One core was selected for biomarker analysis on the basis of the thickness of the black shale unit.
14. K. B. Brody, A. J. Kaufman, J. L. Eigenbrode, G. D. Cody, paper presented at the Geological Society of America Annual Meeting, Denver, CO, 7 to 10 November, 2004.
15. K. Azmy *et al.*, *Precambrian Res.* **112**, 303 (2001).
16. S. B. Jacobsen, A. J. Kaufman, *Geochim. Cosmochim. Acta* **161**, 37 (1999).
17. G. P. Halverson, A. C. Maloof, P. F. Hoffman, *Basin Res.* **16**, 297 (2004).
18. N. P. James, G. M. Narbonne, R. W. Dalrymple, T. K. Kyser, *Geology* **33**, 9 (2005).
19. J. I. Hedges, R. G. Keil, *Mar. Chem.* **49**, 137 (1995).
20. Information on materials and methods is available on *Science* Online.
21. R. E. Summons, L. L. Jahnke, J. M. Hope, G. A. Logan, *Nature* **400**, 554 (1999).
22. R. E. Summons, T. G. Powell, *Geochim. Cosmochim. Acta* **51**, 557 (1987).
23. Trimethylbenzes were identified from their mass spectra (fig. S2). Although they are widely interpreted as products of isorenieratene [e.g., (*43–45*)], one recent report (*46*) has suggested they might also be derived from β-carotene. Biomarker yields are too low to allow confirmatory compound-specific ^{13}C analyses.
24. R. E. Summons, L. L. Jahnke, in *Biological Markers in Sediments and Petroleum: A Tribute to Wolfgang K. Seifert*, J. M. Moldowan, P. Albrecht, R. P. Philp, Eds. (Prentice Hall, Englewood Cliffs, NJ, 1992), pp. 182–200.
25. H. L. ten Haven, M. Rohmer, J. Rullkoetter, P. Bisseret, *Geochim. Cosmochim. Acta* **53**, 3073 (1989).
26. J. S. Sinninghe Damste *et al.*, *Geochim. Cosmochim. Acta* **59**, 1895 (1995).
27. R. E. Summons *et al.*, *Geochim. Cosmochim. Acta* **52**, 2625 (1988).
28. R. E. Summons, M. R. Walter, *Am. J. Sci.* **290-A**, 212 (1990).
29. G. A. Logan, R. E. Summons, J. M. Hayes, *Geochim. Cosmochim. Acta* **61**, 5391 (1997).
30. G. A. Logan *et al.*, *Geochim. Cosmochim. Acta* **63**, 1345 (1999).
31. K. Arouri, P. J. Conaghan, M. R. Walter, G. C. O. Bischoff, K. Grey, *Precambrian Res.* **100**, 235 (2000).
32. C. Li, P. a. Peng, G. Sheng, J. Fu, Y. Yan, *Precambrian Res.* **125**, 337 (2003).
33. F. A. Corsetti, S. M. Awramik, D. Pierce, *Proc. Natl. Acad. Sci. U.S.A.* **100**, 4399 (2003).
34. F. A. Corsetti, A. N. Olcott, C. Bakermans, *Palaeogeogr. Palaeoclimatol. Palaeoecol.*, in press.
35. A. T. Revill *et al.*, *Geochim. Cosmochim. Acta* **58**, 3803 (1994).
36. J. C. Priscu *et al.*, *Science* **280**, 2095 (1998).
37. D. R. Mueller, W. F. Vincent, W. H. Pollard, C. H. Fritsen, *Nova Hedwigia Beih.* **123**, 173 (2001).
38. D. N. Thomas, G. S. Dieckmann, *Science* **295**, 641 (2002).
39. W. F. Vincent, D. R. Mueller, S. Bonilla, *Cryobiology* **48**, 103 (2004).
40. W. O. Smith Jr., L. I. Gordon, *Geophys. Res. Lett.* **24**, 233 (1997).
41. G. A. Knauer, in *Interactions of C, N, P, and S Biogeochemical Cycles and Global Change*, R. Wollast, F. T. Mackenzie, L. Chou, Eds. (Springer-Verlag, New York, 1993), pp. 211–231.
42. W. F. Vincent *et al.*, *Naturwissenschaften* **87**, 137 (2000).
43. D.-J. H. Simons, F. Kenig, C. J. Schroder-Adams, *Org. Geochem.* **34**, 1177 (2003).
44. T. C. Brown, F. Kenig, *Palaeogeogr. Palaeoclimatol. Palaeoecol.* **215**, 59 (2004).
45. K. Grice *et al.*, *Science* **307**, 706 (2005); published online 20 January 2005 (10.1126/science.1104323).
46. M. P. Koopmans *et al.*, *Geochim. Cosmochim. Acta* **60**, 4467 (1996).
47. T. R. Fairchild *et al.*, *Precambrian Res.* **80**, 125 (1996).

48. We thank Companhia Mineira de Metais for samples,

R. Summons and E. Grosjean for helpful discussion and metastable-reaction monitoring gas chromatography–mass spectroscopy (GC-MS) analyses; G. Love, A. Bradley, J. Brocks, C. Li, M. Eek, K. Nealson, and W. Berelson for helpful discussion; J. Pinho and K. B. Brody for help in Brazil; N. Geboy and C. France for TOC abundance data; G. McDonald for lab access; as well as two anonymous reviewers for comments.

Supported by NSF grants EAR0418083 (F.C., A.S., A.O.) and EAR0126378 (A.J.K.) and NASA Exobiology grant 42000-62153 (F.C. and A.O.).

Supporting Online Material
www.sciencemag.org/cgi/content/full/1115769/DC1
Analytical Methods
Figs. S1 and S2
Tables S1 to S3
References and Notes

6 June 2005; accepted 21 September 2005
Published online 29 September 2005;
10.1126/science.1115769
Include this information when citing this paper.

The Evolution of Titan's Mid-Latitude Clouds

C. A. Griffith,[1] P. Penteado,[1] K. Baines,[2] P. Drossart,[3] J. Barnes,[1] G. Bellucci,[4] J. Bibring,[5] R. Brown,[1] B. Buratti,[2] F. Capaccioni,[6] P. Cerroni,[6] R. Clark,[7] M. Combes,[3] A. Coradini,[6] D. Cruikshank,[8] V. Formisano,[4] R. Jaumann,[9] Y. Langevin,[5] D. Matson,[2] T. McCord,[10] V. Mennella,[11] R. Nelson,[2] P. Nicholson,[12] B. Sicardy,[3] C. Sotin,[13] L. A. Soderblom,[14] R. Kursinski[1]

Spectra from Cassini's Visual and Infrared Mapping Spectrometer reveal that the horizontal structure, height, and optical depth of Titan's clouds are highly dynamic. Vigorous cloud centers are seen to rise from the middle to the upper troposphere within 30 minutes and dissipate within the next hour. Their development indicates that Titan's clouds evolve convectively; dissipate through rain; and, over the next several hours, waft downwind to achieve their great longitude extents. These and other characteristics suggest that temperate clouds originate from circulation-induced convergence, in addition to a forcing at the surface associated with Saturn's tides, geology, and/or surface composition.

The atmosphere of Saturn's largest moon, Titan, contains methane, which, like water on Earth, can exist as a gas, ice, and liquid. This moon is hypothesized to resemble Earth, with a methane cycle similar to the terrestrial hydrological cycle, involving methane clouds, rain, and surface liquids. Yet, unlike Earth, only two kinds of clouds have been detected recently on Titan: large storms near the south pole and long clouds predominantly at –40° latitude (*1*–*8*). The south polar clouds reside at the altitude of neutral buoyancy (*2*, *3*), which is indicative of convection (*5*). Their morphologies and Titan's recent south summer solstice (during October 2002) suggest a seasonal explanation for their formation, through a polar updraft resulting from Titan's pole-to-pole circulation and dynamical lifting from surface heating (*3*, *9*, *10*). The narrow mid-latitude clouds, observed between –37° and –44° latitude, extend several hundred to several thousand kilometers in longitude, residing primarily at 0° ± 40° and secondarily at 90° ± 40° west longitude (*4*). The clouds' propensity for particular spots on Titan's disk suggests a tie to the surface (*4*). Yet Cassini images do not display the morphologies expected of orographic clouds nor the dark and uniform appearance expected of seas (*11*, *12*) that would suggest marine clouds. Cloud formation through methane volcanic outgassing could explain the large amounts of methane in Titan's atmosphere (despite its photochemical loss rate of $\sim 6 \times 10^7$ kg/day), in addition to the temperate clouds' locations. However, the volcanoes would have to coincidentally reside at –40° latitude or outgas sufficient methane to instigate widespread deep convection. The longitude most preferred by the mid-latitude clouds coincides with the sub-Saturn point, which experiences large variations in pressure as Titan orbits Saturn (*13*). However, there has been no observed correlation with cloud activity and Titan's orbital position. Alternatively, Titan's general circulation may give rise to latitudinally confined clouds. Yet this answer does not explain the clouds' preferences for certain longitudes. Here we present measurements from the Cassini Visual and Infrared Mapping Spectrometer (VIMS) (*14*) of the structure and evolution of Titan's clouds, which are diagnostic of the physical processes that govern their formations.

Six spectral images of Titan's clouds were recorded by VIMS on 13 December 2004 as Cassini approached Titan on the third (TB) flyby, from a distance of 236,000 to 179,000 km (Fig. 1). The pixel resolution of the clouds ranged from 90 to 130 km and 50 to 70 km in the roughly east-west and north-south directions, respectively, with the highest resolutions achieved in the last image recorded during the 3-hour sequence. Each pixel within the images consists of a spectrum from 0.8 to 5.0 μm, with a resolving power of 143 at 2 μm. Our analysis focuses on the 2- to 2.5-μm section of the spectra that, as a result of variable methane absorption, samples Titan's atmosphere from 100 km to the surface. Within the center of the methane bands (at 2.25 μm), Titan's atmosphere is opaque and sunlight is reflected from the stratosphere, at roughly 100 km altitude. Between the methane bands (at 2.0 μm), Titan's atmosphere is fairly transparent and sunlight reaches the surface. At intermediate wavelengths (2.12 to 2.16 μm), sunlight probes Titan's troposphere at 10 to 40 km, where methane condenses (*1*). Hourly variations in Titan's 2.12- to 2.16-μm albedos occur solely as a result of changes in the opacity of clouds in the middle to upper troposphere (*1*, *5*). Four mid-latitude clouds are readily identified in the six VIMS images. They reside at the latitude and longitude coordinates of [–61:134], [–47:157], [–43,176], and [–41,115] and are referenced as cloud 1 through cloud 4, respectively (Fig. 1).

We approximate the radiative transfer equation with the discrete ordinates algorithm to simulate the absorption and scattering of Titan's atmosphere and surface (*15*). Comparing the calculated spectra to the data, we estimate the optical depths of the stratospheric haze and methane clouds, the cloud altitudes, and surface reflectivity. Methane, the primary absorber, is calculated from line-by-line techniques, using parameters from the HITRAN database (*16*) and assuming a Voigt line profile and the Voyager temperature profile (*17*). We also include pressure-induced absorption (*18*) due to H_2 and N_2. We assume a methane relative humidity of 50% (0.088 mixing ratio) at the surface and a constant mixing ratio (0.017) in the stratosphere (*19*, *20*). A constant methane mixing

[1]Lunar and Planetary Laboratory, University of Arizona, Tucson, AZ 85721, USA. [2]Jet Propulsion Laboratory, California Institute of Technology, Pasadena, CA 91109, USA. [3]Observatoire de Paris, 5 Place Jules Jannsen, Meudon, France. [4]Instituto di Fisica dello Spazio Interplanetario, Consiglio Nationale delle Richerche (CNR), Rome, Italy. [5]Institut d'Astrophysique Spatiale, Université de Paris-Sud, Orsay, France. [6]Instituto di Astrofisica Spaziale e Fisica Cosmica, CNR, Rome, Italy. [7]U.S. Geological Survey, Denver, CO 80225, USA. [8]NASA Ames Research Center, Moffet Field, Mountain View, CA, USA. [9]Institute of Planetary Exploration, German Aerospace Center, Germany. [10]Department of Earth and Space Sciences, University of Washington, Seattle, WA, USA. [11]Osservatorio Astronomico di Capodimonte, Via Moiariello 16, 80131, Napoli, Italy. [12]Department of Astronomy, Cornell University, Ithaca, NY, USA. [13]Laboratoire de Planétologie et Géodynamique, Université de Nantes, France. [14]U.S. Geological Survey, Flagstaff, AZ 86001, USA.

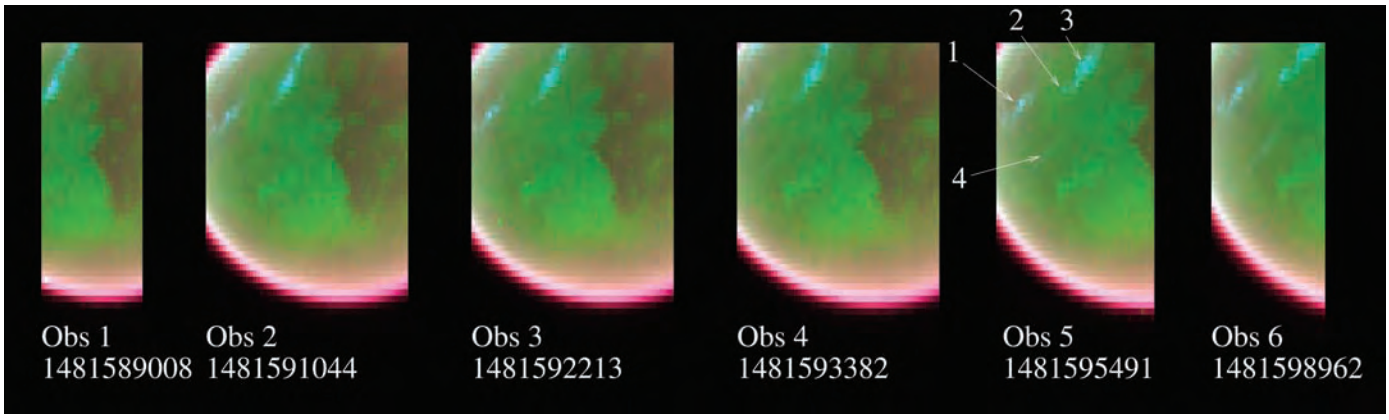

Fig. 1. Six observations (Obs) of Titan's mid-latitude clouds constructed by mapping the 2.13-μm channel to blue, the 2.00-μm channel to green, and the 2.3-μm channel to red. These wavelengths are most sensitive to Titan's clouds, surface, and stratospheric haze, respectively. Obs 1 to 6 (shown with VIMS identification numbers) were recorded at intervals of 34, 20, 20, 35, and 58 min from each other. Clouds 2 to 4 lie near Titan's –40° latitude, whereas cloud 1 resides at –61°. Note the evolution of the clouds with time.

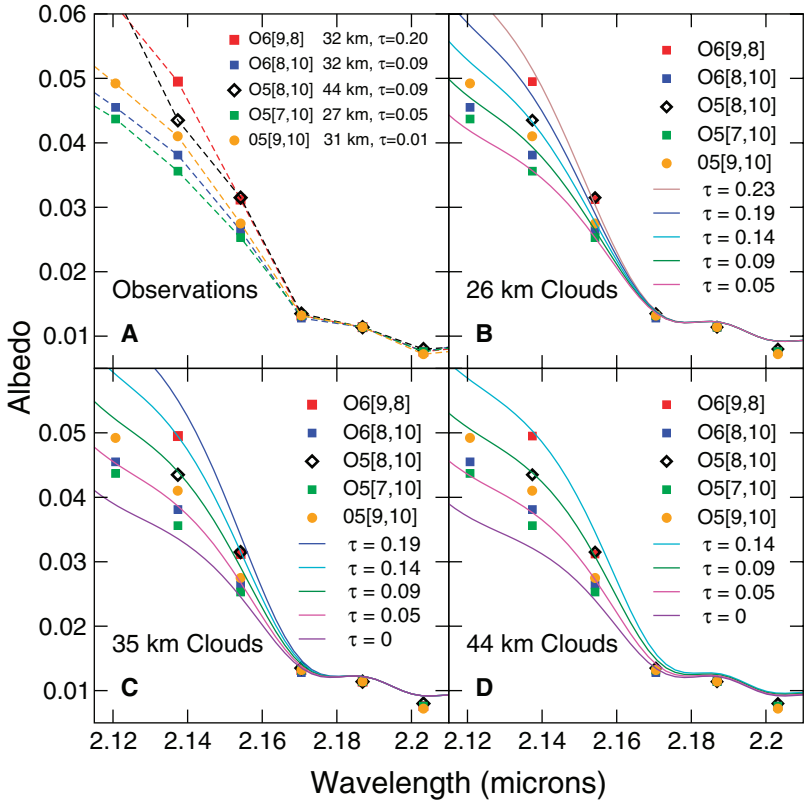

Fig. 2. Observed spectra of cloud 1 are compared to calculated spectra. (**A**) Examples of VIMS spectra resulting from clouds of varying optical depths and altitudes. Indicated are the data observation numbers (Fig. 1), the pixel number (in brackets), and the derived cloud heights and optical depths (τ). Higher clouds affect Titan's spectrum at spectral regions of greater methane opacity (longer wavelengths) for a given optical depth. The dependence of the 2.13- to 2.16-μm slope on the cloud altitudes can be seen by comparing O6[9,8] to O5[8,10]. (**B**) Observations (points) are compared to models (solid lines) calculated with a uniform cloud layer at 26 km altitude for several optical depths. The model spectra between 2.13 and 2.16 μm indicate that pixel O5[7,10] has a cloud near 26 km, of optical depth 0.05. (**C**) Observations O6[9,8], O6[8,10], and O5[9,10[have 2.13- to 2.16-μm slopes similar to models calculated assuming clouds at 35 km, indicating the presence of clouds near this level. (**D**) Observation O5[8,10] matches the model spectrum of a cloud at 44 km, of optical depth 0.09.

ratio is adopted from the surface to the level where saturation is reached, above which methane is saturated up to the tropopause. Uncertainties of a factor of 2 in the methane abundance (greater than expected) cause uncertainties of 5 km in the derived cloud altitudes and 20% in the derived optical depths. We assume spherical haze particles having radii of 0.2 μm from 180 to 90 km altitude. Below 90 km, radii increase with atmospheric pressure to 0.8 μm at 40 km altitude (*21*). We adopt a simple haze profile with a constant density scale height of 120 km above 100 km and a particle density of 1.7 cm^{-3} at 140 km, a constant density of 5 cm^{-3} from 100 to 70 km, and a constant density of 2 cm^{-3} at 70 to 40 km altitude, which fits Titan's cloudless 2.13- to 2.2-μm spectra, although not uniquely. Nonetheless, because the haze optical depth (~0.2) significantly exceeds the gas optical depth (~0.05) above 30 km altitude at 2.13 μm, we estimate fairly accurately the haze optical depth above the clouds. Cloud heights are then derived from the slope of Titan's 2.12- to 2.18-μm spectra, and the 2.13-μm albedo manifests the cloud coverage or optical depth (Fig. 2). Our data do not independently determine the cloud coverage and optical depth. For each pixel, we present the optical depth of a uniform cloud across the pixel, which for a value of τ = 0.3 is equivalent to an optically thick cloud covering 3% of the pixel area.

The four clouds we observed had similar morphologies. Cloud 2 was the simplest; it appeared for the first time in the second observation, O3, as a compact unresolved cloud in one pixel that grew and rose from 20 to 42 km in 35 min (Fig. 3B). Cloud 3 constituted a large area of high (20 to 30 km) clouds within which a small system of clouds rose, penetrated the tropopause at 42 km, and then dissipated within the following 20 min (Fig. 3C). The last image of cloud 3 suggests the beginnings of another rising plume. Multiple centers of activity also appeared in cloud 1 (Fig. 3A) and in the final observations of cloud 4 (Fig. 3D). Cloud 4 displayed the vertical evolution of cumuli from 26 to 42 km in 35 min, followed

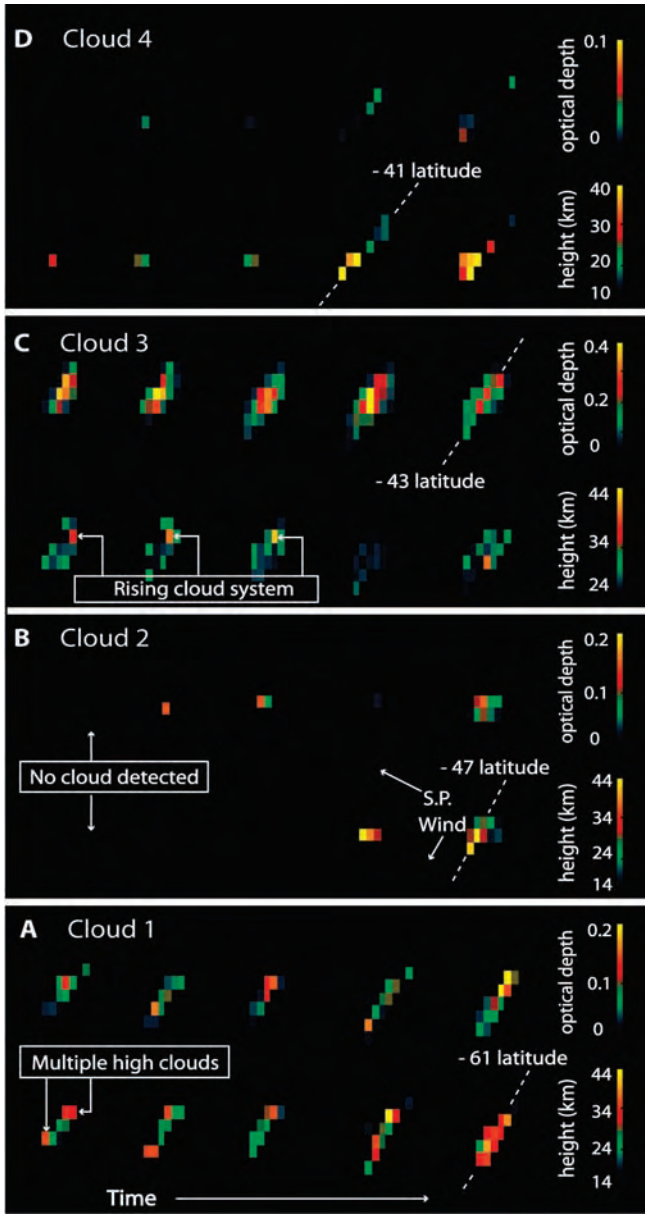

Fig. 3. Images of derived cloud heights (bottom rows) and optical depths (top rows) of Titan's four clouds in a time sequence from left to right indicate the temporal evolution of the clouds (refer to the color bars at right). The orientation of each observation mimics that of Fig. 1, with the south pole in the top left corner of each image, as indicated by S.P. in (B). The clouds extend lengthwise in longitude. (**A**) The optical depths and heights of each pixel comprising the O2 to O6 observations (as referenced in Fig. 1) of cloud 1 (latitude –61°, central longitude 134°). The first observation, O2, is shown in the lefthand column; subsequent observations proceed in order from left to right, recorded at time intervals of 20, 20, 35, and 58 min from the preceding observation (Fig. 1). (**B**) The optical depths and heights of observations O2 to O6 of cloud 2 (latitude –47°, longitude 157°) at intervals of 20, 20, 35, and 58 min. The cloud in O3 and O4 is at ~13 km altitude and thus is not apparent in the bottom row. (**C**) The optical depths and heights of observations O1 to O5 of cloud 3 (latitude –43°, longitude 176°) at intervals of 34, 20, 20, and 35 min. (**D**) The optical depths and heights of observations O2 to O6 of cloud 4 (latitude –41°, longitude 115°) at intervals of 20, 20, 35, and 58 min.

by a growth in size, as seen in the last observation. In both small, perhaps young, clouds (Fig. 3, B and D), horizontal growth followed updrafts, with clouds detected in adjacent eastward pixels (~50 km distance) within 1 hour. If the eastward displaced optical depth results from cloud transport, the implied prograde winds were on the order of 14 m/s, which is consistent with measurements by Cassini's Imaging Science Subsystem (ISS) (*11*). In summary, we detected small centers of vigorous updraft that rose at rates of 2 to 4 m/s in the larger clouds 1 and 3 and 8 to 10 m/s in the more discrete clouds 2 and 4. The slower measured ascent in clouds 1 and 3 may be an artefact of averaging the altitudes of rising plumes with more quiescent ambient clouds within a pixel. High cloud centers were seen to dissipate or fall 10 km to the ambient cloud level within half an hour (Fig. 3, A and C) and to evolve in the eastward direction (Fig. 3, B to D).

The cloud updraft rates agree well with those predicted for convective plumes on Titan (*22*), and incidentally with rates of terrestrial thermals (Fig. 3). The 1/2-hour fall time of the cloud tops from ~40 to 30 km is consistent with the fall velocity of millimeter-sized raindrops (*23*, *24*). The clouds' rapid evolution, discrete high centers, and accompanying increase in optical depth and extent after updrafts indicate that clouds originate as compact convective cells that dissipate through rain and evolve further through zonal wind transport to new longitudes. If fueled by latent heat alone, the convective evolution of a plume requires a parcel to be nearly saturated at the surface; otherwise, thermals would not reach their observed heights at the tropopause (*5*). Alternatively, strong dynamical forcing is required in the form of updrafts, low-level convergence, and/or high-altitude divergence.

The confinement of the clouds primarily to the 0° ± 40° and 90° ± 40° longitudes at –40° latitude suggests a connection to Titan's surface (*4*). However, consistent with Cassini ISS observations (*11*), we detect deviations from this trend. Of the four clouds described here, only one of them (cloud 4) lay near 0° or 90° longitude. Thus, the clouds' association with the surface was either a weak one or would appear to require many surface "events" (such as volcanoes, high winds over mountains, or near-surface methane saturation). Considering ground-based and Cassini observations, event longitudes would include 0°, 39°, 67°, 90°, 115°, 157°, 176°, and 200°, lined up near –40° latitude [(*4*, *11*) and this work]. Additionally we would have to account for the singular presence of similar clouds at –14°, –33°, and –61° latitude [(*11*) and this work] and no cloud detections in the northern hemisphere.

Yet, volcanically outgassed methane would remain confined for a while to a narrow latitude band, because Titan's meridional winds are weak, estimated to be 1 mm/s on average (*25*), in comparison to its zonal winds of tens of meters per second (*11*). One can imagine the humidification of a latitude band, as a result of single volcano, which (if saturation incurred throughout the surface mixing layer) would aid subsequent convective events at the same latitude. We explore this possibility by comparing the mass of a large –40° latitude cloud to the mass of methane required to render the atmosphere unstable to deep convection. We assume the highest optical depth determined in this study, $\tau = 0.4$, and a cloud area of $A = 50{,}000$ km^2, corresponding to a latitude width of 50 km and a downwind longitude extent of 1000 km (*4*). The length of the clouds indicates the airlifted mass transported to new longitudes by one cloud event. The mass of the cloud is given approximately by

$$M = \frac{\tau}{2\pi r^2}\frac{4}{3}\pi r^3 \rho A = 2.3 \times 10^8 \text{kg} \quad (1)$$

where $\rho = 0.06$ g/cm^3 is the mass density of methane ice. The radius of the cloud particles r is taken to be 30 μm: that which survives aloft for the observed cloud lifetimes of 48 hours without falling 10 km out of view. The alternative approach of assuming discrete optically thick clouds covering an effective area of 1000 km^2, a vertical extent of 10 km, and a mass density of 1 g/m^3 (typical of terrestrial clouds) indicates a greater mass of 10^{10} kg.

Assuming an initial humidity of 50%, the mass of methane required to saturate a 0.5-km-thick mixing layer over the entire –37° to –44° latitude band from 0° to 200° longitude, where clouds are observed, is 1.6×10^{14} kg, which is four orders of magnitude greater than the estimated production of one event. However, the cloud mass estimate is uncertain to an order of magnitude, and it is not clear what fraction of the latitude band needs to be saturated to provide the observed activity. In addition, the frequency of potential volcanic events is unknown because of the paucity of observations, leaving open the volcanic possibility. Nonetheless, the volcanic solution is not bolstered by Titan's average –37° to –44° surface albedo at 5 μm, which mimics that between –44° and –50° latitude to within 10% (at 100 km resolution). In addition, the 0° longitude point where clouds are most prevalent (thus the best site for cryvolcanic activity) lies downwind, if prograde as indicated by the ISS observations (*11*), of the less frequent secondary cloud events.

The correlation of Titan's clouds with surface location is only loose, as evidenced by the multiple active centers within the clouds (separated by 200 to 400 km in longitude) and their detections at numerous longitudes. The stronger tie of the clouds to latitude indicates that global circulation plays a role in their formations. To date, clouds have been detected only at southern latitudes, where solar insolation is greatest and the upward branch of the pole-to-pole circulation is expected. In addition, the latitude of –40°, where most clouds are observed, coincides closely with an abrupt decrease in the vast layer of diffuse particles that surrounds the south pole (*26*, *27*). The cutoff of this veil suggests a change in circulation at –40° latitude, which is not predicted in most circulation models of Titan. Yet a recent general circulation model of Titan includes haze caps at Titan's pole (*28*, *29*) and indicates the presence of a converging circulation branch at –40° latitude (*30*). In this model, the thick haze inhibits surface heating at the poles, thereby causing the hottest summer surfaces (which trigger updrafts and convergence) to occur at more temperate latitudes.

The clouds' propensity for 0° and 90° longitude nonetheless suggests a secondary forcing mechanism from the surface. Solar surface heating, Saturn's tidal forcing, and maritime clouds would imply that clouds correlate with surface reflectivity, orbital position, or surface liquids, respectively, which is not observed. Volcanically produced clouds would persist at 0° and 90° longitude and –40° latitude as the seasons change, in contrast to the seasonal latitudinal change expected of circulation-driven clouds. These causes are testable with future observations. Although observations suggest that Titan's circulation dictates the latitude of Titan's clouds, the processes that establish the clouds' longitude remain unclear and involve unknown characteristics of Titan's still largely unexplored surface.

References and Notes

1. C. A. Griffith, T. Owen, G. A. Miller, T. R. Geballe, *Nature* **395**, 575 (1998).
2. H. G. Roe, I. de Pater, B. A. Macintosh, C. P. McKay, *Astrophys. J.* **581**, 1399 (2002).
3. M. E. Brown, A. H. Bouchez, C. A. Griffith, *Nature* **420**, 795 (2002).
4. H. G. Roe, A. H. Bouchez, C. A. Trujillo, E. L. Schaller, M. E. Brown, *Astrophys. J.* **618**, L49 (2005).
5. C. A. Griffith, J. L. Hall, T. R. Geballe, *Science* **290**, 509 (2000).
6. S. G. Gibbard *et al.*, *Icarus* **169**, 429 (2004).
7. E. Gendron *et al.*, *Astron. Astrophys.* **417**, L21 (2004).
8. A. H. Bouchez, M. E. Brown, *Astrophys. J.* **618**, L53 (2005).
9. T. Tokano, *Icarus* **173**, 222 (2005).
10. C. A. Griffith, C. P. McKay, in preparation.
11. C. C. Porco *et al.*, *Nature* **434**, 159 (2005).
12. C. Elachi *et al.*, *Science* **308**, 570 (2005).
13. T. Tokano, F. M. Neubauer, *Icarus* **158**, 499 (2002).
14. R. Brown *et al.*, *Icarus* **164**, 461 (2003).
15. K. Stamnes, S. Tsay, W. Wiscombe, K. Jayweera, *Appl. Opt.* **27**, 2502 (1988).
16. L. S. Rothman *et al.*, *J. Quant. Spectrosc. Radiat. Transfer* **82**, 5 (2003).
17. E. Lellouch *et al.*, *Icarus* **79**, 328 (1989).
18. A. R. W. McKellar, *Icarus* **80**, 361 (1989).
19. H. B. Niemann *et al.*, *Bull. Am. Astron. Soc.* **37**, 621 (2005).
20. F. M. Flasar *et al.*, *Science* **308**, 975 (2005).
21. M. G. Tomasko *et al.*, in *Huygens Science, Payload and Mission* (ESA-SP 1177, European Space Agency Publications Division, Noordwijk, Netherlands, 1997), pp. 345–358.
22. M. Awal, J. I. Lunine, *Geophys. Res. Lett.* **21**, 2491 (1994).
23. O. B. Toon, C. P. McKay, R. Courtin, T. P. Ackerman, *Icarus* **75**, 255 (1988).
24. R. D. Lorenz, *Planet. Space Sci.* **41**, 647 (1993).
25. F. M. Flasar, R. E. Samuelson, B. J. Conrath, *Nature* **292**, 693 (1981).
26. A. Bouchez, thesis, California Institute of Technology, Pasadena, CA (2003).
27. M. Ádámkovics, I. de Pater, H. G. Roe, S. G. Gibbard, C. A. Griffith, *Geophys. Res. Lett.* **31**, 17 (2004).
28. P. Rannou, F. Hourdin, C. P. McKay, *Nature* **418**, 853 (2002).
29. P. Rannou, F. Hourdin, C. P. McKay, D. Luz, *Icarus* **170**, 443 (2004).
30. P. Rannou, F. Hourdin, S. Lebonnois, D. Luz, F. Montmessin, in *COSPAR Scientific Assembly 2004 Abstracts*, 18 to 25 July 2004, Paris, France (Committee on Space Research, Paris, France, 2005), p. 1272.

31. This research was supported by the Cassini Mission of NASA's Planetary Astronomy Program. P.P.'s work is also sponsored by the Brazilian Government through the Coordenação de Aperfeiçoamento de Pessoal de Nivel Superior scholarship. We thank D. Lytle for help with the figures and the reviewers for their constructive suggestions.

20 July 2005; accepted 14 September 2005
10.1126/science.1117702

Geographic Control of Titan's Mid-Latitude Clouds

Henry G. Roe,[1]* Michael E. Brown,[1] Emily L. Schaller,[1] Antonin H. Bouchez,[2] Chadwick A. Trujillo[3]

Observations of Titan's mid-latitude clouds from the W. M. Keck and Gemini Observatories show that they cluster near 350°W longitude, 40°S latitude. These clouds cannot be explained by a seasonal shift in global circulation and thus presumably reflect a mechanism on Titan such as geysering or cryovolcanism in this region. The rate of volatile release necessary to trigger cloud formation could easily supply enough methane to balance the loss to photolysis in the upper atmosphere.

Saturn's largest moon, Titan, is surrounded by a thick atmosphere of nitrogen and methane. Observations of tropospheric clouds (*1*–*6*) and the recent Huygens images of channels show that Titan has an active methane hydrological cycle. The recent discovery (*6*) and continued observations (*7*) of cloud activity at 40°S latitude have led to the suggestion that these mid-latitude clouds are likely the result of seasonally evolving global circulation (*6*). Because photolytic chemistry should deplete methane within 10^7 to 10^8 years (*8*–*10*), the presence of methane in Titan's atmosphere implies that there is a source on Titan's surface, although no sites of active methane release have yet been discovered.

Tropospheric clouds are best observed in a narrow spectral region around a wavelength of 2.12 μm (*11*). Using adaptive optics systems at the W. M. Keck Observatory's 10-m telescope (*12*) and the Gemini Observatory's 8-m telescope (*13*), we imaged Titan's clouds and surface with a resolution of ~300 km in just a few minutes of observing time. During the 2003–2004 and 2004–2005 apparitions of Titan, we acquired usable data on 41 nights with the Keck telescope (*14*) and 47 nights with the Gemini telescope (*15*) (82 separate nights). Although most nights showed cloud activity at latitudes south of 70°S, on 15 nights we observed separate clouds near 40°S

[1]Division of Geological and Planetary Sciences, [2]Caltech Optical Observatories, California Institute of Technology, Pasadena, CA 91125, USA. [3]Gemini Observatory, Hilo, HI 96720, USA.

*To whom correspondence should be addressed. E-mail: hroe@gps.caltech.edu

latitude. (Figs. 1 and 2; table S1) Most of the clouds were clustered tightly near 350°W longitude, with a lesser population apparent between ~45°W and ~160°W (Fig. 3).

In contrast to the south polar clouds, which have been observed to have lifetimes of several weeks (*5*), the mid-latitude clouds had lifetimes of only ~1 Earth day, although remnant wisps below our resolution and contrast limits may have existed for a longer period of time. We possibly observed the same clouds on two consecutive nights on only three occasions (8 and 9 April 2004, 4 and 5 May 2004, and 2 and 3 October 2004). In each case, the cloud appeared to be less prominent on the second night. On 3 November 2004 and 21 February 2005, we observed mid-latitude clouds that were not present in images taken the previous night and the following night. During a full night of observing on 19 December 2004, we observed the development of a mid-latitude cloud system from nothing to full prominence in ~6 hours. By the following night (20 December 2004) this cloud system had disappeared, although we observed new clouds at approximately the same geographic location on 21 December 2004. The short lifetimes of these clouds suggest that methane humidity is substantially less than saturation in the atmosphere on average. A formation mechanism that can cycle on and off in much less than a Titan day is required.

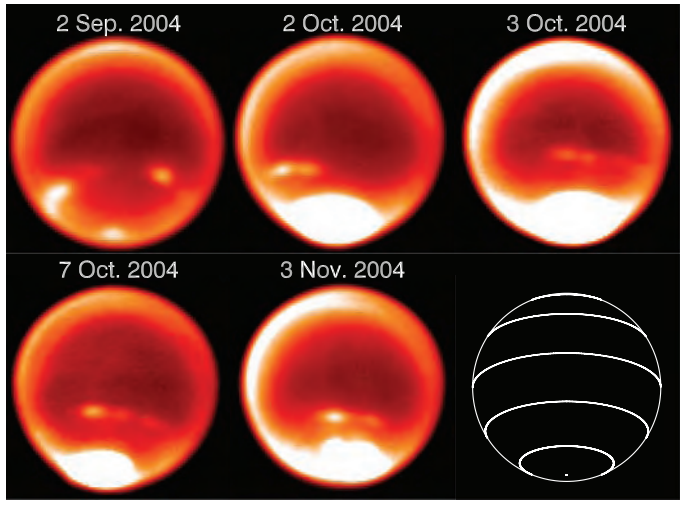

Fig. 1. Images of Titan in a narrowband 2.12-μm-wavelength filter from 5 nights of prominent mid-latitude cloud activity. At lower right, lines of constant latitude for every 30° from equator to pole are plotted at the same scale as the Titan images. Titan's current season is early southern summer, and thus the south pole is visible at the bottom of the image. In October and November 2004, a giant storm was in progress near the south pole. The 2.12-μm-wavelength filter is chosen as it best separates tropospheric cloud features from surface features.

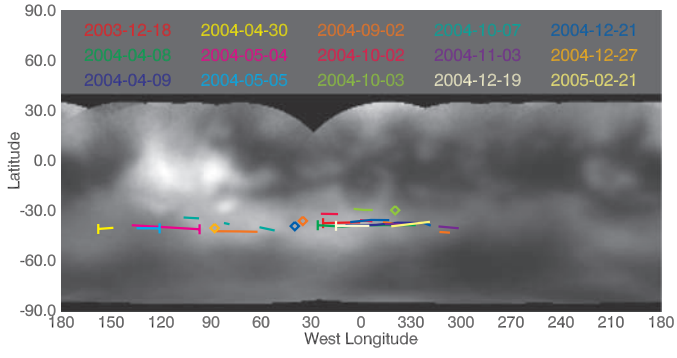

Fig. 2. Locations of all mid-latitude clouds observed to date, shown over a surface map of Titan created from the Keck imagery. Clouds smaller than the spatial resolution of the data (~300 km) are shown as diamonds (◇).

We first observed a mid-latitude cloud on 18 December 2003, and we observed clouds frequently throughout 2004. The sudden appearance after 16 nights of not seeing mid-latitude clouds led us to propose that these clouds were a new phenomenon caused by a seasonal change in the global circulation on Titan (*6*). Coincidently, our observations before December 2003 were significantly biased to the hemisphere nearly opposite the concentrated region of cloud formation, as shown in Fig. 3. A major reason for not seeing mid-latitude clouds before December 2003 could be simply that we had very few observations covering the longitude region in which they are concentrated. To test the statistical significance of the lack of observed clouds before December 2003, we modeled the clouds as two populations, one between 310°W and 30°W longitude with a ~15% probability of a cloud existing at any given moment, and the second population lying between 40°W and 150°W with a ~4% probability. The expected number of observed clouds in the data collected before December 2003 is less than one in both cases, with the probability of observing zero clouds being 0.58 for the first population and 0.66 for the second. Our data set is consistent with these clouds being an ongoing phenomenon on Titan, and we cannot rule out their existence before December 2003 with any statistical significance. Our hypothesis that these clouds only started forming in December 2003 is no longer supported, and thus a seasonal change in global circulation no longer need be invoked to explain the lack of mid-latitude cloud observations before December 2003.

Titan's mid-latitude clouds are nearly always extended in longitude and often appear in groupings of several clouds along a line nearly parallel to longitude. A cloud strung out along a line, parallel to the expected dominant wind flow, is suggestive of a single source forming a cloud that is then sheared out by wind. This morphology and the clustering of the clouds over one small surface region are suggestive of a geographically controlled formation mechanism. If mid-latitude clouds are formed over only a single geographic feature and the tropospheric winds do not shift direction, then the short cloud lifetimes should allow us to pinpoint that source feature. However, a recent study (*16*) of tidal forces shows that Titan's lower tropospheric winds may shift substantially over the course of a Titan day. In one case (2 to 3 October 2004) we saw a cloud that appeared to have moved eastward at 8 m/s and northward at 3 m/s, which is consistent with the expected direction and magnitude of the tidal winds at the time. The extreme clustering of clouds near longitude ~350°W and latitude ~40°S shows that the primary source of the mid-latitude clouds must be nearby. A second, lesser population of clouds at longitudes 40°W to 150°W suggests that additional source regions may exist.

The thermal structure of most of Titan's troposphere is controlled by radiative, rather than convective, processes (*17*). At the troposphere's base, a region of active dry convection maintains a temperature difference of a few degrees between atmosphere and surface. The top of this convective boundary layer (TCBL) is only a few hundreds of meters to a few kilometers above the surface. The level of free convection (LFC) is the altitude at which a parcel of moist air is buoyant as a result of the release of latent heat from condensation. Over most of Titan, the LFC is several kilometers above the TCBL. Convective clouds are formed on Titan when either the TCBL is raised up to the LFC or the LFC is lowered

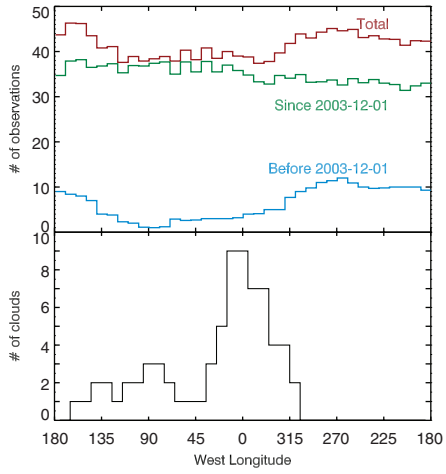

Fig. 3. The number of clouds observed in each 10° bin of planetocentric longitude is shown on the bottom. The total number of nights our observations covered each 10° bin of longitude is shown on the top, as well as divided into the periods of before and after 1 December 2003. In the 2-year data set, the mean number of observations of each 10° bin of longitude was 41 and the minimum number was 37. Through coincidence, the observations taken before 1 December 2003 are heavily biased away from the region where we see the most mid-latitude cloud activity.

down to the TCBL. The TCBL can be lifted by heating of the surface or lower atmosphere, thus requiring more energy to be convectively transported upward. The LFC for a parcel of air can be lowered by injection of methane. The conditional instability of Titan's atmosphere to saturation below ~15 km means that simply raising the humidity to 100% by injecting methane at Titan's surface will lead to a convective cloud (*2*).

Titan's surface can be heated by solar radiation or internal sources, such as cryovolcanism and the subsurface motions of water-ammonia cryo-lava. Solar radiation cannot explain the observed localization of clouds at this season. The time scale for surface temperature changes due to geologic activity is almost certainly much longer than the rate at which mid-latitude cloud formation starts and stops, and geothermal activity seems unlikely to be the sole driver of mid-latitude cloud formation.

Injection of methane into the atmosphere, either by geysers or during cryovolcanic activity, appears to be the most plausible triggering mechanism for the mid-latitude clouds, as any such process would be sporadic and localized geographically. Recent speculation exists that an unusually shaped 30-km feature imaged by Cassini on Titan's surface might be the remnant dome of a cryovolcano (*18*). We have seen no cloud activity in this region (8.5°N latitude, 143.5°W longitude) and no evidence for release of volatiles from this site.

Injection from a geologic source could also solve the conundrum of the long-term existence of Titan's methane atmosphere. Methane is lost from Titan's atmosphere at a rate of ~200 kg/s resulting from photolytic chemistry in the upper atmosphere (*9*, *19*). Assuming a background humidity of 60%, a geyser need only saturate a region of the boundary layer 2 km in diameter and 300 m high once every 7 days to resupply the lost methane. Notably, the rate of mid-latitude cloud formation we observe could easily account for the entire methane resupply needed to explain the current atmospheric methane abundance. A strong sporadic source of methane would not only create clouds in the surrounding region but also raise the background methane abundance in its latitude band. A weaker source of methane, which at other latitudes would not generate substantial clouds, would then more easily generate clouds because of the enhanced background methane abundance. Thus, the lesser population of clouds observed at longitudes ~45°W to 160°W may be the result of one or more weaker sources of methane boosted by the latitudinal band of methane enhancement from the strong methane source near ~350°W longitude.

A possible driver of geologic activity is the tides caused on Titan by the eccentricity of its orbit about Saturn. Titan's subsaturnian point lies at 0° latitude and 0°W longitude, not far from the region in which we see the most significant mid-latitude cloud activity. On Jupiter's moon Io, the largest effect of tidal heating is seen near the sub-jovian point (*20*). From our observations of mid-latitude clouds, the region around ~350°W longitude, ~40°S latitude appears to be the most likely place on Titan to find present-day release of volatiles and geologic activity, including possibly cryovolcanism.

References and Notes

1. C. A. Griffith, T. Owen, G. A. Miller, T. Geballe, *Nature* **395**, 575 (1998).
2. C. A. Griffith, J. L. Hall, T. R. Geballe, *Science* **290**, 509 (2000).
3. M. E. Brown, A. H. Bouchez, C. A. Griffith, *Nature* **420**, 795 (2002).
4. H. G. Roe, I. de Pater, B. A. Macintosh, C. P. McKay, *Astrophys. J.* **581**, 1399 (2002).
5. A. H. Bouchez, M. E. Brown, *Astrophys. J.* **618**, L53 (2005).
6. H. G. Roe, A. H. Bouchez, C. A. Trujillo, E. L. Schaller, M. E. Brown, *Astrophys. J.* **618**, L49 (2005).
7. C. C. Porco *et al.*, *Nature* **434**, 159 (2005).
8. D. F. Strobel, *Icarus* **21**, 466 (1974).
9. J. I. Lunine, D. J. Stevenson, Y. L. Yung, *Science* **222**, 1229 (1983).
10. E. H. Wilson, S. K. Atreya, *J. Geophys. Res.* **109**, E06002 (2004).
11. At 2.12 μm, the combined opacity of methane, nitrogen, and hydrogen is strong enough to obscure the surface but weak enough to allow probing of the tropospheric region of interest (*1*). On most nights we observed in three filters, chosen to probe varying altitude levels in Titan's atmosphere. Images in the K′ filter [2.03 to 2.36 μm (*21*)] are dominated by surface features, although tropospheric clouds are also visible. Images in the $H_2$1-0 filter (2.111 to 2.137 μm) show primarily tropospheric cloud activity. As a result of high methane, opacity images in the Brγ filter [2.154 to 2.183 μm (*21*)] show only the high haze layers approximately above the tropopause. The clouds do not appear in the Brγ filter images, thus allowing us to restrict their altitude range to the troposphere. At these wavelengths the scattering due to haze particles is much weaker than at shorter visible wavelengths, giving the clearest possible view of atmospheric and surface features on Titan.
12. P. Wizinowich *et al.*, *Pub. Astron. Soc. Pac.* **112**, 315 (2000).
13. K. W. Hodapp *et al.*, *Pub. Astron. Soc. Pac.* **115**, 1388 (2003).
14. We acquired images with high enough contrast and resolution to detect the mid-latitude clouds on the Keck telescope on universal time coordinated (UTC) dates: 17 September 2003, 10 to 12 October 2003, 9 November 2003, 11 to 14 November 2003, 18 November 2003, 29 November 2003, 10 December 2003, 15 December 2003, 17 to 18 December 2003, 24 to 27 December 2003, 9 to 10 January 2004, 2 September 2004, 28 September 2004, 2 to 3 October 2004, 7 to 8 October 2004, 23 October 2004, 28 October 2004, 2 to 3 November 2004, 27 November 2004, 19 to 20 December 2004, 14 January 2005, 20 January 2005, 14 to 15 February 2005, 25 February 2005, and 27 to 28 February 2005.
15. We acquired images with high enough contrast and resolution to detect the mid-latitude clouds on the Gemini telescope on UTC dates: 13 November 2003, 15 November 2003, 17 to 18 November 2003, 4 to 9 April 2004, 30 April 2004, 4 to 7 May 2004, 23 to 24 October 2004, 1 to 2 November 2004, 4 to 5 November 2004, 21 December 2004, 24 to 25 December 2004, 27 December 2004, 16 January 2005, 23 to 25 January 2005, 28 January 2005, 8 to 10 February 2005, 12 February 2005, 14 to 16 February 2005, 19 to 22 February 2005, 1 to 2 March 2005, 4 to 5 March 2005, 9 March 2005, and 24 March 2005.
16. T. Tokano, F. M. Neubauer, *Icarus* **158**, 499 (2002).
17. C. P. McKay, J. B. Pollack, R. Courtin, *Icarus* **80**, 23 (1989).
18. C. Sotin *et al.*, *Nature* **435**, 786 (2005).
19. L. M. Lara, M. Banaszkiewicz, R. Rodrigo, J. J. Lopez-Moreno, *Icarus* **158**, 191 (2002).
20. T. V. Johnson *et al.*, *Science* **226**, 134 (1984).
21. H. G. Roe, M. E. Brown, E. L. Schaller, A. H. Bouchez, C. A. Trujillo, data not shown.

22. H.G.R. is supported by an NSF Astronomy and Astrophysics Postdoctoral Fellowship (NSF AST-0401559). E.L.S. is supported by an NSF Graduate Research Fellowship. Additional support was provided by an NSF grant to M.E.B. (NSF AST-0307929). The W. M. Keck Observatory is operated as a scientific partnership among the California Institute of Technology, the University of California, and NASA, and made possible by financial support of the W. M. Keck Foundation. The Gemini Observatory is operated by the Association of Universities for Research in Astronomy, under a cooperative agreement with the NSF on behalf of the Gemini partnership: the NSF, the Particle Physics and Astronomy Research Council (UK), the National Research Council (Canada), Comisión Nacional de Investigación Científica y Tecnológica (CONICYT) (Chile), the Australian Research Council (Australia), Conselho Nacional de Desenvolvimento Científico e Tecnológico (CNPq) (Brazil), and Consejo Nacional de Investigaciones Científicas y Técnicas (CONICET) (Argentina).

Supporting Online Material

www.sciencemag.org/cgi/content/full/310/5747/477/DC1
Table S1

29 June 2005; accepted 30 August 2005
10.1126/science.1116760

Selective Logging in the Brazilian Amazon

Gregory P. Asner,[1]* David E. Knapp,[1] Eben N. Broadbent,[1] Paulo J. C. Oliveira,[1] Michael Keller,[2,3] Jose N. Silva[4]

Amazon deforestation has been measured by remote sensing for three decades. In comparison, selective logging has been mostly invisible to satellites. We developed a large-scale, high-resolution, automated remote-sensing analysis of selective logging in the top five timber-producing states of the Brazilian Amazon. Logged areas ranged from 12,075 to 19,823 square kilometers per year (±14%) between 1999 and 2002, equivalent to 60 to 123% of previously reported deforestation area. Up to 1200 square kilometers per year of logging were observed on conservation lands. Each year, 27 million to 50 million cubic meters of wood were extracted, and a gross flux of ~0.1 billion metric tons of carbon was destined for release to the atmosphere by logging.

Tropical forests have been threatened by increasing rates of deforestation or clear cutting during the past three or more decades (*1*). Although deforestation, largely for the conversion of land to food crops or pastures, is the major destructive force in tropical forests worldwide (*2*), other forest disturbances such as the selective harvest of timber have also increased in frequency and extent (*3*, *4*). In selective logging, a limited number of marketable tree species are cut, and logs are transported off site to sawmills. Unlike deforestation, which is readily observed from satellites, selective logging in the Brazilian Amazon causes a spatially diffuse thinning of large trees, which is hard to monitor by using satellite observations. Selective logging causes widespread collateral damage to remaining trees, subcanopy vegetation, and soils; with impacts on hydrological processes, erosion, fire, carbon storage, and plant and animal species (*3*–*10*).

There is little known about the extent or impacts of selective logging throughout the tropical forests of the world, including the Amazon Basin. A survey of sawmills in the Brazilian Amazon suggested that 9,000 to 15,000 km^2 of forest had been logged in 1996–1997 (*3*). The large uncertainty in this reported area resulted from necessary assumptions of the wood volume harvested per area of forest. Sawmill surveys can, at best, provide only a general idea of where and how much logging occurs, because most operators buy timber at the mill gate rather than harvesting the wood themselves.

Objective spatially explicit reporting on selective logging requires either labor-intensive field surveys in frontier and often violently contested areas or remote detection and monitoring approaches. Previous studies of small areas show the need for high-resolution observations via satellite (*11*–*13*). Moreover, most of the traditional analysis techniques used for localized selective-logging studies have been insufficient for large-scale selective-logging assessments (*11*, *14*, *15*). A detailed comparison of Landsat satellite observations against field measurements of canopy damage after selective logging proved that traditional analytical methods missed about 50% of the canopy damage caused by timber harvest operations (*16*).

We advanced the computational analysis of Landsat Enhanced Thematic Mapper Plus (ETM+) satellite data using the new Carnegie Landsat Analysis System (CLAS) to detect and quantify the amount of selective logging in the major timber-production states of the Brazilian Amazon. This approach provides automated image analysis using atmospheric modeling; detection of forest canopy openings, surface debris, and bare soil exposed by forest disturbances; and pattern-recognition techniques. CLAS provides detailed measurements of forest-canopy damage at a spatial resolution of 30 m × 30 m, and it does so over millions of square kilometers of forest (*17*).

We applied CLAS to five states—Pará, Mato Grosso, Rondônia, Roraima, and Acre (fig. S6)—which account for ~90% of all deforestation in the Brazilian Amazon (*18*). The analysis was conducted on a time series of Landsat ETM+ imagery from 1999 to 2002. Across the five timber-producing Brazilian states, the annual extent of selective logging ranged from 12,075 to 19,823 km^2 (Fig. 1). These logging results represent new forest damage not accounted for in deforestation studies. Each year, the overlap between our results and the Brazilian National Institute for

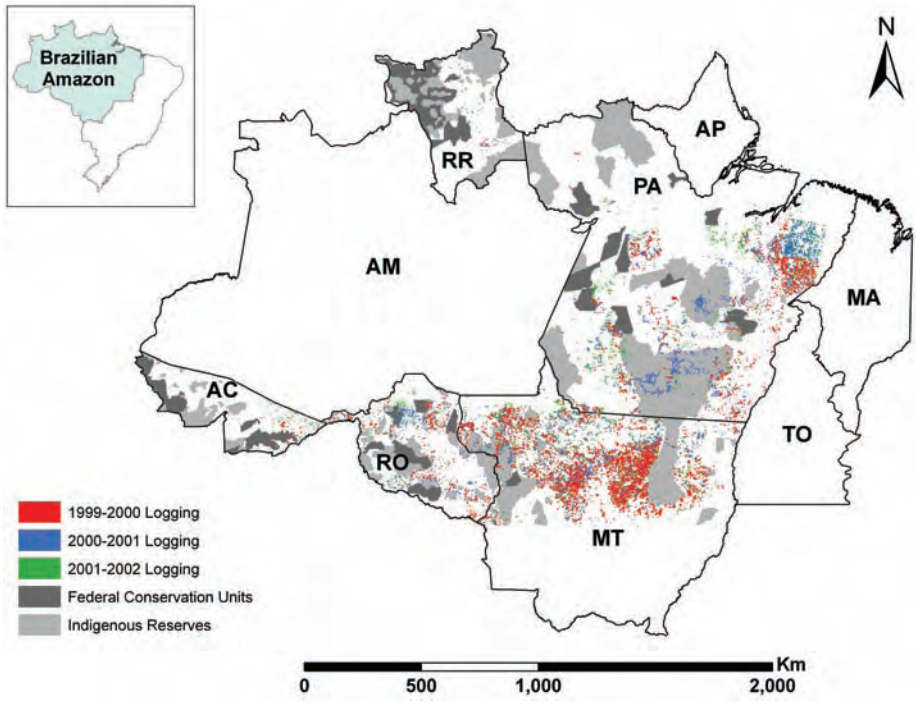

Fig. 1. Spatial distribution of selective logging in five timber-production states of the Brazilian Amazon for the year intervals 1999–2000 (red), 2000–2001 (blue), and 2001–2002 (green). The states of Amazonas (AM), Amapa (AP), Tocantins (TO), Maranhao (MA), and the southern nonforested part of Mato Grosso were not included in the analysis. Light gray areas show the extent of indigenous reserves; dark gray areas delineate federal conservation lands as of 1999 (*29*). RR, Roraima; PA, Pará; MT, Mato Grosso; RO, Rondônia; AC, Acre.

[1]Department of Global Ecology, Carnegie Institution of Washington, Stanford, CA 94305, USA. [2]U.S. Department of Agriculture Forest Service, International Institute of Tropical Forestry, Rio Piedras, PR 100745, USA. [3]Complex Systems Research Center, Morse Hall, University of New Hampshire, Durham, NH 03824, USA. [4]Empresa Brasileira de Pesquisa Agropecuária-Amazonia Oriental, Trav. Dr Eneas Pinheiro SN, Belem CEP 66095–100, Pará, Brazil.

*To whom correspondence should be addressed. E-mail: gasner@globalecology.stanford.edu

Space Research (INPE) annual deforestation maps was only 6% (±5%) (*17*) (Fig. 2). Moreover, only 19% (±11%) of the total area logged in any given year was subsequently deforested 3 years later. Selective logging thus adds 60 to 123% more forest-area damage than has been reported for deforestation alone in the same study period (Table 1). Selective logging was concentrated in the states of Mato Grosso and Pará, where logging areas exceeded or nearly matched deforestation areas. In other smaller states, selective logging increased forest damage area by 10 to 35% over reported deforestation rates (Table 1).

Conservation units such as indigenous reserves, parks, and national forests generally afforded protection against logging. However, exceptions included areas in northern Mato Grosso, where up to 53, 291, and 50 km^2 of logging were measured each year in the Xingu, Aripuanã, and Serra Morena indigenous reserves, respectively (Fig. 1). In the southern portion of Pará state, major logging disturbances were observed in the Menkragnoti and Kayapó indigenous reserves, with up to 261 and 198 km^2, respectively, detected each year between 1999 and 2002. Federal forest reserves of Acre, Gorotire (Pará), and Juruena (Mato Grosso) were harvested for timber at rates of up to 23, 90, and 380 km^2 each year, respectively.

Extensive field validation studies showed that the detection of canopy damage within CLAS is precise and accurate (*17*). Field validation studies showed false-positive and false-negative detection rates of only 5%. Uncertainty caused by errors in atmospheric correction of satellite data, cloud cover, annualization, automated logging-area delineation, and manual auditing were 0.7 to 12.8%, individually. After combining all known sources of error, our analysis suggests an overall absolute uncertainty of up to 14% in total logging area.

Selective logging contributes substantially to gross carbon fluxes from the Brazilian Amazon. We combined forest-damage results from CLAS with field-based forest-canopy gap-fraction (*19*, *20*) and roundwood-extraction data (*21*) to calculate the total wood-extraction rates (*17*). In 2000, 2001, and 2002, roundwood production averaged 49.8, 29.8, and 26.6 million m^3, respectively. The mean annual harvest intensities were 26.6, 21.7, and 21.4 m^3 ha^{-1}, which were generally lower than those reported by sawmill owners in 1996 (*3*, *22*). The total volume harvested equates to 10 million to 15 million metric tons of carbon (MtC) removed (*23*). In addition to roundwood, residual stumps, branches, foliage, and roots are left to decompose in the forest, subsequently returning to the atmosphere as carbon dioxide over about a decade. Our calculated average harvest intensity of 23.2 m^3 ha^{-1} is equivalent to ~8 MgC ha^{-1} contained in roundwood, with an associated 34 to 50 MgC ha^{-1} of fine and coarse debris (*23*–*25*). Integrated to the regional scale, the processing of roundwood and the decomposition of residues lead ultimately to a gross flux of carbon from the forest of up to 0.08 GtC for each year of logging (*26*). This value increases the estimated gross annual anthropogenic flux of carbon from Amazon forests by up to 25% over carbon losses from deforestation alone (*27*). Post-harvest forest regeneration reduces the net flux of carbon to the atmosphere below these values, but the pace of regeneration after logging varies considerably (*9*, *28*).

Selective logging doubles previous estimates of the total amount of forest degraded by human activities (Table 1), a result with potentially far-reaching implications for the ecology of the Amazon forest and the sustainability of the human enterprise in the region. In the future, improved monitoring of tropical forests will require high-performance satellite observations and new computational techniques. Our results, presented with explicit uncertainty analysis and transparency of method (*17*), have located and quantified ubiquitous but previously cryptic disturbances caused by selective logging.

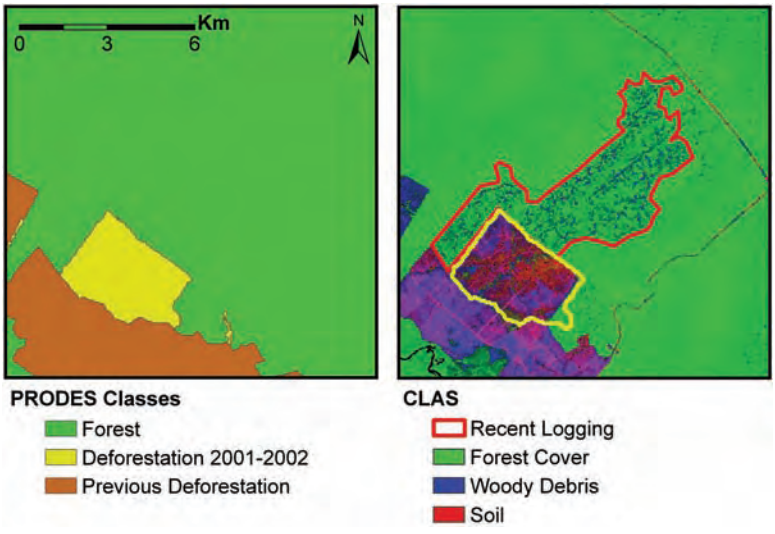

Fig. 2. High-resolution example of selective-logging results in 2001–2002 from the CLAS processing (**right**), compared with deforestation mapping provided by the INPE (**left**) (*18*).

Table 1. Selective-logging rates from 1999–2002 in five major timber-producing states of the Brazilian Amazon, with comparison to the deforestation rates reported by the INPE (*18*).

State	1999–2000 rates (km^2 $year^{-1}$)		2000–2001 rates (km^2 $year^{-1}$)		2001–2002 rates (km^2 $year^{-1}$)	
	Logged	Deforested	Logged	Deforested	Logged	Deforested
Acre	64	547	53	419	111	727
Mato Grosso*	13,015	6,176	7,878	7,504	7,207	6,880
Pará	5,939	6,671	5,343	5,237	3,791	8,697
Rondônia	773	2,465	923	2,673	946	3,605
Roraima	32	253	55	345	20	54
Total	19,823	16,112	14,252	16,178	12,075	19,963

*Only the northern 58% of Mato Grosso containing forested lands was included in the analysis.

References and Notes

1. E. F. Lambin, H. J. Geist, E. Lepers, *Annu. Rev. Environ. Res.* **28**, 205 (2003).
2. We define deforestation as clear cutting and conversion of the forest to other land uses, such as cattle pasture, crop agriculture, and urban and suburban areas.
3. D. C. Nepstad *et al.*, *Nature* **398**, 505 (1999).
4. L. M. Curran *et al.*, *Science* **303**, 1000 (2004).
5. A. Verissimo, P. Barreto, R. Tarifa, C. Uhl, *For. Ecol. Manage.* **72**, 39 (1995).
6. A. Verissimo, P. Barreto, M. Mattos, R. Tarifa, C. Uhl, *For. Ecol. Manage.* **55**, 169 (1992).
7. C. Uhl, A. Verissimo, M. M. Mattos, Z. Brandino, I. C. G. Vieira, *For. Ecol. Manage.* **46**, 243 (1991).
8. R. A. Fimbel, A. Grajal, J. G. Robinson, Eds., in *The Cutting Edge: Conserving Wildlife in Logged Tropical Forests* (Columbia Univ. Press, New York, 2001).
9. M. Keller, G. P. Asner, J. N. M. Silva, M. Palace, in *Working Forests in the Neotropics: Conservation Through Sustainable Management?*, D. J. Zarin, J. R. R. Alavalapati, F. E. Putz, M. Schmink, Eds. (Columbia Univ. Press, New York, 2004), pp. 41–63.
10. N. A. Chappell, W. Tych, Z. Yusop, N. A. Rahim, B. Kasran, in *Forests, Water and People in the Humid Tropics*, M. Bonell, L. A. Bruijnzeel, Eds. (Cambridge Univ. Press, Cambridge, 2005), pp. 513–532.
11. C. Souza, L. Firestone, L. M. Silva, D. Roberts, *Rem. Sens. Environ.* **87**, 494 (2003).
12. J. Reed, *Photogramm. Eng. Rem. Sens.* **69**, 275 (2003).
13. C. de Wasseige, P. Defourney, *For. Ecol. Manage.* **188**, 161 (2004).
14. T. A. Stone, P. Lefebvre, *Intl. J. Rem. Sens.* **19**, 2517 (1998).

15. C. Souza, P. Barreto, *Intl. J. Rem. Sens.* **21**, 173 (2000).
16. G. P. Asner, M. Keller, R. Pereira, J. Zweede, *Rem. Sens. Environ.* **80**, 483 (2002).
17. Materials and methods are available as supporting material on *Science* Online.
18. INPE (Instituto Nacional de Pesquisas Espaciais), *PRODES: Assessment of Deforestation in Brazilian Amazonia* (available at www.obt.inpe.br/prodes/index.html), 2005.
19. G. P. Asner, M. Keller, J. N. M. Silva, *Glob. Change Biol.* **10**, 765 (2004).
20. G. P. Asner, M. Keller, R. Pereira, J. C. Zweede, J. N. M. Silva, *Ecol. Applic.* **14**, S280 (2004).
21. R. Pereira, J. Zweede, G. P. Asner, M. Keller, *For. Ecol. Manage.* **168**, 77 (2002).
22. Nepstad *et al.* (*3*) interviewed sawmill operators to estimate harvest intensities of 19, 28, and 40 m^3 ha^{-1} in 1996.
23. M. Keller, M. Palace, G. P. Asner, R. Pereira, J. N. M. Silva, *Glob. Change Biol.* **10**, 784 (2004).
24. J. J. Gerwing, *For. Ecol. Manage.* **157**, 131 (2002).
25. The conversion of roundwood to carbon assumes an average wood specific gravity of 0.7 Mg m^{-3} and a proportional carbon content of 0.5 as in (*9*). Fallen debris creation was estimated from data in (*23*), based on mean debris amounts found in logged forests (~30 m^3 ha^{-1} harvested) subtracting the woody debris found in undisturbed forests. Upper and lower estimates were based on mean debris amounts plus root mean squared (rms) error, accounting for the uncertainty of estimates for both background and logged sites. Total debris was estimated as 1.4 times fallen debris to account for standing dead and roots. Data are available at ftp://lba.cptec.inpe.br/lba_archives/TG/TG-07/Palace/, with additional synthesis provided by (*30*).
26. The regional gross flux of carbon was estimated by multiplying the range of carbon densities of debris created by the area logged. The range includes both variation in the annual area logged and uncertainty in the amount of debris created during logging.
27. R. S. DeFries *et al.*, *Proc. Natl. Acad. Sci. U.S.A.* **99**, 14,256 (2002).
28. J. N. M. Silva *et al.*, *For. Ecol. Manage.* **71**, 267 (1995).
29. Instituto-Socioambiental. Map of forest types, land-use change, and protected areas in the Amazon. (São Paulo, Brazil, 1999).
30. M. Keller, M. Palace, G. Hurtt, *For. Ecol. Manage.* **154**, 371 (2001).
31. We thank M. Bustamante, K. Carlson, A. Cooper, E. G. Couto, E. C. M. Fernandes, T. Harris, B. Haxo, K. Heidebrecht, J. Hicke, M. S. Johnson, L. Olander, M. Palace, S. Parks, C. A. M. Passos, D. Pendleton, R. Pereira Jr., R. Rabin, A. Warner, A. Villagomez, and J. Zweede for assistance with various portions of this project. We thank D. Williams for managing the acquisition of the Landsat 7 satellite data and D. Wickland for programmatic support. We thank the INPE PRODES program for making its deforestation data and images freely available on the World Wide Web. The CLAS was developed by The Carnegie Institution of Washington. Application of CLAS to Amazonia was funded by NASA's Large-Scale Biosphere-Atmosphere Experiment in Amazonia (LBA-ECO) grant NCC5-675 (LC-21).

Supporting Online Material
www.sciencemag.org/cgi/content/full/310/5747/480/DC1
Materials and Methods
Figs. S1 to S7
Tables S1 to S5
References and Notes

27 July 2005; accepted 20 September 2005
10.1126/science.1118051

Transmission of Equine Influenza Virus to Dogs

P. C. Crawford,[1] Edward J. Dubovi,[2] William L. Castleman,[1] Iain Stephenson,[3] E. P. J. Gibbs,[1] Limei Chen,[3] Catherine Smith,[3] Richard C. Hill,[1] Pamela Ferro,[4] Justine Pompey,[3] Rick A. Bright,[3] Marie-Jo Medina,[3] Influenza Genomics Group,[3]* Calvin M. Johnson,[5] Christopher W. Olsen,[6] Nancy J. Cox,[3] Alexander I. Klimov,[3] Jacqueline M. Katz,[3] Ruben O. Donis[3]†

Molecular and antigenic analyses of three influenza viruses isolated from outbreaks of severe respiratory disease in racing greyhounds revealed that they are closely related to H3N8 equine influenza virus. Phylogenetic analysis indicated that the canine influenza virus genomes form a monophyletic group, consistent with a single interspecies virus transfer. Molecular changes in the hemagglutinin suggested adaptive evolution in the new host. The etiologic role of this virus in respiratory disease was supported by the temporal association of rising antibody titers with disease and by experimental inoculation studies. The geographic expansion of the infection and its persistence for several years indicate efficient transmission of canine influenza virus among greyhounds. Evidence of infection in pet dogs suggests that this infection may also become enzootic in this population.

Transmission of virus from one host species to another is a crucial feature of the ecology and epidemiology of influenza virus (*1*). Two basic mechanisms of interspecies transmission of influenza virus are possible (*2*, *3*). One is the direct transfer of an essentially unaltered virus from one species to another. Examples of this mechanism include the recent human infections with the H5N1 subtype of avian influenza virus (*4*–*6*). The second mechanism is a consequence of the segmented nature of the influenza genome. Simultaneous coinfection of a host with viruses from different species can result in reassortment of the segmented viral genes and the generation of a reassortant virus with the ability to infect other species. For example, novel viruses generated by gene reassortment between avian and human influenza viruses resulted in influenza pandemics in 1957 and 1968 (*2*, *3*, *7*).

Most direct transmissions of whole influenza viruses from the natural host species to a different one do not result in sustained transmission in the new host species. Multiple virus-host interactions are necessary for replication and horizontal transmission and provide a barrier to perpetuation of influenza viruses in the new host (*8*). Therefore, establishment of new, long-lived host-specific lineages of influenza virus is uncommon and has only occurred in domestic poultry, pigs, horses, and humans (*2*, *3*). In this report, we describe an unprecedented interspecies transfer of a complete equine influenza virus to the dog, and the emergence of a new canine-specific influenza virus associated with acute respiratory disease.

In January 2004, an outbreak of respiratory disease occurred in 22 racing greyhounds at a Florida racetrack (supporting online text). Two clinical syndromes were evident: a milder illness characterized by initial fever and then cough for 10 to 14 days with subsequent recovery (14 dogs) or a peracute death associated with hemorrhage in the respiratory tract (8 dogs for a case-fatality rate of 36%). Postmortem examinations were performed on six of the eight fatal cases (*9*). All dogs had extensive hemorrhage in the lungs, mediastinum, and pleural cavity. Histological examination of the respiratory tract revealed tracheitis, bronchitis, bronchiolitis, and suppurative bronchopneumonia (fig. S1). The epithelial lining and airway lumens in these tissues were infiltrated by neutrophils and macrophages. Lung homogenates prepared from these dogs were inoculated into a variety of monkey, human, bovine, and canine cell lines for virus culture (*9*). The lung homogenate from one dog caused cytopathic effects in Madin-Darby canine kidney (MDCK) epithelial cells cultured in the presence of trypsin and the cell culture supernatant agglutinated chicken red blood cells (*9*). Preliminary evidence of an influenza type A virus was provided by a commercial enzyme-linked immunosorbent assay (ELISA) for detection of the nucleoprotein

[1]College of Veterinary Medicine, University of Florida, Gainesville, FL 32611, USA. [2]College of Veterinary Medicine, Cornell University, Ithaca, NY 18453, USA. [3]Division of Viral and Rickettsial Diseases, Centers for Disease Control and Prevention, Atlanta, GA 30333, USA. [4]College of Veterinary Medicine, Texas A&M University, College Station, TX 77841–3040, USA. [5]College of Veterinary Medicine, Auburn University, Auburn, AL 36849–5519, USA. [6]School of Veterinary Medicine, University of Wisconsin-Madison, Madison, WI 53706–1102, USA.

*Influenza Genomics Group members are listed in the Supporting Online Material.
†To whom correspondence should be addressed. E-mail: rvd6@cdc.gov

of influenza A and B viruses, and by polymerase chain reaction (PCR) analysis using primers specific for the matrix gene of influenza A viruses (*9*). In addition, the hemagglutinating activity was inhibited by reference antisera to the equine influenza A H3 subtype, but not by antisera specific for avian, swine, and human influenza A subtypes H1 to H11 and H13 (table S1) (*9*). To characterize the molecular properties of the virus, we determined the nucleotide sequences of the eight RNA segments of the viral genome (*9*). Sequence comparisons with known influenza virus genes and phylogenetic analyses indicated that the eight genes of the canine isolate were most similar to those from contemporary equine influenza A (H3N8) viruses, with which they shared >96% sequence identity (Fig. 1A; table S2). In contrast, representative genes from avian, swine, and human influenza A isolates had 80 to 94% identity with the canine isolate (table S2). These data identified the canine isolate, named A/canine/Florida/43/2004 (canine/FL/04), as an influenza A H3N8 virus closely related to contemporary equine influenza viruses. Because all genes of the canine isolate were of equine influenza virus origin, we concluded that the entire genome of an equine influenza virus had been transmitted to the dog.

To investigate the role of the canine/FL/04 virus in the clinical and pathological observations in the greyhounds, we performed immunohistochemical staining (IHC) on lung tissues using a monoclonal antibody to influenza A H3 (*9*). Viral H3 antigen was consistently detected in the cytoplasm of bronchial and bronchiolar epithelial cells, bronchial gland epithelial cells, and macrophages in airway lumens and alveolar spaces (Fig. 2A). These data supported a diagnosis of pulmonary infection with influenza virus of the H3 subtype in the dogs.

To determine involvement of a canine/FL/04-like virus in the etiology of the respiratory disease outbreak, we analyzed paired acute and convalescent sera from 11 sick dogs and 16 asymptomatic contacts for virus-specific antibodies using hemagglutination inhibition (HI) and microneutralization (MN) assays (*9*). Seroconversion, defined as a greater than fourfold rise in antibody titers to canine/FL/04 from the acute to convalescent phase, occurred in 8 of 11 (73%) sick dogs in both assays (table S3). Seroconversion occurred in 6 of 16 (38%) asymptomatic contacts in the HI assay, whereas 8 of 16 (50%) seroconverted in the MN assay (table S3). The seroconversion data demonstrated infection of the dogs with a canine/FL/04-like virus which coincided temporally with the onset of respiratory disease in most animals.

Single serum samples were collected 3 months after the outbreak from an additional 46 asymptomatic dogs housed with the sick dogs. Of these, 43 (93%) were seropositive in both assays. For the total population of 73 dogs tested, 93% were seropositive in both assays, including 82% (9/11) of the sick dogs and 95% (59/62) of the healthy contacts. The

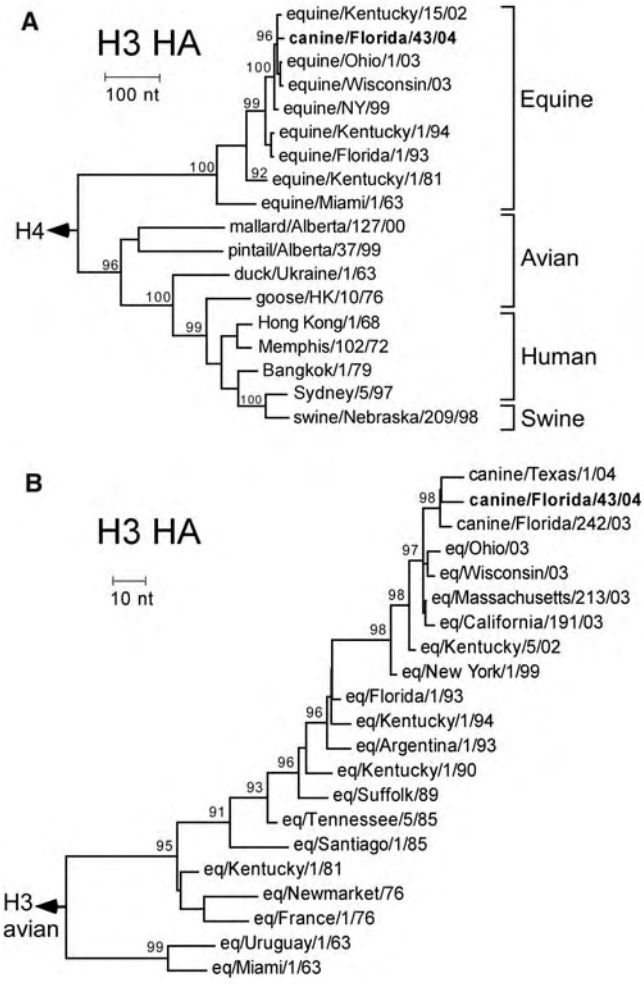

Fig. 1. Phylogenetic relationships among the hemagglutinin genes. (**A**) Tree of HA genes from representative canine, human, avian, swine, and equine isolates, using A/budgerigar/Hokkaido/1/77 (H4) as the outgroup (indicated by arrowhead and H4). (**B**) Tree of the canine influenza virus HA genes with contemporary and older equine HA genes, using A/duck/Ukraine/63 (H3) as the outgroup. Phylogenetic trees were inferred from nucleotide sequences by the neighbor joining method, and bootstrap analysis values ≥90% are shown. The bar denotes the number of nucleotide changes per unit length of the horizontal tree branches.

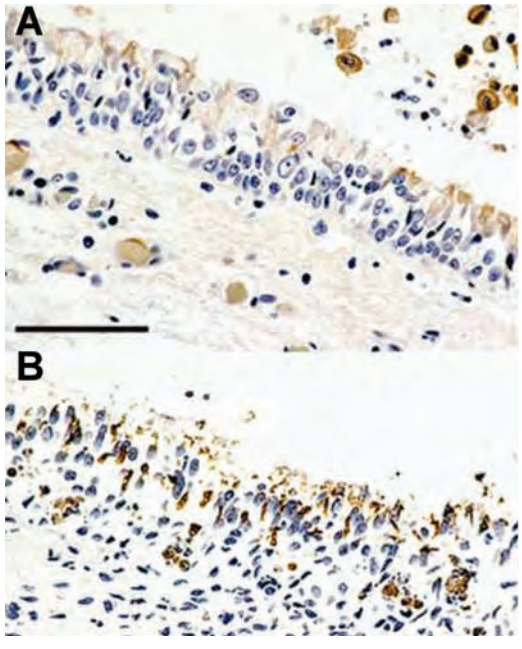

Fig. 2. Immunohistochemical detection of influenza H3 antigen in the lungs. Lung tissue sections were probed with a mouse monoclonal antibody to H3 hemagglutinin and binding was detected by immunoperoxidase reaction (brown precipitate). (**A**) Bronchial epithelium from a greyhound with disease. Viral H3 antigen was detected in bronchial epithelial cell cytoplasm and in macrophages in airway lumens and in alveolar spaces. (**B**) Bronchial epithelium from a beagle dog 5 days after inoculation with A/canine/Florida/43/04 (H3N8). Viral H3 antigen was detected in bronchial epithelial cell cytoplasm. Scale bar, 66 μm.

high seroprevalence in dogs with no history of respiratory disease indicates that infections with canine influenza virus can be subclinical and suggests efficient spread of the virus among dogs.

To better understand the capacity of the canine/FL/04 virus to infect dogs, four 6-month-old purpose-bred beagles were each inoculated with $10^{6.6}$ median tissue culture infectious doses ($TCID_{50}$) by the intratracheal and intranasal routes (*9*). All dogs developed a fever (rectal temperature ≥39°C) for the first 2 days postinoculation (p.i.), but none exhibited respiratory signs such as cough or nasal discharge over a 14-day observation period. Virus shedding was examined by quantification of virus in nasal and oropharyngeal swabs (*9*). Only two of the four dogs shed detectable amounts of virus. One dog shed virus on days 1 and 2 p.i. (1.0 to 2.5 $\log_{10}$ PFU per swab), whereas the other dog shed virus for four consecutive days after inoculation (1.4 to 4.5 $\log_{10}$ PFU per swab). Postmortem examination of two dogs on day 5 p.i. revealed necrotizing and hyperplastic tracheitis, bronchitis, and bronchiolitis similar to that found in the greyhounds, but there was no pulmonary hemorrhage or bronchopneumonia (*9*). Viral H3 antigen was detected in epithelial cells of bronchi, bronchioles, and bronchial glands of both dogs by IHC (Fig. 2B). Infectious virus was recovered from the lung tissue of one of the dogs (*9*). Postmortem examination of the remaining two dogs on day 14 p.i. showed minimal histological changes in respiratory tissues, no viral H3 antigen by IHC, and no recovery of virus from lung homogenates. Seroconversion in the last two dogs was detected in MN assays by day 7 p.i., with a further two- to threefold increase in antibody titers by day 14. These results established the susceptibility of dogs to infection with canine/FL/04, as evidenced by the febrile response, virus shedding from the upper respiratory tract, presence of viral antigen and infectious virus in the lungs, histopathological findings typical for influenza, and seroconversion. The failure to reproduce severe disease and death in the experimentally inoculated beagles is not surprising, because a large proportion of the naturally infected greyhounds were asymptomatic.

To investigate whether a canine/FL/04-like influenza virus had circulated among greyhound populations in Florida before the January 2004 outbreak, we tested archival sera from 65 racing greyhounds for the presence of antibodies to canine/FL/04 using the HI and MN assays (*9*). There were no detectable antibodies in 33 dogs sampled from 1996 to 1998. Of 32 dogs sampled between 2000 and 2003, 9 were seropositive in both assays—1 in 2000, 2 in 2002, and 6 in 2003 (table S4). The seropositive dogs were located at Florida tracks involved in outbreaks of respiratory disease of unknown etiology from 1999 to 2003, which suggests that a canine/FL/04-like virus may have been the causative agent of those outbreaks. To investigate this possibility further, we examined archival tissues from greyhounds that died from hemorrhagic bronchopneumonia in March 2003 (*9*). Lung homogenates from one dog inoculated into MDCK cells yielded H3N8 influenza virus, termed A/canine/Florida/242/2003 (canine/FL/03), in the first passage (*9*). Sequence analysis of the complete genome of canine/FL/03 revealed >99% identity to canine/FL/04 (table S5), indicating that canine/FL/04-like viruses had infected greyhounds before 2004.

From June to August 2004, respiratory disease outbreaks occurred at 14 tracks in 6 states (Florida, Texas, Alabama, Arkansas, West Virginia, and Kansas) with a combined population of ~10,000 racing greyhounds (supporting online text). We collected paired serum samples from 94 dogs during the acute phase of the disease (<7 days from the start of clinical symptoms) and during convalescence (21 days or more after onset of disease). These dogs were located at four Florida tracks: 56% of them had fourfold or greater increases in antibody titers to canine/FL/04, and 100% were seropositive (Table 1 and table S6). Serum samples from 29 convalescent dogs in West Virginia and Kansas also had antibodies to canine/FL/04.

From January to May 2005, respiratory disease outbreaks occurred at 20 tracks in 11 states (Florida, Texas, Arkansas, Arizona, West Virginia, Kansas, Iowa, Colorado, Rhode Island, Wisconsin, and Massachusetts) with a combined population of ~20,000 greyhounds (supporting online text). We collected paired acute phase and convalescent sera from 96 dogs located at seven Florida tracks: 58% of these dogs seroconverted to canine/FL/04 and 100% were seropositive (Table 1 and table S7). From paired samples from 25 dogs at a West Virginia track, we found that 84% of the dogs seroconverted, and 100% were seropositive. From paired samples from 10 dogs at a Wisconsin track, 50% of the dogs seroconverted and 100% were seropositive. Sera from an additional 13 convalescent dogs at this track and 115 dogs at two Arizona tracks contained antibody to canine/FL/04.

We isolated influenza A (H3N8) virus from the lung of a greyhound that died of hemorrhagic bronchopneumonia at a Texas track in July 2004. Sequence analysis of the HA and NA of this isolate, named A/canine/Texas/1/2004 (canine/TX/04), revealed ≥99% identity to canine/FL/04 (table S5). The isolation of three closely related influenza viruses from fatal canine cases over a 16-month period and from different geographic locations, together with the substantial serological evidence of widespread infection among racing greyhounds, suggested sustained circulation of a canine/FL/04-like virus in this population.

Table 1. HI antibody responses to A/canine/Florida/43/04 (H3N8) in racing greyhounds and pet dogs with respiratory disease. Dogs with respiratory disease were tested by HI using A/canine/Florida/43/04 (H3N8). Seroconversion indicates the percentage of dogs with at least a fourfold increase in antibody titer between paired acute phase and convalescent sera. Seropositive indicates a positive antibody titer (HI titer ≥32) in serum samples from convalescent dogs. ND, no data because only serum samples from convalescent dogs were collected from pets. GMT, geometric mean antibody titer for serum samples from convalescent dogs.

HI response	Greyhounds		Pet dogs
	2004	2005	
No. of dogs tested	94*	96†	70‡
Seroconversion (%)	56	58	ND[f]
Seropositive (%)	100	100	97
GMT	381	389	428

*Number of dogs tested at four different tracks in Florida from June to August 2004. †Number of dogs tested at seven different tracks in Florida from January to April 2005. ‡Number of pet dogs tested at one shelter and four veterinary clinics in Florida and one veterinary clinic in New York.

The high prevalence of canine influenza infection in racing greyhounds suggested that the pet dog population might be at risk of infection. Serological tests were performed on 70 dogs with respiratory disease in a shelter facility in northeast Florida, four veterinary clinics located in the northeast, north central, south, and southwest regions of Florida, and one veterinary clinic located in New York (supplemental online text). Ninety-seven percent of the shelter and pet dogs were positive for antibody to canine/FL/04 (Table 1 and table S8). The serologic evidence of influenza virus infection associated with respiratory disease in shelter and pet dogs of various breeds indicated the lack of genetic barriers to infection in the dog population and the spread of the virus to pet populations of regions of the country without greyhound racing.

Phylogenetic analysis (*9*) of the HA genes of canine/FL/03, canine/FL/04, and canine/TX/04 showed that they constitute a monophyletic group with robust bootstrap support. The canine influenza genes were most closely related to the equine H3 "Florida lineage" that emerged in the early 1990s (Fig. 1B) (*10*). Phylogentic analysis and pairwise nucleotide sequence comparisons (*9*) of the other seven genomic segments supported the segregation of the canine genes as a distinct sub-lineage most closely related to the equine virus lineage (tables S2 and S9). Together with identification of infected dogs in widespread geographical locations from 2003 to 2005, these data are most consistent with a single virus transmission event from horses to

Table 2. Amino acid differences between the canine and equine H3 hemagglutinins. Dash denotes no change from the consensus equine H3 HAs. First column shows amino acid residue and position in the mature H3 HA. Single-letter abbreviations for the amino acids are A, alanine; D, aspartic acid; G, glycine; I, isoleucine; K, lysine; L, leucine; M, methionine; N, asparagine; R, arginine; S, serine; T, threonine; V, valine; W, tryptophan.

Equine H3 consensus	Canine/FL/03	Canine/FL/04	Canine/TX/04	Potential functional significance
G7	D	–	–	D also found in duck and human H3 HA
I29	–	M	M	I is conserved in H3 HAs from all species
N83	S	S	S	Various polar amino acids present at this position in H3 HAs of other species
S92	–	N	–	N is present in some duck H3 HAs
L118	–	–	V	L is conserved in all H3 HAs
W222	L	L	L	W is conserved in most H3 HAs of all species; located near the receptor binding site
I328	T	T	T	T is strictly conserved in all avian, swine, or human H3 HAs
G479	G	G	E	E present in equine isolates in 1970s
N483	T	T	T	N occurs in all H3 and other HA subtypes. Replacement results in loss of a glycosylation site.
K541	–	R	–	Basic amino acid conservative change

dogs with subsequent horizontal spread of the adapted virus in the canine population. However, repeated introductions of this unique lineage of influenza virus from an unidentified reservoir species cannot be formally excluded, unlikely as it may be. The presence of virus in the nasal passages and orpharnyx of the experimentally inoculated dogs indicates that shedding is possible, and that dog-to-dog transmission of virus by large droplet aerosols, fomites, or direct mucosal contact could play a role in the epizootiology of the disease.

The viral HA is a critical determinant of host species specificity of influenza virus (*11*). To identify residues within HA that may be associated with adaptation of an equine virus to the canine host, we compared the amino acid sequence of canine HAs to those of contemporary equine viruses. Four amino acid changes differentiate the equine and canine HA consensus amino acid sequences: N83S, W222L, I328T, and N483T (Table 2). The substitution of serine for asparagine at position 83 is a change of unknown functional significance since various polar residues are found in H3 molecules from other species. The strictly conserved isoleucine at position 328 near the cleavage site of the H3 HA has been replaced by threonine. The pivotal role of HA cleavage by host proteases in pathogenesis suggests that this change merits further study. The substitution of leucine for tryptophan at position 222 is remarkable, because it represents a nonconservative change adjacent to the sialic acid binding pocket which could modulate receptor function (*12*). Interestingly, Leu^{222} is not unique to canine H3 HA, because it is typically found in the H4, H8, H9, and H12 HA subtypes (*13*, *14*). The leucine substitution may be more compatible with virus specificity for certain mammalian hosts since infections of swine with subtype H4 (*15*) and humans and swine with subtype H9 (*16*) viruses have been reported. The replacement of asparagine with threonine at position 483 resulted in the loss of a glycosylation site in the HA2 subunit that is conserved in all HA subtypes (*17*). Although the importance of these amino acid changes in the HA for adaptation of an equine virus to dogs remains to be determined, similar amino acid changes have been observed previously in association with interspecies transfer (*18*, *19*).

The interspecies transfer of a whole mammalian influenza virus to an unrelated mammal species is a relatively rare event. Previous studies have provided limited serological or virological evidence, but not both, of transient infection of dogs with human influenza A (H3N2) viruses (*20*–*23*). However, there was no evidence of sustained circulation in the canine host. Although direct transfer of swine influenza viruses from pigs to people is well-documented (*24*–*27*), there is no evidence for adaptation of the swine viruses in human hosts. In this report, we provide virological, serological, and molecular evidence for interspecies transmission of an entire equine influenza A (H3N8) virus to another mammalian species, the dog. Unique amino acid substitutions in the canine virus HA, coupled with serological confirmation of infection of dogs in multiple states in the United States, were correlated with sustained circulation of the virus in the canine population. Evidence of canine influenza infection in pet dogs, a primary companion animal for humans, raises the possibility that dogs may provide a new source for transmission of novel influenza A viruses to humans.

References and Notes

1. R. G. Webster, *Emerg. Infect. Dis.* **4**, 436 (1998).
2. R. G. Webster, W. J. Bean, O. T. Gorman, T. M. Chambers, Y. Kawaoka, *Microbiol. Rev.* **56**, 152 (1992).
3. A. S. Lipatov *et al.*, *J. Virol.* **78**, 8951 (2004).
4. K. Subbarao *et al.*, *Science* **279**, 393 (1998).
5. J. S. Peiris *et al.*, *Lancet* **363**, 617 (2004).
6. Y. Guan *et al.*, *Proc. Natl. Acad. Sci. U.S.A.* **101**, 8156 (2004).
7. Y. Kawaoka, S. Krauss, R. G. Webster, *J. Virol.* **63**, 4603 (1989).
8. R. Webby, E. Hoffmann, R. Webster, *Nat. Med.* **10**, S77 (2004).
9. Materials and methods are available as supporting material on *Science* Online.
10. A. C. Lai, *Virus Res.* **100**, 159 (2004).
11. Y. Suzuki *et al.*, *J. Virol.* **74**, 11825 (2000).
12. W. Weis *et al.*, *Nature* **333**, 426 (1988).
13. E. Nobusawa *et al.*, *Virology* **182**, 475 (1991).
14. A. Kovacova, G. Ruttkay-Nedecky, I. K. Haverlik, S. Janecek, *Virus Genes* **24**, 57 (2002).
15. A. I. Karasin, I. H. Brown, S. Carman, C. W. Olsen, *J. Virol.* **74**, 9322 (2000).
16. M. Peiris *et al.*, *Lancet* **354**, 916 (1999).
17. R. Wagner, D. Heuer, T. Wolff, A. Herwig, H. D. Klenk, *J. Gen. Virol.* **83**, 601 (2002).
18. A. Vines *et al.*, *J. Virol.* **72**, 7626 (1998).
19. M. Matrosovich *et al.*, *J. Virol.* **74**, 8502 (2000).
20. A. Nikitin, D. Cohen, J. D. Todd, F. S. Lief, *Bull. World Health Organ.* **47**, 471 (1972).
21. E. D. Kilbourne, J. M. Kehoe, *Intervirology* **6**, 315 (1975).
22. C. P. Chang, A. E. New, J. F. Taylor, H. S. Chiang, *Int. J. Zoonoses* **3**, 61 (1976).
23. R. E. Houser, W. P. Heuschele, *Can. J. Comp. Med.* **44**, 396 (1980).
24. C. C. Dacso *et al.*, *J. Clin. Microbiol.* **20**, 833 (1984).
25. K. Kimura, A. Adlakha, P. M. Simon, *Mayo Clin. Proc.* **73**, 243 (1998).
26. P. A. Patriarca *et al.*, *Am. J. Epidemiol.* **119**, 152 (1984).
27. F. H. Top Jr., P. K. Russell, *J. Infect. Dis.* **136** (suppl.), S376 (1977).

28. This study was funded by a grant from the Division of Pari-mutuel Wagering, Department of Business and Professional Regulation, State of Florida. We thank J. Barker, L. Bohenko, A. Carlton, S. Coster, W. Dugger, P. Fernandez, B. Fenwick, W. Fortney, M. Harris, S. Marsh, P. McCann, B. Peckham, K. A. Rada, K. Scott, R. Walton, C. Wilkinson, and K.-J. Yoon for provision of samples and expertise. We thank T. Chambers for equine influenza isolates and unpublished prevalence data, C. Macken for access to the Influenza Sequence Database, and the Scientific Resources Program for computer software and hardware. Last, we thank all the greyhound and pet dog owners who participated in this study. The nucleotide sequences of the canine and equine influenza viruses reported here were deposited at NCBI's GenBank, with accession numbers DQ124147 to DQ124197.

Supporting Online Material

www.sciencemag.org/cgi/content/full/1117950/DC1
Materials and Methods
SOM Text
Fig. S1
Tables S1 to S9
References

26 July 2005; accepted 20 September 2005
Published online 29 September 2005;
10.1126/science.1117950
Include this information when citing this paper.

Movement of Eukaryotic mRNAs Between Polysomes and Cytoplasmic Processing Bodies

Muriel Brengues,* Daniela Teixeira,* Roy Parker†

Eukaryotic cells contain nontranslating messenger RNA concentrated in P-bodies, which are sites where the mRNA can be decapped and degraded. We present evidence that mRNA molecules within yeast P-bodies can also return to translation. First, inhibiting delivery of new mRNAs to P-bodies leads to their disassembly independent of mRNA decay. Second, P-bodies decline in a translation initiation–dependent manner during stress recovery. Third, reporter mRNAs concentrate in P-bodies when translation initiation is blocked and resume translation and exit P-bodies when translation is restored. Fourth, stationary phase yeast have large P-bodies containing mRNAs that reenter translation when growth resumes. The reciprocal movement of mRNAs between polysomes and P-bodies is likely to be important in the control of mRNA translation and degradation. Moreover, the presence of related proteins in P-bodies and maternal mRNA storage granules suggests this mechanism is widely adapted for mRNA storage.

A key aspect of the regulation of eukaryotic gene expression is the control of mRNA translation and degradation, which often occurs by decapping, followed by 5′ to 3′ decay (*1*). Translation and mRNA degradation via decapping are tightly linked. To decap, an mRNA exits translation and assembles into a translationally repressed messenger ribonucleoprotein (mRNP) lacking translation initiation factors and containing the decapping enzyme and several accessory proteins (*1*, *2*). These translationally repressed mRNPs accumulate within P-bodies (also referred to as GW or Dcp bodies) (*3*–*8*), where decapping can occur (*9*, *10*). The formation of a P-body mRNP is also important for control of translational repression (*2*, *11*, *12*). An unresolved issue is whether P-bodies can store mRNAs and later release them to reenter translation.

To determine whether mRNAs in P-bodies were committed to decapping, we examined P-bodies in *dcp1*Δ cells where decapping is blocked (*1*) after 10 min of cycloheximide treatment, which prevents mRNAs from exiting translation and entering P-bodies (*7*, *9*, *10*, *13*). We directly observed P-body proteins by using green fluorescent protein (GFP)–tagged versions of the components Dcp2p and Dhh1p, whose presence in P-bodies is dependent on RNA, thus also providing an indirect manner of observing P-body mRNAs (*7*). We observed that P-bodies in *dcp1*Δ (Fig. 1A) and *xrn1*Δ cells (fig. S1) declined after cycloheximide treatment, suggesting that mRNPs can exit P-bodies in the absence of decapping and 5′ to 3′ degradation.

If mRNAs within P-bodies are committed to degradation, then the reduction in P-bodies seen in the *dcp1*Δ strain could be due to 3′ to 5′ degradation. Thus, we examined P-bodies in *dcp*1 mutant strains lacking Ski2p, which is required for 3′ to 5′ degradation of mRNAs. Because blocks to decapping and 3′ to 5′ degradation of mRNA are lethal in combination (*14*), we inhibited decapping in the *ski2*Δ strain by using the temperature-sensitive allele *dcp1-2*. After a shift to 37°C and because of inhibition of mRNA decapping, P-bodies increased in size and number in the *dcp1-2* and *dcp1-2 ski2*Δ strains but still declined after cycloheximide addition (Fig. 1B). Moreover, proteins required for 3′ to 5′ degradation of mRNAs are not concentrated in P-bodies (fig. S2). These results suggest that mRNAs exit P-bodies independent of mRNA degradation, possibly to return to translation.

To determine whether P-body mRNAs could enter translation, we examined translation regulation by the presence of glucose (*15*). We assessed P-bodies by following the subcellular distribution of Dhh1p and Dcp2p as well as the subcellular distribution of two reporter mRNAs (PGK1-U1A and MFA2P-U1A), which are visualized by the binding of a U1A-GFP fusion protein to their 3′

Department of Molecular and Cellular Biology and Howard Hughes Medical Institute, University of Arizona, Tucson, AZ 85721–0106, USA.

*These authors contributed equally to this work.
†To whom correspondence should be addressed. E-mail: rrparker@u.arizona.edu

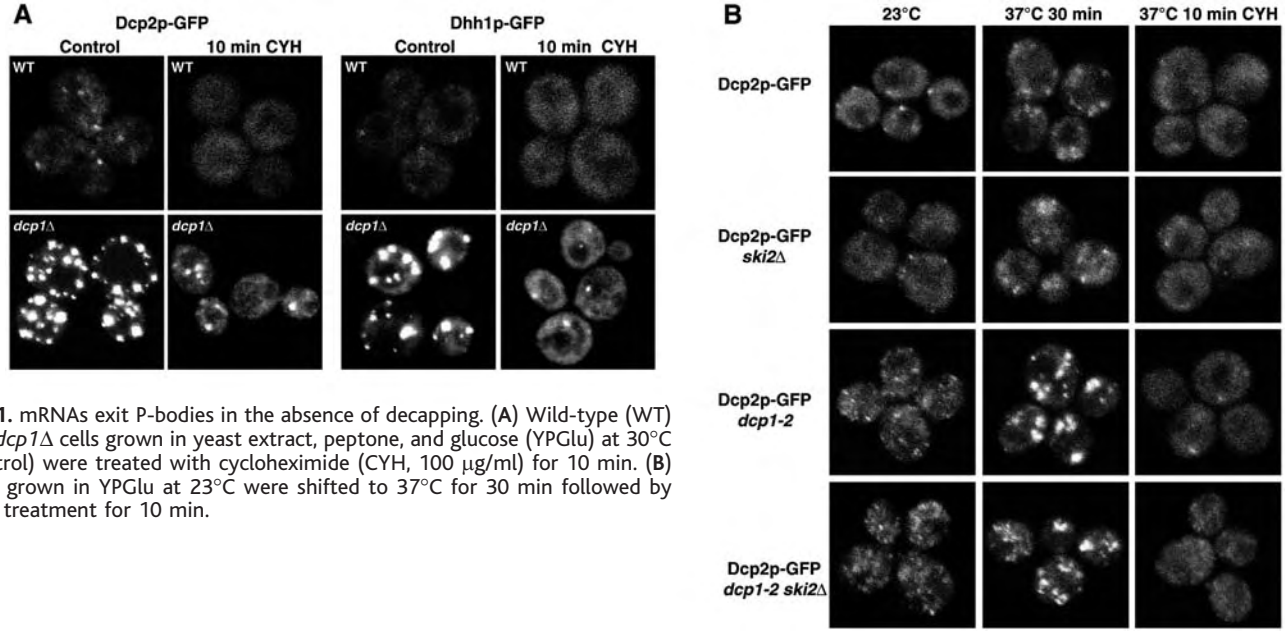

Fig. 1. mRNAs exit P-bodies in the absence of decapping. (**A**) Wild-type (WT) and *dcp1*Δ cells grown in yeast extract, peptone, and glucose (YPGlu) at 30°C (control) were treated with cycloheximide (CYH, 100 μg/ml) for 10 min. (**B**) Cells grown in YPGlu at 23°C were shifted to 37°C for 30 min followed by CYH treatment for 10 min.

untranslated region (UTR) (*16*). Glucose deprivation leads to a rapid loss of polysomes (Fig. 2F) and an increased accumulation of Dcp2p, Dhh1p, and PGK1-U1A and MFA2P-U1A mRNAs in P-bodies (Fig. 2, G to J). Readdition of glucose leads to rapid restoration of polysomes (Fig. 2K) and loss of Dcp2p, Dhh1p, and PGK1-U1A and MFA2P-U1A mRNAs from P-bodies (Fig. 2, L to O). The MFA2P-U1A mRNA accumulated in P-bodies before glucose deprivation and after glucose restoration (Fig. 2, E and O), consistent with the poorer translation of the MFA2 mRNA (~24% untranslated) compared with PGK1 mRNA (~2% untranslated). These observations demonstrate that restoration of translation after glucose deprivation leads to disassembly of P-bodies, either by decapping and degradation of the mRNA within P-bodies or through return of the mRNAs within P-bodies to polysomes.

To evaluate whether decapping was required for the decline of P-bodies after glucose restoration, we examined the response to glucose deprivation and restoration in the *dcp1-2* strain. Similar to wild-type cells at 37°C (Fig. 3A), glucose deprivation in *dcp1-2* cells led to Dhh1p, Dcp2p, PGK1-U1A, and MFA2P-U1A mRNAs accumulating in P-bodies (Fig. 3B, images g to j) and a decline in polysomes (Fig. 3B, image f). Readdition of glucose to the *dcp1-2* strain led to reformation of polysomes (Fig. 3B, image k) and a decline in P-bodies (Fig. 3B, images l to o). The disassembly of P-bodies that occurs upon restoration of glucose is therefore not dependent on decapping and degradation of mRNA within P-bodies. However, because P-bodies do not completely return to basal amounts in the *dcp1-2* strain after glucose restoration, some mRNAs may be targeted for decay under these conditions.

To determine whether translation initiation was required for the disassembly of P-bodies after glucose restoration, we examined the response to glucose deprivation and restoration in a strain carrying a conditional temperature-sensitive allele of a subunit of eukaryotic initiation factor 3 (eIF3), *prt1-63*. Similar to wild-type cells (Fig. 3A), glucose deprivation in *prt1-63* cells led to an accumulation of Dhh1p, Dcp2p, and PGK1-U1A and MFA2P-U1A reporter mRNAs in P-bodies (Fig. 3C, images g to j) and a decline in polysomes (Fig. 3C, image f). Readdition of glucose led to a limited reformation of polysomes (Fig. 3C, image k), and P-bodies largely persisted (Fig. 3C, images l to o). The small decrease in P-bodies seen under these conditions is likely due to the partial restoration of polysomes in the *prt1-63* strain at 37°C and to some mRNAs being degraded by decapping, consistent with the persistence of small P-bodies in the *dcp1-2* strain after glucose restoration. This indicates that the decline of P-bodies that occurs upon restoration of glucose requires translation initiation, presumably to allow the dynamic movement of mRNAs between polysomes and P-bodies to shift to the translating state. This result argues that mRNAs within P-bodies are reentering translation.

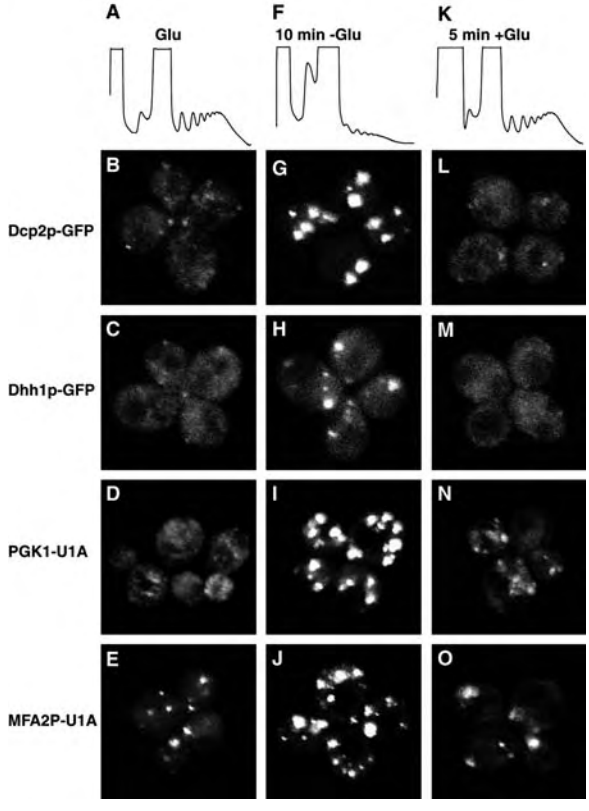

Fig. 2. Disassembly of P-bodies after translation restoration. WT cells expressing a GFP-tagged version of Dcp2p (**B**, **G**, and **L**), Dhh1p (**C**, **H**, and **M**), or co-expressing U1A-GFP with PGK1-U1A (**D**, **I**, and **N**) or MFA2P-U1A (**E**, **J**, and **O**), were grown in glucose containing medium at 30°C (Glu), shifted for 10 min without glucose (10 min –Glu), followed by readdition of glucose (5 min +Glu). Polysome profiles under each condition are shown (**A**, **F**, and **K**).

To demonstrate that P-body mRNAs were reentering translation, we examined the translation status of specific mRNAs on sucrose gradients before and during glucose deprivation and after glucose restoration. The MFA2P-U1A mRNA was primarily associated with polysomes during log growth (~76% polysome-associated), shifted to nontranslating fractions of the gradient during glucose deprivation (~36% polysome-associated) where P-body components sediment (*2*, *17*, *18*), and shifted back into the polysome region of the gradient during glucose restoration (~72% polysome-associated) (Fig. 4A). These results are consistent with the subcellular location of the MFA2P-U1A mRNA, whose concentration in P-bodies is increased during glucose deprivation and then decreased by glucose restoration (Fig. 2). This result argues that mRNAs can return to translation from a P-body state. Similar shifts were observed with endogenous mRNAs, including RPL41A, PGK1, and CYH2 transcripts (Fig. 4B, lower images).

In principle, the transcripts associated with polysomes during glucose restoration could be products of new transcription and not those previously localized to P-bodies. To verify that the appearance of mRNAs in the translating pool does not require new transcription, we performed similar experiments by using a tetracycline repression construct (Tet-Off promoter) with the MFA2pG and the MFA2P-U1A reporters, thereby allowing repression of transcription at the time of glucose deprivation. We observed a similar movement of these mRNAs from the polysome pool to the nontranslating pool and back to translation in response to glucose availability (Fig. 4B), demonstrating that the appearance of MFA2 transcripts in the translating pool after glucose readdition is caused by the restored translation of preexisting transcripts.

The ability of mRNAs to return to translation from P-bodies suggests that P-bodies can serve as sites of mRNA storage. Because P-bodies increase in size with cell density (*7*), we hypothesized that P-bodies might serve as site of mRNA storage during stationary phase in yeast, where cells enter a G0-like state (*19*). In stationary phase yeast, we observed that polysomes are reduced and P-bodies are enlarged, as judged by either proteins (*7*) or the MFA2P-U1A mRNA (Fig. 5).

Several observations indicate that mRNAs within P-bodies at stationary phase enter translation when nutrients are provided. First, in the presence of fresh media, polysomes are restored and P-bodies decrease within 30 min (Fig. 5). Second, when we inhibited the transcription of the Tet-Off MFA2pG reporter

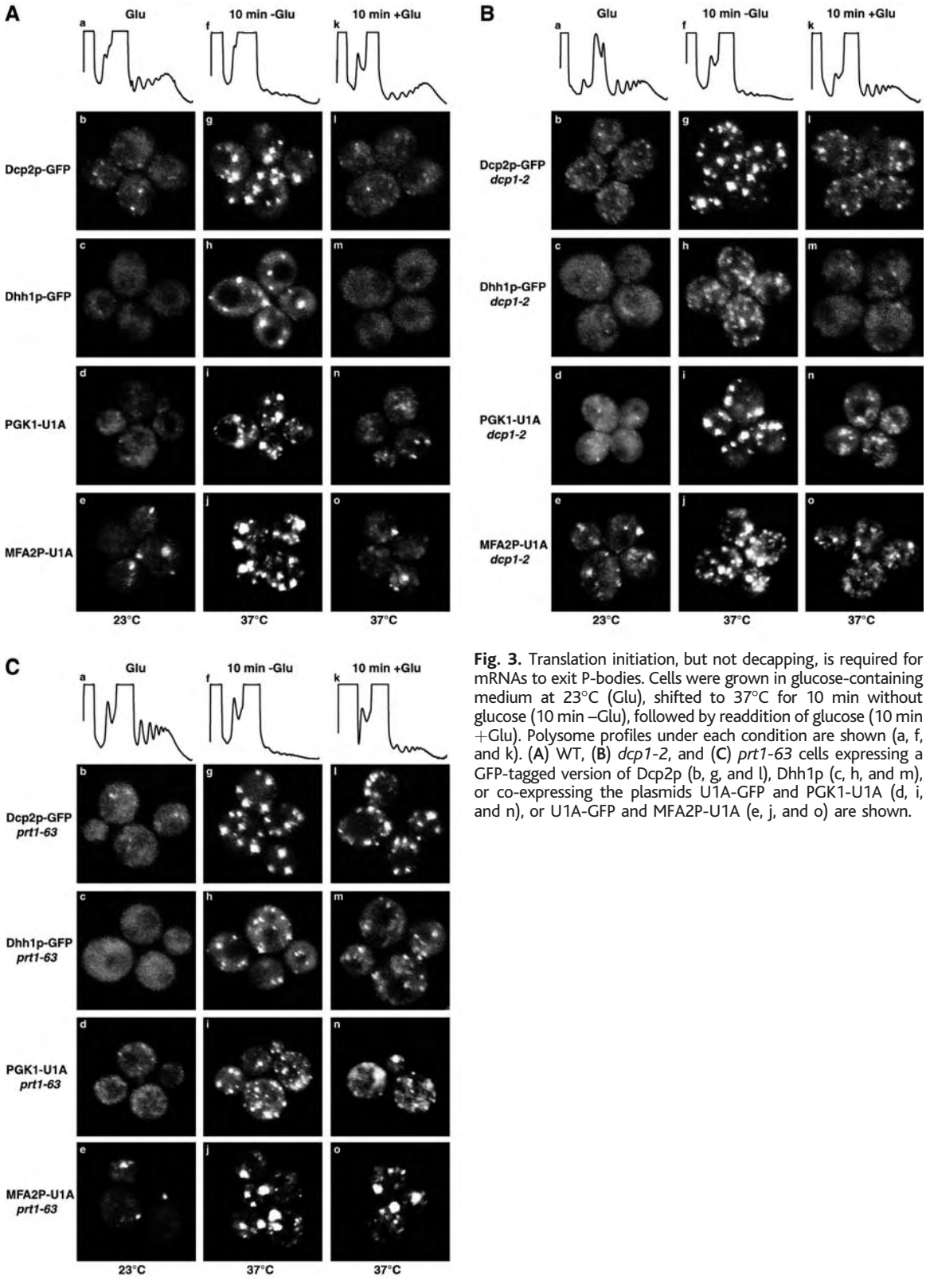

Fig. 3. Translation initiation, but not decapping, is required for mRNAs to exit P-bodies. Cells were grown in glucose-containing medium at 23°C (Glu), shifted to 37°C for 10 min without glucose (10 min –Glu), followed by readdition of glucose (10 min +Glu). Polysome profiles under each condition are shown (a, f, and k). (**A**) WT, (**B**) *dcp1-2*, and (**C**) *prt1-63* cells expressing a GFP-tagged version of Dcp2p (b, g, and l), Dhh1p (c, h, and m), or co-expressing the plasmids U1A-GFP and PGK1-U1A (d, i, and n), or U1A-GFP and MFA2P-U1A (e, j, and o) are shown.

mRNA at the time of nutrient readdition, we observed that these transcripts moved from being predominantly untranslated in stationary phase cells (~22% polysome-associated) to the polysome pool upon media readdition (~73% polysome-associated) (Fig. 5). This demonstrates that during stationary phase P-bodies store mRNAs, which can later enter translation.

Previous work has demonstrated that mRNAs can move from polysomes to P-bodies when translation is repressed (*2*, *7*). Our results indicate that mRNAs can also exit P-bodies to reenter translation, suggesting a movement of yeast mRNAs from polysomes to P-bodies, where they can either be degraded or return to polysomes. Because most yeast mRNAs undergo decapping and therefore associate

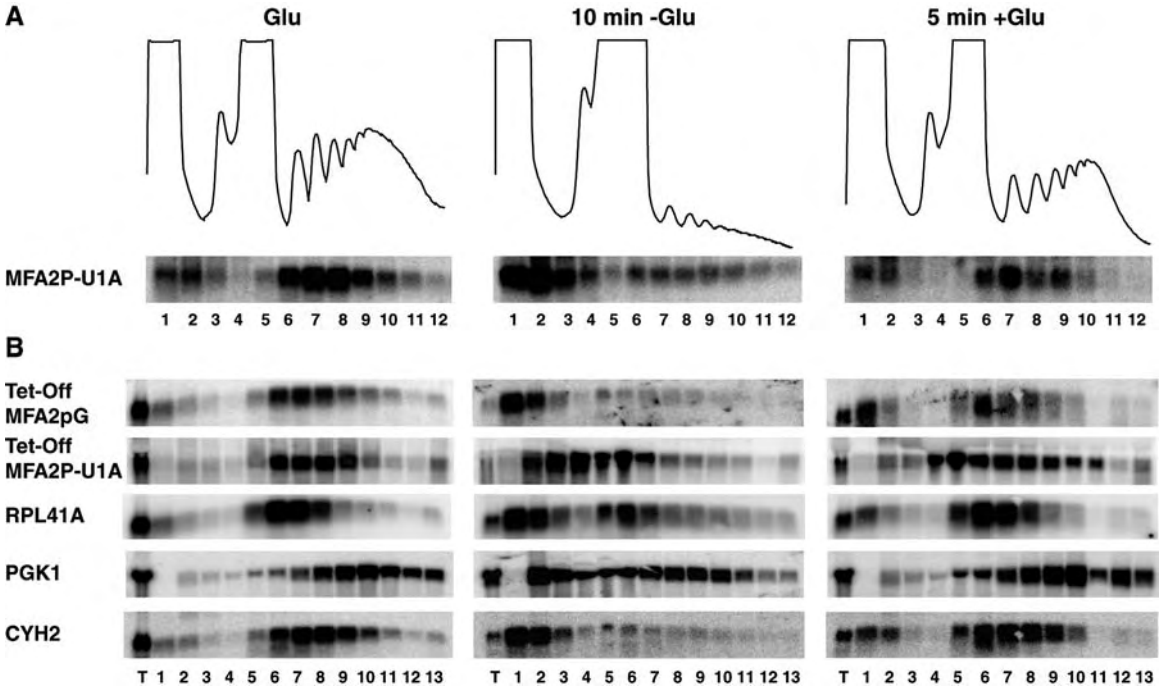

Fig. 4. Movement of mRNAs between a translating and a nontranslating pool. (**A**) WT cells co-expressing U1A-GFP with MFA2P-U1A or (**B**) expressing a plasmid containing MFA2P-U1A or MFA2pG under the control of a tetracycline promoter (Tet-Off MFA2P-U1A and Tet-Off MFA2pG) were grown at 30°C in synthetic complete (SC) medium plus glucose (Glu), shifted for 10 min to (A) SC with no glucose or (B) SC with no glucose containing doxycycline (10 min –Glu), followed by readdition of glucose (5 min +Glu). (A) Polysome profiles of the collected sucrose gradients are shown. Fraction 1 corresponds to the top of the gradient. (A and B) Northern blots for the indicated mRNA are shown.

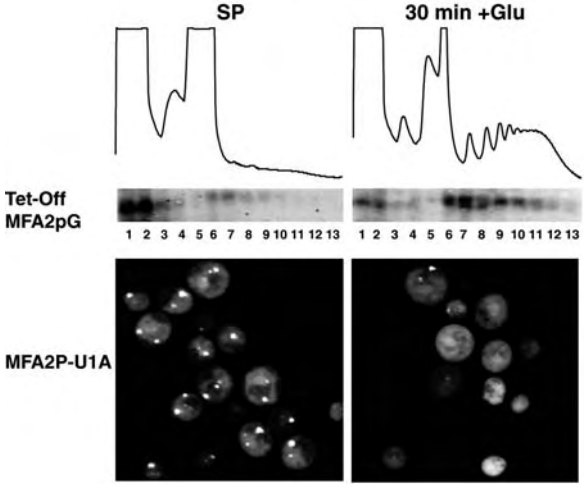

Fig. 5. mRNA present in P-bodies in stationary phase can return to translation. Cells expressing Tet-Off MFA2pG or co-expressing U1A-GFP with MFA2P-U1A were grown until stationary phase (SP). Then glucose, with or without doxycycline, was added to the culture (30 min +Glu). Polysome profiles and Northern blotting of cells expressing the plasmid Tet-Off MFA2pG are shown (**top**). Cells co-expressing U1A-GFP and MFA2P-U1A are visualized (**bottom**). In stationary phase, ~80% of the cells show large foci; after 30 min +Glu, ~20% of the cells have foci, and the remaining foci are considerably diminished.

with P-body components (*1*), and P-body proteins are required for the general repression of translation (*2*), we anticipate that most yeast mRNAs can move between polysomes and P-bodies. Moreover, because P-bodies decline in *dcp1*Δ cells after cycloheximide addition (Fig. 1A), there is likely to be a continual flux of mRNAs in and out of P-bodies. Mammalian P-bodies are similar to yeast P-bodies, suggesting that the movement of mRNAs from P-bodies to polysomes is likely to be a fundamental property of eukaryotic cells. Lastly, ribosomal components and translational factors are not concentrated in yeast P-bodies, even under stress (*7*) (fig. S3), indicating that the movement of mRNAs into P-bodies requires the loss of ribosomes and translation initiation factors.

Movement of mRNAs in and out of P-bodies can function to store mRNAs, one example being yeast in stationary phase, where RNAs enter translation once growth is resumed. Because maternal mRNA storage granules and P-bodies contain related proteins (*1*), we hypothesize that many forms of mRNA storage will share a conserved mechanism. This work also adds evidence that translating and nontranslating pools of mRNAs are spatially segregated in the cytoplasm between polysomes, stress granules, and P-bodies (*20*, *21*). The presence of multiple discrete biochemical and cytological states for cytoplasmic mRNAs strongly implies that mechanisms that control the movement of mRNAs between these states will be important in the regulation of mRNA translation and degradation.

References and Notes

1. J. Coller, R. Parker, *Annu. Rev. Biochem.* **73**, 861 (2004).
2. J. Coller, R. Parker, *Cell,* in press.
3. V. I. Bashkirov, H. Scherthan, J. A. Solinger, J. M. Buerstedde, W. D. Heyer, *J. Cell Biol.* **136**, 761 (1997).
4. D. Ingelfinger, D. J. Arndt-Jovin, R. Luhrmann, T. Achsel, *RNA* **8**, 1489 (2002).
5. J. Lykke-Andersen, *Mol. Cell. Biol.* **22**, 8114 (2002).
6. E. van Dijk *et al.*, *EMBO J.* **21**, 6915 (2002).
7. D. Teixeira, U. Sheth, M. A. Valencia-Sanchez, M. Brengues, R. Parker, *RNA* **11**, 371 (2005).
8. T. Eystathioy *et al.*, *Mol. Biol. Cell* **13**, 1338 (2002).
9. U. Sheth, R. Parker, *Science* **300**, 805 (2003).
10. N. Cougot, S. Babajko, S. B. Seraphin, *J. Cell Biol.* **165**, 31 (2004).
11. J. Liu, M. A. Valencia-Sanchez, G. J. Hannon, R. Parker, *Nat. Cell Biol.* **7**, 719 (2005).
12. G. L. Sen, H. M. Blau, *Nat. Cell Biol.* **7**, 633 (2005).
13. M. A. Andrei *et al.*, *RNA* **11**, 717 (2005).
14. J. S. Anderson, R. P. Parker, *EMBO J.* **17**, 1497 (1998).
15. M. P. Ashe, S. K. De Long, A. B. Sachs, *Mol. Biol. Cell* **11**, 833 (2000).
16. A. S. Brodsky, P. A. Silver, *RNA* **6**, 1737 (2000).
17. C. Bonnerot, R. Boeck, B. Lapeyre, *Mol. Cell. Biol.* **20**, 5939 (2000).
18. P. Hilleren, R. Parker, *RNA* **7**, 753 (2001).
19. J. V. Gray *et al.*, *Microbiol. Mol. Biol. Rev.* **68**, 187 (2004).
20. P. Anderson, N. Kedersha, *J. Cell Sci.* **115**, 3227 (2002).
21. L. Nover, K. D. Scharf, D. Neumann, *Mol. Cell. Biol.* **3**, 1648 (1983).

22. We thank the Parker lab for discussions, especially Kristian Baker and Carolyn Decker for critical reading of the manuscript. Supported by Howard Hughes Medical Institute and NIH (GM45443). D.T. was supported by Fundacao para a Ciencia e Tecnologia (SFRH/BD/2739/2000), Portugal.

Supporting Online Material

www.sciencemag.org/cgi/content/full/1115791/DC1
Materials and Methods
Figs. S1 to S3
Table S1
References

7 June 2005; accepted 23 August 2005
Published online 1 September 2005;
10.1126/science.1115791
Include this information when citing this paper.

The β-Glucuronidase Klotho Hydrolyzes and Activates the TRPV5 Channel

Q. Chang, S. Hoefs, A. W. van der Kemp, C. N. Topala, R. J. Bindels, J. G. Hoenderop*

Blood calcium concentration is maintained within a narrow range despite large variations in dietary input and body demand. The Transient Receptor Potential ion channel TRPV5 has been implicated in this process. We report here that TRPV5 is stimulated by the mammalian hormone klotho. Klotho, a β-glucuronidase, hydrolyzes extracellular sugar residues on TRPV5, entrapping the channel in the plasma membrane. This maintains durable calcium channel activity and membrane calcium permeability in kidney. Thus, klotho activates a cell surface channel by hydrolysis of its extracellular N-linked oligosaccharides.

Calcium, an essential ion in all organisms, plays a crucial role in processes ranging from formation and maintenance of the skeleton to temporal and spatial regulation of neuronal function. Concentration of blood Ca^{2+} decreases with age in both men and women, and several studies suggest that this is linked to aging-associated disorders. The Ca^{2+} balance is maintained by the concerted action of three organ systems—the gastrointestinal tract, bone, and kidney. Until recently, the mechanism by which Ca^{2+} ions enter the absorptive epithelia was unknown. A major breakthrough came with the identification of an epithelial Ca^{2+} channel family consisting of two members of the Transient Receptor Potential (TRP) superfamily, TRPV5 and TRPV6 (*1*, *2*). TRPV5 is predominantly involved in renal Ca^{2+} handling, whereas TRPV6 is postulated to mediate intestinal Ca^{2+} absorption. TRPV5 and TRPV6 are the most Ca^{2+}-selective channels in the TRP superfamily.

Mice lacking TRPV5 display diminished renal Ca^{2+} reabsorption despite enhanced levels of the calciotropic hormone vitamin D, causing severe hypercalciuria (*3*). In addition, compensatory hyperabsorption of dietary Ca^{2+} was observed in the intestines of TRPV5 knockout mice. Furthermore, these mice exhibit abnormalities in bone structure, including reduced trabecular and cortical bone thickness (*3*). In the process of identifying regulatory proteins that maintain the Ca^{2+} balance, we identified klotho as a gene whose expression is decreased in the kidneys of TRPV5 knockout mice. Klotho, a type I membrane glycoprotein of 130 kD (*4*), is abundantly expressed in mouse kidney as determined by quantitative real-time polymerase chain reaction analysis of mRNA (fig. S1) (*4*, *5*). Klotho mRNA expression was at least 500 times lower in all other analyzed tissues, including brain, lung, muscle, heart, liver, spleen, duodenum, ileum, and bone. Immunoblotting indicated a ~130-kD protein in mouse kidney lysates and urine (Fig. 1B).

Inactivation of the klotho gene in mice (*4*) resulted in a syndrome resembling human aging, including short life span, bone aberrations, infertility, skin atrophy, and hypercalcemia, as well as an increase in serum vitamin D. Klotho exhibits homology of 20 to 40% at the amino acid level to β-glucosidase enzymes of bacteria, plants, and eukaryotes (*4*, *6*). In general, β-glucosidases participate in the synthesis and degradation of polysaccharides that are involved in processes such as pathogen defense (*7*), control of signal transduction (*8*), and modification of hormones (*9*). In humans, inheritable deficiencies of glycosidases induce a variety of impairments, such as lysosomal storage diseases, Gaucher's and Krabbe's disease, and lactose intolerance (*10*). In addition to the aging-associated disorders observed in the klotho-null mice, polymorphisms in the klotho gene have been linked to reduced bone mineral density in humans (*11*, *12*). However, the molecular function of klotho and the downstream targets of this hormone remain to be identified.

Previous studies have indicated that the expression of klotho and TRPV5 is tightly controlled by vitamin D, suggesting a functional link between these proteins in the maintenance of the Ca^{2+} balance (*1*, *13*). On the basis of this correlation and an overlap in the pathophysiology of TRPV5 and klotho knockout mice (i.e., disturbed Ca^{2+} homeostasis and vitamin D metabolism), we investigated whether TRPV5 is a downstream target of klotho. Immunohistochemical analysis of mouse kidney cells revealed colocalization of TRPV5, the vitamin D–sensitive Ca^{2+}-transporting protein calbindin-D_{28K}, and klotho in the distal convoluted and connecting tubule, which are nephron segments responsible for active transepithelial Ca^{2+} reabsorption (Fig. 1A). Although klotho mutant mice show systemic aging phenotypes, only limited organs express the klotho gene (*4*).

When TRPV5 was expressed with klotho in human embryonic kidney (HEK293) cells, TRPV5-mediated $^{45}Ca^{2+}$ influx increased (Fig. 2A). Because klotho is detectable in urine, serum, and cerebrospinal fluid (*14*), it may operate from the extracellular site to regulate TRPV5 activity. To investigate this mechanism, transfected HEK293 cells expressing TRPV5 (HEK293-TRPV5) were incubated (16 hours) with culture media (supernatant) collected from klotho-expressing cells.

Klotho was detected in supernatant obtained from transfected HEK293 cells expressing klotho (Fig. 2B). TRPV5 activity increased by 178% when cells were treated with supernatant (Fig. 2B). Klotho did not alter TRPV5 expression, suggesting a specific effect on channel kinetics or trafficking

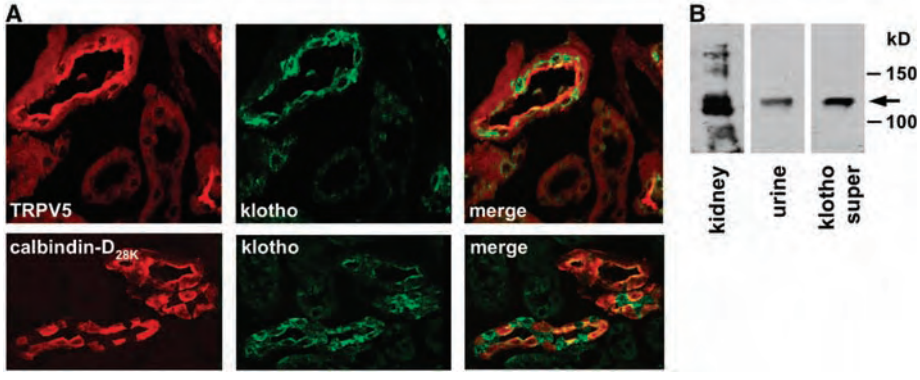

Fig. 1. Localization and expression of klotho. (**A**) Immunohistochemical analysis of klotho (green), TRPV5 (red), and calbindin-D_{28K} (red) in mouse kidney sections. (**B**) Protein lysates were prepared from mouse kidney and from urine ($n = 3$). Both samples were analyzed for the expression of klotho proteins (indicated by arrow) by immunoblotting with the rat antibody to klotho. Klotho-containing supernatant from transfected HEK293 cells expressing klotho was included as a positive control.

Department of Physiology, Nijmegen Centre for Molecular Life Sciences, Radboud University Nijmegen Medical Centre, 6500 HB Nijmegen, Netherlands.

*To whom correspondence should be addressed. E-mail: J.Hoenderop@ncmls.ru.nl

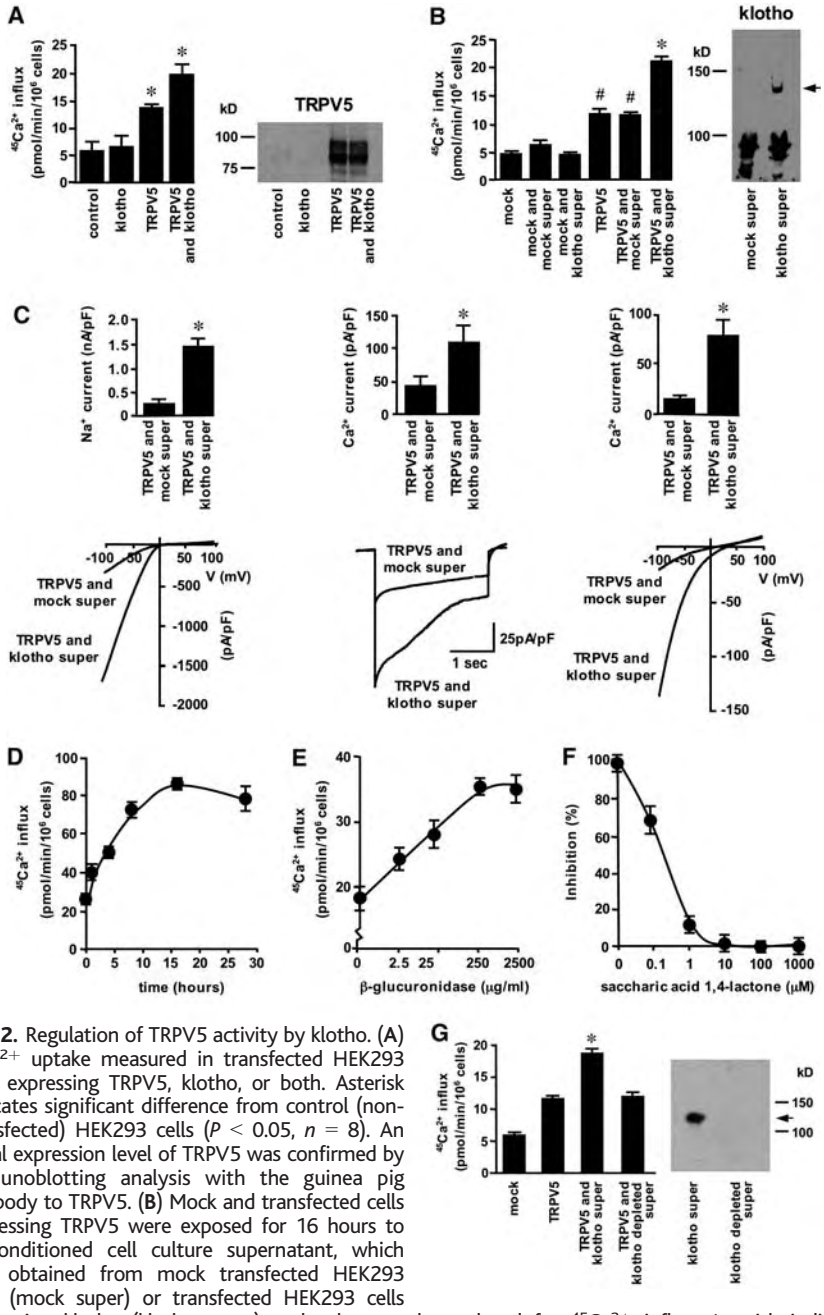

Fig. 2. Regulation of TRPV5 activity by klotho. (**A**) $^{45}Ca^{2+}$ uptake measured in transfected HEK293 cells expressing TRPV5, klotho, or both. Asterisk indicates significant difference from control (non-transfected) HEK293 cells ($P < 0.05$, $n = 8$). An equal expression level of TRPV5 was confirmed by immunoblotting analysis with the guinea pig antibody to TRPV5. (**B**) Mock and transfected cells expressing TRPV5 were exposed for 16 hours to preconditioned cell culture supernatant, which was obtained from mock transfected HEK293 cells (mock super) or transfected HEK293 cells expressing klotho (klotho super) and subsequently analyzed for $^{45}Ca^{2+}$ influx. Asterisk indicates significant difference from HEK293-TRPV5 cells treated with supernatant from mock-transfected cells. Pound sign (#) indicates significant difference from mock-transfected HEK293 cells ($P < 0.05$, $n = 6$). The supernatants of mock and klotho-transfected HEK293 cells were analyzed by immunoblotting analysis with the use of the mouse antibody to hemagglutinin (HA) to detect the secreted klotho that is epitope tagged with HA (indicated by arrow). (**C**) HEK293-TRPV5 cells were treated with klotho-containing supernatant or mock supernatant and analyzed by patch-clamp analysis. The cells treated with klotho-containing supernatant displayed significantly increased currents compared with the mock supernatant. Na^+ current at –80 mV: –1526 ± 250 pA/pF versus –299 ± 106 pA/pF ($n = 6$, left); Ca^{2+} peak current: –115 ± 25 versus –45 ± 10 pA/pF ($n = 6$, middle); and Ca^{2+} current at –80 mV: 88 ± 7 versus –14 ± 5 pA/pF ($n = 6$, right). Errors are SEM. Averaged current responses to voltage ramps and hyperpolarizing pulses are depicted below the histograms. (**D**) HEK293-TRPV5 cells were treated with klotho-containing supernatant for the indicated time and analyzed for $^{45}Ca^{2+}$ influx ($n = 3$). (**E**) HEK293-TRPV5 cells were treated for 16 hours with β-glucuronidase at the indicated concentrations and analyzed for $^{45}Ca^{2+}$ uptake ($n = 3$). (**F**) HEK293-TRPV5 cells were treated with klotho-containing supernatant in the presence of D-saccharic acid 1,4-lactone, a specific inhibitor of β-glucuronidase (*16*) ($n = 3$). (**G**) Klotho was immunoprecipitated from the klotho-containing supernatant and the remaining fluid was analyzed for klotho expression (klotho depleted super). HEK293-TRPV5 cells were treated with depleted and klotho-containing supernatant and analyzed for $^{45}Ca^{2+}$ influx. Asterisk indicates significant difference from HEK293-TRPV5 cells ($P < 0.05$, $n = 3$). Error bars show means + SEM in (A) to (C) and (G); error bars show means ± SEM in (D) to (F).

toward the plasma membrane. HEK293-TRPV5 cells were treated (16 hours) with klotho-containing supernatant and analyzed by whole-cell patch-clamp analysis. Both the Na^+ and Ca^{2+} currents were stimulated by klotho treatment (Fig. 2C). Measurements in divalent-free solution (EDTA 0.1 mM) revealed increased channel activity (Fig. 2C). Application of a hyperpolarizing voltage step from a holding potential of +70 to –100 mV induced an increased Ca^{2+} peak current, whereas no differences in the Ca^{2+}-dependent inactivation behavior of the channel were observed (Fig. 2C). By applying a voltage ramp to cells perfused with a solution containing 10 mM Ca^{2+}, a rise in current amplitude was obtained (Fig. 2C). TRPV5 is a constitutive active Ca^{2+} channel with an open probability of nearly 100% (*15*). Collectively, these findings imply an increased abundance of TRPV5 at the plasma membrane upon exposure to extracellular klotho. The stimulatory effect of klotho on TRPV5 activity was maximal at 16 hours of incubation, but increased channel activity was apparent after 2 hours (Fig. 2D). Because klotho exhibits β-glucuronidase activity (*16*), we examined whether purified β-glucuronidase from bovine liver (Enzyme Commission number 3.2.1.31) could mimic the stimulatory effect of klotho on TRPV5 channel activity. HEK293-TRPV5 cells were incubated (16 hours) with increasing concentrations of β-glucuronidase. β-glucuronidase mimicked the effect of the klotho-containing supernatant on TRPV5 channel activity, with a maximal stimulation at 250 μg/ml (Fig. 2E). To further characterize whether the β-glucuronidase activity of klotho is responsible for the stimulatory action, we assessed the effect of D-saccharic acid 1,4-lactone, a klotho inhibitor (*16*). Klotho-mediated increase of TRPV5 activity was blocked by this inhibitor in a dose-dependent manner, with an apparent median inhibitory concentration (IC_{50}) of 0.5 μM (Fig. 2F). This demonstrates that the stimulatory action of klotho can be attributed to its β-glucuronidase activity. Supernatant that was depleted of klotho by immunoprecipitation failed to increase TRPV5 channel activity (Fig. 2G). Together, these findings demonstrate that the β-glucuronidase activity of klotho activates TRPV5.

The effect of klotho and β-glucuronidase was further evaluated in primary cell cultures from rabbit kidney cells. Connecting tubules and cortical collecting ducts form confluent monolayers that exhibit many characteristics of the original polarized epithelium, including parathyroid hormone and vitamin D–stimulated transepithelial Ca^{2+} transport (*17*). The addition of klotho-containing supernatant or β-glucuronidase to the apical side of the cell monolayers stimulated transcellular Ca^{2+} transport in these primary kidney cells (Fig. 3).

To elucidate the molecular mechanism underlying the stimulatory effect of extracellular klotho on TRPV5 channel activity, we examined the role of glycosylation in this process. Heterologous expression of TRPV5 in HEK293 cells and subsequent immunoblot analysis of cell lysates revealed TRPV5 with a molecular size ranging from 75 to between 90 and 100 kD (Fig. 4A). These protein forms were not detected in control cells. The protein of 75 kD reflects the core TRPV5 protein, whereas the protein of 90 to 100 kD represents the complex glycosylated form (*18*). Sequence analysis predicts an N-glycosylation site at an asparagine residue (N^{358}) positioned between transmembrane segments 1 and 2. The functional role of glycosylation in klotho-mediated TRPV5 stimulation was investigated by mutating this asparagine residue to glutamine (TRPV5-N358Q). This prevented TRPV5 glycosylation when expressed in HEK293 cells, but the cells showed normal Ca^{2+} influx that was not different from cells expressing wild-type TRPV5 channels (Fig. 4A). The stimulatory effect of klotho or β-glucuronidase on TRPV5 was abolished in the HEK293 cells expressing the TRPV5-N358Q mutant, whereas HEK293-TRPV5 cells showed an increased Ca^{2+} influx activity (Fig. 4A). These results indicated that abolishment of glycosylation prevents accumulation of TRPV5 in the plasma membrane. This suggests that the klotho-mediated TRPV5 accumulation is due to the specific hydrolysis of extracellular sugar residues from the channel protein. Because the TRPV5-N358Q mutant did not accumulate in the plasma membrane upon klotho treatment, the klotho-modified TRPV5 glycan is required for trapping the wild-type channel in the plasma membrane. Possibly, the klotho-mediated hydrolysis of TRPV5 exposes a new sugar residue that is a candidate of a plasma membrane retention mechanism. Klotho also increased the activity of the highly homologous TRPV6 channel, whereas a glycosylation-deficient TRPV6 (N357Q) mutant failed to respond to klotho or to the β-glucuronidase (fig. S2). Thus, klotho stimulates TRPV channel activity by sugar hydrolysis at the conserved glycosylation site between transmembrane segments 1 and 2.

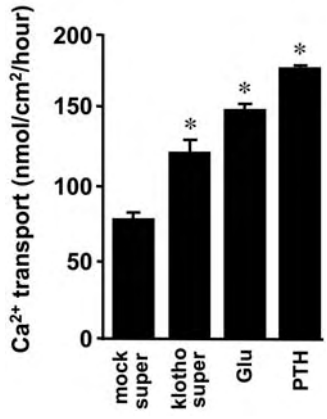

Fig. 3. Transepithelial Ca^{2+} transport is stimulated by klotho. Monolayers of rabbit connecting tubules and cortical collecting ducts primary cell cultures were apically treated with the supernatant from klotho-expressing cells or mock-transfected cells for 16 hours. Net apical to basolateral Ca^{2+} transport was measured in the presence of mock supernatant (apical), klotho-containing supernatant (apical), 250 μg/ml β-glucuronidase (Glu, apical), or 10 nM parathyroid hormone (PTH, basolateral). Asterisk indicates significant difference from cell cultures treated with mock supernatant ($P < 0.05$, $n = 6$). Error bars show means + SEM.

To investigate klotho-mediated hydrolysis of the glycosylated TRPV5 protein, HEK293 cells transiently expressing the channel were labeled for 48 hours with D-[U-^{14}C]glucose. After 32 hours of labeling, the cells were incubated for 16 hours with klotho-containing supernatant, mock supernatant, or β-glucuronidase, TRPV5 was subsequently immunoprecipitated. Incubation of the HEK293-TRPV5 cells with klotho-containing supernatant or β-glucuronidase caused a decrease in D-[U-^{14}C]glucose–labeled TRPV5, indicating cleavage of extracellular ^{14}C-sugars (Fig. 4B). This indicates that klotho exhibits β-glucuronidase activity by hydrolyzing sugars from glycosylated TRPV5 channels.

To determine the functional consequences of the klotho action on TRPV5, the plasma membrane expression of TRPV5 was examined in klotho- and mock-treated HEK293-TRPV5 cells. Klotho-containing supernatant increased the plasma membrane TRPV5 expression, as determined by membrane surface

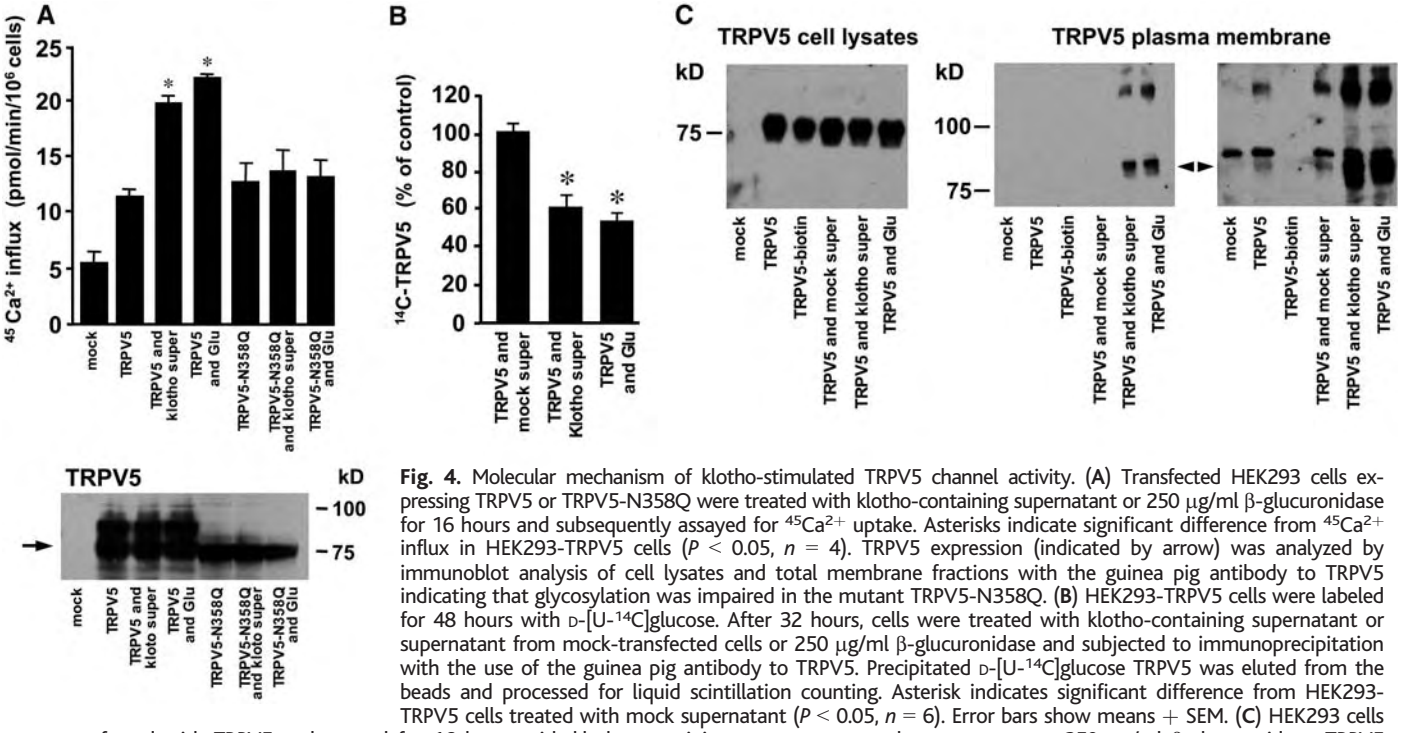

Fig. 4. Molecular mechanism of klotho-stimulated TRPV5 channel activity. (**A**) Transfected HEK293 cells expressing TRPV5 or TRPV5-N358Q were treated with klotho-containing supernatant or 250 μg/ml β-glucuronidase for 16 hours and subsequently assayed for $^{45}Ca^{2+}$ uptake. Asterisks indicate significant difference from $^{45}Ca^{2+}$ influx in HEK293-TRPV5 cells ($P < 0.05$, $n = 4$). TRPV5 expression (indicated by arrow) was analyzed by immunoblot analysis of cell lysates and total membrane fractions with the guinea pig antibody to TRPV5 indicating that glycosylation was impaired in the mutant TRPV5-N358Q. (**B**) HEK293-TRPV5 cells were labeled for 48 hours with D-[U-^{14}C]glucose. After 32 hours, cells were treated with klotho-containing supernatant or supernatant from mock-transfected cells or 250 μg/ml β-glucuronidase and subjected to immunoprecipitation with the use of the guinea pig antibody to TRPV5. Precipitated D-[U-^{14}C]glucose TRPV5 was eluted from the beads and processed for liquid scintillation counting. Asterisk indicates significant difference from HEK293-TRPV5 cells treated with mock supernatant ($P < 0.05$, $n = 6$). Error bars show means + SEM. (**C**) HEK293 cells were transfected with TRPV5 and treated for 16 hours with klotho-containing supernatant, mock supernatant, or 250 μg/ml β-glucuronidase. TRPV5 expression was determined by immunoblotting in total cell lysates to demonstrate equal expression (left). Cell surface proteins were biotinylated extracellularly, precipitated with streptavidin-agarose beads and immunoblotted for TRPV5 (middle, low exposure; right, high exposure). As a negative control, biotin was omitted in the procedure.

protein biotinylation, explaining the observed increase in channel activity (Fig. 4C). Treatment of cells with mock supernatant had no effect. Total expression of TRPV5 in cell lysates was equivalent in all conditions (Fig. 4C). The klotho-mediated increase in channel abundance was mimicked by the addition of 250 μM β-glucuronidase, indicating that extracellular hydrolysis of TRPV5-associated carbohydrates and consequent plasma membrane accumulation depends on the glucuronidase activity of the klotho protein.

N-glycosylation of proteins is highly conserved from yeast to human and has a stabilizing effect on protein structure that facilitates proper folding and trafficking of membrane proteins. Protein glycosylation has been implicated in cellular functions such as modulating protein structure and localization, cell-cell recognition, and signaling in multicellular systems. Protein glycosylation can be modulated by adaptations in the biosynthetic pathway. For instance, dietary variations and hormones such as estradiol can affect the display of cell-surface carbohydrate epitopes (*19*). Our study shows that a glycosylated cell surface protein, TRPV5, can be controlled by the extracellular glucuronidase klotho to regulate its biological function. Because klotho and TRPV5 colocalize in the distal part of the nephron, klotho could exert its stimulatory effect by an auto- and/or paracrine mechanism. Furthermore, TRPV5 and klotho are both positively regulated by the biosynthetic vitamin D pathway. This concomitant control will ensure high Ca^{2+} transport capacity and reduce Ca^{2+} excretion to preserve normal blood Ca^{2+} levels during periods of dietary Ca^{2+} insufficiency.

References and Notes

1. J. G. Hoenderop, B. Nilius, R. J. Bindels, *Physiol. Rev.* **85**, 373 (2005).
2. D. E. Clapham, *Nature* **426**, 517 (2003).
3. J. G. Hoenderop *et al.*, *J. Clin. Invest.* **112**, 1906 (2003).
4. M. Kuro-o *et al.*, *Nature* **390**, 45 (1997).
5. H. Aizawa *et al.*, *Biochem. Biophys. Res. Commun.* **249**, 865 (1998).
6. B. Henrissat, A. Bairoch, *Biochem. J.* **316**, 695 (1996).
7. U. Wittstock, B. A. Halkier, *Trends Plant Sci.* **7**, 263 (2002).
8. L. Wells, K. Vosseller, G. W. Hart, *Science* **291**, 2376 (2001).
9. B. Brzobohaty *et al.*, *Science* **262**, 1051 (1993).
10. R. Schiffmann, R. O. Brady, *Drugs* **62**, 733 (2002).
11. K. Kawano *et al.*, *J. Bone Miner. Res.* **17**, 1744 (2002).
12. N. Ogata *et al.*, *Bone* **31**, 37 (2002).
13. H. Tsujikawa, Y. Kurotaki, T. Fujimori, K. Fukuda, Y. Nabeshima, *Mol. Endocrinol.* **17**, 2393 (2003).
14. A. Imura *et al.*, *FEBS Lett.* **565**, 143 (2004).
15. B. Nilius *et al.*, *J. Physiol.* **527**, 239 (2000).
16. O. Tohyama *et al.*, *J. Biol. Chem.* **279**, 9777 (2004).
17. R. J. Bindels, A. Hartog, J. Timmermans, C. H. Van Os, *Am. J. Physiol.* **261**, F799 (1991).
18. J. G. Hoenderop *et al.*, *EMBO J.* **22**, 776 (2003).
19. D. D. Carson, J. D. Farrar, J. Laidlaw, D. A. Wright, *J. Biol. Chem.* **265**, 2947 (1990).

20. This study was supported by the Dutch Organization of Scientific Research (Zon-Mw 016.006.001), Human Frontiers Science Program (RGP32/2004), and the Dutch Kidney foundation (C03.6017). We thank D. van den Berg for technical assistance and T. van Kuppevelt and the members of our laboratory for discussion, advice, and critical reading of this manuscript.

Supporting Online Material

www.sciencemag.org/cgi/content/full/310/5747/490/DC1
Materials and Methods
References

29 April 2005; accepted 23 September 2005
10.1126/science.1114245

Reciprocal Interference Between Specific CJD and Scrapie Agents in Neural Cell Cultures

Noriuki Nishida,[1,2] Shigeru Katamine,[3] Laura Manuelidis[1]*

Infection of mice with an attenuated Creutzfeldt-Jakob disease agent (SY-CJD) interferes with superinfection by a more virulent human-derived CJD agent (FU-CJD) and does not require pathological prion protein (PrPres). Using a rapid coculture system, we found that a neural cell line free of immune system cells similarly supported substantial CJD agent interference without PrPres. In addition, SY-CJD prevented superinfection by sheep-derived Chandler (Ch) and 22L scrapie agents. However, only 22L and not Ch prevented FU-CJD infection, even though both scrapie strains provoked abundant PrPres. This relationship between particular strains of sheep- and human-derived agents is likely to affect their prevalence and epidemic spread.

In transmissible spongiform encephalopathies (TSEs) such as human CJD, sheep scrapie, and bovine spongiform encephalopathy (BSE), B and T cell adaptive immune responses to a foreign infectious agent have not been detected (*1*). Nonetheless, an attenuated CJD agent, designated SY, was able to prevent superinfection by the more virulent and rapidly lethal FU-CJD agent (*2*). These experiments exploited two human CJD agents that, when passaged in mice, were readily distinguished by profound differences in the incubation time to disease and the distribution of brain lesions. The attenuated "slow" SY produced only small medial thalamic lesions typical of sporadic CJD in mice, whereas the virulent "fast" FU strain, isolated only in Japan, caused widespread severe lesions with many amyloid deposits (Table 1). Clear protective effects of SY-CJD against superinfection by FU-CJD were demonstrable with both intracerebral and peripheral challenges, and SY-protected mice could live free of disease for >600 days, a typical mouse life span (*3*, *4*). By comparison, there was minimal interference between scrapie strains 22C and 22A (*5*). This raised the possibility that protective effects might be restricted to particular strains of CJD or to unusual agent strain combinations. We sought ways to evaluate interference between different combinations of TSE agents, and to determine whether apparently unrelated agents—such as those propagated from human CJD and from sheep scrapie cases—could be antagonistic.

Mice can respond to CJD agents through a variety of myeloid cell and innate defense mechanisms (*6*–*8*). Thus, it was relevant to determine whether different agent strains could prevent superinfection in simplified cell cultures that lack B, T, and myeloid cells. Neural cells, which can be susceptible to TSE agents, would be incapable of producing many of the myeloid cell cytokines that can participate in strain interference in vivo. If interference could be demonstrated in neural cells, it would show that more universal cellular pathways are sufficient for protection. These culture models also might be used to identify crucial, and possibly novel, molecular pathways of innate immunity to TSE agents.

We developed a rapid, simple, and flexible test of interference in GT1-7 cells (hereafter called GT cells), a murine hypothalamic cell line. We previously found that these cells support the replication of a variety of mouse-passaged CJD and scrapie agents (Table 1) (*9*, *10*). A neomycin-resistant plasmid was introduced into the target GT cells (GTneo) to allow their selection by G418 antibiotic treatment (*11*) (Fig. 1). Infected GT challenge cells were killed by adding G418 to cocultures, and the pure GTneo target cells were then passaged and assayed for PrPres, a surrogate marker for infection in GT cells. Although PrPres does not quantitatively correlate with infectious

[1]Yale Medical School, New Haven, CT 06510, USA. [2]Center for Emerging Infectious Diseases, Gifu University, Yanagido 1-1, Gifu 501-1193, Japan. [3]Department of Molecular Microbiology and Immunology, Nagasaki University Graduate School of Medicine, 1-12-4 Sakamoto, Nagasaki 852-8523, Japan.

*To whom correspondence should be addressed. E-mail: laura.manuelidis@yale.edu

Table 1. Cell lines and TSE agents for testing interference. Agents, their source, and the number of cell passages after infection at the time of challenge are shown. By convention, TSE agent names identify the natural host. Thus, scrapie agents are derived from sheep, CJD agents from humans, CWD agents from cervids, and BSE agents from cows. Hence, the terms mouse scrapie and PrP^{Sc} (i.e., PrPres in mice infected with scrapie) indicate infection with sheep-derived agents. The UK Chandler (Ch) "drowsy" strain [equivalent to Rocky Mountain Laboratory (RML) scrapie], from a goat with experimental scrapie, is distinct from 22L scrapie (typical scratching scrapie in sheep from brain pool SSBP1). These scrapie strains are clearly different from CJD and BSE agents propagated in mice (i.e., their separate identities are not made homogeneous by the murine host). CJD encompasses all subsets of human TSE infectious agents except kuru, including those isolated from patients with PrP mutations such as PrP 102L of Gerstmann-Sträussler-Sheinker disease (GSS). SY-CJD causes circumscribed thalamic lesions only after ≥350 days in mice, and it is representative of sporadic CJD agents in the Western hemisphere, including agents isolated from GSS patients (*23*). No CJD agent similar to the representative Japanese fast FU-CJD agent ("CJD-Fukuoka-1") that induces widespread PrP amyloid deposits and severe demyelination has ever been isolated outside of Japan. Because FU-CJD and the Ch and 22L scrapie strains all cause widespread brain pathology, interference between these strains cannot be assessed in mice.

Cell line	Agent strain	Origin	Passages
GT (GT1-7)	—	—	—
SY+GT	SY	CJD sporadic: USA	≥106
FU+GT	FU	CJD (GSS 102L): Japan	≥110
Ch+GT	Ch	"Drowsy" scrapie: UK	≥50
22L+GT	22L	"Scratching" scrapie: UK	≥50
GTneo	Mock	—	≥15
SY+GTneo	SY	CJD sporadic: USA	≥110
Ch+GTneo	Ch	"Drowsy" scrapie: UK	≥15
22L+GTneo	22L	"Scratching" scrapie: UK	≥15

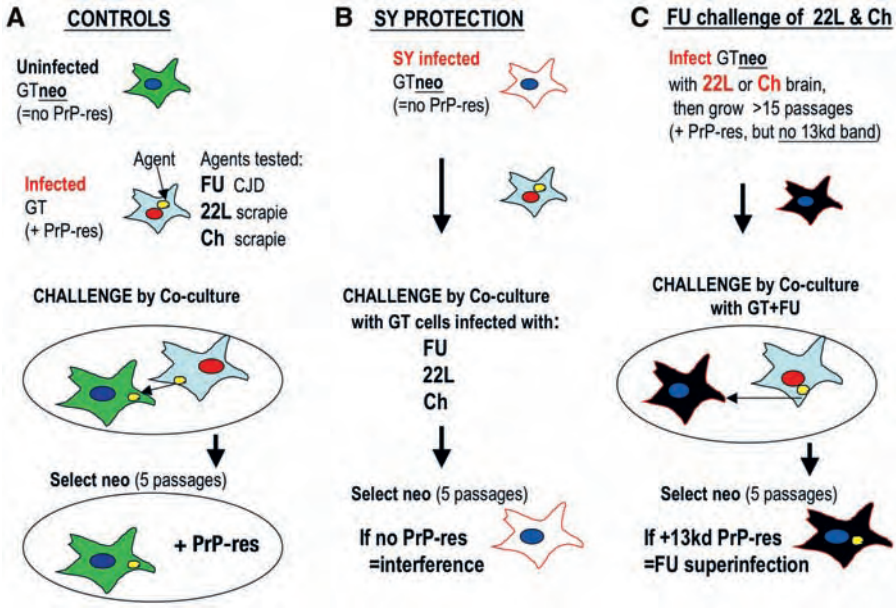

Fig. 1. In vitro interference strategy: Coculture challenges of (**A**) uninfected control cells, (**B**) SY-infected cells, and (**C**) scrapie-infected cells. Target GTneo cells were challenged with mock GT or infected GT cells by coculture for 2 days. GT challenge cells were then killed by G418 treatment, and resistant GTneo cells were analyzed for PrPres (*11*). For FU challenges, GTneo cells were newly infected with 22L or Ch scrapie brain homogenates and passaged >15 times before coculture.

titers, and may not be detectable in all infectious samples [e.g., (*1*, *4*, *12*, *13*)], its presence does indicate infection in GT cells (*10*).

GTneo target cells were exposed to uninfected brain tissue or to equal numbers of uninfected donor cells (i.e., mock-infected as in Fig. 1A). Such control GTneo cells should fail to produce PrPres. In contrast, mock-infected GTneo cells challenged with infected GT cells should become persistently infected and display PrPres long after the GT cells are removed by G418 treatment. Challenges of GTneo cells by GT cells infected with the agents 22L scrapie (GT+22L), Ch scrapie (GT+Ch), or FU-CJD (GT+FU) were rapidly effective (Fig. 2A). A large amount of PrPres was produced by all the control target cells after challenge with infected GT cells, but no PrPres was present after exposure to uninfected brain tissue (in this and in three or more repeat experiments per condition). Further in vitro passages of these GTneo target cells showed stable production of PrPres, indicating persistent infection by each of the challenge agents. Some TSE agents have been associated with variant PrPres band patterns (*14*). The three major PrPres bands were the same in all infected cells. However, an extra, highly reproducible, 13-kD band of PrPres was seen only in FU-infected cells. Antibodies identified this as a C-terminal PrPres fragment (Fig. 2A, C-13). Because this band was not present with any of the other agents, we could use it to specifically diagnose FU superinfection. Moreover, with all challenge agents, rapid infection with de novo production of large amounts of PrPres was apparent by 25 days in culture, whereas intracerebral inoculation with FU homogenates takes more than 90 days to induce brain PrPres (*8*).

In parallel with these controls, we tested whether SY could interfere with FU superinfection in culture as it does in mice, and we also tested whether SY infection could reduce susceptibility to presumably unrelated scrapie agents (Fig. 1B). The neomycin plasmid was added to PrPres-negative but persistently infected SY cells (as verified by repeated bioassays) (*10*, *11*). The lack of PrPres in SY-infected target cells greatly simplified the interference assay. After challenge, a continued lack of PrPres would indicate that covert SY infection protected cells from superinfection. In all these experiments, the number of infectious particles in challenge cells was higher than in target cells by a factor of ≥10,000 (*11*). No PrPres was detected in the GTneo+SY cells challenged with 22L cells (SY/22L lane, Fig. 2B). Thus, SY infection interfered with 22L superinfection. G418 selection also visibly removed all of the abundant PrPres of challenge cells. Persistent SY infection additionally interfered with GT+Ch scrapie agent and GT+FU CJD agent challenges. Only a barely detectable smear of signal was seen in the PrPres gel region (Fig. 2B). Moreover, the 13-kD PrPres band elicited by FU infection was never detectable in the FU-challenged SY cells, and the lack of any distinguishing strain-specific PrPres patterns for the other three common major PrPres bands made it impossible to determine whether the ± signal was due to low levels of the challenge strain. Two repeat experiments reconfirmed that SY interfered with superinfection by 22L, Ch, and FU agents (Table 2). Although the PrPres results do not permit us to conclude that there was complete prevention of superinfection, the interference of SY against 22L, Ch, and FU agents in vitro was manifest, and in marked contrast to the results with unprotected cells.

Because the 13-kD PrPres band was seen only after FU infection (Fig. 2A), it was possible to test whether scrapie agents could protect against the FU-CJD agent (Fig. 1C). We established new persistent infections of GTneo cells by standard application of infected brain homogenates (*9*, *10*), and verified that these newly infected GTneo cells continued to produce substantial amounts of

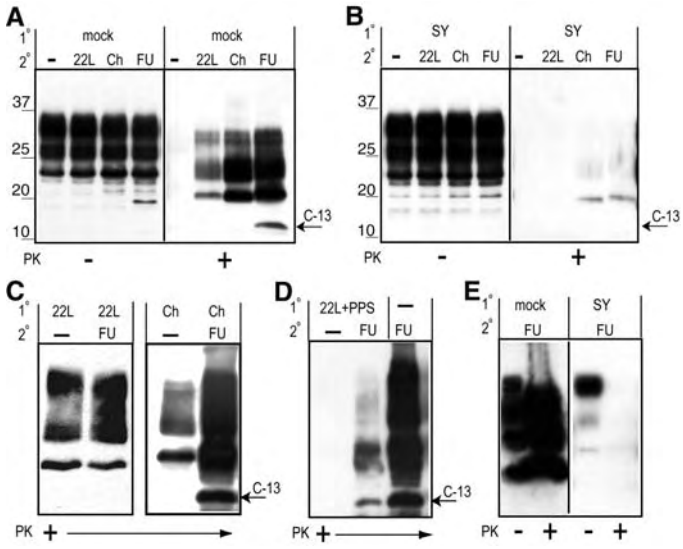

Fig. 2. Immunoblots of control and infected target cells. (**A**) Challenge of mock-infected and (**B**) SY-CJD–infected GTneo target cells by coculture with uninfected GT cells (–) or with infected GT+22L, GT+Ch, and GT+FU cells. Primary agent (1°) and challenge agent (2°) are indicated with total PrP compared to PrPres after limited proteinase K (PK) digestion. No PrPres is detectable in SY-infected cells, and the C-13 band is seen only in FU-infected cells. Markers (in kilodaltons) are at left. (**C**) PrPres after mock (–) and FU-CJD challenge (FU) of 22L scrapie GTneo cells (left) versus challenge of Ch scrapie GTneo cells (right). Mock controls (–) both show high levels of PrPres in scrapie-infected cells before FU challenge. After FU challenge of 22L cells, the pattern and amount of PrPres is unchanged, indicating no appreciable superinfection, and the C-13 band is undetectable. In contrast, massive superinfection by FU is apparent in Ch-infected cells, with markedly increased PrPres and a clear 13-kD band (C-13). (**D**) Superinfection of "cured" 22L cells treated with pentosan polysulfate (22L+PPS). PrPres is not detectable in the "cured" unchallenged cells (left lane) as compared with the original 22L-infected cells in (C). "Cured" cells challenged with FU became susceptible to FU superinfection and showed the C-13 FU diagnostic band (middle lane, arrow). The "cured" cells, however, showed less PrPres than did the parallel FU-challenged uninfected controls (right lane), possibly suggesting residual 22L scrapie agent. (**E**) Mock- and SY-infected target cells (minus neo plasmid or G418 selection) challenged with GT+FU cells separated by a 0.4μ filter. Mock cells became infected (positive for PrPres, left), whereas SY-infected cells were protected (right). C-13 is not seen in whole-cell lysates (*11*).

Table 2. Interference results in three replicate experiments. Symbols: +, strong PrPres signal (positive infection); –, no detectable PrPres; ±, barely detectable or questionable PrPres signal between 19 and 30 kD. C-13 is the FU diagnostic band. FU-CJD, 22L, and Ch scrapie infectious challenges were of greater magnitude than in previous in vivo studies (*11*).

Agent		PrPres		Interference
1° first	2° challenge	19 to 30 kD	C-13	
Mock	FU-CJD	+ / + / +	+ / + / +	No
Mock	22L scrapie	+ / + / +	– / – / –	No
Mock	Ch scrapie	+ / + / +	– / – / –	No
SY-CJD	Mock	– / – / –	– / – / –	—
SY-CJD	FU-CJD	± / – / –	– / – / –	Yes
SY-CJD	22L scrapie	– / ± / ±	– / – / –	Yes
SY-CJD	Ch scrapie	± / – / –	– / – / –	Yes
22L scrapie	FU-CJD	+ / + / +	– / – / –	Yes
Ch scrapie	FU-CJD	+ / + / +	+ / + / +	No

pathologic PrPres for >15 in vitro passages before challenging them with GT+FU cells. Both the 22L and Ch scrapie–infected GTneo cells, but not the parallel mock-infected cells, showed large amounts of the three major PrPres bands, but not the extra 13-kD band that was diagnostic for FU infection. These 22L and Ch scrapie–infected GTneo cells were then challenged with FU+GT cells that displayed the 13-kD band (as in Fig. 2A). A large increase in PrPres and/or the appearance of the extra 13-kD PrPres band in scrapie-infected GTneo cells would show that these particular scrapie agents failed to prevent superinfection by FU. Superinfection would also prove that high levels of PrPres are not protective.

The scrapie strains 22L and Ch displayed markedly different capacities for interfering with FU superinfection (Fig. 2C). Target 22L cells were protected against FU superinfection. The PrPres intensity and band patterns of 22L cells exposed to FU (22L/FU lane, Fig. 2C) were the same as in 22L controls (22L/– lane), and the lack of the FU-diagnostic 13-kD PrPres band further confirmed that only the initial 22L infection was present. The 13-kD PrPres band also did not appear with additional in vitro passages, indicating that FU was probably not covertly contaminating the target cells. These results were reproducible (Table 2).

In sharp contrast, Ch scrapie infection did not protect GTneo cells from FU superinfection. PrPres accumulation in these FU-challenged cells (Ch/FU lane, Fig. 2C) was considerably more intense than in mock cells (Ch/– lane), and consistent with the amount of pathologic PrPres that would be provoked by infection with both agents. Additionally, there was a strong 13-kD PrPres signal indicating FU superinfection (Fig. 2C and Table 2). Hence, enormous amounts of PrPres provoked by the Ch agent did not prevent massive superinfection by a second strain. Because in situ studies show that FU infects most GT cells (*10*), it is likely that a fair proportion of the Ch/FU cells were doubly infected. Brain tissue can also be doubly infected, and each agent breeds true despite cocultivation in that tissue for >200 days (*3*). In sum, two scrapie strains eliciting the same PrPres band pattern show markedly different susceptibilities to a CJD agent that provokes an extra PrPres band.

To further show that interference depended on persistent infection, we "cured" GT+22L neo cells by treating them with pentosan polysulfate (*11*) until PrPres was undetectable (Fig. 2D). We then challenged these "cured" 22L cultures and parallel mock controls with GT+FU as above. These "cured" cultures became susceptible to FU superinfection and showed the diagnostic FU 13-kD band (Fig. 2D), unlike the 22L-protected cells (Fig. 2C). This experiment also shows that the 22L agent, rather than some new cellular characteristic induced by neo plasmid/G418 selection, was the ultimate cause of interference.

Direct cell-to-cell contacts may aid agent transmission in vivo, as in the transfer of infectious agent from follicular dendritic cells to transiting white blood cells (*15*). We found that concentrated supernatants from both 22L- and FU-infected GT cells were less infectious than the remaining whole washed cells by a factor of ~1000, as measured by bioassay. We also prevented direct cell-to-cell contact with 0.4μ filters placed between challenge cells and GT+SY target (minus neoplasmid) cells. This would permit the transit of large viruses and aggregates but not whole cells. Equal numbers of healthy challenge and target cells were plated and exposed for 2 days, and the separated target cells were then passaged and analyzed (*11*). Target control cells required ≥8 in vitro passages to produce PrPres and did not always become positive, unlike the cocultures described above. However, despite this caveat, SY infection did interfere with FU superinfection as compared to more typical controls (Fig. 2E). Thus, SY infection rather than neo transformation and G418 selection was the primary cause of interference.

We have shown that infected neural cells in culture carry all the requisite features for

mounting a substantial TSE interference effect. No immune system cells were necessary for this protection, and stable interfering infections were reproducibly achieved without cloning. Interference did not depend on the presence or absence of abnormal PrP. Only persistent infection protected target cells from superinfection. Additionally, only particular agent-strain combinations showed positive interference, and these could not be predicted from cellular PrPres amounts or banding patterns. Moreover, despite continuous replication in cells with PrPres band patterns very different from those found in brain tissue, SY and FU CJD agents each breed true when reinoculated into mice, as does rodent-passaged scrapie reinoculated in sheep (*10*). The stability of the BSE agent also contrasts with the many different PrPres patterns seen in various affected species. Together, these results are not compatible with the common assumption that TSE strains are encoded by some unresolved type of PrPres folding (*16*, *17*). Indeed, there is still no conclusive evidence that any recombinant or amplified form of abnormal PrP can infect normal animals directly, reproduce meaningful levels of infectivity, or encode all the strain differences observed in mice infected with scrapie, CJD, and BSE agents.

Unlike heterogeneous aggregates of pathological PrP, infectious TSE particles have a discrete viral size of ~25 nm and 10^7 daltons (as assessed by field flow fractionation and high-pressure liquid chromatography, respectively) (*18*), and releasing their tightly bound nucleic acids destroys infectivity (*19*). Thus, some TSE agents such as SY may produce defective interfering particles, as found in many persistent viral as well as noncoding human viroid infections (*20*, *21*). Unlike pathologic host PrP, TSE agents can also provoke innate cellular defenses, including intracellular and diffusible factors that are not restricted to immune system cells (*7*, *8*), and such factors are likely to be involved in interference. Small interfering RNAs with extensive secondary structure may also be evoked by TSE agents, and these can provide even greater strain specificity (*22*). Notably, several small RNAs with extensive secondary structure have been identified in TSE-infected but not in normal brain tissue (*23*), and such motifs deserve further study in TSE culture models.

Cocultures were more efficient than mouse bioassays and can be useful for rapid assessment of agent purification and recovery (*24*). Additionally, they may provide a sensitive test for cells that are infected but show no PrPres (such as white blood cells), and they may be useful for evaluating a wide range of evolving TSE agents that have become important epidemiologically, such as those that cause BSE and chronic wasting disease (CWD). The resistance of cells infected with a prototypic sporadic CJD agent (SY) to two scrapie strains supports the suggestion that a commensal but rarely pathogenic TSE agent may help protect people against infection by sheep TSE strains in nature (*4*), and may explain why so few people have developed BSE-linked CJD (*25*). The clustering of sporadic CJD cases is also consistent with an environmental agent of low virulence (*26*).

References and Notes

1. L. Manuelidis, W. Fritch, Y. G. Xi, *Science* **277**, 94 (1997).
2. L. Manuelidis, *Proc. Natl. Acad. Sci. U.S.A.* **95**, 2520 (1998).
3. L. Manuelidis, Z. Y. Lu, *Neurosci. Lett.* **293**, 163 (2000).
4. L. Manuelidis, Z. Y. Lu, *Proc. Natl. Acad. Sci. U.S.A.* **100**, 5360 (2003).
5. A. Dickinson, H. Fraser, V. Meikle, G. Outram, *Nature New Biol.* **237**, 244 (1972).
6. C. Baker, L. Manuelidis, *Proc. Natl. Acad. Sci. U.S.A.* **100**, 675 (2003).
7. C. Baker, Z. Lu, L. Manuelidis, *J. Neurovirol.* **10**, 1 (2004).
8. Z. Lu, C. Baker, L. Manuelidis, *J. Cell. Biochem.* **93**, 644 (2004).
9. N. Nishida *et al.*, *J. Virol.* **74**, 320 (2000).
10. A. Arjona, L. Simarro, F. Islinger, N. Nishida, L. Manuelidis, *Proc. Natl. Acad. Sci. U.S.A.* **101**, 8768 (2004).
11. See supporting data on *Science* Online.
12. C. Lasmezas *et al.*, *Science* **275**, 402 (1997).
13. Y. G. Xi, A. Ingrosso, A. Ladogana, C. Masullo, M. Pocchiari, *Nature* **356**, 598 (1992).
14. A. Hill *et al.*, *Brain* **126**, 1333 (2003).
15. L. Manuelidis *et al.*, *J. Virol.* **74**, 8614 (2000).
16. S. Prusiner, *Proc. Natl. Acad. Sci. U.S.A.* **95**, 13363 (1998).
17. G. S. Jackson, J. Collinge, *Mol. Pathol.* **54**, 393 (2001).
18. T. Sklaviadis, R. Dreyer, L. Manuelidis, *Virus Res.* **3**, 241 (1992).
19. L. Manuelidis, T. Sklaviadis, A. Akowitz, W. Fritch, *Proc. Natl. Acad. Sci. U.S.A.* **92**, 5124 (1995).
20. A. Barrett, *Curr. Top. Microbiol. Immunol.* **128**, 55 (1986).
21. J. Wu *et al.*, *World J. Gastroenterol.* **11**, 1658 (2005).
22. P. M. Waterhouse, M. B. Wang, T. Lough, *Nature* **411**, 834 (2001).
23. L. Manuelidis, in *Transmissible Subacute Spongiform Encephalopathies: Prion Diseases*, L. Court, B. Dodet, Eds. (Elsevier, Paris, 1966), pp. 375–387.
24. L. Manuelidis *et al.*, unpublished data.
25. L. Linsell *et al.*, *Neurology* **63**, 2077 (2004).
26. P. Smith, S. Cousens, J. d'Huillard Aignaux, H. Ward, R. Will, *Curr. Top. Microbiol. Immunol.* **284**, 161 (2004).

27. Supported by NIH grant NS12674, U.S. Department of Defense grant DAMD-17-03-1-0360, and a grant from the Ministry of Health, Labor and Welfare, Japan.

Supporting Online Material

www.sciencemag.org/cgi/content/full/310/5747/493/DC1
Materials and Methods

29 July 2005; accepted 21 September 2005
10.1126/science.1118155

Interlinked Fast and Slow Positive Feedback Loops Drive Reliable Cell Decisions

Onn Brandman,[1,2]* James E. Ferrell Jr.,[1] Rong Li,[2,3,4] Tobias Meyer[1,2]

Positive feedback is a ubiquitous signal transduction motif that allows systems to convert graded inputs into decisive, all-or-none outputs. Here we investigate why the positive feedback switches that regulate polarization of budding yeast, calcium signaling, *Xenopus* oocyte maturation, and various other processes use multiple interlinked loops rather than single positive feedback loops. Mathematical simulations revealed that linking fast and slow positive feedback loops creates a "dual-time" switch that is both rapidly inducible and resistant to noise in the upstream signaling system.

Studies in many biological systems have identified positive feedback as the key regulatory motif in the creation of switches with all-or-none "digital" output characteristics (*1*). Although a single positive feedback loop (*A* activates *B* and *B* activates *A*) or the equivalent double-negative feedback loop (*A* inhibits *B* and *B* inhibits *A*) can, under the proper circumstances, generate a bistable all-or-none switch (*1*–*5*), it is intriguing that many biological systems have not only a single but multiple positive feedback loops (Table 1). Three examples of positive feedback systems are shown in more detail in Fig. 1.

[1]Department of Molecular Pharmacology, Stanford University School of Medicine, Stanford, CA, 94305, USA. [2]Physiology Course 2004, Marine Biological Laboratory, Woods Hole, MA 02543, USA. [3]Department of Cell Biology, Harvard Medical School, Boston, MA 02115, USA. [4]The Stowers Institute for Medical Research, Kansas City, MO 64110, USA.

*To whom correspondence should be addressed. E-mail: onn@stanford.edu

Polarization in budding yeast depends on two positive feedback loops, a rapid loop involving activity cycling of the small guanosine triphosphatase Cdc42 and a slower loop that may involve actin-mediated transport of Cdc42 (Fig. 1A) (*6*). In many cell types, the induction of prolonged Ca^{2+} signals involves initial rapid positive feedback loops centered on Ca^{2+} release mediated by inositol 1,4,5-trisphosphate (IP3) combined with a much slower loop that induces Ca^{2+} influx mediated by the depletion of Ca^{2+} stores (*7*, *8*) (Fig. 1B). *Xenopus* oocytes respond to maturation-inducing stimuli by activating a rapid phosphorylation/dephosphorylation–mediated positive feedback loop (between Cdc2, Myt1, and Cdc25) and a slower translational positive feedback loop [between Cdc2 and the the mitogen-activated protein kinase (MAPK or ERK) cascade, which includes Mos, MEK (MAPK kinase), and p42] (Fig. 1C).

The presence of multiple interlinked positive loops raises the question of the performance

Table 1. Examples of interlinked positive feedback loops in biological regulation.

System	Positive feedback loops	References
Mitotic trigger	Cdc2 → Cdc25 → Cdc2 Cdc2 -| Wee1 -| Cdc2 Cdc2 -| Myt1 -| Cdc2	(*12*, *13*)
p53 regulation	p53 → PTEN -| Akt → Mdm-2 -| p53 p53 → p21 -| CDK2 -| Rb -|Mdm-2 -| p53	(*14*)
Xenopus oocyte maturation	Cdc2 → Mos → Cdc2 Cdc2 → Cdc25 → Cdc2 Cdc2 → Myt1 → Cdc2	(*11*)
Budding yeast traversal of START	Cdc28 → Cln transcription → Cdc28 Cdc28 -| Sic1 -| Cdc28	(*15*)
Budding yeast polarization	Cdc42 → Cdc24 → Cdc42 Cdc42 → actin → Cdc42	(*6*, *16*, *17*)
Eukaryotic chemotaxis	PIP_3 → Rac/Cdc42 → PIP_3 PIP_3 → Rac/Cdc42 → actin → PIP_3	(*18*)
Muscle cell fate specification	MyoD → MyoD Myogenin → myogenin MyoD → CDO → MyoD MyoD → Akt2 → MyoD	(*19*–*21*)
B cell fate specification	IL-7 → EBF → IL-7 EBF -| Notch-1 -|E2A → EBF → Pax-5 -| Notch-1 -| E2A→ EBF	(*22*, *23*)
Notch/delta signaling	Notch (cell A) -| Delta (cell A) -| Notch (cell A) Notch (cell A) -| Delta (cell A) → Notch (cell B) -| Delta (cell B) → Notch (cell A)	(*24*)
EGF receptor signaling	EGFR -| PTP -| EGFR Sos → Ras → Sos ERK2 → arachidonic acid → ERK2 EGFR → sheddases → EGFR	(*25*–*28*)
S. cerevisiae galactose regulation	Gal2 → galactose -| Gal80 -| Gal2 Gal3 -| Gal80 -| Gal3	(*29*)
Blood clotting	thrombin → Xa:Va → thrombin XIIa → XIIa IXa:VIIIa → Xa → IXa:VIIIa	(*30*)
Platelet activation	activation → ADP secretion → activation activation → 5-HT secretion → activation activation → TxA_2 secretion → activation activation → aggregation → activation	(*31*)
Ca^{2+} spikes/oscillations	Ca^{2+}_{cyt} → PLC → IP_3 → Ca^{2+}_{cyt} Ca^{2+}_{cyt} → IP_3R → Ca^{2+}_{cyt} Ca^{2+}_{cyt} → IP_3R -| Ca^{2+}_{ER} -| SOC → Ca^{2+}_{cyt}	(*7*, *8*)

ADP, adenosine 5′-diphosphate; CDK, cyclin-dependent kinase; cyt, cytochrome; CDO, a component of a cell surface receptor; EGFR, epidermal growth factor receptor; ER, endoplasmic reticulum; 5-HT, serotonin (5-hydroxytryptamine); IL-7, interleukin-7; IP_3R, inositol 1,4,5-trisphosphate receptor; PIP_3, phosphatidylinositol 3,4,5-trisphosphate; PLC, phospholipase C; PTEN, phosphatase and tensin homolog deleted on chromosome 10; PTP, protein tyrosine phosphatase; *S. cerevisiae*, *Saccharomyces cerevisiae*; TxA_2, thromboxane A_2.

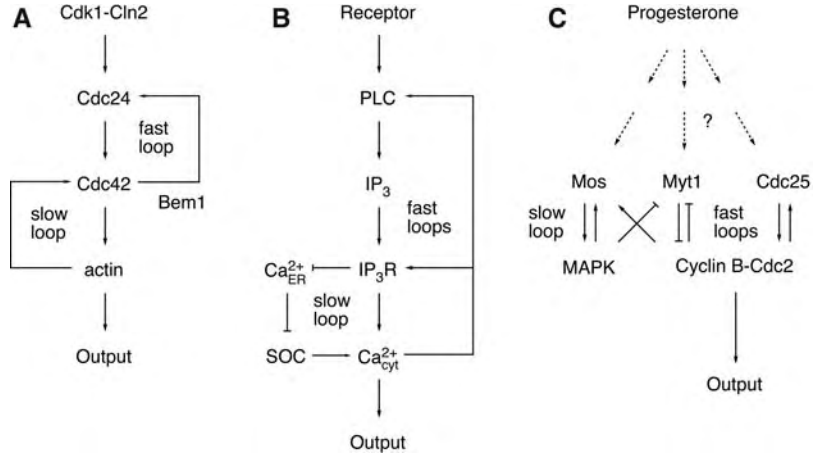

Fig. 1. Schematic views of positive feedback loops in three systems. (**A**) Establishment of polarity in budding yeast. (**B**) Mammalian calcium signal transduction. (**C**) *Xenopus* oocyte maturation.

advantage of the multiple-loop design. One clue is provided by recent studies of budding yeast polarization. When the slow positive feedback loop is selectively compromised by treatment with the actin-depolymerizing agent latrunculin, the result is rapid but unstable cell polarization (*6*). In contrast, cells lacking a functional fast loop (by deletion of Bem1) form stable poles, but with reduced speed (*6*). These experimental observations led us to hypothesize that the slow positive feedback loop is crucial for the stability of the polarized "on" state, whereas the fast loop is critical for the speed of the transition between the unpolarized "off" state and polarized on state.

To test this hypothesis computationally, we created models of positive feedback switches containing either a single positive feedback loop (Fig. 2A) or two interlinked loops (Fig. 2B). For the single-loop switch, we assumed either fast or slow kinetics for the activation and inactivation of loop component *A*. For the dual-loop switch, we assumed either fast kinetics for both the *A* and *B* loops, slow kinetics for both loops, or fast kinetics for the *A* loop and slow for the *B* loop (*9*).

Each model switch responded to a noise-free stimulus (Fig. 2, C to G, left) and a noisy stimulus (Fig. 2, C to G, right) as shown. As expected, the single-slow-loop switch turned on and off slowly and filtered out noise (Fig. 2C). Adding a second slow loop produced a higher basal activity in the off state, a quicker switch from off to on, and a slower switch from on to off (Fig. 2D). The behavior of the two-slow-loop switch was exactly equivalent to that of a single-loop switch in which the concentration of *B* was doubled. Thus, adding a second loop with identical kinetic constants provides a back-up in the event of gene deletion, but does not otherwise alter the behavior of the system beyond what could be achieved with a single loop.

The single-fast-loop switch turned on and off rapidly and was highly susceptible to noise in both the off and on states (Fig. 2E), and adding a second fast loop quickened the transition from off to on and delayed the transition from on to off (Fig. 2F). Thus, the fast-loop switch achieved more rapid responses, but at the cost of increased noise.

In contrast, the system in which a slow and a fast positive feedback loop are linked together introduces marked advantages over single-loop systems, as well as dual-loop systems with the same time constant. In this "dual-time" switch, the output turned on rapidly, as a consequence of the kinetic properties of the fast loop, and turned off slowly as a consequence of the kinetics of the slow loop (Fig. 2G). This allows for independent tuning of the activation and deactivation times. More important, although the dual-time switch exhibited high noise sensitivity when in the off state, as a result of the rapid responses of its fast loop, it became resistant to noise once it settled in its on state as a result of the properties of its slow loop. Thus,

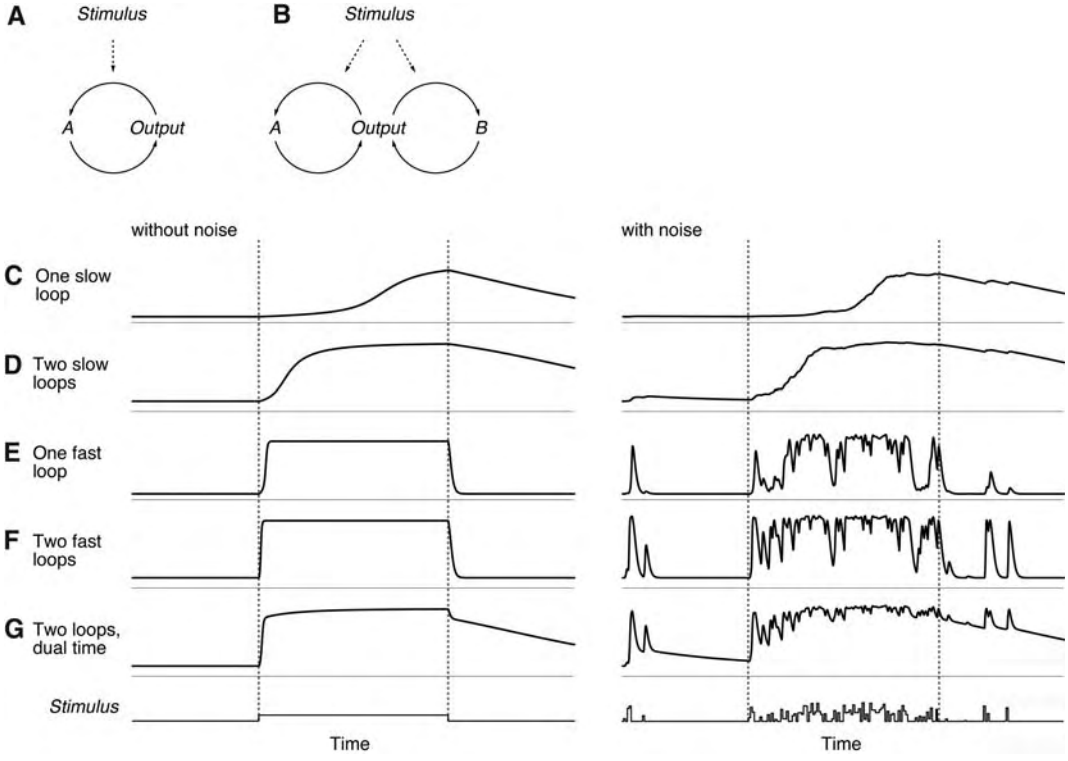

Fig. 2. Calculated responses of single and dual positive feedback loop switches to stimuli. (**A**) A one-loop switch. (**B**) A two-loop switch. (**C** to **G**) Feedback loop output (*y* axis) as a function of time (*x* axis) for single-loop and two-loop switches. (**C**) One slow loop. (**D**) Two slow loops. (**E**) One fast loop. (**F**) Two fast loops. (**G**) One slow loop and one fast loop. The curves on the left assume a noise-free stimulus; the curves on the right assume a noisy stimulus.

the dual-time switch provides the ability to transit rapidly from the off state to the on state together with robust stability of the on state (*10*).

These computational studies help understand the yeast phenotypes described above and provide a rationale for the existence of dual-time positive feedback systems in Ca^{2+} signaling, oocyte maturation, and other biological systems. In the case of Ca^{2+} signaling, the dual-time system enables rapid Ca^{2+} responses from IP3-induced Ca^{2+} release, while also enabling long-term robust Ca^{2+} signals once the store-operated Ca^{2+} influx is triggered. Although weak stimuli or noise have been shown to trigger IP3-mediated Ca^{2+} spikes, more persistent stimuli are needed to induce Ca^{2+} influx and prolonged Ca^{2+} responses (*7*). These long-term Ca^{2+} signals are required for T-cell activation and differentiation and many other cellular processes (*7*, *8*). *Xenopus* oocyte maturation includes a period termed interkinesis, during which Cdc2 becomes partially deactivated (*11*). We conjecture that the slow positive feedback loop helps prevent a transition to the off state during this critical interkinesis period.

Our study suggests that many biological systems have evolved interlinked slow and fast positive feedback loops to create reliable all-or-none switches. These dual-time switches have separately adjustable activation and deactivation times. They combine the important features of a rapid response to stimuli and a marked resistance to noise in the upstream signaling pathway.

References and Notes

1. J. E. Ferrell Jr., W. Xiong, *Chaos* **11**, 227 (2001).
2. M. Laurent, N. Kellershohn, *Trends Biochem. Sci.* **24**, 418 (1999).
3. T. S. Gardner, C. R. Cantor, J. J. Collins, *Nature* **403**, 339 (2000).
4. A. Becskei, B. Seraphin, L. Serrano, *EMBO J.* **20**, 2528 (2001).
5. F. J. Isaacs, J. Hasty, C. R. Cantor, J. J. Collins, *Proc. Natl. Acad. Sci. U.S.A.* **100**, 7714 (2003).
6. R. Wedlich-Soldner, S. C. Wai, T. Schmidt, R. Li, *J. Cell Biol.* **166**, 889 (2004).
7. M. J. Berridge, *Novartis Found. Symp.* **239**, 52 (2001).
8. R. S. Lewis, *Annu. Rev. Immunol.* **19**, 497 (2001).
9. The ordinary differential equations for the one- and two-loop positive feedback switches are

1) One loop

$$\frac{dOUT}{dt} = k_{out\_on} * A * (1 - OUT) - k_{out\_off} * OUT + k_{out\_min}$$

$$\frac{dA}{dt} = [stimulus * \frac{OUT^n}{OUT^n + ec_{50}^n} * (1 - A) - A + k_{min}] * \tau_A$$

2) Two loops

$$\frac{dOUT}{dt} = k_{out\_on} * (A + B) * (1 - OUT) - k_{out\_off} * OUT + k_{out\_min}$$

$$\frac{dA}{dt} = [stimulus * \frac{OUT^n}{OUT^n + ec_{50}^n} * (1 - A) - A + k_{min}] * \tau_A$$

$$\frac{dB}{dt} = [stimulus * \frac{OUT^n}{OUT^n + ec_{50}^n} * (1 - B) - B + k_{min}] * \tau_B$$

$k_{out\_on} = 2$, $k_{out\_off} = 0.3$, $k_{out\_min} = 0.001$, $k_{min} = 0.01$, $n = 3$, $ec_{50} = 0.35$. For a fast loop, $\tau = 0.5$. For a slow loop, $\tau = 0.008$. The equations were solved numerically with Matlab 7.0.
10. An interesting variation on this scheme can be envisioned by assuming that *A* and *B* have distinct effects on the output, and that both effects are required to activate the output. For example, *A* and *B* could phosphorylate different sites on the output protein, so that the protein is only activated when both sites are phosphorylated. The behavior of this dual-time AND switch is essentially the mirror image of the dual-time system shown in Fig. 2E: It turns on slowly, turns off rapidly, and acquires noise resistance when it has been in the off state for a period of time determined by the slow loop.
11. A. Abrieu, M. Doree, D. Fisher, *J. Cell Sci.* **114**, 257 (2001).
12. M. J. Solomon, M. Glotzer, T. H. Lee, M. Philippe, M. W. Kirschner, *Cell* **63**, 1013 (1990).
13. I. Hoffmann, P. R. Clarke, M. J. Marcote, E. Karsenti, G. Draetta, *EMBO J.* **12**, 53 (1993).
14. S. L. Harris, A. J. Levine, *Oncogene* **24**, 2899 (2005).
15. K. Levine, A. H. Tinkelenberg, F. Cross, *Prog. Cell Cycle Res.* **1**, 101 (1995).
16. A. C. Butty *et al.*, *EMBO J.* **21**, 1565 (2002).
17. R. Wedlich-Soldner, S. Altschuler, L. Wu, R. Li, *Science* **299**, 1231 (2003).
18. O. D. Weiner *et al.*, *Nat. Cell Biol.* **4**, 509 (2002).
19. M. J. Thayer *et al.*, *Cell* **58**, 241 (1989).
20. F. Cole, W. Zhang, A. Geyra, J. S. Kang, R. S. Krauss, *Dev. Cell* **7**, 843 (2004).
21. S. Kaneko *et al.*, *J. Biol. Chem.* **277**, 23230 (2002).
22. H. Singh, K. L. Medina, J. M. Pongubala, *Proc. Natl. Acad. Sci. U.S.A.* **102**, 4949 (2005).
23. K. L. Medina *et al.*, *Dev. Cell* **7**, 607 (2004).
24. H. Lodish *et al.*, *Molecular Cell Biology* (Freeman, New York, ed. 5, 2004).
25. A. R. Reynolds, C. Tischer, P. J. Verveer, O. Rocks, P. I. Bastiaens, *Nat. Cell Biol.* **5**, 447 (2003).
26. S. M. Margarit *et al.*, *Cell* **112**, 685 (2003).
27. U. S. Bhalla, P. T. Ram, R. Iyengar, *Science* **297**, 1018 (2002).
28. S. Y. Shvartsman *et al.*, *Am. J. Physiol. Cell Physiol.* **282**, C545 (2002).
29. M. Acar, A. Becskei, A. van Oudenaarden, *Nature* **435**, 228 (2005).
30. E. Beltrami, J. Jesty, *Proc. Natl. Acad. Sci. U.S.A.* **92**, 8744 (1995).
31. H. Holmsen, *Proc. Natl. Sci. Counc. Repub. China B* **15**, 147 (1991).

32. We thank R. Brandman, Y. Brandman, T. Galvez, R. S. Lewis, L. Milenkovic, D. Mochly-Rosen, M. P. Scott, P. M. Vitorino, and R. Wedlich-Soldner who provided helpful suggestions. This work was supported by an NSF predoctoral fellowship awarded to O.B., NIH grants GM46383 to J.E.F., GM057063 to R.L., and MH064801 and GM063702 to T.M.

20 April 2005; accepted 9 September 2005
10.1126/science.1113834

The Biochemical Architecture of an Ancient Adaptive Landscape

Mark Lunzer,[1] Stephen P. Miller,[1] Roderick Felsheim,[1,2] Antony M. Dean[1,3]*

Molecular evolution is moving from statistical descriptions of adaptive molecular changes toward predicting the fitness effects of mutations. Here, we characterize the fitness landscape of the six amino acids controlling coenzyme use in isopropylmalate dehydrogenase (IMDH). Although all natural IMDHs use nicotinamide adenine dinucleotide (NAD) as a coenzyme, they can be engineered to use nicotinamide adenine dinucleotide phosphate (NADP) instead. Intermediates between these two phenotypic extremes show that each amino acid contributes additively to enzyme function, with epistatic contributions confined to fitness. The genotype-phenotype-fitness map shows that NAD use is a global optimum.

The role of epistasis—interactions among mutations that produce nonadditive effects on phenotype and fitness—in evolution remains hotly debated (*1*–*8*). Although routinely detected in natural and in experimental populations (*4*, *9*, *10*), its presence need not imply the existence of multiple peaks in an adaptive landscape (*11*). Indeed, the question remains: Are adaptive landscapes rugged, or are they smooth?

Characterizing the adaptive landscape of an enzyme is conceptually simple. Mutations controlling a phenotype must be identified. Mutants of intermediate phenotype must be engineered so that the connections between genotype and phenotype (the genotype-phenotype map) can be explored. The fitness of each mutant must be determined so that the relationships between genotype and fitness (the genotype-fitness map) can be established. Finally, a model relating phenotype to fitness (the phenotype-fitness map) is needed to specify the mechanism of selection.

We characterized the adaptive landscape governing coenzyme use by isopropylmalate dehydrogenase (IMDH), an enzyme that catalyzes a step in the biosynthesis of leucine, an essential amino acid. All IMDHs use nicotinamide adenine dinucleotide (NAD) as a coenzyme, although some related isocitrate dehydrogenases (IDHs) lie at the other phenotypic extreme and use nicotinamide adenine dinucleotide phosphate (NADP) instead. Six amino acid residues critical to coenzyme use have been identified (*12*–*15*) (Fig. 1). Enzyme performance ($P = k_{cat}/K_m$) and preference (P^{NAD}/P^{NADP}—the number of NADs turned over for each NADP turned over when both coenzymes are present in equimolar concentrations) are phenotypes relevant to fitness (*16*). The fitnesses of engineered mutants are estimated using the *Escherichia coli* chemostat competition assay (*17*). Finally, the physiological basis of fitness is described using a simple model of metabolism.

[1]BioTechnology Institute, [2]Department of Entomology, [3]Department of Ecology, Evolution and Behavior, University of Minnesota, St. Paul, MN 55108, USA.

*To whom correspondence should be addressed. E-mail: adean@biosci.umn.edu

Protein engineering (*18*) was used to switch the coenzyme specificity of *E. coli* IMDH from NAD to NADP. Unlike most IMDHs, *E. coli* IMDH already has the Arg-341 found in all NADP-dependent IDHs. The remaining five replacements (Asp236Arg, Asp289Lys, Ile290Tyr, Ala296Val and Gly337Tyr) were introduced into the coenzyme-binding pocket of *E. coli* IMDH by site-directed mutagenesis. Specificity was changed by a factor of 20,000, from a 100-fold preference for NAD ($P^{NAD} = k_{cat}^{NAD}/K_m^{NAD} = 82 \times 10^3\ M^{-1}\ s^{-1}$ and $P^{NADP} = k_{cat}^{NADP}/K_m^{NADP} = 0.84 \times 10^3\ M^{-1}\ s^{-1}$) to a 200-fold preference for NADP ($P^{NAD} = 0.18 \times 10^3\ M^{-1}\ s^{-1}$ and $P^{NADP} = 37 \times 10^3\ M^{-1}\ s^{-1}$). The engineered "RKYVYR" enzyme is both as active and as specific toward NADP as the wild-type enzyme is toward NAD.

To characterize the genotype-phenotype map, we engineered various combinations of amino acids at the six sites (table S1) (*18*). The kinetic performances of 164 mutant enzymes toward NAD and NADP were estimated. Nested analyses of variance (NANOVA) (*19*) of $\log_e$-transformed performances and preferences show that a simple linear additive model of the form

$$\log_e(y) = m + \sum_{j=1}^{6} a_{i,j}, \mathrm{df} = 14 \quad (1)$$

explains most of the data (y is performance or preference, m is the sample mean and $a_{i,j}$ is the additive deviation caused by amino acid i at site j): $r^2 = 0.95$ for $\log_e(P^{NAD})$, $r^2 = 0.92$ for $\log_e(P^{NADP})$, and $r^2 = 0.97$ for $\log_e(P^{NADP}/P^{NAD})$. Performance and preference are dominated by additive effects (Table 1). There is no evidence for epistasis in these genotype-phenotype maps.

Statistical additivity implies thermodynamic additivity. Simple enzyme transition state theory (*16*) suggests

$$\Delta\Delta G^{\ddagger mut} = \sum_{j=1}^{6} \Delta\Delta G^{\ddagger}_{i.j} = RT \sum_{j=1}^{6} (a_{i.j} - a_{i.wt}) \quad (2)$$

where $\Delta\Delta G^{\ddagger mut} = \Delta G^{\ddagger wt} - \Delta G^{\ddagger mut}$ is the total difference in free energies between the enzyme transition states of the mutant (mut) and the wild type (wt), and $\Delta\Delta G^{\ddagger}_{i.j} = \Delta G^{\ddagger.wt}_{i} - \Delta G^{\ddagger.mut}_{i.j} = RT(a_{i.j} - a_{i.wt})$ represents the difference attributable to replacing a single wt amino acid at site j with an amino acid i. Thermodynamic additivity has been seen in a number of studies of protein folding (*20*), protein-protein interactions (*21*), and catalysis (*22*). The lack of epistasis in coenzyme performance by IMDH is typical of many molecular genotype-phenotype maps, although nonadditive effects arise in some (*23*–*25*).

No enzyme performs well with both coenzymes (Fig. 2A). Given thermodynamic additivity, the performances of each of the remaining 512 − 164 = 348 mutant intermediates can be predicted by summing the additive effects (Table 1). Again, the interior of the plot is

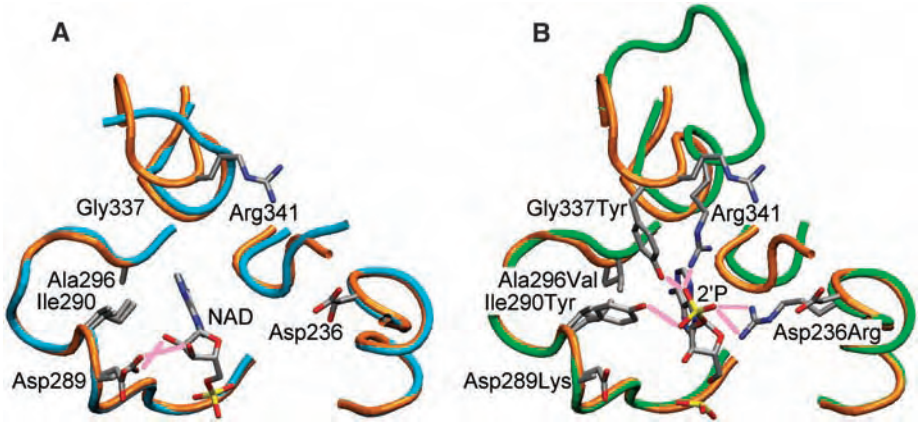

Fig. 1. Crystallographic structures identify amino acids determining coenzyme use. Only key residues are shown (gray, carbon; red, oxygen; blue, nitrogen; yellow phosphorus). (**A**) Structural alignment of *E. coli* IMDH (*13*) (brown main-chain; labels designate the amino acid followed by the site number) and *Thermus thermophilus* IMDH (*14*) (blue main-chain) showing the double H-bond (pink lines) critical to NAD use. (**B**) Structural alignment of *E. coli* IMDH and *E. coli* IDH (green main-chain) with NADP bound (*15*) showing IDH residues (following the IMDH site number) H-bonding to the 2′-phosphate (2′P) of bound NADP (H-bonds from the disordered 289Lys not shown).

empty (Fig. 2B). Evidently, a performance trade-off restricts severely the possible phenotypes upon which selection can act.

The genotype-fitness map reveals strong epistasis in fitness. Ninety IMDH mutants, representing a stratified sample of kinetic performances, were recombined individually into the *leu* operon on the *E. coli* chromosome and their fitnesses relative to those of the wild type determined in chemostat competition (*17*, *18*). A NANOVA (*19*) (residues within sites) of fitness assuming only additive effects produced a poor fit ($r^2 = 0.85$). Interactions were not modeled because they required many more degrees of freedom than our NANOVA design permited. Eliminating "transitional" residues (table S1) (*18*) from the analysis allows pairwise interactions to be modeled. The resulting NANOVA included six significant pairwise interactions ($r^2 = 0.99$) and was a marked improvement over the strictly additive model ($r^2 = 0.87$). Hence, epistasis is present in the genotype-fitness map.

The phenotype-fitness map shows how epistasis, absent in the genotype-phenotype map, arises in the genotype-fitness map. Fitness is commonly a concave function of enzyme performance (*26*, *27*). Assume fitness (w) is a hyperbolic function of intracellular IMDH performance toward isopropylmalate (V_{max}/K_m^{ipm})

$$w = w_{max}\frac{V_{max}}{K_m^{ipm}}\Big/\left(K + \frac{V_{max}}{K_m^{ipm}}\right) \qquad (3)$$

where w_{max} is maximum fitness when $V_{max}/K_m^{ipm} \rightarrow \infty$, K is the performance necessary to produce $w_{max}/2$, V_{max} is the maximum intracellular rate when isopropylmalate is saturating, and K_m^{ipm} is the concentration of isopropylmalate necessary to produce $V_{max}/2$. The concave nature of Eq. 3 is typical of the nonlinear responses in metabolic flux to changes in enzyme activities that produce genetic dominance, phenotypic robustness, and epistasis at higher levels of biological organization (*28*, *29*). Epistasis in fitness arises because the same mutation producing the same proportional increase in activity in a wild type as in a mutant compromised by mutation will cause a smaller increase in fitness in the wild type (because $w \approx w_{max}$ when $V_{max}/K_m^{ipm} \gg K$) than it will in the mutant [because $w = (w_{max}/K)V_{max}/K_m^{ipm}$ when $V_{max}/K_m^{ipm} \ll K$].

Substituting a kinetic model describing the IMDH random bi-ter kinetic mechanism for V_{max}/K_m^{ipm} in Eq. 3 and collecting terms produces the phenotype-fitness map in terms of the coenzyme kinetics,

$$w = w_{max}\left(\frac{k_{cat}^{NAD}}{K_m^{NAD}} + \frac{k_{cat}^{NADP}}{K_m^{NADP}}R\right)\Big/ \left(A\left(1 + \frac{B}{K_m^{NAD}} + \frac{C}{K_m^{NADP}}\right) + \left(\frac{k_{cat}^{NAD}}{K_m^{NAD}} + \frac{k_{cat}^{NADP}}{K_m^{NADP}}R\right)\right) \qquad (4)$$

Table 1. Additive effects ($a_{i,j}$) of amino acid replacements on coenzyme use.

Site	Residue	Performance effects				Preference effect*	
		NAD	SE	NADP	SE	NAD-NADP	SE
236	Arg	–0.250	±0.039	0.735	±0.046	–0.985	±0.041
	Asp	0.250	±0.039	–0.735	±0.046	0.985	±0.041
289	Lys	–0.657	±0.060	1.547	±0.071	–2.204	±0.062
	Asp	0.850	±0.057	–0.722	±0.069	1.572	±0.062
	Asn†	–0.019	±0.059	0.506	±0.072	–0.509	±0.045
	Glu†	–0.183	±0.074	–1.332	±0.089	1.148	±0.079
290	Tyr	–0.680	±0.082	0.659	±0.092	–1.367	±0.102
	Ile	2.218	±0.078	0.255	±0.094	1.963	±0.083
	His†	–0.824	±0.099	0.684	±0.119	–1.508	±0.106
	Leu†	2.267	±0.076	1.058	±0.120	1.209	±0.109
	Phe†	–0.516	±0.099	–0.869	±0.119	0.353	±0.102
	Lys†	0.159‡	±0.109	0.911	±0.123	–0.729	±0.107
	Asn†	–1.981	±0.096	–1.713	±0.116	–0.268	±0.112
	Gln†	–0.633	±0.094	–1.039	±0.112	0.406	±0.109
296	Val	–0.672	±0.038	–0.577	±0.047	–0.095	±0.041
	Ala	0.672	±0.038	0.577	±0.047	0.095	±0.041
337	Tyr	–0.193	±0.094	0.058‡	±0.046	–0.139	±0.040
	Gly	0.193	±0.094	–0.058‡	±0.046	0.139	±0.040
341	Arg	0.291	±0.047	0.375	±0.058	–0.084‡	±0.050
	Ser	–0.291	±0.047	–0.375	±0.058	0.084‡	±0.050
	m	–0.095	±0.055	0.013	±0.065	–0.108	±0.056

*The preference effect is defined as $a_{wt,j} - a_{i,j}$. †Possible transitional replacements attributable to multiple base substitutions needed to exchange Asp for Lys at site 289 and Ile for Tyr at site 290. ‡Not significantly different from zero.

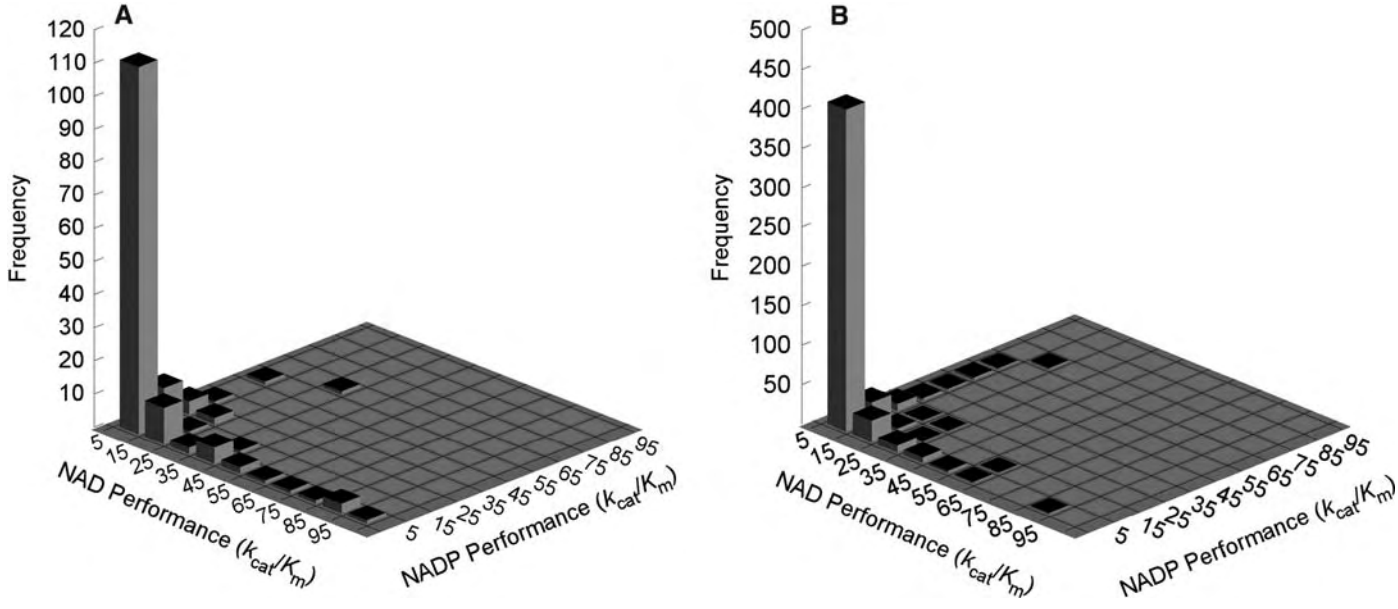

Fig. 2. Performances (10^3 $M^{-1}s^{-1}$) of engineered IMDH mutants toward NAD and NADP reveal a trade-off in enzyme function. (**A**) Distribution of performances for the 164 engineered enzymes constructed. (**B**) Distribution of performances for 512 genotypic intermediates predicted on the assumption of thermodynamic additivity. Symptomatic of a trade-off in performance, the interiors of both plots are devoid of mutants.

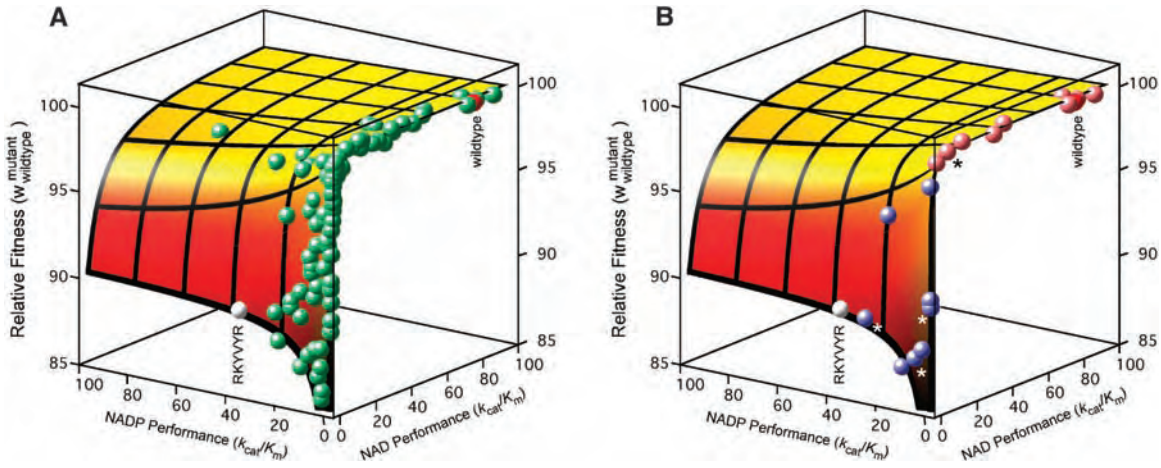

Fig. 3. The phenotype-fitness map of IMDH. (**A**) The fitnesses (green spheres of fitness radius $w = 0.5\% \approx 2$ SE) of 90 engineered mutants plotted against their coenzyme performances (10^3 $M^{-1}s^{-1}$). The fitted surface is the estimated phenotype-fitness map (Eq. 4). It reveals a single broad adaptive peak on which resides the NAD-specific wild-type enzyme (red sphere). NADP use is advantageous only in mutants with very poor NAD performance (e.g., the RKYVYR mutant, white sphere). (**B**) Escape from the lower NADP-use plateau to the higher NAD-use plateau is possible because some single amino acid replacements (blue spheres from the RKYVYR mutant, pink spheres from the wild type; asterisks denote fitness values predicted from kinetic data) produce sufficiently large effects on performance and fitness that the maladaptive valley near the origin is bypassed.

where A, B, C, D, and R are constants associated with kinetic terms and coenzyme pools unaffected by our mutations (*18*). Equation 4 is a hypothesis that describes fitness in terms of the kinetic parameters obtained for each mutant enzyme. It fits the data well—nonlinear regression yields $r^2 = 0.97$.

Noting that the $1/K_m^{NAD(P)}$ values are necessarily correlated with—and hence can be collapsed into—the $k_{cat}^{NAD(P)}/K_m^{NAD(P)}$ values allows the phenotype-fitness map to be visualized (Fig. 3A). IMDH fitness is maximized exclusively by high performance with, and high preference for, NAD (the wild type on the right fitness plateau). NADP use is suboptimal.

Product inhibition by NADPH lowers the fitness of NADP users. Most intracellular NADP is in the reduced form, NADPH, which has a 30-fold higher affinity for IMDH ($K_m^{NADP}/K_i^{NADPH} \approx 30$). Thermodynamic additivity ensures that mutations in the coenzyme-binding pocket that improve performance with NADP also increase affinity for NADPH (fig. S1) (*18*). Consequently, any benefit gained by improved performance with NADP is offset by intensified product inhibition by abundant NADPH. A similar correlation for NAD use does not generate a measurable cost because so little intracellular NAD is in the reduced NADH form ($B \ll C$, Eq. 4) (*18*).

The phenotype-fitness map has a single peak (the broad NAD-use plateau in Fig. 3A). In principle, the trade-off in performance (Fig. 2) could combine with mutations of small functional effect to force all paths from the NADP-dependent RKYVYR mutant to the NAD-dependent wild type through the maladaptive valley at the origin. The result would be two peaks on the genotype-fitness map, with the higher NAD-use plateau inaccessible from the lower NADP-specific allele.

The genotype-fitness map has just one adaptive peak. The fitnesses of all 512 mutant genotypes were predicted using Eq. 4 with enzyme performances calculated assuming thermodynamic additivity (Table 1 and Fig. 2B). A fitter genotype was mutationally accessible to every genotype—except for the NAD-dependent wild type, which was predicted to be fittest. Only one peak is expected because some mutations have sufficiently large phenotypic effects that the maladaptive valley at the origin of the phenotype-fitness map is bypassed (Fig. 3B).

Defining all mutational connectivities between the genotypes on the phenotype-fitness map completes the IMDH adaptive landscape. With its single peak, the landscape is far less rugged than those envisioned by Wright (*1*). With epistasis consigned to a minor role, this landscape lies closer to Fisher's conception (*2*) than to any other. Ironically, the landscape might have been more rugged, with two adaptive peaks, had another of Fisher's assumptions, that of many mutations each of small effect (*2*), proven correct.

Coenzyme use by IMDH is likely representative of a large class of adaptive landscapes in which thermodynamic additivity in molecular function (Table 1) (*20*–*22*) combines with concave fitness functions at the organismal level (Eq. 3) (*26*, *27*). Nevertheless, landscapes are likely to be more rugged whenever epistasis in genotype-phenotype maps (*23*–*25*) combines with complex phenotype-fitness maps (*26*).

Our landscape provides a mechanism sufficient to explain why all IMDHs use NAD. Conservation of this phenotype implies that we have characterized an ancient adaptive landscape—unchanged in all lineages, in all habitats, since the last common ancestor. Such ancient landscapes can explain adaptive processes at the very dawn of life's diversity.

References and Notes

1. S. Wright, in *Proceedings of the Sixth International Congress of Genetics*, D. F. Jones, Ed. (Brooklyn Botanic Garden, Menasha, WI, 1932), pp. 356–366.
2. R. A. Fisher, *The Genetical Theory of Natural Selection* (Clarendon, Oxford, 1930).
3. J. Maynard Smith, *Nature* **225**, 563 (1970).
4. M. C. Whitlock, P. C. Phyllips, F. B.-G. Moore, J. Tonsor, *Annu. Rev. Ecol. Syst.* **26**, 601 (1995).
5. C. L. Burch, L. Chao, *Nature* **406**, 625 (2000).
6. J. A. Coyne, N. H. Barton, M. Turelli, *Evol. Int. J. Org. Evol.* **51**, 643 (1997).
7. M. J. Wade, C. J. Goodnight, *Evol. Int. J. Org. Evol.* **52**, 1537 (1998).
8. D. M. Weinreich, L. Chao, *Evol. Int. J. Org. Evol.* **59**, 1175 (2005).
9. S. J. Schrag, V. Perrot, B. R. Levin, *Proc. R. Soc. Lond. B. Biol. Sci.* **264**, 1287 (1997).
10. S. Maisnier-Patin, O. G. Berg, L. Lijas, D. I. Andersson, *Mol. Microbiol.* **46**, 355 (2002).
11. D. M. Weinreich, R. A. Watson, L. Chao, *Evol. Int. J. Org. Evol.* **59**, 1165 (2005).
12. G. Zhu, G. B. Golding, A. M. Dean, *Science* **307**, 1279 (2005).
13. G. Wallon *et al.*, *J. Mol. Biol.* **266**, 1016 (1997).
14. J. H. Hurley, A. M. Dean, *Structure* **2**, 1007 (1984).
15. J. H. Hurley, A. M. Dean, D. E. Koshland Jr., R. M. Stroud, *Biochemistry* **30**, 8671 (1991).
16. A. Fersht, *Structure and Mechanism in Protein Science: A Guide to Enzyme Catalysis and Protein Folding* (Freeman, New York, 1999).
17. M. Lunzer, A. Natarajan, D. E. Dykhuizen, A. M. Dean, *Genetics* **162**, 485 (2002).
18. Materials and methods are available as supporting material on *Science* Online.
19. R. R. Sokal, F. J. Rohlf, *Biometry* (Freeman, New York, ed. 3, 1995).
20. J. A. Wells, *Biochemistry* **29**, 8509 (1990).
21. W. S. Sandberg, T. C. Terwilliger, *Proc. Natl. Acad. Sci. U.S.A.* **90**, 8367 (1993).
22. T. Aita, M. Iwakura, Y. Husimi, *Protein Eng.* **14**, 633 (2001).
23. M. A. Qasim *et al.*, *Biochemistry* **42**, 6460 (2003).
24. X. Wang, G. Minasov, B. K. Shoichet, *J. Mol. Biol.* **320**, 85 (2002).
25. M. A. DePristo, D. M. Weinreich, D. L. Hartl, *Nat. Rev. Genet.* **6**, 678 (2005).
26. D. L. Hartl, D. E. Dykhuizen, A. M. Dean, *Genetics* **111**, 655 (1985).
27. A. M. Dean, *Genetics* **139**, 19 (1995).
28. H. Kacser, J. Burns, *Genetics* **97**, 639 (1981).
29. U. Alon, M. G. Surette, N. Barkai, S. Leibler, *Nature* **397**, 168 (1999).

30. We thank B. Kerr, L. Merlo and four anonymous reviewers for constructive criticism of the manuscript. Supported by NIH grant GM060611 (A.M.D.).

Supporting Online Material

www.sciencemag.org/cgi/content/full/310/5747/499/DC1
SOM Text
Materials and Methods
Figs. S1 and S2
Table S1
References and Notes

2 June 2005; accepted 15 September 2005
10.1126/science.1115649

Assortative Mating as a Mechanism for Rapid Evolution of a Migratory Divide

Stuart Bearhop,[1]* Wolfgang Fiedler,[2] Robert W. Furness,[3] Stephen C. Votier,[5] Susan Waldron,[4] Jason Newton,[6] Gabriel J. Bowen,[7] Peter Berthold,[2] Keith Farnsworth[1]

There have been numerous recent observations of changes in the behavior and dynamics of migratory bird populations, but the plasticity of the migratory trait and our inability to track small animals over large distances have hindered investigation of the mechanisms behind migratory change. We used habitat-specific stable isotope signatures to show that recently evolved allopatric wintering populations of European blackcaps *Sylvia atricapilla* pair assortatively on their sympatric breeding grounds. Birds wintering further north also produce larger clutches and fledge more young. These findings describe an important process in the evolution of migratory divides, new migration routes, and wintering quarters. Temporal segregation of breeding is a way in which subpopulations of vertebrates may become isolated in sympatry.

There have been numerous observations of changes in the behavior and dynamics of migratory bird populations (*1*–*7*). Migration is naturally a plastic trait, and tracking migratory birds is problematic because of the distances and areas involved (*2*, *7*). Thus it has proved almost impossible to investigate the mechanisms behind, and the consequences of, migratory change. However, the recent formation of a migratory divide in a breeding population of European passerines (*1*), together with developments in stable isotope techniques, mean that we can now gain insights into these processes.

Fifty years ago, the blackcap *Sylvia atricapilla* was considered a summer visitor to northern Europe and the British Isles. However, an increasing number of birds began overwintering in Britain and Ireland, in numbers growing from a few individuals in the early 1960s to the point where a recent survey of birdwatchers found that 31% of their gardens had blackcaps visiting bird tables from October 2003 to March 2004 (*8*). Work in the early 1990s showed that the birds overwintering in Britain and Ireland actually bred in south central Europe and that this newly evolved migratory behavior had a genetic basis (*1*, *9*). The normal wintering areas associated with blackcaps breeding in south central Europe (and therefore the ancestral wintering areas for the British and Irish birds) are southern Iberia and North Africa. The new wintering area is disjunct from the original, and birds wintering in Britain and Ireland display a completely different migratory orientation (*1*).

Berthold *et al*. (*1*) argued that the rate of increase in the wintering population suggests that birds wintering in Britain and Ireland gain some fitness benefits by adopting this strategy. They also suggested that because the critical photoperiods that trigger migratory urges and the onset of gonadal development are reached around 10 days earlier at the more northerly wintering latitudes, assortative mating among early arrivals may be an important factor driving the increases in the British and Irish wintering populations (*1*, *2*).

Stable hydrogen isotope ratios {$\delta^2H = ([^2H/^1H_{sample} \div {}^2H/^1H_{reference}] - 1) \times 1000$} and stable carbon isotope ratios ($\delta^{13}C$) in the tissues of migrant birds can be used to infer their breeding or wintering origins (*4*, *10*–*12*). Given the patterns of δ^2H in European rainfall (Fig. 1) and those measured in the feathers of several bird species (*13*), we hypothesized that measurements of δ^2H in tissues grown in the two wintering areas (Britain and Ireland or Iberia) may be sufficiently distinct isotopically to infer the wintering origins of blackcaps in the breeding grounds. We measured δ^2H (*14*–*16*) in proximal sections of claw tips (most recently synthesized) from wintering blackcaps in the two wintering areas (Britain and Ireland or Iberia), as well as from resident birds from Britain and Ireland (blue tits *Parus*

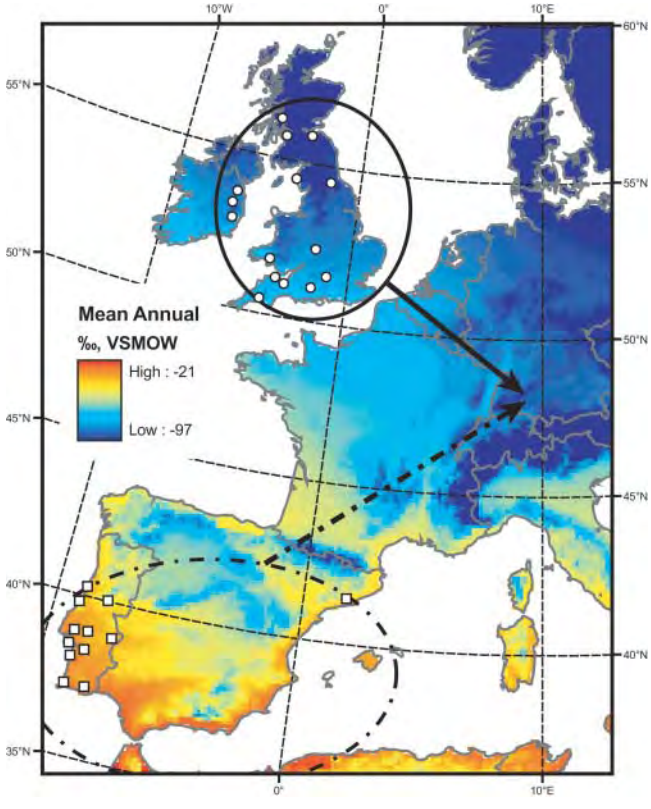

Fig. 1. Mean annual δ^2H in Western European rainfall and locations of blackcap winter sampling sites (white circles and squares). Map values were derived using a detrended interpolation model (*26*) and the data of the Global Network for Isotopes in Precipitation (*27*). A clear separation of δ^2H values over northern (British Isles) and southern (Iberia) blackcap wintering regions provides the basis for distinguishing the wintering area of birds sampled at summer breeding grounds. The international standard for δ^2H is Vienna standard mean ocean water (VSMOW). δ^2H values at more northerly latitudes (including the British Isles) are considerably lower than those in the south. Ellipses indicate the approximate wintering ranges of migratory blackcaps from the German breeding areas in Britain and Ireland (solid circle) and Spain and Portugal (dashed circle). Although blackcaps do occur in France during the winter, they are not thought to come from the central European breeding population. The arrows represent approximate spring migration directions.

[1]School of Biology and Biochemistry, Medical Biological Centre, Lisburn Road, Queen's University Belfast, Belfast BT6 7BL, UK. [2]Max Planck Institute for Ornithology, Vogelwarte Radolfzell, Schlossallee 2, D-78315 Radolfzell, Germany. [3]Institute of Biomedical and Life Sciences, Graham Kerr Building; [4]Centre for Geosciences, Department of Geography and Geomatics; University of Glasgow, Glasgow G12 8QQ, UK. [5]Department of Biological Sciences, University of Plymouth, Drake Circus, Plymouth PL4 8AA, UK. [6]Life Sciences Community Stable Isotope Facility, Scottish Universities Environmental Research Centre, East Kilbride, Glasgow G75 0QF, UK. [7]Department of Biology, University of Utah, 257 South 1400 East, Salt Lake City, UT 84112, USA.

*To whom correspondence should be addressed. E-mail: s.bearhop@qub.ac.uk

caeruleus and great tits *P. major*) and from resident birds from Portugal and Spain (Sardinian warblers *S. melanocaphala*) to provide two independent measures of over-winter isotope signatures.

Having sampled birds at multiple sites (Fig. 1) over two winters (December to March 2001–2002 and 2002–2003), we found that the δ^2H values measured in the claws of residents from Britain and Ireland were significantly lower than those in resident birds from Portugal and Spain (Fig. 2A). δ^2H signatures in the claws of overwintering blackcaps showed a similar pattern (Fig. 2B), with northerly wintering blackcaps having lower δ^2H signatures than those from much further south (*14*). δ^2H signatures in the tissues of birds are primarily a function of the signature in local rainfall (assimilated through the diet), with little or no additional species-level effects (*13*), and the patterns in both wintering blackcaps and residents correspond to those in precipitation (Figs. 1 and 2). Indeed, there was almost no overlap in values (Fig. 2A) among residents, meaning that this isotope ratio provided an excellent marker for discriminating between birds from these two regions (*14*). Because claws are metabolically inert and grow very slowly (*17*), measurement of δ^2H in the oldest claw material (the distal portion of the claw tip) collected from birds soon after they return to the breeding grounds (*17*) should allow us to infer the relative wintering latitudes of individuals.

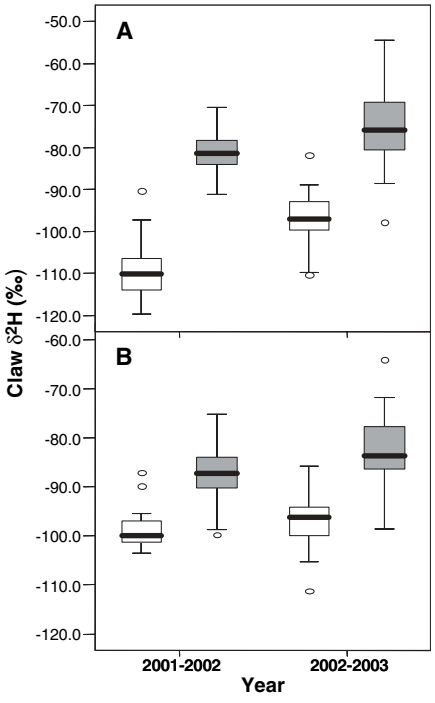

Fig. 2. Box plots (median, interquartile ranges, and outliers) for claws of birds captured during the winters of 2001–2002 and 2002–2003 at sites throughout Portugal (solid boxes) and the British Isles (open boxes). Data for resident birds are shown in (A) and for blackcaps in (B). The results of general linear models (GLMs) in which claw δ^2H was the dependent variable, with year and status [four levels: Portuguese resident (n = 63 birds), Portuguese blackcap (n = 120), British Isles resident (n = 43), and British Isles blackcap (n = 42)] as factors, demonstrated that there was significant annual variation (residents only: $F_{1,264}$ = 52.6, $P < 0.001$). This model was well supported (adjusted r^2 = 0.63); however, most of the variation is explained by status ($F_{3,264}$ = 147.4, $P < 0.001$). (**A**) Scheffe tests indicated highly significant differences between the signatures of resident birds from Britain and Ireland and those in Portugal [mean difference = –23 per mil (‰), $P < 0.001$]. (**B**) Scheffe tests also demonstrated that δ^2H signatures in the claws of wintering blackcaps differ significantly from those of residents in the same country in 2001–2002 (Portugal mean difference –5.4‰, P = 0.002; Britain and Ireland mean difference –6.0‰, P = 0.001), This is probably due to a small amount of the claw sample being synthesized away from the wintering areas. However, the difference between blackcaps wintering in either region was over double this (mean difference –12.7‰, $P < 0.001$).

During the summers of 2002 and 2003, breeding blackcaps were captured at eight sites in southern Germany and Austria (*14*). Birds were caught as soon as possible after establishment of their breeding territories. Where possible, both birds of a pair were captured, and in all cases the subsequent breeding attempt was followed. We found a highly significant relation between δ^2H signatures in the claws of males and those in the females they were paired with (Fig. 3). To provide a direct estimate of the incidence of assortative mating, wintering area–specific reciprocal-normal probability density functions were modeled by smoothing the empirical distributions from winter populations, and these were used to assign a probability of origin to each breeding bird (*14*). We found that observed values for assortative pairings were significantly higher than expected (χ^2 = 40.1, $P \ll 0.001$, Yates correction for 1 degree of freedom applied). Birds were 2.5 times more likely to pair assortatively than randomly (*14*), with "relative risks" for assortative pairing being 2.63 [95% confidence interval (CI) 1.3 to 28.5] for Iberian pairs and 2.63 (95% CI 1.2 to 5.8) for British and Irish pairs. This provides the strongest evidence yet for assortative mating (*1*, *9*).

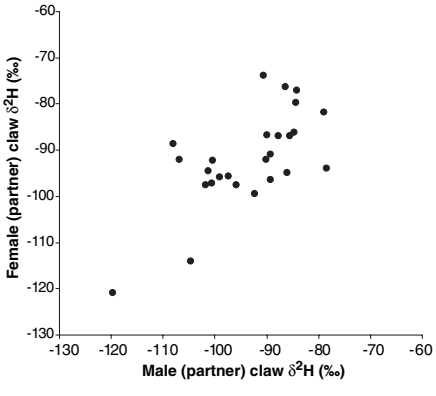

Fig. 3. There is a highly significant relation between δ^2H signatures in the claws of male blackcaps and in those of the female they are paired with (GLM: $F_{1,30}$ = 28.719, $P < 0.001$, r^2 = 0.5, year NS). This relation remains significant even when the two points with the lowest y values are ignored ($F_{1,28}$ =12.2, P = 0.002, r^2 = 0.3).

In 2003, the time of arrival on the breeding grounds was estimated for a subsample of blackcap males, and this was positively correlated with relative wintering latitude inferred from claw δ^2H signatures (Fig. 4), indicating that British and Irish males tend to arrive earlier than their southern European counterparts (Fig. 4). This is consistent with the hypothesis that earlier onset of the critical photoperiods required to stimulate migratory restlessness and gonadal development at higher wintering latitudes drives assortative mating with respect to wintering area (*1*, *2*). Assortative mating in this blackcap population could be further favored by strong selection against the offspring of hybrid pairings, because they inherit migration directions and distances intermediate to those of their parents, which would lead them on flights that would cross out over the Bay of Biscay: routes that tend not to be observed in orientation experiments with adults (*1*, *9*).

Finally, we investigated whether we could detect any potential fitness benefits associated with the new migration route. We found that females paired with males having lower δ^2H signatures, indicating higher wintering latitudes, produced significantly larger clutches [multiple logistic regression: Wald = 7.02, P = 0.008, egg-laying date not significant (NS), n = 38 males] (*14*). These results seem likely to be a consequence of male territory quality. Because differences in arrival times (Fig. 4) mean that males from more northerly wintering areas have more opportunity to settle in high-quality territories, the effect could arise in one of two ways: First, females on high-quality territories may enhance their body condition because of better foraging opportunities. It has been noted in a number of territorial passerine species that one of the most important aspects of territory selection is food availability (*18*), and provisioning experiments have shown that females can respond to high levels of food availability by producing larger clutches (*19*). Second, high-quality females may choose to settle in high-quality territories. Although there are studies demonstrating that male territory quality can influence clutch size (*18*), it is often extremely difficult to distinguish the effect of intrinsic female quality from the extrinsic quality of the territory she has selected (*18*).

We also found that females with lower δ^2H signatures, (indicating more northerly wintering areas) were more likely to have a success-

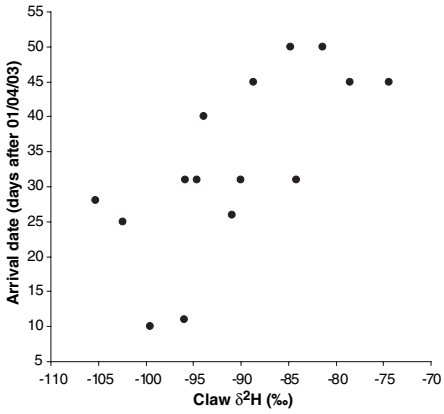

Fig. 4. There is a significant relation between estimated arrival dates (in 2003 only) of males and the δ^2H signatures in their claws ($F_{1,14}$ = 11.2, P = 0.005, r^2 = 0.44), suggesting that birds from further north arrive earlier. Three birds that were first detected more than 60 days after the first of April were excluded from these analyses because we could not be certain that these observations represented their first breeding attempt.

ful breeding attempt than those from further south (multiple logistic regression: Wald = 5.88, P = 0.015, clutch size and lay date NS, n = 48 females) (*14*). Although incubation and brood-rearing duties are shared, this finding could also be an effect of female body condition or intrinsic quality.

There are several other ways in which birds wintering at higher latitudes may benefit over southern conspecifics. Blackcaps breeding in Central Europe that migrate to the Iberian Peninsula have much further to travel than those wintering in Britain and Ireland. Thus, birds that come from the northern wintering areas may have more resources to devote to their reproductive attempt (*1*), which can enhance offspring viability (*20*, *21*). Changes in urbanization patterns in Britain and Ireland have led to good feeding opportunities for several bird species in the form of garden feeders and planting of exotic plants that fruit year round (*1*). Although blackcaps do use these food resources heavily during winter months, their impact on migratory condition is yet to be quantified. It has also been suggested that the harsher conditions experienced by blackcaps at high wintering latitudes (when compared to Iberia) may make them better able to survive early-season conditions on the breeding grounds (*2*).

It is becoming increasingly clear that events outside of the breeding season have major impacts on the fitness of migratory birds (*7*, *12*, *22*), and our results provide further evidence of this. However, in contrast to other studies which do not distinguish among the roles of genetic variability or phenotypic plasticity, our results are primarily a consequence of a genetically controlled change in behavior (*1*). In addition, this blackcap population provides a rare example of assortative mating being driven by changes in the timing of breeding, and the stable isotope techniques used here are probably the only way in which this could be estimated at this point in time.

Speciation through temporal segregation of breeding populations has been proposed as a mechanism for differences in Madeiran storm petrel *Oceanodroma castro* populations (*23*). Although we have no evidence for morphometric or genetic differences between the two types of migratory blackcaps in our study, it has been shown that there are genetic differences among different migratory blackcap populations (*24*). Thus, our findings provide compelling support for a mechanism by which sympatric vertebrate populations may become isolated and thus how divergence and ultimately sympatric speciation could occur. Our findings also have implications for our understanding of migratory connectivity, indicating that higher levels of connectivity may influence adaptation to the breeding areas and lead to speciation (*25*).

References and Notes

1. P. Berthold, A. J. Helbig, G. Mohr, U. Querner, *Nature* **360**, 668 (1992).
2. P. Berthold, *Bird Study* **42**, 89 (1995).
3. P. A. Cotton, *Proc. Natl. Acad. Sci. U.S.A.* **100**, 12219 (2003).
4. D. R. Rubenstein *et al.*, *Science* **295**, 1062 (2002).
5. G. E. Hill, R. R. Sargent, M. B. Sargent, *Auk* **115**, 240 (1998).
6. C. B. Viverette, S. Struve, L. J. Goodrich, K. L. Bildstein, *Auk* **113**, 32 (1996).
7. M. S. Webster, P. P. Marra, S. M. Haig, S. Bensch, R. T. Holmes, *Trends. Ecol. Evol.* **17**, 76 (2002).
8. D. Glue, *Br. Trust Ornithol. News* **254**, 8 (2004).
9. A. J. Helbig, *Behav. Ecol. Sociobiol.* **28**, 9 (1991).
10. K. A. Hobson, L. I. Wassenaar, *Oecologia* **109**, 142 (1997).
11. C. P. Chamberlain *et al.*, *Oecologia* **109**, 132 (1997).
12. D. R. Norris, P. P. Marra, R. Montgomerie, T. K. Kyser, L. M. Ratcliffe, *Science* **306**, 2249 (2004).
13. K. A. Hobson, G. J. Bowen, L. I. Wassenaar, Y. Ferrand, H. Lormee, *Oecologia* **141**, 477 (2004).
14. Materials and methods are available as supporting material on *Science* Online.
15. L. I. Wassenaar, K. A. Hobson, *Environ. Sci. Technol.* **34**, 2354 (2000).
16. L. I. Wassenaar, K. A. Hobson, *Isotopes Environ. Health Stud.* **39**, 211 (2003).
17. S. Bearhop, R. W. Furness, G. M. Hilton, S. C. Votier, S. Waldron, *Funct. Ecol.* **17**, 270 (2003).
18. R. Przybylo, D. A. Wiggins, J. Merila, *J. Avian Biol.* **32**, 214 (2001).
19. S. J. Reynolds, S. J. Schoech, R. Bowman, *Oecologia* **134**, 308 (2003).
20. H. E. Gorman, R. G. Nager, *Proc. R. Soc. London Ser. B.* **271**, 1923 (2004).
21. S. Rytkonen, M. Orell, K. Koivula, M. Soppela, *Oecologia* **104**, 386 (1995).
22. P. P. Marra, K. A. Hobson, R. T. Holmes, *Science* **282**, 1884 (1998).
23. L. R. Monteiro, R. W. Furness, *Philos. Trans. R. Soc. London Ser. B.* **353**, 945 (1998).
24. J. Perez-Tris, S. Bensch, R. Carbonell, A. J. Helbig, T. L. Telleria, *Evolution* **58**, 1819 (2004).
25. M. S. Webster, P. P. Marra, in *Birds of Two Worlds*, R. Greenberg, P. P Marra, Eds (John Hopkins Univ. Press, Balitmore, MD, 2005), chap. 16.
26. G. J. Bowen, J. Revenaugh, *Water Resour. Res.* **39**, 1299 (2003).
27. See the IAEA/WMO GNIP database (http://isohis.iaea.org/).
28. We thank R. McDonald, R. Phillips, T. Van Lamsweerde, M. Fowlie, and three anonymous referees for their advice; the Vogelwarte Radolfzell ringers, B. Kavanagh, J. Callion, P. Burton, B. Ross, P. Catry, A. Campos, R. Lopes, W. J. Webber, C. Honan, T. Keely, S. Fagan, S. Alves, M. Eaton, J. Pemberton, S. MacMahon, A. Slade, and S. Wooley for help with the fieldwork; and L. Wassenaar for the provision of keratin standards to correct for exchangeable hydrogen. S.B. was funded by a Natural Environment Research Council postdoctoral fellowship.

Supporting Online Material
www.sciencemag.org/cgi/content/full/310/5747/502/DC1
Materials and Methods
References

2 June 2005; accepted 20 September 2005
10.1126/science.1115661

New Products

http://science.labvelocity.com

Fluorospectrometer

The NanoDrop ND-3300 Fluorospectrometer can perform full spectrum fluorescent analysis of 1 µl samples without the use of cuvettes or capillaries. The instrument's patented sample retention system makes use of surface tension to hold the sample in place on the fiber optic measurement surface. Through the unconventional use of a white LED in addition to commonly used ultraviolet and blue LED sources, a broad excitation range is achieved without cumbersome and costly filter changes. The space-saving fluorospectrometer offers unique features that allow investigators to use fluorometry in valuable new ways. For example, the 9×5 in instrument provides the benefits of measuring two picograms of DNA in a 2µl PicoGreen reaction. With assays in microgenomics, proteomics, and drug discovery requiring progressively smaller sample analysis, the ND-3300 allows for sample conservation because of its ability to measure minute amounts of biomolecules.

NanoDrop Technologies For information 302-479-7707 www.nanodrop.com

ImmunoglobulinG Kit

The Melon Gel Kit quickly processes sera to produce purified immunoglobulin G (IgG) ready to use for downstream modification or conjugation. There is no need to desalt. Melon Gel saves time compared with classical protein A or protein G purifications without compromising the quality of the IgG.

Pierce For information 800-874-3723 www.piercenet.com

Hepatocyte Drug Transport Assay

To help choose better drug candidates, B-Clear identifies compounds with desirable hepatobiliary disposition properties or adverse drug–drug interaction potential, avoiding costly product development challenges. B-Clear, a patented sandwich-cultured hepatocyte approach, is an in vitro method to predict hepatic uptake and biliary excretion and assess drug transporter inhibition. It can make use of human, monkey, dog, rat, or mouse hepatocytes.

Qualyst For information 919-313-6500 www.qualyst.com

Capto MMC Chromatography Medium

Capto MMC is the second in a new family of chromatography media intended for large-scale biopharmaceutical manufacturing. It is a multimodal cation exchanger used in the early stages of downstream purification, designed to meet a growing need in the biopharmaceutical market to process large feed volumes in a fast, efficient, and cost-effective way. Adsorption to Capto MMC is salt-tolerant, enabling the finding of proteins at the conductivity level of the feed material. It binds proteins at all the ionic strengths normally used during protein fermentation. This means that clarified feedstocks can be loaded directly onto the medium, eliminating the need for prior dilution to reduce the conductivity of the starting material. Furthermore, the ligand adds selectivity, which increases the chances of solving challenging purification problems. Based on a highly rigid agarose matrix, Capto MMC allows for a wide working range of flow velocities, column bed heights, and sample viscosities.

GE Healthcare For information 732-457-8082 www.gehealthcare.com

DNA Polymerase

MasterAmp Tth DNA Polymerase is a thermostable enzyme that has both DNA-directed DNA polymerase activity and an efficient reverse transcriptase activity. The enzyme is active at temperatures up to 70° C, which minimizes nonspecific priming and RNA secondary structure and ensures more accurate and sensitive reverse transcription–polymerase chain reaction.

Epicentre Biotechnologies For information 800-284-8474 www.EpiBio.com

Proteomics System

The NanoLC-1D Plus liquid chromatography system for nanospray mass spectrometry analysis is configured with a third pump for rapid sample loading and washing. Suitable for proteomics and biomarker discovery applications, the system allows sample loading at high flow rates, for time savings and flexibility. The system features a new pump and flow controller technology that allows precise operation at higher pressure—5500 psi—for higher resolution in nanobore columns. An innovative flow meter design improves flow precision for a wider variety of mobile phases. By eliminating flow splitting, Eksigent's proprietary microfluidic technology improves reproducibility and sensitivity and eliminates solvent waste.

Eksigent Technologies For information 925-960-8869 www.eksigent.com

Imaging Family

A new collection of cell systems and software tools provides a flexible and modular family of imaging products. Comprising seven members, the cell^ family ranges from simple image acquisition and documentation systems to complete solutions for live cell imaging. Each member is made up of cameras, microscopes, and illumination systems controlled by advanced Windows-based software. Due to their modular set up, all cell^ family members are fully upgradeable to grow with evolving research requirements, so users do not have to get used to new interfaces as their needs develop. The cell^A and cell^B are entry-level systems for image acquisition, reporting, and archiving. The cell^D offers more advanced functions, allowing rapid image acquisition, direct web transfer, numerous processing functions, and interactive measurements. The cell^F is a standard-level system for fluorescent applications and cell^P is for advanced automated capture and analysis of multi-fluorescent images, time-lapse photography, and three-dimensional composites.

Olympus For information +49 40 2 37 73-5426. www.olympus-europa.com

Direct Marker Visualization

The MagicMark XP Western Protein Standard makes use of innovative technology for direct marker band visualization on protein immunoblots. Each protein in the standard set contains an immunoglobulin binding site, allowing marker visualization using the same antibody–conjugate reagents and protocol for the target protein as your immunoassay. The standard offers a broad molecular weight range of 20 to 220 kDa.

Invitrogen For information 800-955-6288 www.invitrogen.com

Published by AAAS

Master Mixes

The FastStart Taqman Probe Master and the FastStart SYBR Green Master are new ready-to-use reagent mixes that simplify the preparation of samples for quantitative polymerase chain reaction (PCR) and two-step quantitative reverse transcription (RT) PCR. These master mixes are optimized for use with most real-time PCR instruments other than the LightCycler 2.0 system. They are available in two formulations, with and without ROX reference dye. The Probe Master allows sensitive detection and quantification of defined DNA sequences. The Green Master is suitable for quantitative, real-time DNA detection assays when the user performs quantitative PCR and two-step quantitative RT-PCR assays in the SYBR Green I detection format.

Roche Applied Science For information 317-521-2464 www.roche-applied-science.com

Phosphatase Inhibitor

The Halt Phosphatase Inhibitor Cocktail preserves phosphorylation of proteins in cell and tissue lysates. The cocktail contains a mixture of four phosphatase inhibitors of broad specificity, including sodium fluoride, sodium orthovanadate, sodium pyrophosphate, and β-glycerophosphate. Unlike other commercially available cocktails, which protect against either serine/threonine phosphatases or protein tyrosine phosphatases, the Halt Phosphatase Inhibitor Cocktail protects phosphoproteins from both families of phosphatases. The cocktail is compatible with standard protein assays.

Pierce For information 815-968-0747 www.piercenet.com

DNA Polymerase

PrimeStar HS DNA Polymerase is a novel, high-fidelity polymerase chain reaction (PCR) enzyme that provides maximum fidelity as well as extended product length (8.5 kb for human genomic DNA; 22 kb for lambda DNA). Targeted for PCR cloning applications, it offers high accuracy and high priming efficiency. The antibody-mediated hot-start formulation prevents false initiation events during reaction assembly due to mispriming or primer digestion, thus lowering background.

Takara Mirus Bio For information 888-251-6618 www.takaramirusbio.com

Screening Chip

The newest addition to the Topaz System for protein crystallization is the 8.96 Screening Chip, which delivers the ability to run 768 experiments in parallel with less than 15 nl of protein sample per trial. This higher density of experiments and lower protein consumption, compared with traditional drop-based formats, dramatically reduces the overhead involved with protein crystallization. The 8.96 Chip screens 96 reagents against eight samples, which opens the door to the simultaneous processing of multiple reagents. The feature allows researchers to use nano-volume crystallization to qualify which among multiple constructs or protein-ligand preparations are "crytallizable." Researchers can use the information to determine how their protein production resources should be allocated.

Fluidigm For information 650-266-6000 www.fluidigm.com

Phosphoproteome Profiles

The ProteoExtract Phosphoproteome Profiler Kit is a convenient kit for the precipitation and digestion of protein fractions and subsequent enrichment of phosphopeptides. Isolated phosphopeptide-containing fractions are directly compatible with matrix-assisted laser desorption ionization and electrospray ionization-liquid chromatography/mass spectrometry. Applications include small molecule profiling (for example, drug or inhibitor); monitoring of cellular effects of gene silencing, and measuring effector overexpression effects in signal transduction phosphorylation events.

EMD Biosciences For information 800-854-3417 www.emdbiosciences.com

Systems for In Vivo Molecular Imaging

The Kodak Image Station In-Vivo F and FX systems feature cooled charge-coupled device camera technology and selectable multi-wavelength illumination for sensitive, quantitative imaging of luminescent-, fluorescent-, and radiographic-labeled biomolecules in vivo. The FX system also provides an integrated digital x-ray imaging source and a phosphor-based radiographic imaging screen, enabling digital radiography. By precisely co-registering anatomical x-rays of tissues, organs, and whole animals with near-infrared, isotopic, or luminescent optical imaging modalities, a significant improvement in anatomical localization of molecular signals is achieved. With true 16-bit imaging performance, 4-million pixel resolution, a 10× optical zoom, and comprehensive analysis capability, the Image Station In-Vivo systems produce high performance molecular imaging results for the widest range of labels and sample formats on an easy-to-use platform. Both systems feature the Kodak Animal Management Center, which provides an enclosed, animal-friendly environment for multi-modal imaging of up to four mice simultaneously, and Kodak Molecular Imaging software for quantitative image analysis and multi-modal image overlay capability.

Eastman Kodak For information 877-747-HELP www.kodak.com/go/molecular

Taq DNA Polymerase

Contaminating DNA in polymerase preparations often interferes with the interpretation of results, especially when targeting conserved sequences. MTP Taq DNA Polymerase is a recombinant thermostable enzyme from *Thermus aquaticus* expressed in *E. coli* and purified using a proprietary process to minimize the levels of contaminating DNA. The enzyme has both five-prime and three-prime DNA polymerase and exonuclease activities, is approximately 95 kD, and has no detectable endonuclease or three-prime or five-prime exonuclease activities.

Sigma-Aldrich For information 314-286-7626 www.sigmaaldrich.com

Newly offered instrumentation, apparatus, and laboratory materials of interest to researchers in all disciplines in academic, industrial, and government organizations are featured in this space. Emphasis is given to purpose, chief characteristics, and availability of products and materials. Endorsement by *Science* or AAAS of any products or materials mentioned is not implied. Additional information may be obtained from the manufacturer or supplier by visiting www.science.labvelocity.com on the Web, where you can request that the information be sent to you by e-mail, fax, mail, or telephone.

Published by AAAS

EDITORIAL FEATURE

The Class of 2005

These days, the path to scientific independence is long and steep. But every year, a new cohort of scientists makes it to the top, thanks to lots of hard work, determination, talent, and at least a little good luck. This week, we celebrate the success of the new faculty class by profiling eight early-career researchers from the United States and Europe who this year came of age, beginning their first permanent jobs as independent scientists

United States: Two Scientists and a Baby

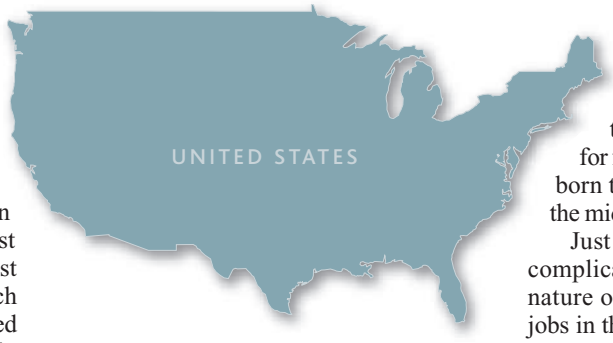

The conventional wisdom for job seekers is "keep it simple." It's hard enough to get a tenure-track job without any complications; forget about finding two jobs in the same place, for instance, or adding children to the mix. By that standard, earth scientist Alexis Templeton and biophysical chemist Amy Palmer did a lot wrong in their search for tenure-track jobs. They were determined to stay together, seeking faculty positions in the same city, even the same institution, and they started a family just as they began searching for jobs. Yet Palmer and Templeton have ended up together at the University of Colorado, in jobs that they each wanted.

If they did so many things wrong, how did things end up so right? The conventional wisdom, it seems, is no longer always so wise. It's been eroded by cultural changes at leading institutions. And, as Templeton and Palmer's experience indicates, talent, hard work, audacity, and—especially—being ready can overcome some high barriers. "We felt ready," says Templeton. "We just felt that we had to go for it."

Together in Colorado. Alexis Templeton (*left*) and Amy Palmer.

Convergence and scientific divergence

Palmer and Templeton have been aligning their plans and ambitions since they met as undergraduates at Dartmouth College. Templeton graduated first and began working on a master's degree at Dartmouth. When Palmer finished her bachelor's degree, she took a technician job in a Dartmouth laboratory while Templeton finished her master's degree. Then they headed west together, where Palmer enrolled at Stanford University in bioinorganic chemistry and Templeton did a technician stint of her own, in a stable-isotope lab at the nearby Lawrence Berkeley lab.

Later, Templeton joined Palmer in graduate school at Stanford, and soon they were deep into their first dual job search. "We actually co-interviewed for postdocs at some places," says Templeton. "That was our first run-through." They decided to stay in California but headed south, to the University of California, San Diego: Palmer in the department of pharmacology and Templeton at the UCSD-affiliated Scripps Institution of Oceanography.

Both scientists changed direction with their postdocs. Templeton took up the study of the ecology and chemistry of microbial communities that live on the flanks of submarine volcanoes. "We're looking at the ways life can exist in these systems. We're at the early stages of trying to figure out who's present, and then we want to look mechanistically at how they do it." Palmer studies the movement of signaling molecules within and between "living cells, and in real time."

Two scientists and a baby

As their scientific paths diverged, Templeton and Palmer's personal lives became more tightly intertwined: Just as they began looking for faculty positions together, Ethan was born to Palmer on 29 November 2004—the middle of the interviewing season.

Just a few years ago, any one of these complicating factors—the unconventional nature of their relationship; requiring two jobs in the same place; having a baby in the midst of the job search—could have caused problems. But "what we found is that many institutions have worked very hard in the last few years to be very open" to assisting new parents and dual-career couples, as well as about lifestyle choice, says Templeton: "I think the landscape has changed a lot."

"Institutions were very good about helping us, if one had an offer, trying to accommodate the other," adds Palmer. "We had no idea going into this that that would even be an option."

Universities also went out of their way to accommodate the demands of the baby. Several rescheduled interviews, and even when her hosts didn't know what to do, "they were always willing to ask," says Palmer.

And what about the fact that they were two women in a relationship? "There wasn't a blink, which was really astounding," says Templeton.

Arrival

Although things were going very well for the couple—top institutions were expressing interest in both of them—the experience was exhausting. When Templeton wasn't interviewing, she was off in the South Pacific collecting data. "It was great and hard all at the same time," says Palmer. "I've never been as deeply tired as I was from November until about April when we finally decided where we would end up."

Templeton remembers when the call came and their collective future began to gel. Palmer already had an offer from the University of Colorado, Boulder, and they were waiting to hear from the earth science department, which had interviewed Templeton independently. "I was totally out of touch, in Samoa, which is where we were working,"

CREDIT: SARA SHRIVER

Published by AAAS

she says. "There was very little telephone contact, and we had no e-mail or anything like that." Templeton's offer finally got through, and the family converged on Colorado. Now, even the obligatory working dinners were family affairs. "We ate and mixed together, each of the individual initiatives that were hiring us, we worked out our kinks with each of them."

Now that they're settled in, Templeton and Palmer spend much of their time ordering equipment, setting up their labs, and writing research grants. Both received start-up packages sufficient to buy essential equipment and support students, but support for professional staff was not a part of the deal, so Templeton is trying to scrape together funds to pay a technician to help get her lab up and running. Graduate students will soon start "rotating" into Palmer's lab, but Templeton won't have students until next year at the earliest because at Colorado's earth science department, students are admitted only after hooking up with a research group. Neither scientist is teaching yet—both got teaching-load reductions for the first year—but Palmer will begin teaching later in the semester and Templeton in the spring.

The secrets of their success

In an era when most postdocs fail to get even a single tenure-track offer, Templeton and Palmer received several, and a handful of institutions offered both of them jobs. What made them so successful?

One factor was the receptiveness of universities that, just a few years earlier, might not have been prepared to deal with the complexities they presented. This is largely a result of policy recommendations from the American Council on Education and recent, well-publicized scholarship by academics such as Bob Drago, Mary Ann Mason, and Marc Goulden, believes Cathy Trower of the Collaborative on Academic Careers in Higher Education, an organization that aims to "improve the quality of faculty work life." "Academe is finally, slowly, waking up," says Trower.

Apart from that, Palmer and Templeton's success was due partly to the usual virtues: talent, hard work, strong records of research accomplishments, strong letters of recommendation from well-known mentors, and so on. Yet Palmer and Templeton had one other thing going for them: They took their time, and by the time they went on the job market, they were ready.

After considering going on the market following their first postdoctoral year, the couple decided to put off their job search for another year so that they could focus all their attention on their postdoctoral research. That extra year, they figure, changed everything. "Suddenly, it was a feeling of real independence in terms of the directions we wanted to go in," says Templeton. "We felt very well established in what we were working on in our postdocs and really excited about new opportunities and looking for ways to make those new opportunities come into being."

"Looking back on it," Palmer adds, "I would say that was the smartest decision I ever made because the next year, the reason I knew I was ready is that I had all these ideas of my own that I wanted to pursue. I felt that I really wanted to study them in my own way. I felt like I was cutting the cord."

Together in Boulder

Now the cord is cut, and the three of them are thrilled with the result. Ethan, now 10 months old, "has been very happy since we've gotten to Colorado," says Templeton, "because he's not traveling across the country all the time, and he has a stable routine." As for the parents, they're both busy but fulfilled. "It feels really good to just know what it is we're trying to do and just focus on it," she adds.

Yet Palmer and Templeton still face all the challenges of beginning a new faculty position: recruiting students and staff, finding research funding, teaching, integrating themselves into the academic community, and establishing a steady flow of ideas and data. It's daunting. "I wish that there was double the amount of time in each and every single day," says Palmer. "There are so many different draws on your time that you're just not used to. No matter how many times people tell you what it's like, you just don't know until you experience it. But it's just great."

—JIM AUSTIN

Jim Austin is the editor of *Science*'s Next Wave. He can be contacted at jaustin@aaas.org.

Germany: Deciphering Cellular Processes

To German-born biochemist Anne Spang, a researcher's role is similar to that of a police detective: "putting evidence together to solve a riddle." Her scientific snooping has led her to uncover fundamental cellular processes such as intracellular transport mechanisms and mitosis and taken her to four countries. At each stage, Spang has ventured into new territory and taken risks. As a reward, in a few months, she'll take up her first tenured faculty position at the Biozentrum in Basel, Switzerland.

In career terms, this is the icing on the cake for Spang, who already has an independent and prestigious—but untenured—position. But she wasn't prepared to take the first job she was offered. In fact, after 2 years of applying and interviewing, she believes that persevering for the right faculty job—a position that can fulfil your career ambitions—is worth the investment of time and risk. "The most important thing," she says, "is figuring out what you really want."

CREDIT: A. SPANG

Discovering biology

Spang "came into biochemistry through the back door," as she puts it. She started her scientific life as a chemical engineering student at the University of Applied Science in Darmstadt, Germany, where basic courses in biochemistry and microbiology turned her on to biochemistry.

After finishing her chemical engineering diploma thesis in 1990, Spang moved to France to study biochemistry as an undergraduate at the Pierre and Marie Curie University in Paris. Although she says the challenge of catching up with her fellow students "was a shock," her exposure to biochemical research cemented her choice: "I knew I wanted to do a Ph.D."

So in 1992, Spang moved back to Germany to pursue a Ph.D. at the Max Planck Institute for Biochemistry at Martinsried, near Munich. There she worked with Elmar Schiebel investigating a core cell-biology question: the role of the centrosome analog—important in mitosis—in the yeast *Saccharomyces cerevisiae*. "I had a great time," she says. "It was clear to me that I loved doing research." Next stop, California.

With her newly minted Ph.D., Spang joined Randy Schekman's lab at the University of California, Berkeley, where she stayed for three-and-a-half years. There she developed an in vitro assay to measure intracellular transport mechanisms: the trafficking route from the Golgi to the endoplasmic reticulum. It was a high-risk project, but the gamble paid off, not just in immediate terms but—by establishing a novel technique—also in terms of her career. "It was clear from the beginning that because the project was risky, I could take

[it] with me when I left Randy's lab."

Spang took the project back to Germany. In 1999, after interviewing for several jobs, she was offered a prestigious 5-year position as a junior group leader at the Max Planck Society's Friedrich Miescher Laboratory (FML) in Tübingen, Germany. The job came with funding for five staff positions and the possibility of a 2-year extension. FML, says Spang, is a "special institute" comprised of four young group leaders in different fields of life sciences who work together to manage the institute's budget and communal resources.

At FML, Spang took advantage of her independence to develop two major research lines. One originates from her previous work: elucidating intracellular traffic processes in yeast; how vesicles are formed and how and when cargo is included in transport to the various organelles. The other focuses on cytokinesis—the final stage of mitosis, in which the mother and daughter cell separate and move apart—in the roundworm *Caenorhabditis elegans*.

Finding the right faculty job

Although she has complete research freedom at FML, it is not a long-term option. So 2 years ago, Spang started applying for faculty jobs. She hit the jackpot earlier this year when one of the first places she applied, the Biozentrum, offered her a tenured professorship this year. Spang and her group of eight from Tübingen—everyone but one technician in the lab—will move with her to Basel. "I'm totally excited about starting."

What really attracted her is the lack of distractions. "There is no overload of administration and teaching. I can still do research." It was a good fit—just as she was looking for a research-focused job, Basel was looking for a research-focused candidate—and Spang believes this is key. The interview process, she points out, goes both ways: They are interviewing you, and you are interviewing them. "You immediately develop a feeling for the position. Would this be good for me or not?" Warning bells would have rung loudly, she says, if during an interview she had been asked, "Would you think about becoming dean within the next 2 years?"

Now that she has secured her own tenured position, Spang urges other early-career researchers not be disheartened. "Don't take it personally. Now that I'm on selection committees, I see how difficult it is to decide between the last candidates."

"When I watch cell division in *C. elegans*," says Spang, "I still think this is a fascinating and beautiful process. Only study problems that you really find interesting," she advises. "Only then have you the energy to keep going." **–ANNE FORDE**

Anne Forde is the European Editor, North and East, for *Science*'s Next Wave.

France: A Knot Mathematician, With a Twist

On 1 September, Julien Marché joined the ranks of the Maîtres de Conférences at the Pierre and Marie Curie University in Paris. As in many other countries, permanent academic positions like this are highly competitive in France. Although he is quick to dismiss his achievement—"It doesn't mean much," he says—he has accomplished this at an age when most scientists are still doing their Ph.D. work.

Marché's path to his current position—"I'm 25, so it will be short," he says—began early. He earned a scientific baccalauréat magna cum laude at 16, 2 years ahead of the normal schedule. Instead of university, he went to the highly selective Classes Préparatoires, where he spent 2 years preparing for the competition to enter the French Grandes Écoles. He won entry into the prestigious École Normale Supérieure (ENS) in Paris in 1998. There, Marché earned a B.Sc. and M.Sc. in mathematics after his first year, and an agrégation—a qualification for higher-education teaching—a year later. In his third year, Marché did a Diplôme d´Etudes Approfondies, a prerequisite to starting a Ph.D. in France.

Like most students at ENS, Marché began a thesis in his last year, working on knot theory—a branch of topology—at Denis Diderot University, studying "algebraic constructions related to knots, inspired from theoretical physics," he says. Three years later, in December 2004, Marché was awarded his Ph.D. with distinction.

Next, Marché tried his luck at getting a permanent position, which in France usually means becoming a Chargé de Recherche at a public research organization such as the Centre National de la Recherche Scientifique (CNRS) or a Maître de Conférences at a university. "I wasn't accepted at the CNRS," he says, so he applied for a Maître de Conférences position. He was hired by the Department of Algebraic Analysis at the Jusseiu Mathematics Institute, which is affiliated with both the Pierre and Marie Curie and Denis Diderot universities, in a very competitive search. "You can count on one hand the number of positions you can have access to," says Marché. "I was lucky to find this position very quickly, in 6 months"; for many people, the search can take 2 to 3 years. He is happy now to be able to relax and focus on his work. "I have gained some peace of mind. My career will not be put at risk every year."

In France, new faculty appointees join an existing team rather than starting up their own. Although "the researcher is free to do whatever he wants," says Marché, "I will be working in a team, so I will necessarily get interested in their field of research." He sees this as an advantage, as it offers connections that he intends to explore. "I want to open myself to new ideas and start new collaborations." **–ELISABETH PAIN**

Elisabeth Pain is Contributing Editor for Europe, South and West, for *Science*'s Next Wave.

Spain: A Physicist Keen to Put Things in Order

Rebeca de Nalda Minguez, 34, has just started her first permanent position, as Cientifico Titular of the Spanish Consejo Superior de Investigaciones Científicas (CSIC) Rocasolano Institute for Chemical Physics in Madrid. She was only 2 years into her 5-year Ramón y Cajal contract, a research position created by the Spanish government in 2001 to bridge postdoctoral and permanent positions. At a time when many Ramón y Cajal scientists in their last year still have no permanent position in sight, de Nalda Minguez considers herself lucky, not least because she will begin her new position with management skills that she picked up during her time abroad.

After obtaining a 5-year degree in physics at the Universidad Complutense de Madrid in 1994, de Nalda Minguez did a 4-year Ph.D. at the Rocasolano Institute on laser-matter interactions. She went on to do a postdoc at the Madrid Institute of Optics in 2000; then she was off to the United Kingdom for a research-associate position at Imperial College London. She returned to Madrid in 2003 with a Ramón y Cajal at the Universidad Complutense.

"There is a tremendous bottleneck" to get a Cientifico Titular position, she says; when she applied in 2004, only 100 positions were offered by CSIC, for all fields and in the whole of Spain.

Still, for de Nalda Minguez, achieving true independence will be challenging. In Spain, "most people integrate into an existing

CREDITS (LEFT TO RIGHT): J. MARCHÉ; R. DE NALDA MINGUEZ

and functioning lab," which gives them less freedom. Alternatively, "people can start afresh, but they do struggle for each aspect of research." She is seeking middle ground, joining some of her institute's activities while developing her own lines of research.

Molecular bonds are not the only things that de Nalda Minguez would like to break and rearrange during her career. "There are many problems in the Spanish system," she says: Newcomers are not welcomed, there are long delays in the processing of applications, and many scientists become permanent staff only in their 40s. Most of all, "we all have a lot to learn in this country on managerial skills—on setting up active and creative teams and working together with a common aim," she says. **–E.P.**

Norway: A Neuroscientist Making Connections

Norwegian neuroscience researcher Farrukh A. Chaudhry trained as a medical doctor, but his heart has always been in basic science. In August this year, the 36-year-old Chaudhry began an appointment as a group leader at the Biotechnology Centre in Oslo. The position is funded for 10 years and comes with an associate professorship at the Centre for Molecular Biology and Neuroscience at the University of Oslo. A 2003 winner of the Norwegian King's Gold Medal for Science, Chaudhry is one of only a handful of young scientists to win their first faculty position in Norway this year.

When he finished his medical studies at the University of Oslo, Chaudhry began studying for a Ph.D. with Jon Storm-Mathisen at the university's Anatomical Institute. There he investigated amino acid transporters, proteins that ferry signals across the synapse, the gap between nerve cells. The work was done in collaboration with Robert Edwards at the University of California, San Francisco (UCSF), where Chaudhry conducted most of his experimental work. During this period, he uncovered a new family of transporter proteins.

As a postdoc, Chaudhry returned to Storm-Mathisen's lab and secured a "career stipend" from the Norwegian Research Council, which gave him independent funding and a lot of intellectual freedom.

Chaudhry saw an ad for the group-leader position at the Biotechnology Centre by chance, and he says he didn't think too much about his application. In retrospect, he realizes how fortunate he was to get a group-leader position in a research institute in Norway. "This is an unusual position; I will have little bureaucracy and limited teaching."

Chaudhry will investigate whether the family of amino acid transporters he discovered while at UCSF may play a role outside the synapse, perhaps in non-neurological diseases such as chronic metabolic acidosis or even cancer. **–A.F.**

Belgium: A Particle Physicist On Track

On 1 November, Caroline Collard, a 29-year-old Belgian national, will join the French CNRS Department of Nuclear and Particle Physics with a permanent Chargé de Recherche position. Getting one of these positions is hard enough for French nationals; foreigners have the added difficulty of understanding the French system. "For me it was really a possibility to apply because I was [already] working inside France, so I had lots of advice about it," she says.

Collard earned a 4-year degree in physics at the Université Libre de Bruxelles in Belgium, then stayed on to do a Ph.D. in fundamental particle physics, analyzing electron-proton accelerator data. She finished in 2002, then left for a postdoc at the École Polytechnique in Palaiseau, France, where she contributed to the building of a new detector, laying the foundations for future data analysis while "taking part in more experimental work."

The next career step for Collard was to obtain one of the six CR2 positions available at CNRS this year in her section. CNRS scientists are assigned a definite project and host lab, according to their preferences and the needs of research departments; Collard was appointed at the Laboratoire de l'Accélérateur Linéaire in Orsay to search for the Higgs boson. "I will go to a lab that is doing exactly the kind of research that I want to do; I am really happy about this."

If a permanent position has advantages over a postdoc, a job at a public research institution in France also has advantages over the typical academic post. Although some CNRS scientists choose to teach, a job at CNRS has no teaching obligations. Chargés de Recherche also enjoy greater mobility and after a 1-year probationary period can choose to move to another project, even a different research centre.

Collard was successful the first time she applied, partly, she reckons, because she has been thinking for a while about how to improve her chances. "It is important to look objectively at your CV and see if it is complete," she says, and to ask others for advice. Other than that, "you have to be lucky, because there is a lot of good people, and they [too] deserve the position." **–E.P.**

Germany: Tracking Pollutants

Next January, German postdoc Martin Elsner, currently based in Toronto, will start his first independent position as a Helmholtz Association Young Investigator in Germany. The tenure-track job, which will fund his salary and that of four group members, will be based at the GSF National Research Center for Environment and Health in Neuherberg, near Munich. Elsner represents a new generation of young scientists based in Germany who have the opportunity to establish their scientific independence at an age far younger than their predecessors.

While he was an undergraduate studying chemistry at the Swiss Federal Institute of Technology in Zurich, Elsner developed an interest in environmental chemistry. That led to a Ph.D. at the Swiss Federal Institute of Aquatic Science and Technology, where, along with René Schwarzenbach and Stefan Haderlein, he investigated the degradation of chlorinated solvents in groundwater.

Last year, he began a postdoc in Barbara Sherwood Lollar's lab at the Department of Geology at the University of Toronto. The Toronto group uses stable isotopes to trace the origin, route, and degradation of pollutants in groundwater. Elsner developed a method to determine the chemical pathway by which a pollutant is degraded.

For Elsner, a research group leader position at GSF is "really an attractive possibility. … I can concentrate on my research."

How has he managed to make the transition to independence at the relatively young age of 32? "It is very important to find your own research field, something original," Elsner says. "Go abroad for some time. That is how I got into a field that I could make a significant contribution to." **–A.F.**

CREDITS (LEFT TO RIGHT): GUNNAR LOTHE; C. COLLARD; M. ELSNER